Heat Transfer from a Convecting Crystallizing, Replenished Magmatic Sill and Its Link to Seafloor Hydrothermal Heat Output

A Dissertation
Presented to
The Academic Faculty

By

Lei Liu

In Partial Fulfillment
Of the Requirements for the Degree
Doctor of Philosophy in the
School of Earth and Atmospheric Sciences

Georgia Institute of Technology

December, 2010

Heat Transfer from a Convecting Crystallizing, Replenished Magmatic Sill and Its Link to Seafloor Hydrothermal Heat Output

Approved by:

Dr. Robert Lowell, Advisor
Professor Emeritus
School of Earth and Atmospheric Sciences
Georgia Institute of Technology

Dr. Leonid Germanovich
School of Civil and Environmental Engineering
Georgia Institute of Technology

Dr. Andrew Newman
School of Earth and Atmospheric Sciences
Georgia Institute of Technology

Dr. Josef Dufek
School of Earth and Atmospheric Sciences
Georgia Institute of Technology

Dr. Martial Taillefert
School of Earth and Atmospheric Sciences
Georgia Institute of Technology

Date Approved: November 3, 2010

To my dear family, friends and my teachers

ACKNOWLEDGEMENTS

First and foremost, I would like to express my sincere gratitude to my advisor, Dr. Robert Lowell, for offering me the opportunity to pursue my Ph.D. degree at Georgia Tech. I appreciate his close guidance and great efforts to prepare me to become a mature researcher. He has always been supportive of me not only when I made progress but also when I made mistakes. He taught me how to strive for excellence in my academic pursuits and helped me to develop critical thinking and presenting skills. I appreciate his guidance, support, endurance, and encouragement during my graduate studies at Georgia Tech. What I have learned from him is by no means limited to geophysics knowledge, but rather is applicable to the entire life.

This research was supported in part by NSF Grants 0527208 and 0976418 to Dr. Robert Lowell. This support is gratefully acknowledged.

I would like to thank my dissertation committee members: Dr. Andrew Newman, Dr. Josef Dufek, Dr. Martial Taillefert, and Dr. Leonid Germanovich for taking the time to serve on my PhD defense committee and for their helpful suggestions on my dissertation.

My sincere thanks also go to my group members, Kayla Lewis, Kate Craft, Liang Han, and friends at both Georgia Tech and Virginia Tech, Lujia Feng, Gence Genc, Kevin Zhao, Chunquan Wu, Liying Li, Hina Shah, Tao Jiang, Youyi Ruan and Kai Wang, for the insightful discussions and help along the way.

Last but not least, I would like to express my deepest gratitude to my family. I would like to thank my parents, my husband, and my sister for their unconditional and

eternal love and support. Their encouragement is always with me and has given me the strength to complete this work.

TABLE OF CONTENTS

LIST OF TABLES

LIST OF FIGURES

LIST OF SYMBOLS

Values of the physical parameters for magma chamber and hydrothermal vent fields

Symbol	Physical meaning	Value	Units
a_m	Thermal diffusivity of magma	8×10^{-7}	m^2/s
A_d	Area of hydrothermal discharge zone	10^3-10^4	m^2
A_m	Horizontal magma area in chamber	variable	m^2
A_{m0}	Initial magma chamber area	10^6-10^7	m^2
b	Exponential factor	10^{-9}-10^{-10}	
c_m	Andesitic magma specific heat	1000	J /kg ºC
	Basaltic magma specific heat	1400	
c_f	Fluid specific heat	6×10^3	J /kg ºC
C	Diopside concentration		
C_e	Diopside concentration at eutectic point	58%	
C_{in}	Di concentration of the added magma		
D	Magma chamber thickness		m
D_0	Initial magma thickness	10-100	m
D_{in}	The thickness of added magma		m
D_m	Liquid magma thickness		m
D_s	Crystal magma layer thickness		m
F_c	Heat flux added by conductivity		W/m^2
F_h	Heat flux carried by the hydrothermal fluid		W/m^2
F_m	Magmatic heat flux		W/m^2

F_r	Heat flux added by magma replenishment		W/m^2
g	Acceleration due to gravity	9.81	m/s^2
k	Permeability	10^{-11}-10^{-13}	m^2
L_a	Latent heat of crystallization of andesite	3×10^5	J/kg
L_b	Latent heat of crystallization of basalt	4.2×10^5	
L_{an}	Latent heat of solid anorthite	3.9×10^5	J/kg
L_{di}	Latent heat of solid diopside	6.6×10^5	J/kg
P	Magma replenishment period		year
M	Mass of magma		kg
Nu	Nusselt number		-
Ra	Rayleigh number		-
Ra_c	The critical Rayleigh number	$\sim10^3$	-
T_{aL}	Andesite liquidus temperature	1100	ºC
T_{awL}	3 wt% andesite liquidus temperature	1010	ºC
T_{aS}	Andesite solidus temperature	970	ºC
T_{awS}	3 wt% andesite solidus temperature	900	ºC
T_{bL}	Basalt liquidus temperature	1200	ºC
T_{bS}	Basalt solidus temperature	1030	ºC
T_{dwL}	4 wt% dacite liquidus temperature	950	ºC
T_{dwS}	4 wt% dacite solidus temperature	800	ºC
T_{anL}	Anothrite liquidus temperature	1553	ºC
T_{diL}	Diopside liquidus temperature	1391	ºC
T_e	Eutectic temperature	1275	ºC

T_h	Hydrothermal temperature	250-400	ºC
T_{in}	The temperature of replenished magma		ºC
T_m	Magma temperature		ºC
u	Replenishment rate		m/s
u_0	Initial replenishment rate		m/s
u_d	Darcian velocity		m/s
V	Volume of magma		m^3
w	Magma replenishment frequency		$year^{-1}$
α_f	Thermal expansion coefficient of fluid	10^{-3}	$ºC^{-1}$
α_m	Thermal expansion coefficient of magma	5×10^{-5}	$ºC^{-1}$
δ	Conduction boundary layer		m
κ	Thermal diffusivity	8×10^{-7}	m^2/s
λ	Thermal conductivity	2	Wm/ ºC
ν_f	Kinematic viscosity of fluid	10^{-7}	m^2/s
ν_m	kinematic viscosity of magma		m^2/s
ν_{m0}	Kinematic viscosity of magma at liquidus		m^2/s
ρ_a	Anhydrous andesite density	2.5×10^3	kg/m^3
ρ_{aw}	3 wt % H_2O andesite density	2.4×10^3	kg/m^3
ρ_b	Basaltic magma density	2.7×10^3	kg/m^3
ρ_d	4 wt.% Dacitic magma density	2.2×10^3	kg/m^3
ρ_f	Fluid density	10^3	kg/m^3
χ	Volume fraction of crystals		-
χ_c	Critical crystal fraction	60%	-

χ_{in}	The crystal content of input magma	-
ϕ	The solid factor	-

Notes: Subscripts '*m*' refers to magma, '*b*', '*a*' '*aw*', and *'d'* refer to basaltic magma, dry andesitic magma, 3wt% H_2O andesitic magma, and 4 wt.% dacitic magma respectively; '*f*' refers to fluid; '*h*' refers to hydrothermal system; '*L*' and '*S*' refer to the liquidus and solidus temperatures, respectively. For example, T_{bL} denotes the temperature of the basaltic magma at the liquidus stage.

SUMMARY

Hydrothermal systems at oceanic spreading centers play an important role in the composition of seawater, the formation of ore deposits, the support of microbial and macrofaunal ecosystems, and even for the development of life on early earth. These circulation systems are driven by heat transport from the underlying magma chamber, where latent heat of crystallization and sensible heat from cooling are transferred by vigorous, high Rayleigh number convection through a thin conductive boundary layer.

The traditional study of magmatic-hydrothermal systems is primarily based on the time-series observation, which takes the form of repeat visits, continuous offline monitoring by autonomous instruments, or continuous online monitoring by instruments with satellite or cable links to shore. Although a number of studies have deployed autonomous monitoring instruments at vents and around mid-ocean ridges to investigate geophysical and hydrothermal processes, the data are still rather limited and a comprehensive understanding of magma-hydrothermal processes at oceanic spreading centers is lacking. Numerical modeling needs to be employed to elucidate the dynamic behavior of magmatic hydrothermal systems and for testing completing hypotheses in these complex, data-poor environments.

In this dissertation, I develop a mathematical framework for investigating heat transport from a vigorously convecting, crystallizing, cooling, and replenished magma chamber to an overlying hydrothermal system at an oceanic spreading center. The resulting equations are solved numerically using MATLAB. The simulations proceed step-by-step to investigate several different aspects of the system.

First, I consider a hydrothermal system driven by convection, cooling and crystallization in a ~ 100 m thick basaltic magma sill representing an axial magma chamber (AMC) at an oceanic spreading center. I investigate two different crystallization scenarios, crystal-suspended and crystal-settling, and consider both un-replenished and replenished AMCs. In cases without magma replenishment, the simulation results for crystals-suspended models show that heat output and the hydrothermal temperature decrease rapidly and crystallinity reaches 60% in less than ten years. In crystals-settling models, magma convection may last for decades, but decreasing heat output and hydrothermal temperatures still occur on decadal timescales. When magma replenishment is included, the magmatic heat flux approaches steady state on decadal timescales, while the magma body grows to double its original size. The rate of magma replenishment needed ranges between 5 x 10^5 and 5 x 10^6 m^3/yr, which is somewhat faster than required for seafloor spreading, but less than fluxes to some terrestrial and subseafloor volcanoes on similar timescales. The heat output from a convecting, crystallizing, replenished magma body that is needed to drive observed high-temperature hydrothermal systems is consistent, with gabbro glacier models of crustal production at mid-ocean ridges.

Secondly, I study the heat transfer model from a parametric perspective and examine the effects of both initial magma chamber thickness and magma replenishment rate on the hydrothermal heat output. The initial rate of convective heat transfer is independent of the initial sill thickness; but without magma replenishment, the rate of decay of the heat output varies linearly with thickness, resulting in short convective lifetimes and decaying hydrothermal temperatures for sills up to ~ 100m thick. When magma replenishment is included in crystals settling scenarios at constant or

exponentially decreasing rates of ~ 10^{-8} m/s to the base of the sill, growth of the sill results in stabilized heat output and hydrothermal temperature on decadal timescales and a relatively constant to increasing thickness of the liquid layer. Sills initially ~ 10 m thick can grow, in principal, to ~ 10 times their initial size with stable heat output and a final melt thickness less than 100m. Seismic data provides evidence of AMC thickness, but it can not discriminate whether it denotes initial magma thickness or is a result of replenishment. These results suggest that magma replenishment might not be seismically detectable on decadal time scales. Periodic replenishment may also result in quasi-stable heat output, but the magnitude of the heat output may vary considerably in crystals suspended models at low frequencies; compared to crystals settling models. In these models the direct coupling between magmatic and hydrothermal heat output suggests that heat output fluctuations might be recorded in hydrothermal vents; but if damping effects of the basal conductive boundary layer and the upflow zone are taken into account, it seems unlikely that heat output fluctuations on a time scale of years would be recorded in hydrothermal vent temperatures or heat output.

Thirdly, I extend the work to the binary system motivated by the fact that the real magmas are multi-component fluids. I focus on the extensively studied binary system, diopside-anorthite (Di-An), and investigate the effects of convection of a two-component magma system on the hydrothermal circulation system through the dynamic modeling of both temperature and heat output. I model the melt temperature and viscosity as a function of Di concentration, and incorporate these relations in the modeling of the heat flux. Simulations comparing the effects of different initial Di concentrations indicate that magmas with higher initial Di concentrations convect more vigorously, which results in

faster heat transfer, more rapid removal of Di from the melt and growth of crystals on the floor. With magma replenishment, I assume that the magma chamber grows either horizontally or vertically. In either case magma replenishment at a constant rate of ~ 10^{-8} m^3/a can maintain relatively stable heat output of 10^7-10^9 Watts and reasonable hydrothermal vent temperatures for decades. The final stabilized heat flux increases with increasing Di content of the added magma. Periodic replenishment with a 10 year period results in temperature perturbations within the magma that also increase as a function of increasing Di. With the simple magma model used here, one can not discern conclusively whether the decrease in magma temperature between the 1991/1992 and the 2005/2006 eruptions at EPR 9°50′ involved replenishment with more or less evolved magmas.

Fourthly, I investigate a high-silica magma chamber as the hydrothermal circulation driver. I construct viscosity models for andesite and dacite melts as a function of temperature and water content and incorporate these expressions into a numerical model of thermal convective heat transport from a high Rayleigh number, well-mixed, crystallizing and replenished magma sill beneath a hydrothermal circulation system. Simulations comparing the time dependent heat flux from basalt, 0.1wt.% andesite, 3wt.% andesite, and 4wt.% dacite, indicate that higher viscosity magmas convect less vigorously, which results not only in lower heat transport and hydrothermal vent temperatures, but also in a lower decay rate of the vent temperature. Though somewhat colder, hydrothermal systems driven by unreplenished high-silica melts tend to have a longer lifetime than those driven by basalts, assuming a heat output cutoff of 10^7 Watts. As in the basaltic case, magma replenishment at a rate of ~ 3 x 10^5 – 3 x 10^6 m^3/a can maintain relatively stable heat output of 10^7-10^9 Watts and hydrothermal vent

temperatures for decades. Idealized models of porous flow through the lower crust suggest such replenishment rates are not likely to occur, especially for high-viscosity magmas such as andesite and dacite. Long term stability of hydrothermal systems driven by these magmas requires an alternate means of magma replenishment.

Finally, the dissertation concludes by discussing some avenues for future work. Most important of these are to: (1) couple magma convection with more realistic hydrothermal models and (2) link magma chamber processes to better physical models of replenishment and eruption.

CHAPTER 1. INTRODUCTION

1.1 Magma-Hydrothermal Activity at Oceanic Spreading Centers

1.1.1 Seafloor hydrothermal systems

Mid-ocean ridges play an important role in the plate-tectonic cycle of our planet. The global mid-ocean ridge system extends around approximately 50,000–60,000 km across the ocean-floor. At the mid-ocean ridges, oceanic crust and lithosphere are created at an average rate of ~3.3 km^2/yr [*Parsons*, 1981; *White et al*., 1992]. Along the volcanic mid-ocean ridges, seawater percolates downward through fractured oceanic crust where it is heated and chemically modified through the reaction with the surrounding host rock. Eventually, the seawater can reach the maximum temperature that exceeds 400°C. At these high temperatures the fluids become extremely buoyant and rise rapidly back to the seafloor, where they are expelled into the overlying water column. These seafloor hydrothermal systems play an important role in the transport of mass and energy between the lithosphere, biosphere and ocean. The heat transfer in submarine hydrothermal systems accounts for nearly 25% of the global heat flux from Earth's interior, and approximately 33% of the heat flux through the ocean floor [*Williams and Von Herzen*, 1974; *Stein and Stein*, 1994]. The transfer of mass affects the geochemistry of seawater and the crust [e.g., *Wolery and Sleep*, 1976; *Edmond et al.*, 1979; *Von Damm et al*.,

1985;] and is responsible for the formation of ore deposits on the seafloor [e.g., *Hekinian et al.*, 1980; *Hannington et al.*, 1995; *Rona and Scott*, 1993].

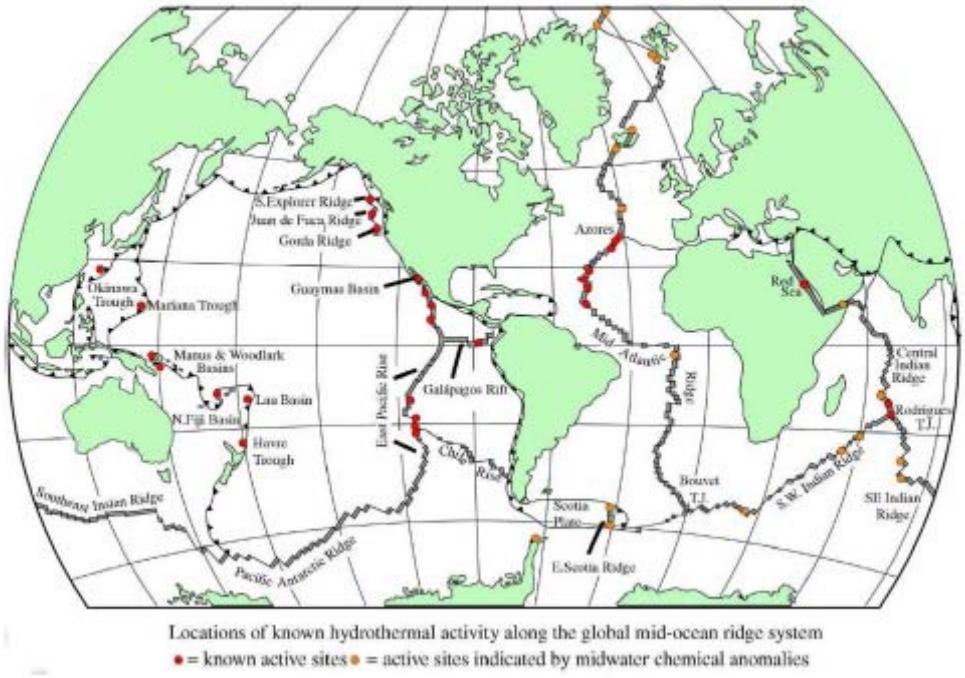

Figure 1.1 Map of the global ridge crest system indicates the major mid-ocean ridge sections [*German and Von Damm*, 2004]. Red circles represent sites where active hydrothermal vents have already been found. Orange circles show sites where hydrothermal activity is known to exist from the detection of characteristic chemical signals in the overlying water column.

The discovery of high-temperature hydrothermal vent sites on the seafloor is the best evidence of hot hydrothermal circulation at ridge crests. The global distribution of hydrothermal vents is shown in Figure 1.1. The first active fields of hot springs in the deep sea on the mid-ocean ridges were discovered in 1977 at the Galapagos Spreading

Center (GSC) [*Corliss et al.*, 1979]. This was also the first observation of a vent biological ecosystem based on chemosynthetic bacteria [*Jannasch*, 1983]. Subsequently, the first high temperature (~ 350 °C) sulfide-laden "black smokers" were discovered on the East Pacific Rise (EPR) at latitude 21ºN [*Spiess et al.*, 1980]. In the past three decades, more than 300 sites of hydrothermal venting have been discovered and explored on the ocean floor [*Baker and German*, 2004]. High temperature metal-rich, magnesium- and sulfate-poor hydrothermal fluids that form black and white smoker chimneys are formed along oceanic spreading centers in several major geodynamic settings, including the fast [*Haymon et al.*, 1991; *Baker et al.*, 1994], intermediate [*Baker and Massoth*, 1987], slow [Rona, 1985; *Langmuir et al.*, 1993] and ultraslow-spreading ridges [*Baker et al.*, 2004; *Edmonds et al.*, 2003], back-arc basins [*Fouquet et al.*, 1991] , arcs [*de Ronde et al.*, 2003], and fore arcs [*Herzig and Hannington*, 1995].

Hydrothermal venting occurs on mid-ocean ridge axes with a diversity of thermal, structural, and petrological characteristics. Hydrothermal fields exhibit different forms depending on the spreading rate. On the fast-spreading East Pacific Rise, black smokers (250°C ~ 400°C) typically occur through discrete individual chimneys and chimney clusters. Sulfide chimneys are rarely more than 15 m tall [*Kelley et al.*, 2002]. On the intermediate-spreading Juan de Fuca Ridge, the most common structures are the large multi-flanged irregular sulfide mounds (up to 18 - 20 m tall) that host multiple vigorously venting black smoker chimneys on their summits [*Tivey and Delaney*, 1986; *Kelly et al.*, 1997]. On the slow-spreading Mid-Atlantic Ridge, for example, the Transatlantic

Geotraverse (TAG) hydrothermal field, the black smokers exist on the top of a large single large deposit with the diameter of 200 m and height of about 50 m [*Humphris et al.*, 1995]. The TAG hydrothermal activity has been episodically active over relatively long periods (10^5 years) [*Rona*, 1984; 1993b]. Distinctly different from all other known sea floor hydrothermal fields, a new class of tectonically hosted hydrothermal field, including the low-temperature Saldanha and Lost City sites [*Barriga et al.*, 1998; *Kelly et al.*, 2001] and the high-temperature Logatchev and Rainbow vent sites [*Charlou et al.*, 2002], were discovered on the Mid-Atlantic Ridge. Lost City is located about 15 km away from a mid-oceanic ridge and on 1.5 million years old ocean crust. It is a peridotite-hosted system, characterized by massive carbonate–brucite structures, up to 60 m high, rather than sulfide structures typical of black smokers. It represents the first observation of the low-temperature venting (40°C ~ 75°C) that may be associated with serpentinization-related heat release [*Lowell and Rona*, 2002] and is the first major occurrence of active carbonate chimneys at a vent site [*Kelley et al.*, 2001].

Hydrographic, optical, and chemical tracers have all been used to successfully identify the venting [*Baker et al.*, 1995]. The first one of such studies was return visits during the 1980s to vent fields at 13°N on the East Pacific Rise and in the Galápagos Spreading Center. Comparison of known sites between visits revealed that the activity of individual vents and entire vent fields can vary substantially at a scale of years, and that these fluctuations can strongly affect the abundance and distribution of specialized vent fauna [*Fustec et al.*, 1987; *Hessler et al.*, 1988]. During the 1990s, with the capability to

access the acoustic listening network in the Northeastern Pacific, researchers were able to remotely detect seafloor eruptions on the Juan de Fuca and Gorda Ridges [*Fox et al.*, 1995]. Meanwhile, our understanding of the hydrothermal and biological consequences of magma injection and eruption events have been enhanced greatly through the event-response studies at eruption sites in this region [*Embley et al.*, 1999] and the serendipitous discovery and follow-up investigation of a seafloor eruption at 9°N on the East Pacific Rise [*Haymon et al.*, 1993; *Shank et al.*, 1998]. The global importance of seafloor hydrothermal processes and the apparent interconnectedness of magma transport, crustal structure, seawater circulation and biogeochemical processes have led to focused studies at the RIDGE 2000 Integrated Study Sites (ISS), which currently are located on the Endeavour Segment of the Juan de Fuca, and the East Lau Spreading Center in the Lau Basin [see more detailed information at www.ridge2000.org/science]. These pioneering studies documented the impressive capacity of microorganisms [*Juniper et al.*, 1995; *Huber et al.*, 2003] and vent fauna [*Tunnicliffe et al.*, 1997] to quickly colonize and exploit new sources of venting, and motivated new researches into the propagation of vent species along the mid-ocean ridges.

Estimating the heat transfer by hydrothermal circulation through oceanic crust is important to understand the evolution of the oceanic crust and its effects on the chemistry and the biology of the oceans. Before the discovery of submarine hydrothermal venting, a comparison of conductive heat flow data based on the numerical models of the global

heat loss from cooling, spreading lithosphere suggested that hydrothermal heat loss was an important component of the Earth's energy budget.

Figure 1.2 summarizes the early work on heat loss models of hydrothermal venting and shows the observed and predicted heat flow versus the age of the ocean basins. Figure (a) is summary of earlier results from [*Anderson and Skilbeck*, 1981]. Figures (*b*), (*c*) and (*d*) are the results from *Stein and Stein* [1994] compared to predictions of reference models GDH1 [*Stein and Stein*, 1992] and PSM [*Parsons and Sclater*, 1977]. Stein and Stein [1994] compare theoretical and observed heat flow data to parameterize hydrothermal circulation and find that the advected heat flux caused by hydrothermal circulation is significant. About 33% of the total oceanic heat flux occurs by advection and approximately 30% of the advected portion of the flux occurs in crust younger than 1 Ma. Although the models estimate the global importance of hydrothermal heat loss, they do not provide information for an individual vent or vent field.

Various techniques have been used to determine the heat output from focused high-temperature vents. These include measurement of the buoyant plumes above discrete vents [e.g., *Bemis et al.*, 1993; *Little et al.*, 1987], and measurements of flow velocity, temperature and area of individual vent orifices [e.g. *Converse et al.*, 1984; *Ginster et al.*, 1994; *Ramondenc et al.*, 2006] Studies from a number of hydrothermal sites show that total heat output from high-temperature vents at a given sites ranges between 10^7-10^8 Watts.

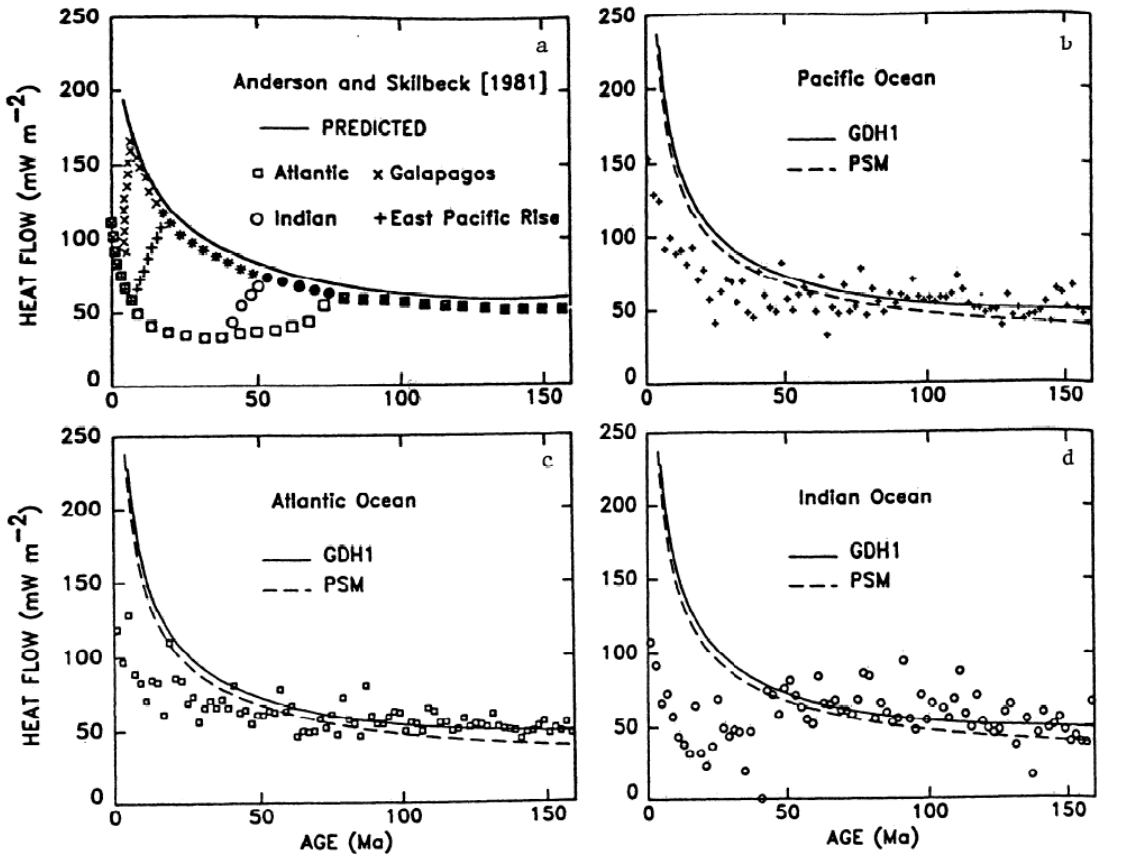

Figure 1.2 Observed and predicted heat flow versus the age of the ocean basins. Figure (a) is the summary of earlier results from [*Anderson and Skilbeck*, 1981]. The predicted curve is schematic. Figures (*b*), (*c*) and (*d*) are results from *Stein and Stein* [1994] compared to predictions of reference models GDH1 [*Stein and Stein*, 1992] and PSM [*Parsons and Sclater*, 1977]. The symbols for observed heat flow are shown in (a). Similar sealing ages for all the oceans are indicated, in contrast to the earlier compilation which shows the sealing at younger ages in the Pacific [From *Stein and Stein*, 1994].

Diffuse flow has received less attention than focused flow, even though it might account for a significant amount of the total hydrothermal heat output at mid-ocean ridges. For example, *Schultz et al.*, [1992] estimate that diffuse flow accounts for nearly 90% of the total heat output at the Main Endeavor Field on the Juan de Fuca Ridge,

though *Veirs et al.* [2006] obtain an estimate of ~50%. Geochemical data shows that diffuse flow is a mixture of seawater and high-temperature vent fluid [*Von Damm and Lilley*, 2004], and recent assessments of this data suggest that most of the diffuse heat output is ultimately due to the high-temperature component [*Germanovich et al.*, 2010]

Measurements in the neutrally buoyant plume in the water column above a vent field are also used to estimate the total heat flux. Such integrated heat outputs typically give larger values than the sum of discrete measurements at individual vents, suggesting that these measurements include some part of the diffuse flow. Water column measurements typically range between 10^8 and 10^9 Watts [see *Baker*, 2007; *Lowell et al.*, 2008]. Observed heat output and vent temperature data are summarized in Table 1.1 (see corresponding reference for details).

Table 1.1 Vent flow characteristics for some seafloor hydrothermal systems

Reference	Location	Vent temperature (°C)	Vent Heat Flux (MW)	Integrated Heat Flux H_t (GW)
Rona and Trivett [1992]	Axial Volcano (JdFR)	108 - 326	2.4 - 6.4	
Rosenberg et al. [1988]	Endeavour (JdFR)	up to 400		1 - 5
Schultz et al. [1992]	Endeavour (JdFR)	7 - 13	53.5 – 62.9	
Veirs et al. [2006]	Endeavour (JdFR)		8 - 42	
Ginster et al. [1994]	Endeavour (JdFR)	296 - 374	3.6 - 87.3	0.29 - 0.44
Baker and Massoth [1986]	South Cleft (JdFR)			0.29 - 0.87
Baker and Massoth [1987]	Endeavour (JdFR)			0.6 - 2.8
Baker et al. [1993]	North Cleft (JdFR)	104 - 324	161 - 319	0.48 - 0.96
Baker [1994]	North Cleft (JdFR)			0.38 - 0.94
Gendron et al. [1994]	North Cleft (JdFR)			1.4 – 4
Stein and Fisher [*2001*]	Middle Valley (JdFR)	180 - 276	0.13	
Lonsdale and Becker [1985]	Southern Trough (GB)	270 - 314	86 - 201	
Ramondenc et al. [2006]	9°50′ N (EPR)	345 - 388	40	
McConachy et al. [1986]	11°N (EPR)	347	3.0 - 25	
Macdonald et al. [1980]	21°N (EPR)	344 - 356	0.2 - 0.3	
Converse et al. [1984]	21°N (EPR)	275 - 350	140 - 300	
Rudnicki and Elderfield [1992]	TAG (MAR)	360 - 364		0.5 - 0.9
Rona et al. [1993]	TAG (MAR)	365	200 - 250	
Rudnicki and German [2002]	Kairei (CIR)	360		0.07 - 0.12

Notes: In this table, JdFR stands for Juan de Fuca Ridge, GB for Guaymas Basin, EPR for East Pacific Rise, MAR for Mid-Atlantic Ridge and CIR for Central Indian Ridge. Modified from [*Lowell et al.*, 2008].

1.1.2 Link between hydrothermal activity and sub-axial magma chamber

The interplay between the sub-axial magma chamber (AMC) and hydrothermal system is shown schematically in Figure 1.3. At nearly all sites of observed high-temperature venting, seismic reflection data shows the presence of shallow subsurface magma bodies beneath the active hydrothermal systems regardless of the spreading rate. It is now generally accepted that the AMC represents the heat source that drives the hydrothermal circulation [e.g., *Kelley et al.*, 2002; *Maclennan*, 2008; *Lowell* et al., 2008, 2010]. Even at the TAG hydrothermal systems at the slow spreading Mid-Atlantic Ridge where no shallow or mid-crustal magma has been detected, the presence of deeper magmatic sources has not been ruled out [*Canales et al.*, 2007]. Hydrothermal activity also appears to be associated with the recent volcanism at the ultra-slow spreading Gakkel Ridge in Arctic Ocean [*Michael et al.*, 2003; *Baker et al.*, 2004] and the Southwest Indian Ridge [*Sauter et al.*, 2002; *Dick et al.*, 2003]. Observations from the 21°N sites on EPR have indicated the considerable stability of hydrothermal venting in temperature and composition lasting for more than two decades [*Campbell et al.*, 1988; *Von Damm et al.*, 2002]. The TAG hydrothermal field at the Mid-Atlantic Ridge has a near constant fluid composition from 1986 until 2003 [*German and Lin*, 2004]. The steady state character of seafloor hydrothermal systems has been linked to magma replenishment at rates similar to those observed at basaltic volcanoes [*Lowell and Germanovich*, 1994; *Humphris and Cann*, 2000]. However, such constancy can be

interrupted. Both the temperature and composition of fluids existing at vent sites can change significantly with time, apparently in direct response to volcanic activity and/or dike emplacement beneath the seafloor [*Butterfield and Massoth*, 1994; *Von Damm et al.*, 1995, 1997; *Lilley et al.*; 2003].

Episodic magma supply has been recognized to be an important feature in behavior of seafloor hydrothermal activity. The seismic reflection suggests that the episodicity is important event along about 60% of the surveyed East Pacific Rise [*Detrick et al.*, 1987]. Evidence of large-scale episodic venting of hydrothermal fluids was discovered at Juan de Fuca Ridge in 1986 [*Baker et al.*, 1989]. A detailed study of magnetization and morphology coupled with seismic reflection has shown that the magmatic processes on the Valu Fa Ridge are episodic [*Collier and Sinha*, 1992]. In addition, the evidence for episodic replenishment of the AMC at relatively high frequency includes eruption scenarios and non-eruptive diking events. For instance, the eruptions occurred at the fast-spreading East Pacific Rise near 9°50′N in 1991 and 1992 [*Haymon et al.*, 1993]. Time series studies of vent fluid composition at this site in direct response to this volcanic episode show the continuously evolving chemical compositions over more than a decade [*Von Damm et al.*, 1995, 1997, 2004]. Temporal changes in hydrothermal activity related to the more recent eruptions in 2005/2006 [*Rubin et al.*, 2006; *Soule et al.,* 2007] are still being investigated. There is evidence of non-eruptive diking activity that may cause perturbations to the hydrothermal systems [*Ramondenc et al*., 2008; *Germanovich et al.*, 2010]. A non-eruptive diking event that affected vent

temperature and chemistry has also been observed at Main Endeavour Field (MEF) on Juan de Fuca ridge (JDFR) [*Johnson et al.*, 2000, *Lilley et al.*, 2003].

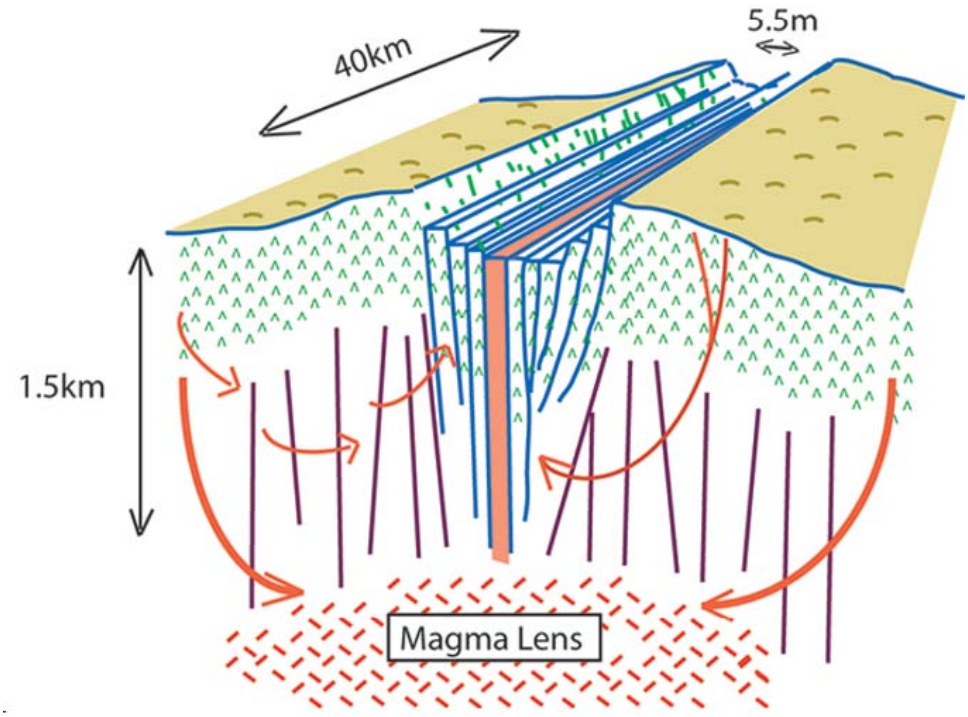

Figure 1.3 Illustration showing possible routes of hydrothermal circulation (arrows) through a section of fast- or medium-spreading ridge crest above an axial magma lens. The heat releases from crystallization and cooling melt lens to the overlaying hydrothermal systems to generate hydrothermal vents [after *German and Lin*, 2004].

1.2 Models of Magma-Hydrothermal Systems

1.2.1 Hydrothermal circulation system

Quantitative understanding of the interconnected heat transfer and biogeochemical processes at oceanic spreading centers requires the development of mathematical and numerical models. Such models can address the physical processes of fluid circulation and heat transfer or geochemical processes in both temporal and spatial scale, and can be used to explain the observational data and infer subsurface conditions as well as to guide further experimental and field studies. In general, hydrothermal convection models can be classified into three categories: cellular convection models, single-pass models, and downward cracking models. Reviews of various models of hydrothermal systems can be found in [*Lowell*, 1991a; *Lowell et al.*, 1995; *Lowell and Germanovic*h, 2004].

Cellular convection models were initially developed by *Horton and Rogers* [1945] and *Lapwood* [1948] served as a starting point for studying geothermal convection problems. They investigate the convection in a saturated homogeneous porous material layer which is heated from below. The upper and lower boundaries are generally impermeable and isothermal. In these models, Rayleigh number *Ra*, a dimensionless parameter that determines the character of convective patterns, must be greater than the critical Rayleigh number Ra_c for convection to occur [*Lapwood*, 1948]. Early work on cellular convection models attempted to explain the heat flow anomaly patterns observed

in young sediment lithosphere [*Williams et al.*, 1974; *Ribando et al.*, 1976; *Green et al.*, 1981; *Fehn et al.*, 1983]. Cellular convection models have been applied to off-axis circulation [*Lowell*, 1980; *Fisher et al.*, 1990; *Fisher and Becker*, 1995] and hydrothermal circulation above a sub-axial magma body [*Brikowski and Norton*, 1989; *Wilcock*, 1998; *Rabinowicz et al.*, 1999]. *Schoofs and Hansen* [2000] investigated the depletion of the brine layer at the base of a vigorously convecting system. *Jupp and Schultz* [2000] argued that the thermodynamic properties of water may control black smoke at the temperature of 400 °C.

Single pass models examine the general behavior of the hydrothermal system without considering the details of the temperature and velocity distribution. Single-pass models describe the deep circulation system in which fluids circulate downward into the ocean crust, flow horizontally near the top of the magma chamber at the base of the sheeted dikes, and ascend back to the surface. Focused high-temperature flow is thought to occur in the main single-pass limb; diffuse flow may occur as a result of the mixing of the deep circulation with the shallower circulation in the pillow basalts. Hydrothermal fluid is assumed to pass through the system only once through a recharge zone, a discharge zone, along with a reaction zone near the base of the hydrothermal system. A cartoon description of the model is illustrated in Figure 1.4. The single-pass models can be viewed as a special case of the cellular convection models, in which an extremely heterogeneous distribution of permeability restricts the flow paths to pipe-like zones. Based on the scale analysis arguments in [*Lowell*, 1991; *Lowell and Germanovich*, 2004],

the single-pass model explains high-heat output venting more easily than the high Rayleigh number convection model, for the case of an imposed heat flux lower boundary condition. Single-pass models have been used in hydrothermal modeling since the earliest works tried to explain the low conductive heat flow values measured on young crust and in terms of hydrothermal heat loss [*Bodvarsson and Lowell*, 1972; *Lowell*, 1975]. Single-pass models have been applied in many seafloor hydrothermal problems to describe the general behavior of hydrothermal systems, such as the formation of sulfide ore deposits at seafloor spreading centers [*Lowell and Rona*, 1985], the temporal evolution of heat transfer from solidifying magma to black smokers [*Lowell and Germanovich*, 1994], the formation of catastrophic event plumes associated with dike injections [*Lowell and Germanovich*, 1995], and the thermal stresses effect on the evolution of permeability [*Lowell et al.*, 1993; *Germanovich et al.*, 2001]. *Pascoe and Cann* [1995], *Lowell et al*., [2003], and *Ramondence et al*., [2008] developed a two-limb single-pass model to investigate the mixing between deep seated hydrothermal circulation and fluid circulation in the extrusive layer of the oceanic crust.

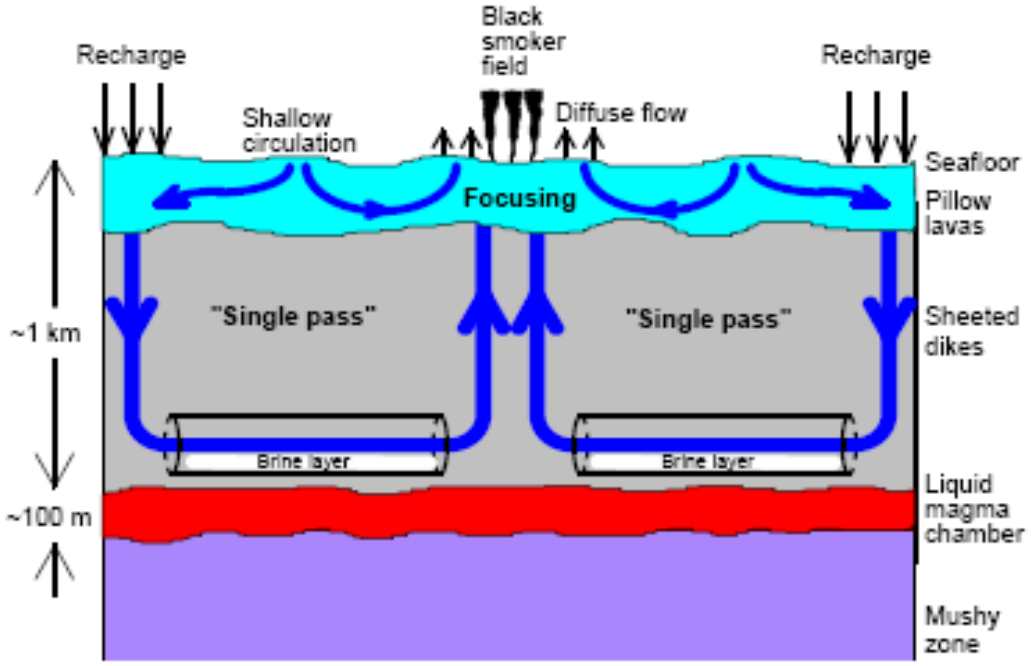

Figure 1.4 Cartoon of a single-pass hydrothermal circulation model at an ocean ridge crest at local ridge crest circulation scale [*Germanovich et al.*, 2000].

Downward cracking models for hydrothermal circulation were initially proposed by *Lister* [1974]. It is assumed that tensile thermal stresses, provided by temperature differences, could cause fracture propagation, so that hydrothermal circulation would migrate downward and extract heat from the cracked hot rocks. *Lister* [1983] argues that, to sustain a high output hydrothermal system, one not only needs support from an active magma chamber but also requires an active cracking front. *Lowell and Germanovich* [1994] develop this idea and suggested that hydrothermal systems migrate downward into an impermeable frozen layer, in conjunction with dike emplacement into the crust. Their model suggests that thermal stresses associated with dike injection may be preferable to

Lister's original mechanism. In consequence, as magma crystallizes the hydrothermal system migrates downwards and high heat flux is maintained.

The downward cracking concept is still prevalent in the literature. Field studies suggest that the reaction zone with the highest temperature may be characterized by a downward propagating set of fluid-filled fractures [*Kelley and Delaney*, 1987; *Kelley et al.*, 1993]. At the cracking front, hydrothermal fluids migrate downwards and obtain their final compositions before rising buoyantly back to the seafloor [*Alt*, 1995; *Seyfried and Ding*, 1995; *Alt and Teagel*, 2000]. *Wilcock and Delaney* [1996] argue that a downward penetrating cracking front supports high hydrothermal fluxes when the magma supply to the crust decreases, leading to the formation of large sulfide deposits at intermediate spreading rate ridges, such as the Endeavour Segment of the Juan de Fuca Ridge. Recent seismic reflection data [*Van Ark et al.*, 2007] suggests that an AMC likely provides the heat for hydrothermal circulation at the Main Endeavour Fiedl, however.

Even though Lister's idea of a downward propagating cracking front has been accepted at least conceptually [e.g., *Wilcock and Delaney*, 1996] as a mechanism of hydrothermal heat transfer, the evidence from [*Manning et al.*, 2000] is not consistent with the original Lister model. For example, *Manning et al.*, [2000] argue that: (a) the first cracks to form are microcracks rather than the macro-scale cracks envisioned by Lister; (b) the crack propagation rate is orders of magnitude less than suggested by *Lister* [1974]; and (c) the cracking temperature predicted in Lister model decreases with depth, which is counter to observations from Oman ophiolite and the East Pacific Rise.

Hydrothermal circulation is mainly driven by the underlying magma chambers, since magma chamber provides the heat source to sustain hydrothermal circulation. Hydrothermal circulation and heat transfer models also show the important role of magmatic heat sources in the hydrothermal systems [*Cann and Strens*, 1982; *Lowell and Rona*, 1985]. [*Lowell and Burnell*, 1991] and [*Lowell and Germanovich* 1994] considered heat transfer from an axial crystallizing magma body using a single-pass hydrothermal system model (see Figure 1.3). Scaling analysis of the heat loss from the magma that decreases with time as $t^{-1/2}$ suggests an analogous decline of the hydrothermal heat output and vents temperature. Hydrothermal systems driven by sub-axial magma chambers often exhibit relatively stable vent temperatures and vent fluid chemistry on decadal time scales [*Campbell et al.*, 1988; *Von Damm et al.*, 2002]. To maintain the observed black smoker temperatures and heat output in a steady state for decades requires a thin conductive boundary layer between the magma and hydrothermal circulation [*Lowell and Germanovich*, 1994, 2004; *Fontaine and Wilcock*, 2006], a highly permeable discharge zone [*Lowell and Germanovich*, 1994, 2004], and magma replenishment [*Lowell and Germanovich*, 1994, 2004]. In addition, the characteristics of hydrothermal systems are closely related to magmatic activity. Both the temperature and composition of hydrothermal fluids can change significantly with time in direct response to magmatic and tectonic vents. For example, hydrothermal responses to earthquake eruptions and dike emplacement are studied by [*Lilley et al.*, 2003; *Ramondenc et al.*, 2008]. However, to better understand the behavior of magma-hydrothermal systems at mid-ocean ridges,

these models must consider the coupling between hydrothermal circulation and magma convection, including possible replenishment.

1.2.2 Magma chamber convection

The dynamics of the cooling, crystallizing magma chambers have been a subject of scientific interest for decades. The study of magma chamber dynamics focuses on two different mechanisms: (i) the thermally well-mixed magma body is cooled by conduction through the wall rocks [*Cathles*, 1977; *Norton and Taylor*, 1979]; and (ii) cooling of the magma chamber is dominated by magma convection [*Spera*, 1980; *Spera et al.*, 1982; *Lister*, 1983; *Hupert and Sparks*, 1988]. Different opinions exist in the literature regarding the role of convection. For examples, *Brandeis and Jaupart* [1986] and *Marsh* [1989] have argued that convection is weak or absent. Theoretical and experimental studies indicate that magma should convect vigorously [*Huppert and Sparks*, 1988; *Martin and Nokes*, 1988, *Worster et al.*, 1990, *Kerr*, 1994]. Although the role of convection on nucleation, growth, and the redistribution of crystals in magma chambers is under debate, the dominant role of the convection in magma cooling and crystallization is widely accepted. Heat transfer by convection is more efficient, by one to two orders of magnitude, than by conduction in cooling magma bodies.

As magmatic systems cool below their liquidus temperatures, generally denser crystals form at the cooling boundaries. There has been much debate concerning the mechanism of fractional crystallization in magma chambers. Crystals may nucleate at the

roof, near the floor or within the interior of the magma body where they can remain in suspension or settle down afterwards [*Martin and Nokes*, 1989; *Sparks et al.*, 1984]. *Huppert and Sparks* [1984] assumed that crystals formed in the interior of the magma chamber were small and remained suspended as a result of vigorous convective motions. This assumption is counter to traditional models in which crystals settle and accumulate on the floor [*Martin*, 1990; *Martin and Nokes*, 1989; *Worster et al*., 1990]. The crystals settling rate depends upon the rate of cooling, the density of the particles, and the viscosity of the magma. Experimental studies indicate that convection delays but does not stop crystal settling. [*Jarvis and Woods*, 1994] argued that crystals grow in the interior of a turbulently convecting fluid and subsequently settle gravitationally to the bottom boundary. They also suggested that the residence time of crystals within the convecting bulk is relatively short compared to the overall cooling time of the fluid. Crystal settling is believed to be an efficient differentiation mechanism, even though the convective velocities are much larger than settling velocities using Stokes' law [*Martin and Nokes*, 1989].

Convection in magma chambers results from two different driving forces: thermal convection and compositional convection. Thermal convection results from the cooling of the magma as heat is transported to the surrounding rocks [*Brandeis and Jaupart*, 1986]. Compositional convection is driven by the density and chemical composition differences between the crystals and liquids that stem from the injection of new magma into a chamber, partial melting, or fractional crystallization [*Sparks et al.*, 1984]. Double

diffusive convection occurs when gradients in both temperature and composition exist in the crystallizing magma [*Huppert and Sparks*, 1984].

1.2.3 Linked Models of Magma and Hydrothermal Convection

Studies of the temporal evolution in hydrothermal processes indicate the existence of a close coupling between magma supply and hydrothermal processes on individual ridge segments [*Haymon et al*. 1991, 1993, 1996; *Embley et al*. 1995; *Von Damm et al*. 1995; *Haymon and White,* 2004; *Maclennan*, 2008]. The first models linking magmatic heat transfer to the overlying hydrothermal system assumed that crystallization occurs at the roof of the magma [e.g., *Lowell and Rona*, 1985; *Lowell and Burnell*, 1991]. In this case, the thermal boundary layer rapidly thickens due to the accumulation of crystals on the roof of the magma chamber, which results in heat transfer from the magma decreasing rapidly with time. Consequently, the temperature and heat output of the hydrothermal systems decay rapidly too. However, the details of the connection between the ridge axis hydrothermal flux and subsurface magma chamber processes have not been studied comprehensively.

1.3 Motivation

Most models of hydrothermal circulation are coupled to magmatic processes only loosely. In the most common situation, the temperature is fixed at the bottom of the magma chamber. This condition assumes that magma serves as an infinite reservoir of heat, and heat transport is controlled by the vigor of hydrothermal systems, which is

characterized by the Rayleigh number *Ra* [e.g., *Bejan*, 1995; *Lowell and Germanovich*, 2004]. On the other hand, if a constant heat flux is assumed at the base of the hydrothermal system, then hydrothermal heat output is controlled by the rate at which the heat is conducted from the magma body [e.g., *Lowell and Germanovich*, 1994, 2004; *Germanovich et al.*, 2000, 2001]. Neither of these boundary conditions is realistic because heat transfer from a convecting magma body near its liquidus will cause magma to cool and crystallize [e.g., *Cann and Strens*, 1982; *Lowell and Rona*, 1985].

The hydrothermal models of *Lowell and Burnell* [1991] and *Lowell and Germanovich* 1994] considered heat transfer from a crystallizing magma body. These assumed that crystallization occurred at the roof of the magma chamber. As the frozen layer grew downward, heat loss from the magma decreased with time as $t^{-1/2}$ resulting in an analogous decline in hydrothermal heat output and vents temperature. Although hydrothermal heat loss following diking events such as occurred at Co-Axial in 1993 or at Axial Volcano in 1998 may decay faster than $t^{-1/2}$ [*Baker et al.*, 2004*b*], hydrothermal systems driven by sub-axial magma chambers often exhibit relatively stable vent temperatures and vent fluid chemistry on decadal time scales [*Campbell et al.*, 1988; *Von Damm et al.*, 2002]. Although time series data on hydrothermal heat output are limited, heat output is generally assumed to be stable as well. The data suggest that ridge crest hydrothermal systems typically transport between 10^8 and 10^9 Watts of heat [*Ramondenc et al.*, 2006; *Baker*, 2007].

Lowell and Germanovich [1994] and *Humphris and Cann* [2000] suggested that magma inputs at rates similar to those observed on terrestrial volcanoes could help maintain steady hydrothermal heat output. These results, however, were not linked to quantitative models of magma convection and crystallization.

The observations of quasi-steady state hydrothermal heat output and vent temperature, which are not adequately predicted by current magma-hydrothermal models, argue for models that investigate different ways to link magmatic processes and hydrothermal circulation. Therefore, my research on developing models of magma convection that may be more appropriate representations of the magmatic-hydrothermal coupling is well motivated.

1.4 Objectives

The objective of this dissertation is to provide a suite of effective models to characterize the coupling between hydrothermal systems and magma chamber. In the literature, a large number of mathematical models have been developed to study the seafloor hydrothermal systems. However, relatively few of these models have addressed the link between high-temperature hydrothermal systems and magma supply or provided a basis for understanding heat transport from a convecting magma chamber to the overlaying hydrothermal system. I seek to address the linkages between hydrothermal heat output and heat transfer from a cooling, crystallizing, replenished magma chamber beneath oceanic spreading centers. Specifically, I consider the heat transfer from a

vigorously convecting basaltic magma chamber of certain thickness to the overlying hydrothermal system. Also, I consider not only the common case in which crystals stay suspended in the magma, but also the end-member case in which crystals rapidly settle or crystallization occurs at the base of the magma chamber. In addition, I investigate the role of magma replenishment in maintaining quasi steady heat output on decadal timescales.

Though many of the pioneering studies entailed high-temperature flow, they generally assume a single-component fluid. In reality, the magmas are multi-component fluids. Although the results on one-component systems provide insights on the interaction between the magma and hydrothermal systems, the convection mechanism can not apply to multi-component systems since they do not consider the dependence among multiple components. Thus, I address the modeling of the hydrothermal system driven by multiple-component magmas. Specifically, I consider the Di-An system and focus on the Di rich side, since it represents a chemical analogue to the basaltic melts at mid-ocean ridges. A phase diagram is employed to evaluate the formation and crystallization processes, and the dynamic features of the system are characterized with respect to the time-varying Di concentration.

Although most hydrothermal systems at oceanic spreading centers are driven by basaltic magma, high-silica magmas have been discovered at several different locations. High-silica magmas, typically andesites and dacites, have higher viscosity. Different viscosities between basaltic and high-silica magmas result in different thermal

characteristics and evolution of the overlying hydrothermal systems. However, studies of hydrothermal systems driven by high-silica melts are less detailed and not as thoroughly understood as their mid-ocean ridge basaltic counterparts. I aim to better characterize hydrothermal systems driven by high-silica melts and focus on both andesites and dacites magma. Specifically, I examine the dependence of viscosity on different factors such as temperature, composition and water content, because melt viscosity exerts a strong control on the heat flux from the convecting magma.

In summary, this dissertation addresses the following topics:

- Modeling and parametric studies of heat output from a convecting, crystallizing, replenished basalt magma chamber beneath an oceanic spreading center
- Effect of multi-component chemical composition on the evolution and heat transfer from a cooling, crystallizing, replenished magma chamber
- Models of heat transfer from a convecting, crystallizing, replenished high silica andesitic dacitic magma chambers at an oceanic spreading center

1.5 Outline

The rest of the dissertation is organized as follows:

Chapter 2 introduces the magmatic-hydrothermal models at oceanic spreading centers including a turbulent convecting, crystallizing, and replenished magma body, and briefly reviews some of the previous modeling work. Then, I present a mathematical framework to perform numerical analysis of the magma chamber and overlying

hydrothermal system. I consider two scenarios of magma convection and crystallization models. One assumes the convective motions in the magma chamber are sufficiently vigorous to keep crystals in suspension and well mixed within the interior of the magma. The other assumption is that crystallization occurs at the boundary layer of a magma chamber and crystals settle and accumulate on the floor. In addition, I discuss magma replenishment as a mechanism to maintain steady state heat flux from the magma system for decades.

Chapter 3 considers hydrothermal systems at oceanic spreading centers with heat transfer from a vigorously convecting, crystallizing, and replenished basaltic magmatic sill beneath an ocean ridge axis. Based on the fundamental theory for magma convection and hydrothermal circulation presented in Chapter 2, I develop the numerical models for the dynamic heat flux and temperature for both the magma chamber and overlying hydrothermal systems.

Chapter 4 focuses on the effects of the initial magma chamber size and episodic magma replenishment on heat flux and responses of hydrothermal vents. In addition, I discuss the implication of the model in terms of the evolution of the magma chamber and the linkages between magmatic heat output and hydrothermal venting for EPR.

Chapter 5 extends the work to two-component melts and investigates the effect of magma chemical composition on magmatic heat transfer and the dynamic characteristics of overlying hydrothermal system. I focus on the Di-An system, because it is a reasonable yet simple analog for a basaltic magma chamber. Since the heat transfer behavior of

magmatic mixtures is determined by the presence of different chemical components, the system characteristics, such as heat flux, crystal content, etc., are examined through a dynamic model of the Di concentration. The goal is also to link magma chamber dynamics to the composition of lavas that may be erupted.

Chapter 6 examines the magmatic heat flux and behavior of hydrothermal temperature in the presence of high-silica melts, focusing on both andesite and dacite magmas. Due to the significant difference of viscosity between different magmas, the thermal characteristics and evolution of the overlying hydrothermal systems are different. I investigate the dependence of viscosity on different factors, including chemical composition, temperature, pressure, volatile content, and crystal content, and propose new viscosity models for andesites and dacites. Then, adopting the proposed framework in Chapter 2, I describe the heat flux of hydrothermal system based on the proposed viscosity model.

Finally, Chapter 7 summarizes this dissertation and suggests topics for future research. For the reader's convenience, I have attempted to keep every chapter as self contained as possible.

1.6 References

Alt J.C. (1995). Subseafloor processes in mid-ocean ridge hydrothermal systems. In Humphris, S.E., Zierenberg, R., Mullineaux, L., and Thomson, R. (Eds.), *Seafloor Hydrothermal Systems: Physical, Chemical, Biological and Geological Interactions within Hydrothermal Systems*. *Geophys. Monogr.*, *91*:85–114.

Alt J.C. and Teagle D.A.H. (2000). Hydrothermal alteration and fluid fluxes in ophiolites and oceanic crust. In *Ophiolites and Oceanic Crust: New Insights from Field Studies and the Ocean Drilling Program*, ed. Y. Dilek, E. Moores, D. Elthos, A. Nicoals, pp. 273–82. Geol. Soc. Am. Spec. Pap. 349. Boulder, CO: Geol. Soc. Am. 552 pp.

Anderson, R.N and J.N. Skilbeck (1981). Oceanic heat flow, in *The Sea*, *7*, *The Oceanic Lithoshphere*, ed. by C. Emiliani, 489-523, Wiley-Interscience, New York.

Babcock, J.M., A.J. Harding, G.M. Kent, and J.A. Orcutt (1998). An examination of along-axis variation of magma chamber width and crustal structure on the East Pacific Rise between 13°30'N and 12°20'N, *Journal of Geophysical Research*, 103(B12), 30451-30467

Baker, E.T. and G.J. Massoth (1986). Hydrothermal plume measurements: A regional perspective, *Science*, *234*, 980-982.

Baker, E.T. and G.J. Massoth (1987). Characteristics of hydrothermal plumes from two vent fields on the Juan de Fuca Ridge, northeast Pacific Ocean, *Earth Planet. Sci. Lett., 85*, 59–73

Baker, E.T., G.J. Massoth, S.L. Walker, and R.W. Embley (1993). A method for quantitatively estimating diffuse and discrete hydrothermal discharge, *Earth Planet. Sci. Lett.*, *118*, 235-249.

Baker, E.T. (1994). A six-year time series of hydrothermal plumes over the Cleft segment of the Juan de Fuca Ridge, *J. Geophys. Res.*, *99*, 4889-4904.

Baker, E.T., R.A. Feely, M.J. Mottl, F.J. Sansone, C.G. Wheat, J.A. Resing, and J.E. Lupton (1994). Hydrothermal plumes along the East Pacific Rise, 8°40 to 11°50N: Plume distribution and relationship to the apparent magmatic budget, *Earth Planet. Sci. Lett., 128*, 1–17

Baker, E.T., C.R. German, and H. Elderfield (1995). Hydrothermal plumes over spreading center axes: Global distributions and geological inferences. In *Seafloor*

Hydrothermal Systems: *Physical, Chemical, Biological and Geological Interactions*, *Geophys. Monogr.*, *91*, ed. by S.E. Humphris, R.A. Zierenberg, L.S. Mullineaux, and R.E. Thomson, pp. 47-71, AGU, Washington, D.C.

Baker, E.T. (1996). Geological indexes of hydrothermal venting, *J. Geophys. Res.*, vol. 101, no. B6, pp.13,741-13,753

Baker, E.T. and C.R. German (2004). On the global distribution of hydrothermal vent fields, in *Mid-Ocean Ridges*: *Hydrothermal Interactions Between the Lithosphere and Oceans*, *Geophys. Monogr., 148*, ed. by C.R. German, J. Lin and L.M. Parson, pp. 245-266, Amer. Geophys. Union, Washington, D.C.

Baker, E.T., H.N. Edmonds, P.J. Michael, W. Bach. H.J.B. Dick, J.E. Snow, S.L. Walker, N.R. Banerjee, and C.H. Langmuir (2004). Hydrothermal venting in magma deserts: The ultraslow-spreading Gakkel and South West Indian Ridges, *Geochem., Geophys., Geosyst., 5*(8), Q08002, doi:10.1029/2004GC000712

Barriga, F.J.A.S., Y. Fouquet, A. Almeida, M.J. Biscoito, J.L. Charlou, R.L.P. Costa, A. Dias, A.M.S.F. Marques, J.M.A. Miranda, K. Olu, F. Porteiro and M.G.P.S. Queiroz (1998). Discovery of the Saldanha Hydrothermal Field on the FAMOUS segment of the MAR (36° 30'N). *EOS, Trans. Am. Geophys. U.*, 79(45), F67 (abstr.).

Becker, K., R. Von Herzen, J. Kirklin, R. Evans, D. Kadko, M. Kinoshita, O. Matsubayashi, R. Mills, A. Schultz, and P. Rona (1996). Conductive heat flow at the TAG active hydrothermal mound: Results from 1993-1995 submersible surveys, *Geophys., Res. Lett.*, *23*, 3463-3466.

Bejan, A. (1995). *Convection Heat Transfer*, 2nd ed., p. 623, John Wiley, Hoboken, N. J.

Bemis, K.G., R.P. Von Herzen, and M.J. Mottl (1993). Geothermal heat flux from hydrothermal plumes on the Juan de Fuca Ridge, *J. Geophys. Res. 98*. 6351–6365.

Bodvarsson, G. (1950). Geophysical methods in prospecting for hot water in Iceland (translated from Danish), *Timarit Verkfraed Islands*., *35*, 49-59.

Bodvarsson, G. (1961). Physical characteristics of natural heat resources in Iceland, Proc. Conf. *New Sources Energy*, *2*, 82-89

Bodvarsson, G. and R.P. Lowell (1972). Ocean-floor heat flow and the circulation of interstitial waters, *J. Geophys. Res.*, *77*, 4472-4475.

Brandeis, G. and C. Jaupart (1986). On the interaction between convection and crystallization in cooling magma chambers. *Earth Planet. Sci. Lett.* 77: 345-61

Brikowski, T. and D. Norton (1989). Influence of magma chamber geometry on hydrothermal activity at mid-ocean ridges, *Earth Planet. Sci. Lett.*, *93*, 241-155.

Burnett, M.S., D.W. Caress, and J.A. Orcutt (1989). Tomographic image of the magma chamber at 12°50' on the East Pacific Rise, *Nature*, 339, 206-208.

Butterfield, D. A., and G. J. Massoth (1994). Geochemistry of North Cleft segment vent fluids: temporal changes in chlorinity and their possible relation to recent volcanism, *J. Geophys. Res., 99,* 4951–4968.

Calvert, A.J. (1995). Seismic evidence for a magma chamber beneath the slow-spreading Mid-Atlantic Ridge, *Nature*, *377*, 410-414.

Campbell, A.C., T.S. Bowers, C.I. Measures, K.K. Falkner, M. Khadem, and J.M. Edmond (1988). A time series of vent fluid compositions from 21°N, East Pacific Rise (1979,1981,1985), and the Guaymas Basin, Gulf of California (1982,1985), *J. Geophys. Res.*, *93*, 4537-4549.

Canales, J.P, R.S. Detrick, S.M. Carbotte, G.M. Kent, J.B. Diebold, A. Harding, J. Babcock, M.R. Nedimovic, and E. Van Ark (2005). Upper crustal structure and axial topography at intermediate spreading ridges: Seismic constraints from the southern Juan de Fuca Ridge, *J. Geophys., Res.*, *110*, B12104.

Canales, J. P., S. C. Singh, R. S. Detrick, S. M. Carbotte, A. Harding, G. M. Kent, J. B. Diebold, J. Babcock, and M. R. Nedimovic (2006). Seismic evidence for variations in axial magma chamber properties along the southern Juan de Fuca Ridge, *Earth. Planet. Sci. Lett.*, *246*, 353-366.

Canales, J.P., R.A. Sohn, B.J. deMartin (2007). Crustal structure of the Trans-Atlantic Geotraverse (TAG) segment (Mid-Atlantic Ridge, 26 degrees 10'N); implications for the nature of hydrothermal circulation and detachment faulting at slow spreading ridges *Geochemistry, Geophysics, Geosystems*, vol. 8, no. 8, 18 pp.

Cann, J.R. and M.R. Strens, (1982). Black smokers fuelled by freezing magma, *Nature*, *298*, 147-149.

Cathles, L.M. (1977). An analysis of the cooling of intrusives by groundwater convection which includes boiling. *Econ. Geol.* 72: 804-26

Charlou, J. L., J. P. Donval, Y. Fouquet, P. Jean-Baptiste, and N.Holm (2002). Geochemistry of high H2 and CH4 vent fluids issuing from ultramafic rocks at the Rainbow hydrothermal field (36°14'N, MAR), *Chemical Geology, 191,* 345–359.

Collier, J. S., and M. C. Sinha (1990). Seismic images of a magma chamber beneath the Lau Basin back-arc spreading centre, *Nature*, *346*, 646-648.

Collier, J. S. and M. C. Sinha, (1992). Seismic mapping of a magma chamber beneath the Valu Fa Ridge, Lau Basin, *J. Geophys. Res.*, vol. *97*, no. B10, pp.14,031-14,053

Converse, D. R., H. D. Holland, and J. M. Edmond (1984). Flow rates in the axial hot springs of the East Pacific Rise (21°N): implications for the heat budget and the formation of massive sulfide deposits, *Earth Planet. Sci. Lett.*, *69*, 159-175.

Corliss, J.B., J. Dymond, L.I. Gordon, J.M. Edmond, R.P.Von Herzen, R.D. Ballard, K. Green, D. Williams, A. Bainbridge, K. Crane, and T.H. Van Andel. (1979). Submarine thermal springs on the Galapagos Rift, *Science*, *203*, 1073-1083.

Day, A.J., Peirce, C. and Sinha, M.C. (2001) Three-dimensional crustal structure and magma chamber geometry at the intermediate-spreading, back-arc Valu Fa Ridge, Lau Basin - results of a wide-angle seismic tomographic inversion. *Geophysical Journal International*, 146, (1). 31-52.

de Ronde, C. E. J., G. J. Massoth, E. T. Baker, and J. E. Lupton (2003). Submarine hydrothermal venting related to volcanic arcs, Giggenbach Memorial Volume, in *Volcanic, geothermal and ore-forming fluids: Rulers and witnesses of processes within the Earth*, edited by S. F. Simmons and I. Graham, *Soc. of Econ. Geolog., 10*, 91–110

Detrick, R. S., P. Buhl, E. Vera, J. Mutter, J. Orcutt, J. Madsen, and T. Brocher (1987). Multi-channel seismic imaging of a crustal magma chamber along the East Pacific Rise, *Nature*, *326*, 35-41.

Detrick, R.S., A.J. Harding, G.M. Kent, J.A. Orcutt, J.C. Mutter, and P. Buhl (1993). Seismic structure of the southern East Pacific Rise, *Science*, *259*, 499-503.

Dick, H. J. B., J. Lin, and H. Schouten (2003). An ultraslow-spreading class of ocean ridge, *Nature*, *426,* 405–412.

Edmonds, H. N., C. R. German, D. R. H. Green, Y. Huh, T. Gamo, and J. M. Edmond (1996). Continuation of the hydrothermal fluid chemistry time series at TAG and the effects of ODP drilling, *Geophys. Res. Lett*., *23,* 3487–3489.

Edmonds, H. N., P. J. Michael, E. T. Baker, D. P. Connelly, J. E. Snow, C. H. Langmuir, H. J. B. Dick, R. Mühe, C. R. German, and D. W. Graham (2003). Discovery of abundant hydrothermal venting on the ultraslow-spreading Gakkel Ridge, Arctic Ocean, *Nature, 421*, 252–256,.

Embley, R.W, W.W. Chadwick, Jr., I.R. Jonasson, D.A. Butterfield, and E.T. Baker (1995). Initial results of the rapid response to the 1993 CoAxial event: relationships between hydrothermal and volcanic process, *Geophys. Res. Lett*., *22*, 143-146.

Embley, R.W., W.W. Chadwick Jr., D. Clague, and D. Stakes. (1999). 1998 eruption at Axial Volcano: Multibeam anomalies and seafloor observations. *Geophysical Research Letters 26*:3,425– 3,428.

Fehn, U., K.E. Green, R.P. Von Herzen, and L.M. Cathles (1983). Numerical models for the hydrothermal field at the Galapagos spreading center, *J. Geophys. Res.*, *88*, 1033-1048.

Fisher, A.T., K. Becker, T.N. Narasimhan, M.G. Langseth and M.J. Mottl (1990). Passive, off-axis convection through the southern flank of the Costa Rica rift, *J. Geophys. Res.*, *95*, 9343-9370.

Fisher, A.T. and K. Becker (1995). Correlation between seafloor and basement relief: Observational constraints and numerical examples and implications for upper crustal permeability, *J. Geophys. Res.*, *100*, 12641-12657.

Fontaine, F. J. and W. S. D. Wilcock (2006). Dynamics and storage of brine in mid-ocean ridge hydrothermal systems, *J. Geophys. Res.*, 111, B06102, doi:10.1029/2005JB003866.

Fouquet, Y., U. Von Stackelberg, J.L. Charlou, J.P. Donval, J. Erzinger, J.P. Foucher, P. Herzig, R.K. Muehe, S. Soakai, M. Wiedicke, and H. Whitechurch (1991). Hydrothermal activity and metallogenesis in the Lau back-arc basin, *Nature*, *349*, 778-781.

Fox, C.G., W.E. Radford, R.P. Dziak, T.K. Lau, H. Matsumoto, and A.E. Schreiner (1995). Acoustic detection of a seafloor spreading episode on the Juan de Fuca Ridge using military hydrophone arrays, *Geophys. Res. Letts.*, *22*, 131–134.

Fustec, A., D. Desbruyères, and S.K. Juniper, (1987). Deep- sea hydrothermal vent communities at 13°N on the East Pacific Rise: Microdistribution and temporal variations. *Biological Oceanography 4*:121–164.

German, C.R and J. Lin, (2004). The thermal structure of the oceanic crust, ridge spreading, and hydrothermal circulation: How well do we understand their inter-connections? *In: Mid-ocean ridges: Hydrothermal interactions between the lithosphere and oceans, ed.* C.R. German, J.Lin and L.M. Parson*, American Geophysical Union Geophysical Monograph, 148, 1-18, doi:10.1029/148GM01,2004.*

German, C.R., and K.L. Von Damm (2004). Hydrothermal processes, in *The oceans and marine geochemistry*, *Treatise on geochemistry*, vol. 6, edited by H. D. Holland, et al., pp. 181-222, Elsevier-Pergamon, Oxford, UK.

Germanovich, L.N., R.P. Lowell, and D.K. Astakhov (2000). Stress-dependent permeability and the formation of seafloor event plumes, *J. Geophys. Res.*, *105*, 8341-8354.

Germanovich, L.N., R.P. Lowell, and D.K. Astakhov (2001). Temperature-dependent permeability and bifurcations, in hydrothermal flow, *J. Geophys. Res.*, *106*, 473-495.

Germanovich, L. N., R. P. Lowell, and P. Ramondenc (2010). Hydrothermal response to the earthquake swarm at 9°50 N, East Pacific Rise: Magmatic origin and constraints from heat flow and geochemical data, *J. Geophys Res.* (in press).

Glickson, D.A., D.S. Kelley, and J.R. Delaney (2007). Geology and hydrothermal evolution of the Mothra Hydrothermal Field, Endeavour Segment, Juan de Fuca Ridge. *Geochem. Geophys. Geosyst. 8*: 23.

Ginster, U., M.J. Mottl, and R.P. Von Herzen (1994). Heat flux from black smokers on the Endeavor and Cleft segments, Juan de Fuca Ridge, *J. Geophys. Res., 99,* 4937-4950.

Gendron, J.F., J.F. Todd, R.A. Feely, E.T. Baker, and D. Kadko (1994). Excess ^{222}Rn over the Cleft segment, Juan de Fuca Ridge, *J. Geophys. Res.*, *99*, 5007-5015.

Green, K.E., R.P. Von Herzen, and D.L. Williams (1981). The Galapagos Spreading Center at 86W: A detailed geothermal field study, *J. Geophys. Res.*, *86*, 979-986.

Hannington, M.D., I.R. Jonasson, P.M. Herzig, and S. Petersen (1995). Physical and chemical processes of seafloor mineralization at mid-ocean ridges, In *Seafloor hydrothermal systems; physical, chemical, biological, and geological interactions*, edited

by Humphris, S.E., R.A. Zierenberg, L.S. Mullineaux, R.E. Thomson, *Geophysical Monograph*, *91*, pp.115-157,

Harding, A.J., J.A. Orcutt, M. E. Kappus, E. E. Vera, J. C. Mutter, P. Buhl, R. S. Detrick, and T. M. Brocher (1989). Structure of young oceanic crust at 13°N on the East Pacific Rise from expanding spread profiles, *J. Geophys. Res.*, 94(B9). 12163-12196.

Haymon, R.M., D.J. Fornari, M.H. Edwards, S. Carbotte, D. Wright, and K. C. Macdonald (1991). Hydrothermal vent distribution along the East Pacific Rise crest (9°09'–54'N) and its relationship to magmatic and tectonic processes on fast-spreading mid-ocean ridges, *Earth Planet. Sci. Lett., 104*, 513–534

Haymon, R.M., D.J. Fornari, K.L. Von Damm, M.D. Liley, M.R. Perfit, J. M. Edmond, W. C. Shanks, III, R. A. Lutz, J. M. Grebmeier, S. Carbotte, D. Wright, E. McLaughlin, M. Smith, N. Beedle, and E. Olson (1993). Volcanic eruption of the mid-ocean ridge along the east Pacific Rise crest at 9°45′- 52′N: direct submersible observations of seafloor phenomena associated with an eruption event in April, 1991. *Earth Planet. Sci. Lett.*, *119*, 85–101.

Haymon, R.M. (1996). The response of ridge-crest hydrothermal systems to segmented, episodic magma supply, *Geological Society Special Publication*, *118*, 157-168.

Hekinian, R., M. Fevrier, J. L.Bischoff, P. Picot, W. C. Shanks, (1980). Sulfide deposits from the East Pacific Rise near 21 degrees N, *Science*, vol.207, no.4438, pp.1433-1444

Herzig, P.M. and Hannington, M.D. (1995). Hydrothermal activity, vent fauna, and submarine gold mineralization at alkaline fore-arc seamounts near Lihir Island, Papua New Guinea. Proceedings Pacific Rim Congress 1995, *Australasian Institute of Mining and Metallurgy*: 279-284.

Horton, C.W., and F.T. Rogers, Jr., (1945). Convection currents in porous media, *J. Appl. Phys.*, *16*, 367-370.

Huber, J.A., D.A. Butterfield, and J.A. Baross, (2003). Bacterial diversity in a subseafloor habitat following a deep-sea volcanic eruption. FEMS Microbial Ecology 43:393–409.

Humphris, S.E. and J.R. Cann (2000). Constraints on the energy and chemical balances of the modern TAG and ancient Cyprus seafloor sulfide deposits, *J. Geophys. Res.*, *105*, 28477-28488.

Humphris S.E., P.M. Herzig, D.J. Miller, J.C. Alt, K. Becker, D. Brown, G. Burgmann, H. Chiba, Y. Fouquet, J.B. Gemmell, G. Guerin, M.D. Hannington, N.G. Holm, J.J. Honnorez, G.J. Iturrino, R. Knott, R. Ludwig, K. Nakamura, S. Petersen, A.L. Reysenbach, P.A. Rona, S. Smith, A.A. Sturz, M.K. Tivey, and X. Zhao (1995). The internal structure of an active sea-floor massive sulphide deposit. *Nature*, *377*, 713–6.

Huppert, H.E. and R.S.J. Sparks (1984). Double-diffusive convection due to crystallization in magmas, *Annual Review of Earth and Planetary Science*s, vol.12, pp.11-37

Huppert, H.E., and R.S.J. Sparks, (1988). Melting the roof of a chamber containing a hot turbulently convecting fluid. *J. Fluid Mech.* 1 88: 107-31

Jarvis, R.A. and A.W. Woods (1994). The nucleation, growth and settling of crystals from a turbulently convecting fluid, *J. Fluid Mech*, Vol. 273, pp. 83-107

Jenner G.A., P.A. Cawood, M.Rautenschlein, and W. M White., (1987). Composition of back-arc basin volcanics, Valu Fa ridge: evidence for a slab-derived component in their mantle source. *Journal of Volcanology and Geothermal Research*, 32:209-222.

Johnson, H.P., M. Hutnak, R.P. Dziak, C.G. Fox, I. Urcuyo, J.P. Cowen, J. Nabelek, and C. Fisher (2000). Earthquake-induced changes in a hydrothermal system on the Juan de Fuca mid-ocean ridge, *Nature*, *407*, 174-177.

Juniper S.K., P. Martineu, J. Sarrazin, and Y. Gelinas, (1995). Microbial mineral floc associated with nascent hydrothermal activity on CoAxial segment, Juan de Fuca Ridge. *Geophysical Research Letters 22*:179–182.

Jupp, T. and A. Schultz (2000). A thermodynamic explanation for black smoker temperatures, *Nature*, *403*, 880-883.

Kelley, D.S. and J.R. Delaney (1987). Two-phase separation and fracturing in mid-ocean ridge gabbros at temperatures greater than 700±C. *Earth Planet. Sci. Lett. 83*:53–66

Kelley D.S, K.M. Gillis, and G. Thompson (1993). Fluid evolution in submarine magma-hydrothermal systems at the Mid-Atlantic Ridge. *J. Geophys. Res.* 98:19579–96

Kelley, D.S., J.R. Delaney, M.D. Lilley, and D.A. Butterfield (1997). Unusual sulfide structures and venting style in the newly discovered Mothra hydrothermal field, Endeavour Segment of the Juan de Fuca Ridge, *Eos, Transactions*, AGU, *78*, no.46, Suppl., pp.773

Kelley, D.S., J.A. Karson, D.K. Blackman, G.L. Früh-Green, D.A. Butterfield, M.D. Lilley, E.J. Olson, M.O. Schrenk, K.K. Roe, G.T. Lebon, P. Rivizzigno, and the AT3-60 Shipboard Party. (2001). An off-axis hydrothermal vent field near the Mid-Atlantic Ridge at 30°N. *Nature*, *412*:145–149.

Kelley, D.S., J.A. Baross, and J.R. Delaney (2002). Volcanoes, fluids, and life at mid-ocean ridge spreading centers, *Annu. Rev. Earth Planet. Sci*., *30*, 385-491.

Kent, G.M., A.J. Harding, and J.A. Orcutt (1990). Evidence for a smaller magma chamber beneath the East Pacific Rise at 9º30´N, *Nature*, *344*, 650-652.

Kerr, R.C. (1994). Melting driven by vigorous compositional convection. *J. Fluid Mech*. 280, 255-285

Langmuir, C.H., D. Fornari, D. Colodner, J.L. Charlou, I. Costa, D. Desbruyeres, D. Desonie, T. Emerson, A. Fiala-Medioni, Y. Fouquet, S. Humphris, L. Saldanha, R. Sours-Page, M. Thatcher, M. Tivey, C. Van Dover, K. Von Damm, K. Wiese, C. Wilson, (1993). Geological setting and characteristics of the Lucky Strike vent field at 37°17' N on the Mid- Atlantic Ridge, *Eos Trans*. *AGU* 74:99

Lapwood, E. (1948). Convection of a fluid in a porous media, *Proc. Cambridge Philos. Soc.*, *44*, 508-521.

Lilley, M. D., D. A. Butterfield, J. E. Lupton, and E. J. Olson (2003). Magmatic events can produce rapid changes in hydrothermal vent chemistry, *Nature*, *422*, 878-881, doi:10.1038.

Lister, C.R.B. (1983). On the intermittency and crystallization mechanisms of sub seafloor magma chambers. *Geophys. J. R.* Astron. Soc. 73: 351-66

Little, S.A., K.D. Stolzenbach, and R.P. Von Herzen (1987). Measurements of plume flow from a hydrothermal vent field, *J. Geophys. Res. 92*. 2587–2596.

Lonsdale, P. and K. Becker (1985). Hydrothermal plumes, hot springs, and conductive heat flow in the Southern Trough of Guaymas Basin, *Earth Planet. Sci. Lett.*, *73*, 211-225.

Lowell, R.P. (1980). Topographically driven sub-critical hydrothermal convection in the oceanic crust. *Earth Planet. Sci. Lett.*, *49*, 21-28.

Lowell, R.P. (1991). Modeling continental and submarine hydrothermal systems, *Rev. Geophys.,* 29, 457-476.

Lowell, R.P. (2010). Hydrothermal circulation at slow spreading ridges: analysis of heat sources and heat transfer processes, in *Diversity of Hydrothermal Systems on Slow Spreading Ocean Ridges*. *Geophysical Monograph Series 188*, AGU

Lowell, R.P. and D.K. Burnell (1991). A numerical model for magma-hydrothermal boundary layer heat transfer in the oceanic crust, *Earth and Planet. Sci. Lett., 104,* 59-69

Lowell, R.P. and L.N. Germanovich (1994). On the temporal evolution of high-temperature hydrothermal systems at ocean ridge crests, *J. Geophys. Res., 99,* 565-575

Lowell, R.P. and L.N. Germanovich (1995). Dike injection and the formation of megaplumes at ocean ridges, *Science, 267,* 1804-1807

Lowell, R.P. and P.A. Rona (1976). On the interpretation of near bottom water temperature anomalies, *Earth Planet. Sci. Lett.*, 32, 18-24.

Lowell, R.P., and P.A. Rona (1985). Hydrothermal models for the generation of massive sulfide ore deposits, *J. Geophys. Res., 90,* 8769-8783

Lowell, R.P. and P.A. Rona (2002). Seafloor hydrothermal systems driven by the serpentinization of peridotite. *Geophys. Res. Lett. 29*, 1531, doi 10.1029/2001GL014411.

Lowell, R.P., Y. Yao, and L.N. Germanovich (2003). On the relationship between focused and diffuse flow in seafloor hydrothermal systems, *J. Geophys. Res., 108(B9).* 2424, doi: 10.1029/2002JB002371,.

Lowell, R.P. and L.N. Germanovich (2004). Seafloor hydrothermal processes: Results from scale analysis and single-Pass models, in *Mid-Ocean Ridges*: *Hydrothermal Interactions Between the Lithosphere and Oceans, Geophys. Monogr. Ser.*, *148*, ed. by C.R. German, J. Lin and L.M. Parson, pp.219-244, Amer. Geophys. Union, Washington, D.C.

Lowell, R.P., B.W. Crowell, K.C. Lewis, L. Liu (2008). Modeling multiphase, multicomponent processes at oceanic spreading centers, *Geophysical Monograph*, *Ser.*, *178*, pp.15-44

Manning C.E., MacLeod C.J., Weston P.E. (2000). Lower-crustal cracking front at fast-spreading ridges: evidence from the East Pacific Rise and Oman ophiolites. In *Ophiolites*

and Oceanic Crust: New Insights from Field Studies and the Ocean Drilling Program, ed. Y. Dilek, E. Moores, D. Elthos, A. Nicoals, pp. 261–72, Geol. Soc. Am. Spec. Pap. 349. Boulder, CO: Geol. Soc. Am. 552 pp.

Martin, D. (1990). Crystal settling and in situ crystallization in aqueous solutions and magma chambers, *Earth Planet. Sci. Lett.*, *96*, 336-348.

Martin, D. and R. Nokes (1988). Crystal settling in a vigorously convecting magma chamber. *Nature* 332, 534-536.

Martin, D. and R. Nokes (1989). A fluid-dynamical study of crystal settling in convecting magmas, *Journal of Petrology*, vol.30, no.6, pp.1471-1500

Marsh, B.D. (1989). On convective style and vigor in sheet-like magma chambers *J.Petrol.*, 30, 479-530.

McConachy, T. F., R. D. Ballard, M. J. Mottl, and R. P. Von Herzen (1986). Geologic form and setting of a hydrothermal vent field at lat 10°56'N, East Pacific Rise: A detailed study using Angus and Alvin, *Geology*, *14*, 295-298.

Parsons, B. (1981). The rates of plate creation and consumption, *Geophys. J. R. Astr. Soc., 67*, 437–448.

Parsons, B. and J.G. Sclater (1977). An analysis of the variation of ocean floor bathymetry and heat flow with age, *J. Geophys. Res.*, *82*, 803-827.

Michael, P. J., C.H. Langmuir, H. J. B. Dick, J. E. Snow, S. J. Goldstein, D. W. Graham, K. Lehnert, G. Kurras, W. Jokat, R. Muehe, H.N. Edmonds, , (2003). Magmatic and amagmatic seafloor generation at the ultraslow-spreading Gakkel Ridge, Arctic Ocean *Nature* (London). vol.423, no.6943, pp.956-961

Norton, D., and H.P.Jr. Taylor (1979). Quantitative simulation of the hydrothermal systems of crystallizing magmas on the basis of transport theory and oxygen isotope data: an analysis of the Skaergaard intrusion. *J. Petrol.* 20: 421~86

Rabinowicz, M., J.C. Sempere, and P. Genthon (1999). Thermal convection in a vertical permeable slot: Implications for hydrothermal circulation along mid-ocean ridges, *J. Geophys. Res.*, *104*, 29275-29292.

Ramondenc, P., L.N. Germanovich, K.L. Von Damm, and R.P. Lowell (2006). The first measurements of hydrothermal heat out at 9°50´N, East Pacific Rise, *Earth Planet. Sci. Lett.*, *245*, 487-497.

Ramondenc, P., L.N. Germanovich, R.P. Lowell (2008). Modeling hydrothermal response to earthquakes at oceanic spreading centers, *Geophysical Monograph*, vol. 178, pp.97-121

Ribando, R.J., K.E. Torrance, and D.L. Turcotte (1976). Numerical models for hydrothermal circulation in the oceanic crust, *J. Geophys. Res.*, *81*, 3007-3012.

Rohr, K.B., B. Mildreit and C.J. Yorath (1988). Asymmetric deep crustal structure across the Juan de Fuca Ridge, *Geology*, *16*, 533-537

Rona, P.A. (1984). Hydrothermal mineralization at seafloor spreading centers, *Earth Sci. Rev.*, 20, 1-104.

Rona, P.A. (1985). Black smokers and massive sulfides at the TAG hydrothermal field, Mid-Atlantic Ridge 26°N, *Eos, Trans. AGU*, vol.*66*, no.46, pp.936, 12 Nov 1985

Rona, P.A. and S.D. Scott (1993). Preface to special issue on sea-floor hydrothermal mineralization: new perspectives. *Econ. Geol. 88*, pp. 1935–1976.

Rona, P. A., M. D. Hannington, C. V. Raman, G. Thompson, M. K. Tivey, S. E. Humphris, C. Lalou, and S. Petersen (1993b). Active and relict Sea-Floor Hydrothermal Mineralization at the TAG Hydrothermal Field, Mid-Atlantic Ridge, *Econ. Geol.*, *88*, 1989-2017.

Rona, P.A. and D.A. Trivett (1992). Discrete and diffuse heat transfer at ASHES vent field, Axial Volcano, Juan de Fuca Ridge, *Earth Planet. Sci. Lett., 109,* 57-71.

Rosenberg, N.D., J.E. Lupton, D. Kadko, R. Collier, M.D. Lilley, and H. Pak (1988). Estimation of heat and chemical fluxes from a seafloor hydrothermal vent field using radon measurements, *Nature, 344*, 604-607.

Rubin, K. H., M. Perfit, D. J. Fornari, S. A. Soule, M. Tolstoy, and F. Waldhauser (2006). Geochronology and composition of the 2005-06 volcanic eruptions of the East Pacific Rise, 9°46'-56'N, *Eos Trans. AGU*, *87*(52), Fall Meet. Suppl., Abstract V23B-0602.

Rudnicki, M. D., and H. Elderfield (1992). Theory applied to the Mid-Atlantic Ridge hydrothermal plumes: the finite-difference approach, *J. Volcanol. Geotherm. Res.*, *50*, 161-172.

Rudnicki, M. D., and C. R. German (2002). Temporal variability of the hydrothermal plume above the Kairei vent field, 25°S, Central Indian Ridge, *Geochem. Geophys. Geosyst.*, *3*(2), doi:10.1029/2001GC000240.

Sauter, D., L. Parson, V. Mendel, C. Rommevaux-Jestin, O. Gomez, A. Briais, C. Mével, K. Tamaki, and the FUJI Scientific Team, TOBI sidescan sonar imagery of the very slow-spreading Southwest Indian Ridge: Evidence for along-axis magma distribution, *Earth Planet. Sci. Lett., 199*, 81–95, 2002.

Seyfried W.E. Jr and Ding K. (1995). Phase equilibria in subseafloor hydrothermal systems: a review of the role of redox, temperature, pH and dissolved Cl on the chemistry of hot spring fluids at mid-ocean ridges. In Humphris, S.E., Zierenberg, R., Mullineaux, L., and Thomson, R. (Eds.). *Seafloor Hydrothermal Systems: Physical, Chemical, Biological and Geological Interactions within Hydrothermal Systems*. Geophys. Monogr., 91: 248–72

Scheirer, D.S., T.M. Shank, D.J. Fornari (2006). Temperature variations at diffuse and focused flow hydrothermal vent sites along the northern East Pacific Rise *Geochem. Geophys. Geosyst.*, 7, Q03002, doi: 10.1029/2005GC001094.

Schoofs, S. and U. Hansen (2000). Depletion of a brine layer at the base of ridge-crest hydrothermal system, *Earth Planet. Sci. Lett.*, *180*, 341-353.

Schultz, A., J.M. Delaney, and R.E. McDuff (1992). On the partitioning of heat flux between diffuse and point source venting, *J. Geophys. Res., 97,* 12229-12314.

Shank, T.M., D.J. Fornari, K.L. Von Damm, M.D. Lilley, R.M. Haymon, and R.A. Lutz, (1998). Temporal and spatial patterns of biological community development at nascent deep-sea hydrothermal vents along the East Pacific Rise. *Deep-Sea Research* 45:465–515.

Silantyev, S.A., M.V. Mironenko, A.A. Novoselov (2009). Hydrothermal systems hosted in peridotites at slow-spreading ridges. Modeling phase t*ransformations and material balance: Upwelling limb of the hydrothermal cell,* Petrology. Vol. 17, no. 6, pp. 523-536.

Singh, S.C., G.M. Kent, J.S. Collier, A.J. Harding, and J.A. Orcutt (1998). Melt to mush variations in crustal magma properties along the ridge crust at the sourthern East Pacific Rise, *Nature*, 394, 874-878.

Singh, S. C., J. S. Collier, A. J. Harding, G. M. Kent, and J. A. Orcutt (1999). Seismic evidence for a hydrothermal layer above the solid roof of the axial magma chamber at the southern East Pacific Rise, *Geology*, *27*, 219-222.

Singh, S. C., W. C. Crawford, H. Carton, T. Seher, V. Combier, M. Cannat, J. P. Canales, D. Dusunur, J. Escartin, and J. M. Miranda (2006). Discovery of a magma chamber and faults beneath a Mid-Atlantic Ridge hydrothermal field, *Nature*, *442*, 1029-1032.

Sinha, M.C. (1995). Segmentation and rift propagation at the Valu Fa Ridge, Lau Basin: evidence from gravity data, *J. Geophys. Res.*, *100*, 15025-15043.

Sinha, M.C., S.C. Contable, C. Peirce, A. White, G.S. Heinson, L.M. MacGregor, and D.A. Navin (1998). Magmatic processes at slow spreading ridges: implications of the RAMESSES experiment at 57°45'N on the Mid-Atlantic Ridge, *Geophys. J. Int.*, *135*, 731-745.

Sinton, J. M., L. L. Ford, B. Chappell, M. T. McCulloch, (2003). Magma genesis and mantle heterogeneity in the Manus back-arc basin, Papua New Guinea, *Journal of Petrology*, vol.44, no.1, pp.159-195.

Sohn, R.A., D.J.Fornari, K. L. Von Damm, J. A. Hildebrand, and S.C. Webb (1998). Seismic and hydrothermal evidence for a cracking event on the East Pacific Rise crest at 9°50'N, *Nature*, 396, 159-161.

Soule, S.A., D.J. Fornari, M.R. Perfit, K.H. Rubin (2007). New insights into mid-ocean ridge volcanic processes from the 2005-2006 eruption of the East Pacific Rise, 9°46'N-9° 56'N, *Geology, 35*, 1079-1082

Spera, F. J. (1980). Thermal evolution of plutons: a parameterized approach. *Science* 207: 299-301

Spera, F. J., D.A. Yuen, and S.J. Kirschvink (1982). Thermal boundary layer convection in silicic magma chambers: effects of temperature- dependent rheology and implications for thermogravitational chemical fractionation. *J. Geophys. Res.* 87: 8755-67

Spiess, F.N., K.C. Macdonald, T. Atwater, R. Ballard, A. Carranza , D.Cordoba, C. Cox, V.M. Diaz Garcia, J. Francheteau, J. Guerrero, J. Hawkins, R. Haymon, R. Hessler, T.

Juteau, M. Kastner, R. Larson, B. Luyendyk, J.D. Macdougall, S. Miller, W. Normark, J. Orcutt, and C. Rangin (1980). East Pacific Rise: Hot springs and geophysical experiments, *Science*, *207*, 1421-1433.

Stein, C.A. and S. Stein (1992). A model for the global variation in oceanic depth and heat flow with lithospheric age, *Nature*, *359*, 123-129.

Stein, C.A. and S. Stein (1994). Constraints on hydrothermal heat flux through the oceanic lithosphere from global heat flow, *J. Geophys. Res.*, *99*, 3081-3095.

Stein, J.S. and A.T. Fisher (2001). Multiple scales of hydrothermal circulation in Middle Valley, northern Juan de Fuca Ridge: Physical constraints and geologic models, *J. Geophys. Res.*, *106*, 8563-8580.

Sparks, R.S.J., H.E. Huppert, J.S. Turner (1984). The fluid dynamics of evolving magma chambers, *Philosophical Transactions of the Royal Society of London*, Series A: Mathematical and Physical Sciences, vol.310, no.1514, pp.511-534

Tolstoy, M., D.R. Bohnenstiehl, M.H. Edwards, G.J. Kurras (2001). Seismic character of volcanic activity at the ultraslow-spreading Gakkel Ridge, *Geology* (Boulder). vol.29, no.12, pp.1139-1142

Tivey, M.K. and J.R. Delaney (1986). Growth of large sulfide structures on the Endeavour Segment of the Juan de Fuca Ridge, *Earth. Planet. Sci. Lett.*, *77*, 303-317.

Tunnicliffe, V., R.W. Embley, J.F. Holden, D.A. Butterfield, G. Massoth, and S.K. Juniper, (1997). Biological colonization of new hydrothermal vents following an eruption on Juan de Fuca Ridge. *Deep-Sea Research 44*:1,627–1,644

Turner, I.M.C. Peirce, M.C. Sinha, (1999). Seismic imaging of the axial region of the Valu Fa Ridge, Lau Basin; the accretionary processes of an intermediate back-arc spreading ridge, *Geophysical Journal International*, vol.138, no.2, pp.495-519

Van Ark, E.M., R.S. Detrick, J.P. Canales, S.M. Carbotte, A.J. Harding, G..M. Kent, M.R. Nedimovic, W.S.D. Wilcock, J.B. Diebold, J.M. Babcock (2007), Seismic structure of the Endeavour Segment, Juan de Fuca Ridge; correlations with seismicity and hydrothermal activity, *J. Geophys. Res.*, *112*, B02401, doi: 10.1029/2005JB004210.

Veirs, S.R., R.E. McDuff, and F.R. Stahr (2006). Magnitude and variance of near-bottom horizontal heat flux at the Main Endeavour hydrothermal vent field, *Geochem. Geophys. Geosyst.*, *7*, Q02004, doi:10.1029/2005GC000952

Vera, E.E., J.C. Mutter, P. Buhl, J.A. Orcutt, A.J. Harding, M.E. Kappus, R.S. Detrick, and T.M. Brocher (1990). The structure of 0- to 0.2-m.y.-old oceanic crust at 9°N on the East Pacific Rise from expanded spreading profiles, *J. Geophys. Res.*, 95(B10), 15529-15556.

Von Damm, K.L. (2004). Evolution of the hydrothermal system at East Pacific Rise 9 degrees 50'N; geochemical evidence for changes in the upper oceanic crust *Geophysical Monograph*, vol.148, pp.285-304, 2004, Editor: German, Christopher R; Lin, Jian; Parson, Lindsay M

Von Damm, K.L., and M.D. Lilley (2004). Diffuse flow hydrothermal fluids from 9°50'N East Pacific Rise: Origin, evolution and biogeochemical controls, in The Subsurface Biosphere at Mid-Ocean Ridges, *Geophys. Monogr. Ser.*, vol. *144*, edited by W. S. D. Wilcock et al., pp. 245–268, AGU, Washington, D. C.

Von Damm, K.L. and J.L. Bischoff (1987). Chemistry of hydrothermal solutions from the southern Juan de Fuca Ridge, *J. Geophys. Res.*, vol. 92, no. B11, pp.11,334-11,346

Von Damm K.L., J.M. Edmond, B. Grant, C.I. Measures, B. Walden, and R.F. Weiss. (1985). Chemistry of submarine hydrothermal solutions at 21°N, East Pacific Rise. *Geochimica et Cosmochimica Acta* 49:2,197–2,220.

Von Damm, K. L., S. E. Oosting, R. Kozlowski, L. G. Buttermore, D. C. Colodner, H. N. Edmonds, J. M. Edmond, and J. M. Grebmeier (1995). Evolution of East Pacific Rise hydrothermal vent fluids following a volcanic eruption, *Nature, 375,* 47–50.

Von Damm, K.L., L. G. Buttermore, S. E. Oosting, A. M. Bray, D. J. Fornari, M. D. Lilley, and W. C.Shanks III (1997). Direct observation of the evolution of a seafloor "black smoker" from vapor to brine, *Earth Planet. Sci. Lett., 149,* 101–112.

Von Damm, K.L., C.M. Parker, R.M. Gallant, and J.P. Loveless (2002). Chemical evolution of hydrothermal fluids from EPR 21°N: 23 years later in a phase separating world, *EOS Trans*., Amer. Geophys. Union, *83*, Suppl., 1421.

White, R. S., D. McKenzie, and R. K. O'Nions (1992). Oceanic crustal thickness from seismic measurements and rare earth element inversions, *J. Geophys. Res., 97,* 19683–19715.

Williams, D.L. and R.P. Von Herzen (1974). Heat loss from the Earth: New estimate, *Geology*, *2*, 327-328.

Williams, D.L., R.P. Von Herzen, J.G. Sclater, and R.N. Anderson (1974). The Galapagos Spreading Center: lithospheric cooling and hydrothermal circulation, *Geophys. J. Roy. Astr. Soc.*, *38*, 587-608.

Wilcock, W.S.D. (1998). Cellular convection models of mid-ocean ridge hydrothermal circulation and the temperatures of black smoker fields, *J. Geophys. Res.*, *103*, 2585-2596.

Wilcock W.S.D, Delaney J.R. (1996). Mid-ocean ridge sulfide deposits: evidence for heat extraction from magma chambers or cracking fronts? *Earth Planet. Sci. Lett.* 145:49–64

Wolery, T.J. and N.H. Sleep (1976). Hydrothermal circulation and geochemical flux at mid-ocean ridges, *J. Geol.*, *84*, 249–275.

Worster, M. G., H. E. Huppert, and R. S. J. Sparks (1990). Convection and crystallization in magma cooled from above, *Earth Planet. Sci. Lett.*, *101*, 78-89.

CHAPTER 2. MATHEMATICAL FORMULATION

In this chapter, I propose to more realistically model magma hydrothermal processes at oceanic spreading centers by including a turbulent convecting, crystallizing, and replenished magma body. Figure 2.1 depicts the basic model geometry consisting of a layer of vigorously convecting magma that transfers heat to an overlaying hydrothermal system through a thin thermal boundary layer, with new magma replenished from its underlying mush zone. Hydrothermal circulation system follows a single-pass model, in which cold seawater penetrates into the oceanic crust where it is heated and form the hydrothermal fluid at a temperature T_h. At the top of the magma chamber, the temperature is constant at the solidus magma temperature T_S. Due to the large temperature difference between the hydrothermal fluid and the top of magma chamber, heat is transferred from the convecting magma at temperature T_m across a thin thermal conductive boundary layer with thickness $\delta(t)$. Denoting F_m and A_m as the heat flux and area of the magma chamber, respectively, the total heat output from the magma chamber is $F_m(t)A_m$. I assume that all the heat output from the magma chamber is transported across the conductive boundary layer and is taken up by the overlying hydrothermal system. With the heat transfer into the hydrothermal fluids, the buoyant fluids rise rapidly and discharge into the ocean through hydrothermal vents. As a result of the heat

transported from the magma chamber to the hydrothermal fluid, the magma chamber cools down and crystallizes.

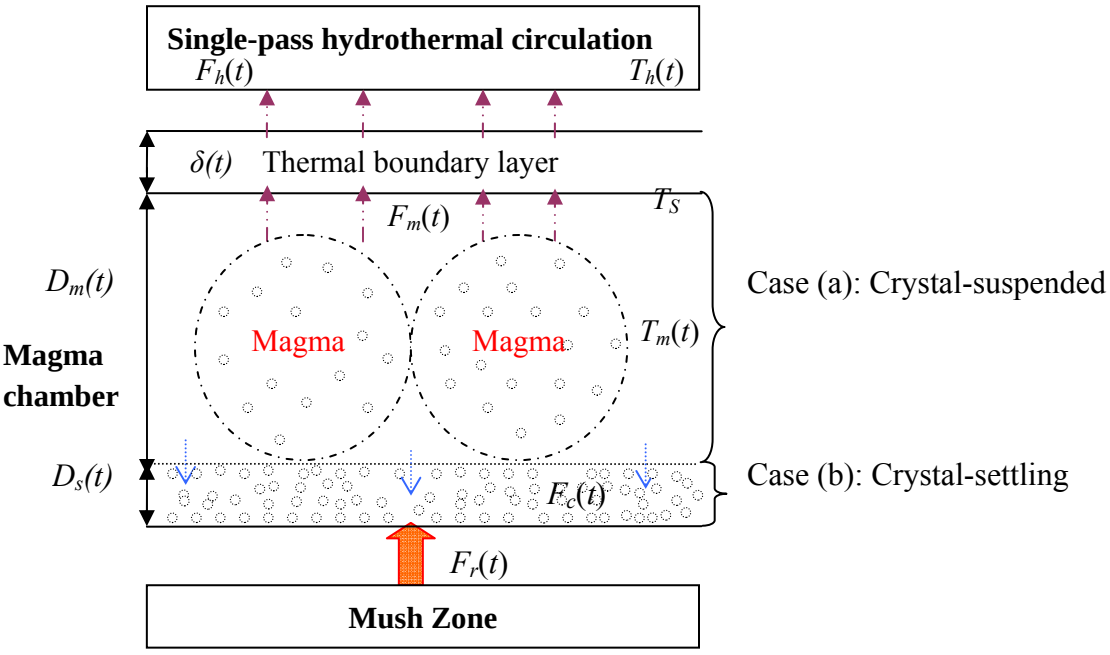

Figure 2.1 Schematic of magma convection model with crystals suspended in case (a) and crystals settling in case (b). Turbulent magma convection provides heat flux F_m to power the overlying hydrothermal system at a temperature T_h and heat flux F_h. The top of the magma chamber is maintained at its solidus T_s and heat from the magma to the hydrothermal system is transported across a conductive boundary layer of thickness δ(t). The underlying mush zone provides a source of magma and heat flux to the magma chamber. Details of magma dynamics are neglected in this model.

In this work, I consider two scenarios of magma convection and crystallization. One assumes the convective motions in the magma chamber are sufficiently vigorous to keep crystals in suspension and well mixed within the interior of the magma, which is similar to the model of [*Huppert and Sparks*, 1988]. The other scenario assumes that, as

crystallization occurs, crystals settle rapidly and accumulate on the floor, similar to the models of [*Martin*, 1990; *Martin and Nokes*, 1989; *Worster et al*., 1990]. In this case, the crystal layer grows with time and, as a result, the depth of liquid magma decreases. This assumption allows me to calculate the maximum lifetime of the magma convection since magma convection is driven only by the liquid magma. Homogeneous crystallization of a well-mixed magma is likely to be possible only in the early stages of magma convection processes because, as the crystal size increases, gravitational forces will overcome the convective forces keeping the crystals in suspension [*Brandies and Jaupart*, 1986]. Thus, in the crystals suspended model I neglect the density difference between the crystals and the liquid magma; and in the crystal-settling model, I assume that crystals instantly fall out of suspension and settle onto the chamber floor as they form within the magma.

In the following sections, the mathematical models are presented to describe the interactive characteristics of both the magma convection system and the hydrothermal system. Section 2.1 introduces the basic system geometry and the fundamentals of convection in the magma system, and presents the heat balance for a convecting, crystallizing, replenished magma chamber; Section 2.2 develops the magma heat flux models for both crystals suspended and crystals settling; Section 2.3 develops the magma heat flux models with magma replenishment for two different crystals distribution assumptions; Section 2.4 describes the hydrothermal circulation models.

2.1 Heat Conservation of the Magma Chamber

Almost all convective motions come from a layer of fluid heated from below and/or cooled from above. Within the liquid magma body, the thermal convection results from the temperature difference between the hot magma and the cold upper boundary. Heat is transferred by conduction between the cold rock and hot magma. The vigor of this convection is expressed by the dimensionless Rayleigh number *Ra*, which is defined as the ratio of thermal buoyancy force to the viscous and thermal resistance

$$Ra = \frac{\alpha_m g D^3 \Delta T}{a_m \nu_m} \tag{1}$$

where α_m (°C^{-1}) is the thermal expansion, g (m/s^2) is the acceleration due to gravity, D is the thickness of the laterally extensive magma body, a_m (m^2/s) is thermal diffusivity, ν_m (m^2/s) is kinematic viscosity, and $\Delta T = T_m(t) - T_s$ is the difference between the mean temperature of the convecting magma $T_m(t)$ and the magma solidus temperature T_s. The subscript m refers to properties of the magma.

During cooling and crystallization of magma chamber, T_m, ΔT, and ν_m are time-dependent. Therefore, the Rayleigh number is also a function of time. Rayleigh number is a measurement of the strength of the convection and of the rate of heat transfer. As shown by *Huppert and Sparks* [1988], *Martin and Nokes* [1989], *Huppert and Turner* [1990], *Worster et al.* [1990], *Jaupart and Tait* [1995] and *Jellinek and Kerr* [1999], a magma body would undergo vigorous convection when the Rayleigh number is greater or equal to a critical value ,i.e., $Ra >> Ra_c$. Instability and convective motions start only

when the Rayleigh number reaches a minimum value of ~10^3; and convection becomes fully turbulent when $Ra > 10^6$. As ΔT decreases and ν_m increases as a result of cooling, the motion becomes increasingly less vigorous with time and eventually becomes laminar. Since the Rayleigh number is proportional to the third power of thickness of magmatic chamber, the size of the system is the most important parameter concerning the existence and vigor of magma convection. Seismic data at several mid-ocean ridges show the presence of a thin mostly liquid lens of magma is typically several tens of meters to perhaps ~ 100 m thick [e.g., *Kent et al*., 1990; *MacLeod and Yaoyancq*, 2000]. In nearly all cases, the initial *Ra* is much greater than the critical value. For ΔT = 100°C, D = 100 m, $Ra \sim 10^{11}$; for $D \sim 10$ m and $\Delta T \sim 1$°C, then $Ra \sim 10^6$.

To characterize the heat flux of the magma chamber, I first introduce the Nusselt number. Following *Huppert and Sparks* [1988], the heat flux $F_m(t)$ from the convecting magma body can be expressed in terms of the Nusselt number *Nu*, which is defined as the ratio of the heat transport as a result of convection to the heat flux conducted across the layer of thickness D in the absence of convection:

$$Nu = \frac{F_m(t)D}{\lambda_m\left(T_m(t) - T_S\right)} \tag{2}$$

where t (s) is the time, $\lambda_m = a_m \rho_m c_m$ is the thermal conductivity, ρ_m (kg/m^3) is the magma density, and c_m (J/kg°C) is the specific heat. The classical relationship between the Nusselt number and the thermal Rayleigh number is given by [*Jarvis and Peltier*, 1989]

$$Nu \approx (Ra / Ra_c)^{1/3} \tag{3}$$

Upon substituting equations (1) and (3) into equation (2), I obtain the heat flux F_m (W/m^2) transferred as a result of convection in the magma chamber [*Turner*, 1973]

$$F_m(t) = \rho_m c_m 0.1(\alpha_m g a_m{}^2 / \nu_m(t))^{1/3}(T_m(t) - T_S)^{4/3} \tag{4}$$

Next, I discuss the heat balance for the convecting, crystallizing, replenished magma chamber. Considering that a layer of crystal-free magma emplaces into the crust and forms a magma chamber, the magma is cooled by the surroundings. The heat content of magma chamber is given by

$$H(t) = V_m(t)[\rho_m c_m T_m\ (t) + \rho_m(1 - \chi(T_m(t))L] \tag{5}$$

where L (J/kg) is the latent heat of the crystallization of the magma, $\chi(T_m(t))$ is the volume fraction of crystals in the crystal-melts mixture, which is a function of the magma temperature $T_m(t)$ since the magma crystallization is controlled by its temperature. $V_m(t)$ denotes the volume of liquid magma

$$V_m(t) = A_m(t)D_m(t) \tag{6}$$

where $A_m(t)$ is surface area of magma chamber, and D_m(t) is the thickness of liquid magma. In general, both the area and thickness of the liquid magma may be time varying. The details of modeling are discussed later. Moreover, the first term on the right-hand side of equation (5) represents sensible heat per unit volume of magma, and the second term represents the latent heat yet to be released as crystallization occurs.

For simplicity, I neglect the difference in the density between liquid magma and crystals, and the volume decrease that occurs as a result of crystallization. Moreover, I

assume that the magma body is a sill-like structure and that heat loss from the vertical walls is negligible. The conservation of energy at the magma-hydrothermal system interface requires that

$$\frac{dH(t)}{dt} = -F_m(t)A_m(t) + F_r(t)A_m(t) + F_c(t)A_m(t) \tag{7}$$

where $F_r(t)$ is the heat flux added to the magma chamber as a result of replenishment, and $F_c(t)$ is the rate at which the conductive heat transfers from the growing crystal layer to the convecting liquid magma.

In order to solve equation (7), I need an expression for $\chi(T_m(t))$. One commonly used expression assumes that the crystal content χ varies linearly with the magma temperature, which is limited between the liquidus and solidus temperature [*Hort*, 1997], i.e.,

$$\chi(T_m(t)) = \frac{T_L - T_m(t)}{T_L - T_s} \tag{8}$$

where T_L denotes the liquid magma temperature. As an alternative, *Huppert and Sparks* [1988] relate χ to the magma temperature through the following formula

$$\chi\big(T_m(t)\big) = \frac{7200}{T_m(t)} - 6 \tag{9}$$

In the following, I discuss four different scenarios to solve the differential equation (7). I consider the case in which magma replenishment is absent or present. Within each case, I consider two scenarios depending on the existence form of the crystals: (a) crystals remain suspended with the liquid magma as it crystallizes; and (b)

crystallization occurs at the floor of the magma chamber or crystals instantly settle to the chamber floor (see Figure 2.1). For simplicity I refer to these two cases as "crystals suspended" and as "crystals settling", respectively. The real situation probably lies between these extremes, and some crystals may also grow from the roof. I neglect this effect because I wish to diminish the growth rate of a conductive thermal boundary layer at the top of the magma chamber, and thus provide an upper estimate for the magmatic heat flux. In the following discussion, I denote $D(t)$, D_0, and A_{m0} to be the magma chamber thickness at time t, the initial values of the magma chamber thickness and area, respectively.

2.2 Magma Convection without Replenishment

Without new magma being added to the magma chamber, the heat from magma replenishment $F_r(t) = 0$. Both the thickness and the area of magma chamber are assumed to be time invariant as a result of neglecting the density difference between the magma and crystals, i.e., $D(t) = D_0$ and $A_m(t) = A_{m0}$.

2.2.1 Crystals suspended

In the crystal-suspended scenario, the crystals are well mixed with liquid magma during cooling and crystallization (Figure 2.1, case (a)). The crystals and liquid magma have the same temperature and $F_c(t) =0$. In addition, without magma replenishment, both the magma chamber thickness and area remain constant at their initial values, respectively. The thickness of the liquid magma is the same as the thickness of the

magma chamber, i.e., $D_m(t) = D(t) = D_0$. Correspondingly, the volume of magma $V_m(t)$ is a constant

$$V_m(t) = D_0 A_{m0} \tag{10}$$

Therefore, the equation (7) is simplified to

$$\frac{dH(t)}{dt} = -F_m(t) A_{m0} \tag{11}$$

2.2.2 Crystals settling

If crystallization occurs at the floor of the magma chamber or crystals instantly settle there, then the volume of the liquid magma $D_m(t)$ decreases as magma crystallizes (Figure 2.1, case (b)). Thus, the thickness of the liquid magma depends on the crystal content, i.e.,

$$D_m(t) = D_0(1 - \chi(T_m(t))) \tag{12}$$

Correspondingly, the volume of liquid magma $V_m(t)$ is

$$V_m(t) = A_{m0} D_m(t) \tag{13}$$

As the magma chamber cools and crystals settle to the floor, a temperature gradient may exist across the crystal layer resulting in conductive heat transfer from the growing crystal layer to the convecting liquid. The rate of conductive heat flux from the crystal pile back to the liquid magma is approximately expressed as

$$F_c(t) = \lambda_m \frac{T_L - T_m(t)}{D_s(t)} \tag{14}$$

where $D_s(t)$ is the thickness of the crystal layer,

$$D_s(t) = D_0 \chi(T_m(t)) \tag{15}$$

Therefore, the equation (7) is simplified to

$$\frac{dH(t)}{dt} = -F_m(t)A_{m0} + F_c(t)A_{m0} \tag{16}$$

2.3 Magma Convection with Replenishment

During magma replenishment, additional heat and fluid mass is added to the magma chamber. As a result, the heat content increases with time. Denote $u(t)$ to be the magma replenishment rate. The rate of heat input due to replenishment $F_r(t)$ is given by

$$F_r(t) = (\rho_m c_m T_L + \rho_m L)u(t) \tag{17}$$

In addition, the magma chamber volume grows as the new magma refills. Denote $V(t)$ to be the magma chamber volume. It can be obtained as

$$V(t) = V_0 + \int_0^t A_b(s)u(s)ds \tag{18}$$

where $V_0 = D_0 A_{\mathrm{m0}}$ is the initial volume, $A_b(t)$ is the area through which magma replenishment occurs. For simplicity, I assume that the additional magma is added at its liquidus across the entire area at the base of the magma chamber, i.e, $A_b(t) = A_m(t)$.

I again consider the two cases: “crystals suspended” and “crystals settling”. I assume that the magma entering the base of the magma chamber mixes rapidly with the existing magma so that a single temperature $T_m(t)$ can still be used to describe the convection system. To model the magma chamber growth in equation (18), I assume that the magma chamber grows either horizontally or vertically, i.e., either the area $A_m(t)$ or thickness $D(t)$ of the magma body varies with time.

2.3.1 Magma replenishment with the growth of magma thickness

In this section, I assume the thickness of magma chamber $D(t)$ changes and the area of magma is a constant $A_m(t) = A_{m0}$ during magma replenishment. The thickness of magma chamber is

$$D(t) = D_0 + \int_0^t u(s)ds \tag{19}$$

Note that although the magma chamber thickness grow the same way in both crystals suspended and crystal settling cases, the thickness of liquid magma are different in each case. In the crystals suspended, the thickness of magma is the same as that of the magma chamber, i.e., $D_m(t) = D(t)$, since no separation of magma and crystals are considered. In the crystals settling case, the thickness of magma depends on the crystal content

$$D_m(t) = D(t)(1 - \chi(T_m(t))) \tag{20}$$

2.3.2 Magma replenishment with growth of horizontal area

One can also consider the effects of magma replenishment on the heat output from the convecting, crystallizing magma chamber by keeping the thickness of the magma chamber fixed, i.e., $D(t) = D_0$, and allowing the area to increase with time. First, I express the volume of liquid magma chamber with the magma replenishment rate $u(t)$

$$V_m(t) = V_0 - V_s(t) + \int_0^t A_m(s)u(s)ds \tag{21}$$

where $V_o = A_{m0}D_0$ is the initial magma chamber size, and $V_s(t)$ is the volume of crystals that have formed. In the following, I consider the evolution of the magma horizontal area by considering the crystals suspended and crystals settling cases, respectively.

In the crystals suspended case, $V_s(t)$ is zero since the crystals are mixed evenly in the residual melts, and the liquid magma thickness is the same as that of the magma chamber, i.e., $D_m(t) = D(t) = D_0$. Taking the derivative of equation (21) leads to

$$\frac{dV_m(t)}{dt} = D_0 \frac{dA_m(t)}{dt} = A_m(t)u(t) \tag{22}$$

Solving (22) results in the area of the magma chamber

$$A_m(t) = A_{m0} \exp\left(\frac{\int_0^t u(s)ds}{D_0} \right) \tag{23}$$

In the crystals settling case, the crystal volume $V_s(t)$ depends on the crystal content and is related to the liquid magma volume by

$$V_s(t) = \frac{\chi(T_m(t))}{1 - \chi(T_m(t))} V_m(t) \tag{24}$$

Substituting (24) into equation (21) yields

$$\frac{1}{(1 - \chi(T_m(t)))} V_m(t) = V_0 + \int_0^t A_m(s)u(s)ds \tag{25}$$

Combining equations (6) and (12), I obtain the volume of the liquid magma

$$V_m(t) = D_0(1 - \chi(T_m(t)))A_m(t) \tag{26}$$

Substitution of equation (26) into (25) and taking derivative results in differential equation of the magma horizontal area

$$D_0 \frac{dA_m(t)}{dt} = A_m(t)u(t) \tag{27}$$

Note I obtained the same results for the crystal settling (equation (27)) and crystal suspended (the right equality in equation (22)) cases, although they originate from different mechanisms.

2.3.3 Magma replenishment rates

In this section, I discuss the modeling of the magma replenishment rate. I consider two basic models of replenishment. First, magma replenishment occurs with a constant velocity for a certain time period t_f. Thus, the replenishment rate is expressed as

$$\begin{aligned} u(t) &= u_0 \qquad 0 \le t_f \\ u(t) &= 0 \qquad t > t_f . \end{aligned} \tag{28}$$

In the second model, the velocity of replenishment is assumed to decay exponentially

$$u(t) = u_0 e^{-bt} \tag{29}$$

where u_0 is the initial velocity, b is the exponential factor.

2.4 Hydrothermal Systems

I assume that the total heat flux from the subsurface magma body is transferred to the base of the hydrothermal system through an impermeable conductive boundary layer with thickness $\delta(t)$. Then if $F_h(t)$ denotes the advective heat flux transported by the hydrothermal fluid, and A_d is the area of the discharge zone,

$$F_m(t) A_m(t) = F_h(t) A_d \tag{30}$$

The heat flux of the hydrothermal system is related to its temperature as

$$F_h(t) = \rho_f c_f u_d T_h(t) \tag{31}$$

where $T_h(t)$ denotes the temperature of hydrothermal system, ρ_f is the density and c_f is the specific heat of the fluid, and u_d is the Darcian upflow velocity. I assume that buoyancy drives circulation in a porous medium. For simplicity, I assume the temperature of the recharge zone is zero and the flow resistance is dominated by the discharge zone [*Lowell and Germanovich*, 2004]. Then the Darcian upflow velocity u_d is given by

$$u_d = \frac{\alpha_f g k T_h(t)}{v_f} \tag{32}$$

where α_f is the coefficient of the thermal expansion of fluid, k is the permeability, and v_f is the kinematic viscosity of fluid. Substituting equation (32) into (31) leads to

$$F_h(t) = \rho_f c_f \frac{\alpha_f g k}{v_f} T_h^2(t) \tag{33}$$

Hydrothermal and magmatic heat fluxes are linked to vent temperature by substituting equation (33) into equation (30). Therefore, the temperature of the hydrothermal temperature is obtained from

$$T_h(t) = \sqrt{\frac{F_m(t) A_m v_f}{\rho_f c_f \alpha_f g k A_d}} \tag{34}$$

Solving equation (7) is the key to determining all the system properties, including heat flux and temperature, etc. In the following chapters, I will show the equation (7) can be simplified to a first-order non-linear ordinary differential equation in terms of the magma temperature as a function of time. A MATLAB program (Appendix A) is developed to solve for the magma temperature. To determine the first-order derivative of temperature, the finite difference approximation is applied by using Euler method. Once

the magma temperature is solved, other quantities are available through their relationship to the magma temperature.

This chapter describes a general framework for mathematical modeling of the hydrothermal system driven by magma convection. Chapters 3, 4, 5, and 6 discuss different magma systems. Although each chapter follows the same framework as in this chapter, each is written as an individual paper. Chapter 3 has been published in the Journal of Geophysical Research. Chapter 4 has been submitted to Geophysical Journal International. Chapters 5 and 6 will be submitted soon.

2.5 References

Brandeis G., and C. Jaupart (1986). On the interaction between convection and crystallization in cooling magma chambers, *Earth Planet. Sci. Lett.*, *77*, 345-361.

Hort, M. (1997). Cooling and crystallization in sheet-like magma bodies revisited, *J. Volcanol. Geotherm. Res.*, *76*, 297-317.

Huppert, H.E. and R.S.J. Sparks (1988). The generation of granitic magmas by intrusion of basalt into continental crust, *J. Petrol.*, *29*, 599-624.

Huppert, H.E. and J.S. Turner (1991). Comments on "On convective style and vigor in sheet-like magma chambers" by Bruce D. Marsh, *J. Petrol.*, *32*, 851-854.

Jarvis, G.T. and W.R. Peltier (1989). Convection models and geophysical observations, in *Mantle Convection*: *Plate Tectonics and Global Dynamics*, ed. W. R. Peltier, Gordon and Breach Science Publishers, 479-595.

Jaupart, C. and S. Tait (1995). Dynamics of differentiation in magma reservoirs, *J. Geophys. Res.*, *100*, 17,615-17,636.

Jellinek, A.M. and R.C. Kerr (1999). Mixing and compositional stratification produced by natural convection. Part 2. Applications to the differentiation of basaltic and silicic magma chambers and komatiite lava flows, *J. Geophys. Res.*, *104*, 7203-7218.

Kent, G.M., A.J. Harding, and J.A. Orcutt (1990). Evidence for a smaller magma chamber beneath the East Pacific Rise at 9º30´N, *Nature*, *344*, 650-652.

Lowell, R.P. and L.N. Germanovich (2004). Seafloor hydrothermal processes: Results from scale analysis and single-Pass models, in *Mid-Ocean Ridges*: *Hydrothermal Interactions Between the Lithosphere and Oceans, Geophys. Monogr. Ser.*, *148*, ed. by C. R. German, J. Lin and L. M. Parson, pp. 219-244, AGU, Washington, D.C.

MacLeod, C.J. and G. Yaouancq (2000). A fossil melt lens in the Oman ophiolite: Implications for magma chamber processes at fast spreading ridges, *Earth Planet. Sci. Lett.*, *176*, 357-373.

Martin, D. (1990). Crystal settling and in situ crystallization in aqueous solutions and magma chambers, *Earth Planet. Sci. Lett.*, *96*, 336-348.

Martin, D. and R. Nokes (1988). Crystal settling in a vigorously convecting magma chamber, *Nature*, *332*, 534-536.

Turner, J.S. (1973). *Buoyancy effects in fluids*, Cambridge University Press, London.

Worster, M.G., H.E. Huppert, and R.S.J. Sparks (1990). Convection and crystallization in magma cooled from above, *Earth Planet. Sci. Lett.*, *101*, 78-89.

CHAPTER 3. MODELS OF HYDROTHERMAL HEAT OUTPUT FROM A CONVECTING, CRYSTALLIZING, REPLENISHED MAGMA CHAMBER BENEATH AN OCEANIC SPREADING CENTER[1]

Abstract

The temperature and heat output of hydrothermal systems at oceanic spreading centers place strong constraints on the mechanism of heat transfer in oceanic crust. In this paper, we investigate time-dependent heat transfer from a vigorously convecting, crystallizing, and replenished magmatic sill beneath an ocean ridge axis and an overlying hydrothermal system. We first consider two different crystallization scenarios: crystals-suspended and crystals-settling, coupled with crystallinity-dependent and temperature-dependent magma viscosity. The large-scale convection is assumed to rapidly homogenize the magma, resulting in a characteristic temperature T_m. In cases without magma replenishment, the simulation results for crystals-suspended models show that heat output and the hydrothermal temperature decrease rapidly and crystallinity reaches 60% in less than ten years. In crystals-settling models, magma convection may last for decades, but decreasing heat output and hydrothermal temperatures still occur on decadal timescales. When magma replenishment is included, the magmatic heat flux approaches

[1]The material is essentially reproduced from Liu, L. and R.P. Lowell (2009). Models of hydrothermal heat output from a convecting, crystallizing, replenished magma chamber beneath an oceanic spreading center, *J. Geophys. Res.*, 114, B02102, doi:10.1029/ 2008JB005846.

steady state on decadal timescales, while the magma body grows to double its original size. The rate of magma replenishment needed ranges between 5 x 10^5 and 5 x 10^6 m^3/yr, which is somewhat faster than required for seafloor spreading, but less than fluxes to some terrestrial volcanoes on similar timescales. The heat output from a convecting, crystallizing, replenished magma body that is needed to drive observed high-temperature hydrothermal systems is consistent, with gabbro glacier models of crustal production at mid-ocean ridges.

3.1 Introduction

Hydrothermal systems at oceanic spreading centers are closely linked to magmatism. At nearly all sites of observed high-temperature venting, seismic reflection data shows the presence of shallow subsurface magma bodies beneath active hydrothermal systems regardless of spreading rate [e.g., *Detrick et al.*, 1987; *Collier and Sinha*, 1990; *Canales et al.*, 2006; *Singh et al.*, 2006; *Van Ark et al.*, 2007]. Even at the TAG hydrothermal system at the slow spreading Mid-Atlantic Ridge where no shallow or mid-crustal magma has been detected, the presence of deeper magmatic sources has not been ruled out [*Canales et al.*, 2007]. At the ultra-slow spreading Gakkel Ridge, hydrothermal activity also appears to be associated with recent volcanism [*Michael et al.*, 2003; *Baker et al.*, 2004*a*]. More importantly, recent evidence suggest the properties of subaxial magma lenses vary along the ridge axis and that high-temperature venting lies above regions with high liquid fraction [*Singh et al.,* 1999; *Canales et al.*, 2006]. Moreover, at the fast-spreading East Pacific Rise near 9°50′N, where eruptions occurred in 1991 [*Haymon et al.*, 1993] and again in late 2005/early 2006 [*Rubin et al.*, 2006; *Soule et al.,* 2007], there is evidence of non-eruptive magmatic activity as suggested by vent chemistry [e.g., *Von Damm*, 2004] and changes in the permeability structure [e.g., *Sohn et al.*, 1998; *Scheirer et al.*, 2006] that may be related to magmatism [e.g., *Ramondenc et al*., 2008].

Most models of hydrothermal circulation are coupled to magmatic processes

only loosely. In the most common situation, the temperature is fixed at the bottom. This condition assumes that magma serves as an infinite reservoir of heat and heat transport is controlled by the vigor of the hydrothermal system, which is characterized by the Rayleigh number *Ra* [e.g., *Bejan*, 1995; *Lowell and Germanovich*, 2004]. On the other hand, if a constant heat flux is assumed at the base of the hydrothermal system, then hydrothermal heat output is controlled by the rate at which the heat is conducted from the magma body [e.g., *Lowell and Germanovich*, 1994, 2004; *Germanovich et al.*, 2000, 2001]. Neither of these boundary conditions is realistic because heat transfer from a convecting magma body near its liquidus will cause magma to cool and crystallize [e.g., *Cann and Strens*, 1982; *Lowell and Rona*, 1985].

The hydrothermal models of *Lowell and Burnell* [1991] and *Lowell and Germanovich* 1994] considered heat transfer from a crystallizing magma body. These assumed that crystallization occurred at the roof of the magma chamber. As the frozen layer grew downward, heat loss from the magma decreased with time as $t^{-1/2}$ resulting in an analogous decline in hydrothermal heat output and vent temperature. Although hydrothermal heat loss following diking events such as occurred at Co-Axial in 1993 or at Axial Volcano in 1998 may decay faster than $t^{-1/2}$ [*Baker et al.*, 2004*b*], hydrothermal systems driven by sub-axial magma chambers often exhibit relatively stable vent temperatures and vent fluid chemistry on decadal time scales [*Campbell et al.*, 1988; *Von Damm et al.*, 2002]. Although time series data on hydrothermal heat output are limited, heat output is generally assumed to be stable as well. The data suggest that ridge crest

hydrothermal systems typically transport between 10^8 and 10^9 Watts of heat [*Ramondenc et al.*, 2006; *Baker*, 2007].

Lowell and Germanovich [1994] and *Humphris and Cann* [2000] suggested that magma inputs at rates similar to those observed on terrestrial volcanoes could help maintain steady hydrothermal heat output. These results were not linked to quantitative models of magma convection and crystallization, however.

The observations of quasi-steady state hydrothermal heat output and vent temperature, which aren't adequately predicted by current magma-hydrothermal models, argue for models that investigate different ways to link magmatic processes and hydrothermal circulation. In the following section of this paper, we discuss models of magma convection that may be more appropriate representations of the magmatic-hydrothermal coupling. In section 3.3, we formulate the mathematical model for magma chamber convection with and without replenishment. In section 3.4, we present the results of the numerical simulations; and in section 3.5, we discuss the implications of the modeling results.

3.2 Magma Convection and Crystallization

The dynamics of cooling, crystallizing magma chambers has long been a subject of scientific interest [e.g., *Lovering*, 1955; *Jaeger*, 1968; *McBirney and Noyes*, 1979; *Irvine*, 1980]. Because the density and chemical composition of the crystals are generally different from that of the liquid, crystallization often results in convective transport and

chemical differentiation within the magma body. The role of convection on nucleation, growth, and the redistribution of crystals in magma chambers has been a matter of some debate. Although *Brandeis and Jaupart* [1986] and *Marsh* [1989] have argued that convection is weak or absent, the more common view is that convection is vigorous [e.g., *Huppert and Sparks*, 1988; *Martin and Nokes*, 1988, *Worster et al.*, 1990, *Kerr*, 1994].

Convection in magma chambers results from two different driving forces: thermal convection and compositional convection. Thermal convection results from cooling of the magma as heat is transported to the surrounding country rock. Compositional convection results from buoyancy-driven density differences that stem from injection of a new composition into a chamber, partial melting, or fractional crystallization.

The detailed dynamics of a crystallizing magma body is extremely complex. Crystals may nucleate at the roof, near the floor or within the interior of the magma body, and the rate at which crystals settle depends upon the rate of cooling, the density of the particles, and the viscosity of the magma. *Huppert and Sparks* [1988] assumed that crystals formed in the interior of the magma chamber, were small, and remained suspended as a result of vigorous by convection. This assumption is counter to traditional models in which crystals settle and accumulate on the floor [*Martin*, 1990; *Martin and Nokes*, 1989; *Worster et al*., 1990]. *Jellinek et al*. [1999] and *Jellinek and Kerr* [1999] investigate convection and magma mixing in laboratory experiments and *Jellinek and Kerr* [2001] applied these results to convection and crystallization within the Kilauea Iki lava lake. In these papers, magma replenishment has been neglected, and cooling is

assumed to occur as a result of thermal conduction to the country rock. Magma convection models that include replenishment have focused on cases in which the entering magma has significantly different composition than the magma in place [e.g., *Huppert and Sparks*, 1981; *Huppert et al.*, 1986; *Snyder and Tait*, 1995]. Such models are not directly relevant to mid-ocean ridge settings.

In this paper, we seek to address the linkages between hydrothermal heat output and heat transfer from a cooling, crystallizing, replenished magma chamber beneath an oceanic spreading center. For this analysis we do not consider the detailed dynamics of magma chamber crystallization. Because the composition of mid-ocean ridge basalts is relatively homogenous locally [e.g., *Batiza and Niu*, 1992; *Perfit et al.*, 1994], we neglect the effects of compositional convection and magmatic differentiation and consider a model of magma thermal convection based on that of *Huppert and Sparks* [1988]. They considered heat transfer from a vigorously convecting basaltic magma chamber of thickness D emplaced into the cold continental crust and developed a simple heat balance to describe how the bulk temperature of the magma $T_m(t)$ decayed as heat was transferred across the roof as a result of high Rayleigh number convection. The focus of their model was to determine the extent of roof melting and convection within a growing silicic magma, while crystallization and cooling occur within the subjacent basaltic magma chamber.

Although we use *Huppert and Sparks* [1988] as a starting point, we consider several different scenarios. First, rather than investigating the effect of convective heat

transfer from the magma on heating the overlying rock, we link this heat transfer to the overlying hydrothermal circulation system. The upper boundary of the convecting magma is maintained at the solidus temperature T_s. Because the hydrothermal circulation rapidly removes heat from the crustal rocks, no induced melting occurs on the chamber roof. Second, in addition to considering the case in which crystals stay suspended in the magma, we also consider the end-member case in which crystallization occurs at the floor (or crystals settle rapidly to the base of the magma chamber). These two situations are both qualitatively and quantitatively different from earlier models [*Lowell and Rona*, 1985; *Lowell and Burnell*, 1991; *Lowell and Germanovich*, 2004], which assumed freezing proceeded downward from the roof. These models resulted in a rapidly thickening conductive thermal boundary layer and a rapid decay in hydrothermal heat output. If crystallization occurs at the base of the magma chamber or if the crystals rapidly settle there, the lower boundary layer grows with time, resulting in a decreasing depth of liquid magma with time. This assumption yields an estimate of the maximum lifetime of magma convection in the absence of replenishment, because convection in crystal-free magma maintains a lower viscosity. Third, because we find that magmatic heat flux and hydrothermal temperature still decay more quickly than observed, we investigate the role of magma replenishment in maintaining a quasi-steady heat output on decadal time scales.

3.3 The Mathematical Model

3.3.1 Basic system geometry and mathematical formulation

Seismic data from studies at several mid-ocean ridges show the presence of a thin mostly liquid lens of magma extending between ~ 0.5 and 4 km across the ridge axis and often for 10s of kilometers along the axis [e.g., *Detrick et al.*, 1987; *Sinton and Detrick*, 1992, *Collier and Sinha*, 1990; *Kent et al.*, 1990; *Singh et al.*, 2006; *Van Ark et al.*, 2007]. The magma lens is typically several tens of meters to perhaps ~ 100 m thick [*Kent et al*., 1990; *MacLeod and Yaoyancq*, 2000]. Heat is transferred by conduction between the magma and the overlying cold country rock. As shown by *Huppert and Sparks* [1988], *Martin and Nokes* [1989], *Huppert and Turner* [1991], *Worster et al.* [1990], *Jaupart and Tait* [1995] and *Jellinek and Kerr* [1999], such a magma body would undergo vigorous convection. The vigor of this convection is expressed by the dimensionless Rayleigh number *Ra*, must exceed a critical value $Ra_c \sim 10^3$. For a laterally extensive magma body of thickness *D*, *Ra* is

$$Ra = \frac{\alpha_m g D^3 \Delta T}{a_m v_m} \tag{1}$$

where α_m is the coefficient of thermal expansion, g is the acceleration due to gravity, a_m is the thermal diffusivity, v_m is the kinematic viscosity, and $\Delta T = T_m\,(t)\text{-}T_s$ is the difference between the average temperature of the convecting magma $T_m(t)$ and the solidus temperature of basalt T_s that defines the roof of the magma body, respectively. The subscript *m* refers to properties of the magma. Because magma is cooling and

crystallizing T_m is a function of time. The symbols used in this paper are listed in Table 3.1.

Table 3.1 Values of the physical parameters for hydrothermal vent fields

Physical meaning	Parameter	Value	Units
Latin symbols			
Area of magma replenishment	A_b		m^2
Area of hydrothermal discharge zone	A_d	10^3-10^4	m^2
Horizontal magma area in chamber	A_m	$<2\times10^6$	m^2
Initial magma chamber area	A_{m0}	10^6-10^7	m^2
Exponential factor	b	10^{-9}	S
Fluid specific heat	c_f	6×10^3	J /kg ºC
Magma specific heat	c_m	1400	J /kg ºC
Magma chamber depth	D	100	M
Liquid magma thickness	D_m		M
Crystal magma layer thickness	D_s		M
Heat flux added by conductivity	F_c		W/m^2
Heat flux carried by the hydrothermal fluid	F_h		W/m^2
Magmatic heat flux	F_m		W/m^2
Heat flux added by magma replenishment	F_r		W/m^2
Acceleration due to gravity	g	9.81	m/s^2
Permeability	k	10^{-11}-10^{-13}	m^2
Latent heat of crystallization of magma	L	4.2×10^5	J/kg
Nusselt number	Nu		-
Rayleigh number	Ra		-
The critical Rayleigh number	Ra_c	$\sim10^3$	-
Replenishment final time	t_f		s
Mean magma temperature	T_m		ºC
Hydrothermal temperature	T_h	250-400	ºC
Basalt liquidus temperature	T_L	1200	ºC
Basalt solidus temperature	T_S	1030	ºC
Darcian velocity	u_d		m/s
Replenishment rate	u		m/s
Volume of magma	V_m		m^3
Volume of crystals	V_s		m^3

Greek symbols			
Thermal expansion coefficient of magma	α_m	5×10^{-5}	$^oC^{-1}$
Thermal expansion coefficient of fluid	α_f	10^{-3}	$^oC^{-1}$
Conduction boundary layer thickness	δ		m
Thermal diffusivity	κ	8×10^{-7}	m^2/s
Thermal conductivity of magma	λ_m	2	Wm/ ^oC
Thermal conductivity of rock	λ_r	2	Wm/ ^oC
Kinematic viscosity of magma	ν_m		m^2/s
Kinematic viscosity of magma at liquidus	ν_{m0}	0.1	m^2/s
Kinematic viscosity of fluid	ν_f	10^{-7}	m^2/s
Density of magma	ρ_m	2.7×10^3	kg/m^3
Density of fluid	ρ_f	10^3	kg/m^3
Volume fraction of crystals	χ		-
Critical crystal fraction	χ_c	60%	-

In nearly all cases, Ra is much greater than the critical value of 10^3. For ΔT = 100°C, D = 100 m, and the other parameters in Table 3.1, $Ra \sim 10^{11}$; for $D \sim 10$ m and $\Delta T \sim 1$°C, then $Ra \sim 10^6$. Therefore, following *Huppert and Sparks* [1988], the heat flux $F_m(t)$ transferred from the convecting magma body can be expressed in terms of the Nusselt number Nu and the classical relationship between Nu and Ra [e.g., *Jarvis and Peltier*, 1989],

$$F_m(t) = \frac{\lambda_m (T_m(t) - T_s)}{D} Nu$$
$$Nu \approx (Ra / Ra_c)^{1/3} \qquad (2)$$

where λ_m is the thermal conductivity of magma. Substituting equation (1) into equation (2) yields the heat flux transferred as a result of convection in the magma chamber [*Turner*, 1973]

$$F_m(t) = \rho_m c_m J (T_m(t) - T_S)^{4/3} \quad (3)$$

where $J = 0.1(\alpha_m g a_m{}^2 / \nu_m)^{1/3}$, and $a_m = \lambda_m / \rho_m c_m$. As a result of heat flux $F_m(t)$ transferred through the top boundary of area A_m, the magma body cools and crystals begins to form.

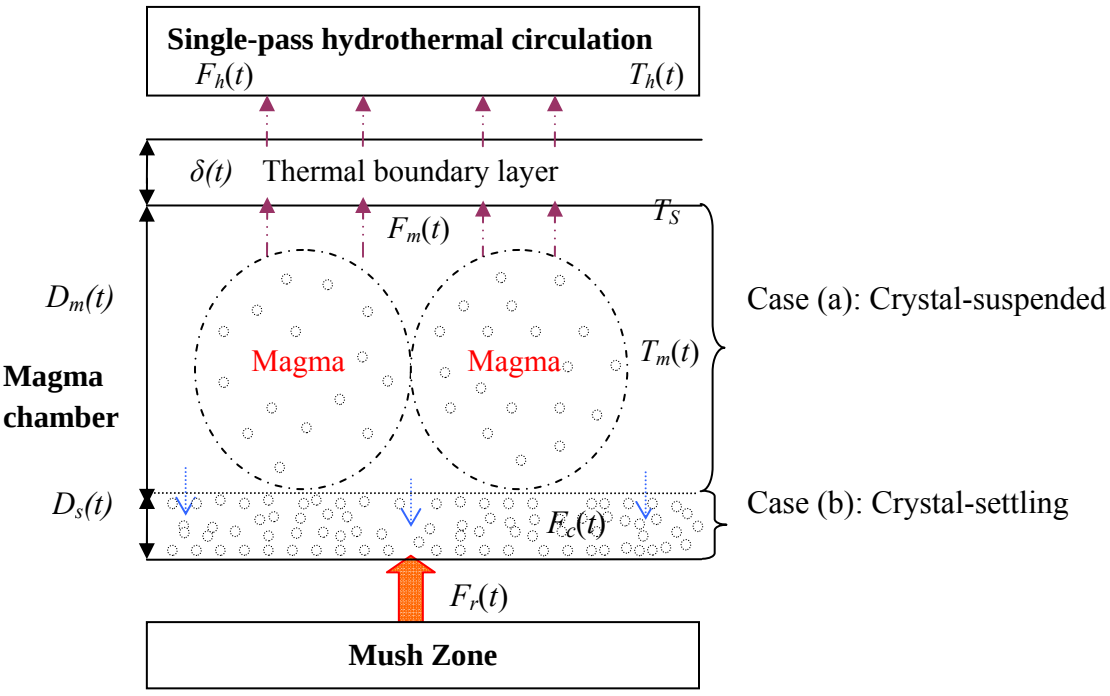

Figure 3.1 Schematic of magma convection model with thickness D_m and mean temperature T_m. Turbulent magma convection provides heat flux F_m to power the overlying hydrothermal system at a temperature T_h and heat flux F_h. The top of the magma chamber is maintained at its solidus T_s and heat from the magma to the hydrothermal system is transported across a conductive boundary layer of thickness δ. The underlying mush zone provides a source of magma and heat flux to the magma chamber. (a) depicts the situation with crystals suspended and (b) depicts the situation with crystals settling. [modified from *Lowell et al.*, 2008]

In this paper, we assume that the total heat flux from the magma chamber $F_m(t)A_m$ is transported across a conductive boundary layer $\delta(t)$, where it is taken up by a

convecting hydrothermal system. Figure 3.1 depicts the basic model geometry consisting of: a layer of vigorously convecting basaltic magma underlying a hydrothermal system. In the hydrothermal circulation system, cold seawater penetrates the oceanic crust, where it is heated to a temperature T_h. The buoyant fluid then rises rapidly and discharges into the ocean through a hydrothermal vent field of area A_d.

Following [*Lowell and Germanovich*, 2004], we link heat transfer from magma to the heat transfer by the hydrothermal circulation through a heat balance equation

$$F_m(t)A_m = \lambda_r \frac{T_S - T_h(t)}{\delta(t)} A_m = F_h(t)A_d \tag{4}$$

where λ_r is the thermal conductivity of rock and $F_h(t)$ is the advective heat flux transported by the hydrothermal fluid. Equation (4) simply states that the heat conducted from the turbulently convecting magma body into the base of the hydrothermal system equals the heat transported to the top of the discharge zone A_d by hydrothermal advection.

For a hydrothermal system venting at temperature $T_h(t)$, the heat flux is

$$F_h(t) = \rho_f c_f u_d T_h(t) \tag{5}$$

where ρ_f is the density and c_f is the specific heat of the fluid, and u_d is the Darcian upflow velocity. We assume buoyancy driven flow; and for simplicity, we assume the temperature of the recharge zone temperature is zero and the flow resistance is dominated by the discharge zone [*Lowell and Germanovich*, 2004]. Then u_d is given by

$$u_d = \frac{\alpha_f g k T_h(t)}{\nu_f} \tag{6}$$

where α_f is the coefficient of the thermal expansion of fluid, k is the permeability, and ν_f

is the kinematic viscosity of fluid. In equation (6), we recognize that the permeability may be a function of time. Substituting equation (6) into (5) leads to

$$F_h(t) = \rho_f c_f \frac{\alpha_f g k}{\nu_f} T_h^2(t) \tag{7}$$

Hydrothermal and magmatic heat fluxes are linked to vent temperature by substituting equation (7) into equation (4).

3.3.2 The heat balance for a convecting, crystallizing, replenished magma chamber

The heat content $H(t)$ of a volume of magma $V(t) = A_m(t)D(t)$ is

$$H(t) = V(t)[\rho_m c_m T_m\ (t) + \rho_m (1 - \chi(T_m(t))L] \tag{8}$$

where L is the latent heat of the crystallization of the magma and $\chi(T_m(t))$ is the volume fraction of crystals at temperature $T_m(t)$, respectively. The first term on the right-hand side of equation (8) represents sensible heat per unit volume of magma, and the second term represents the latent heat yet to be released as crystallization occurs. For simplicity, we neglect the slight difference in density between liquid and crystals, and the volume decrease that occurs as a result of crystallization. Conservation of energy requires that

$$\frac{dH(t)}{dt} = -F_m(t)A_m(t) + F_r(t) + F_c(t)A_m(t) \tag{9}$$

where $F_r(t)$ is the rate at which heat is added to the magma chamber as a result of replenishment and $F_c(t)$ is the rate at which heat is conducted into the magma from below. Substituting equation (8) into equation (9) yields

$$\frac{dV_m(t)}{dt}[\rho_m c_m T_m(t) + \rho_m(1-\chi(T_m(t))L] + V_m(t)\frac{d}{dt}[\rho_m c_m T_m(t) + \rho_m(1-\chi(T_m(t))L] \tag{10}$$

$$= -F_m A_m(t) + F_r(t) + F_c(t)A_m(t)$$

Using equation (10), we consider four different scenarios. First we consider the case in which magma replenishment is absent. Within this scenario, we consider two member situations: (a) crystals remain suspended with the liquid magma as it crystallizes or (b) crystallization occurs at the floor of the magma chamber or crystals instantly settle there (Figure 3.1). For simplicity we refer to these two cases as "crystals suspended" and as "crystals settling", respectively. The real situation probably lies between these extremes, and some crystals may grow from the roof. We neglect this effect because we wish to diminish the rate at which a conductive thermal boundary layer may grow at the top of the magma chamber. Then we consider the case in which magma replenishment occurs, and again we consider the two cases of "crystals suspended" and "crystals settling".

In order to solve equation (10), we need expressions for $\chi(T_m(t))$, the magma viscosity $\nu_m(T_m(t))$, and a number of other parameters. One commonly used expression assumes χ varies linearly with temperature between the liquidus and solidus temperature [*Hort*, 1997]. That is:

$$\chi(T_m(t)) = \frac{T_L - T_m(t)}{T_L - T_s} \tag{11}$$

Huppert and Sparks [1988], relate χ to magma temperature through the formula

$$\chi\big(T_m(t)\big) = \frac{7200}{T_m(t)} - 6 \tag{12}$$

Equation (12) yields a liquidus temperature of 1200°C, a solidus temperature of 1030°C; the temperature at which crystallinity reaches 60% is 1091°C. This analytical expression is displaced toward slightly lower temperatures, but it exhibits a similar χ-T trend to that calculated by MELTS [*Ghiorso and Sack*, 1995; *Asimow and Ghiorso*, 1998] for a standard dry MORB. Because the solidus temperature in (12) is greater than for MORB, equation (12) slightly overestimates the amount of latent heat released during crystallization. Equation (11) gives a slightly higher temperature at which χ = 60%, resulting in a shorter lifetime for the convecting system [*Liu*, 2007]. Having an analytical expression for the χ-T relationship is useful for the mathematical analysis developed here. We use equation (12) for the computations in this paper because it is a good approximation to the χ-T relationship for basalt.

In equation (3), heat flux $F_m(t)$ depends upon magma viscosity, which is mainly dependent on the crystal content of the magma [*Roscoe*, 1952*; Lejeune and Richet*, 1995]:

$$\nu_m = \nu_{m0}(1-\chi/\chi_c)^{-n} \tag{13}$$

where n is a constant, and χ_c is the critical crystal fraction beyond which the flow is prevented (i.e., $\nu = \infty$). In this formulation we neglect the dependency of viscosity on temperature as well as non-Newtonian rheology that occurs when crystal content reaches about 40% [*Lejeune and Richet*, 1995]. As the temperature $T_m(t)$ decreases and the crystal content increases according to equation (12), magma viscosity increases. Empirical data suggest χ_c = 60% and n = 2.5 [*Shaw*, 1980; *Marsh*, 1981; *Lejeune and Richet*, 1995]. For crystal-free basalt $\nu_{m0} \approx 0.1$ m^2/s, equation (13) becomes

$$\nu_m = 0.1(1 - 1.67\chi)^{-2.5} \tag{14}$$

The relationship between magma viscosity and crystal content is shown in Figure 3.2. As crystallinity increases, the viscosity increases moderately at first; but when crystal content reaches ~ 60%, the viscosity increases so rapidly over a short range of crystallinity that the magma behaves essentially as a solid. Because $Ra \to 0$ as $\nu_m \to \infty$, we cease the calculations when $\chi(T_m(t) = 60\%$.

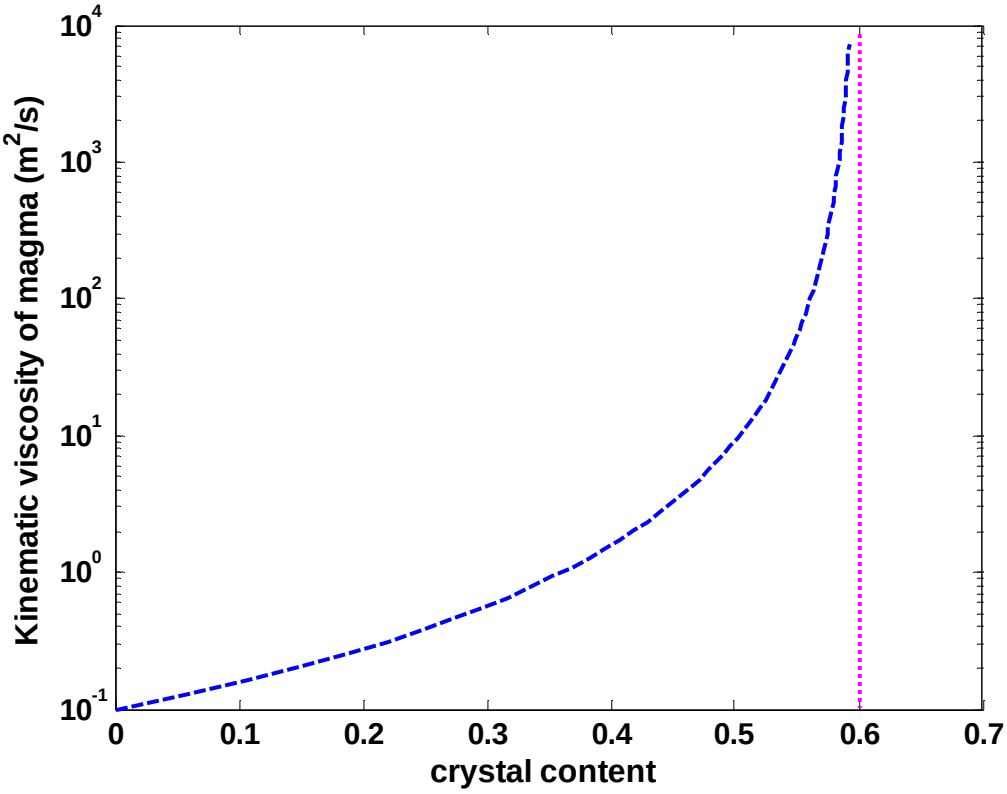

Figure 3.2 The relationship between magma viscosity and crystal content from equation (14), showing the rapid increase in magma viscosity as crystal content reaches 60%.

In models which assume crystal settling, the magma is assumed to be crystal free as it cools. For these models we assume

$$v_m = v_{m0}(T_L / T_m(t))^{8.5} \tag{14a}$$

Equation (14a) gives an increase in the viscosity of a factor of 3 as magma cools from 1,200°C to 1,050°C. This equation gives a reasonable fit to the data for dry basaltic magma given in *Spera* [2000]. Then *Ra* decreases as the thickness of the magma layer *D* and the temperature difference ΔT decrease. In principle, we stop the calculations when $Ra \sim 10^6$; however, in actual simulations we stop when the heat output becomes less than that observed in seafloor hydrothermal systems.

Equation (10) is solved numerically in conjunction with equations (3), (12) and (14) to obtain the total magmatic heat output $F_m(t)A_m$, which is then linked to hydrothermal heat output and vent temperature through equations (4) and (7), respectively. The other parameters needed in theses equations are given in Table 3.1. In particular, we use ρ_m = 2,700 kg/m^3 for basaltic magma [*Trial and Spera*, 1990; *Spera*, 2000], T_L = 1,200 °C [*Sinton and Detrick*, 1992], and T_s = 1,030 ºC. The shape and the size of the magma body are the most important parameters during heat transfer. For simplicity we consider a rectangular-shaped magmatic sill is considered with planar area A_m and thickness D ($D << A_m$). In this model, we assume D = 100 m, initially.

To estimate the area for heat extraction by a hydrothermal system, we note that axial magma chamber typically ranges between 0.5 and 4 km wide across the ridge axis [e.g., *Collier and Sinha*, 1990; *Kent et al.*, 1990; *Singh et al.*, 2006] while extending for

dozens of kilometers along the axis in some places [e.g., *Detrick et al*., 1987; *Van Ark et al.*, 2007; *Jacobs et al.*, 2007], and less than 10 km in others [e.g., *Canales et al.*, 2005; *Singh et al.*, 2006]. Vent field spacing along ridge axes is somewhat irregular. Along the Endeavour segment of the Juan de Fuca Ridge, vent fields are spaced approximately 2 km apart [e.g., *Kelley et al.*, 2002], but along other ridge segments vent fields may be spaced more closely or farther apart. As a reasonable estimate, we will assume that the hydrothermal circulation taps heat from an area of subsurface magma $A_m \sim 10^6$-10^7 m^2. In models with magma replenishment, either the area A_m or thickness D of the magma body may vary with time. The cases in which the area increases are described in the Appendix.

3.3.3 Magma convection without replenishment

3.3.3.1 Crystals suspended

If we assume that all the crystals are suspended within the interior of the magma then $V_m(t) = A_{m0}D_0$, is a constant. Because there is no replenishment, $F_r(t) = 0$ in equation (10). Upon taking the time derivative of the second term on the left hand side of equation (10), we obtain

$$\rho_m c_m D_0 \frac{dT_m}{dt} - \rho_m L D_0 \chi'\left(T_m(t)\right)\frac{dT_m}{dt} = -F_m(t) \qquad (15)$$

where $\chi'(T_m(t))$ is the derivative of χ with respect to T_m (from equation (12)), and $F_m(t)$ is given by equation (3), where ν is given by equation (14). Equation (15) is solved for $T_m(t)$ and the result is inserted into (4) to obtain the total heat flux from magma convection as a function of time.

3.3.3.2 Crystals settling

If crystallization occurs at the floor of the magma chamber or instantly settles there, then the volume of the magma chamber decreases as the thickness D decreases with time (Figure 3.1 case (b)). The volume of liquid magma $V_m(t)$ is the initial volume V_0 minus the volume of crystals formed V_s. Hence

$$\frac{dV_m}{dt} = A_m \frac{dD_m(t)}{dt} = -V_0 \frac{d\chi(t)}{dt} = -V_0 \frac{d\chi(T_m(t))}{dT_m} \frac{dT_m(t)}{dt} \tag{16}$$

As the magma chamber cools and crystals settle to the floor a temperature gradient may exist across the crystal layer resulting in conductive heat transfer from the growing crystal layer to the convecting liquid. The rate of conductive heat flux from the crystal pile back to the liquid magma is approximately

$$F_c = \lambda_m \frac{T_L - T_m(t)}{D_s(t)} \tag{16a}$$

where λ_m is the thermal conductivity of the frozen magma and $D_s(t) = \chi(T_m(t))D_0$ is the thickness of the crystal layer. By comparing results of simulations with and without the term given by equation (16a), it can be shown that this term exerts only a small effect on the thermal evolution of the magma chamber [*Liu*, 2007].

Substituting equations (16) into equation (10) and recognizing that $D_m(t) = D_0[1-\chi(T_m(t))]$, we obtain the result

$$\frac{dT_m}{dt} = \frac{F_m - F_c}{\rho_m D_0 \chi'\left(c_m T_m(t) + L(1-\chi(T_m(t))\right) + D_0 \rho_m [1-\chi(T_m(t))](\chi' L - c_m)} \tag{17}$$

Equation (17) is now solved with F_m given by equation (3), F_c given by equation (16a),

and ν_m given by equation (14a).

3.3.4 Magma convection with replenishment

During magma replenishment, additional heat and fluid mass is added to the magma chamber. As a result both the magma chamber volume and heat content increase with time. The increase in heat content is given by the factor $F_r(t)$ in equation (10). We will assume that additional magma is added at its liquidus through an area at the base of the magma $A_b(t)$ at a velocity $u(t)$. Again we consider the two cases: "crystals suspended" and "crystals settling". For simplicity we assume the magma entering the base of the magma chamber mixes rapidly with the existing magma so that a single temperature $T_m(t)$ can still be used to describe the convection system.

3.3.4.1 Crystals suspended

In this case the magma volume is

$$V(t) = V_0 + \int_0^t A_b(s)u(s)ds \tag{18}$$

For simplicity, we assume that the area of the magma remains constant and that magma replenishment occurs over the entire area A_m. Then

$$\frac{dV_m(t)}{dt} = A_m \frac{dD_m(t)}{dt} = A_m u(t) \tag{19}$$

We consider two different models of replenishment. In the first model, magma replenishment occurs at a constant velocity for a certain time period t_f, which corresponds to the time for the magma chamber to double in size or the magmatic heat flux to decay

to less than 10^7 Watts

$$\begin{aligned} u(t) &= u_0 \qquad 0 \le \mathrm{t_f} \\ u(t) &= 0 \qquad \mathrm{t} > t_f . \end{aligned} \tag{20}$$

The depth of the magma can be obtained by integrating equation (19) yielding:

$$D_m(t) = u_0 t + D_0 \tag{21}$$

In the second model, the velocity of replenishment is assumed to decay exponentially

$$u(t) = u_0 e^{-bt} \tag{22}$$

where u_0 is the initial velocity. Similarly, the depth of the magma is given by

$$D_m(t) = -\frac{u_0 \exp(-bt)}{b} + D_0 + \frac{u_0}{b} \tag{23}$$

The rate of heat input $F_r(t)$ is given by

$$F_r(t) = (\rho_m c_m T_L + \rho_m L) A_m u(t) \tag{24}$$

Substituting equations (18), (19), and (24) into equation (10) leads to the necessary equation for magma temperature:

$$\frac{dT_m}{dt} = \frac{F_m(t) - \rho_m u(t)\left(c_m\left(T_L - T_m(t)\right) + \chi\left(T_m(t)\right)L\right)}{D_m(t)\rho_m\left(\chi'\left(T_m(t)\right)L - c_m\right)} \tag{25}$$

where $D_m(t)$ is given by either equation (21) or (23).

3.3.4.2 Crystals settling

If crystals form on or instantly settle to the floor of the magma chamber, the magma volume is given by

$$V_m(t) = V_0 - V_s + \int_0^t A_b(s)u(s)ds \tag{26}$$

where V_s is the volume of crystals that have formed. Because we have no independent constraint on the surface area, we assume that $A_m(t) = A_{m0}$, a constant. Substituting $V_s = \chi/(1-\chi)V_m(t)$ into equation (26) then

$$\frac{1}{(1-\chi)}V_m = V_0 + A_{m0}\int_0^t u(s)ds \tag{27}$$

Substituting $V_m(t) = A_{m0}D_m(t)$ into (27) yields the result

$$D_m(t) = (1-\chi)\left[D_0 + \int_0^t u(s)ds\right] \tag{28}$$

The thickness of magma chamber is

$$D(t) = D_0 + \int_0^t u(s)ds \tag{28a}$$

and the rate at which the magma volume changes with time is

$$\begin{aligned}\frac{dV_m}{dt} &= A_{m0}\frac{dD_m(t)}{dt} = A_{m0}\left[-\chi' D_0\frac{dT_m}{dt} + (1-\chi)u(t) - \chi'\int_0^t u(s)ds\frac{dT_m}{dt}\right] \\ &= A_{m0}\left[-\left(D_0 + \int_0^t u(s)ds\right)\chi'\frac{dT_m}{dt} + (1-\chi)u(t)\right]\end{aligned} \tag{29}$$

Then upon substituting equations (16a), (24), (28) and (29) into equation (10) we obtain the equation for magma temperature:

$$\frac{dT_m}{dt} = \frac{F_m - F_c + \rho_m u(t)[(1-\chi)(c_m T_m + (1-\chi)L) - (c_m T_L + L)]}{\rho_m D(t)\chi'\left(c_m T_m(t) + L(1-\chi(T_m(t))\right) + D(t)\rho_m[1-\chi(T_m(t))](\chi' L - c_m)} \tag{30}$$

Simulations using equation (30) are run for set periods of time using the different replenishment velocities given by either equation (20) or (22). The simulation stops when $D(t)$ doubles.

3.4 Results

3.4.1 Magma convection without replenishment

Figure 3.3 shows total heat output $F_m(t)A_m$ from the convecting basaltic magma with two different values of A_m for "crystals suspended". The dotted lines located at 10^9 and 10^7 Watts denote the approximate range of total hydrothermal heat output measured in hydrothermal systems at oceanic spreading centers [*Ramondenc et al.*, 2006; *Baker*, 2007]. As the magma temperature drops, the crystallinity and viscosity increase (Figure 3.2), resulting in decreasing values of Ra and $F_m(t)$ with time. The simulation ceases when the crystal content reaches 60% and the viscosity become infinite. Figure 3.3 shows that magmatic heat output decreases rapidly within a ten-year period and the convective lifetime is less than 10 years. This results primarily from the decrease in Rayleigh number as the viscosity increases with crystallinity. Such a rapid decay may be appropriate for a system driven by a diking event, but it would not be expected for a system driven by an axial magma chamber. Area A_m plays a role in determining the total heat flux, but it has no influence on the lifetime of magma convection.

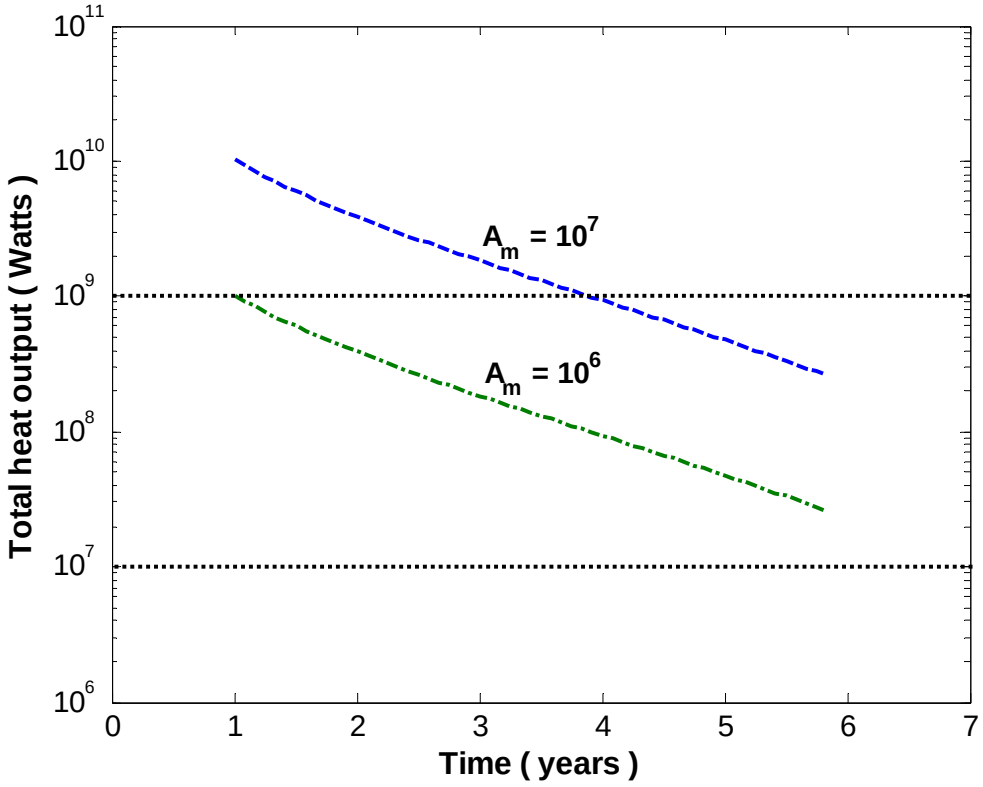

Figure 3.3 Total heat output from the convecting crystallizing magma for the crystals suspended model without magma replenishment. The dotted lines located at 10^9 Watts and 10^7 Watts denote the approximate range of total hydrothermal heat output measured at oceanic spreading centers.

Figure 3.4 shows the total heat output, for case "crystals settling". In comparison with Figure 3.3, Figure 3.4 shows that for the same value of A_m, the initial rate of heat loss from the convecting magma is greater for the "crystals settling" case; but the rate of decline heat loss is much slower in this case, and the convective lifetime of the magma body increases. For larger surface area A_m, the lifetime exceeds 80 years with a heat output of more than 10^7 Watts. Although in principle the simulation stops when *Ra*

decreases to 10^6, this limit is not reached within the 100 year timescale shown in Figure 3.4.

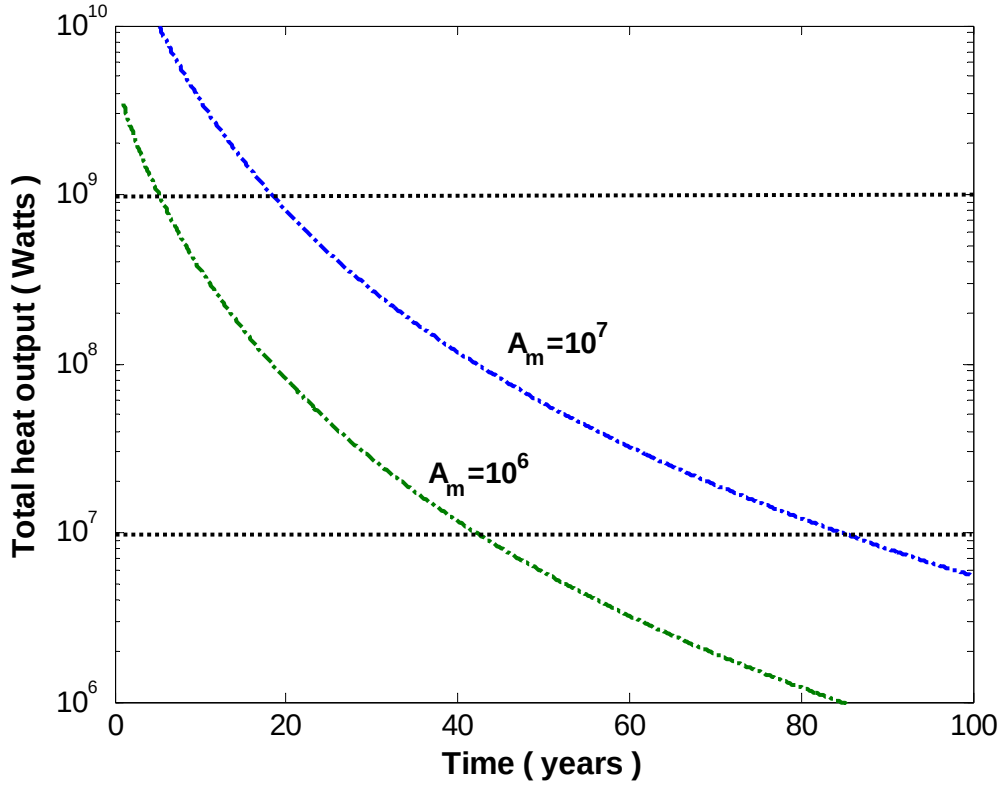

Figure 3.4 Same as Figure 3.3, except using the crystals settling model. In this case, the lifetime of magma convection increases significantly although heat output gradually declines below 10^7 Watts.

The principal difference between the models with crystals suspended and crystals settling stems from the role of viscosity. With crystals suspended, the rapid increase of viscosity with crystal content exerts the main control on *Ra* and the rate of heat loss from the magma chamber. With crystals settling, the viscosity of the liquid magma changes

slowly (equation (14a)), and only the gradual change in the thickness D and the temperature difference ΔT affect the Rayleigh number. In this case, even after 60% crystallization, $D \approx 40$ m and $Ra \sim 3 \times 10^9$. Although the magmatic heat loss decays more slowly in the case of crystals settling, and the overall lifetime increases, Figure 3.4 shows that heat output drops from 10^9 to 10^8 Watts in less than 2 decades. For systems with an initial heat output of $\sim 10^8$ Watts, the decay rate is significantly slower, and given the limited data available for hydrothermal systems, the crystal settling model may be reasonable (but see also section 3.4.2).

3.4.2 The behavior of the hydrothermal system

To further emphasize the implications of the heat output results shown in Figure 3.4 and Figure 3.5, Figure 3.6 shows the hydrothermal vent temperature as a function of time for different values of permeability k and magma area A_m, assuming a hydrothermal discharge area $A_d = 10^4$ m^2. Temperature $T_h = 250$ °C denotes the lower limit for observed black smoker vent temperatures. Equations (4) through (7) show that the hydrothermal heat flux is controlled by the magmatic heat flux from below The equations also show that for a given magma surface area A_m the hydrothermal temperature decreases with increases in permeability (or mass flux). These equations also show that there is a tradeoff between magma surface area and permeability as depicted in Figure 3.5 and Figure 3.6. Figure 3.5 shows that the temperature of the hydrothermal system drops very quickly during the brief lifetime of the system. Figure 3.6 shows that although the magma

convection system lasts for several decades, the hydrothermal temperature still drops rapidly on a decadal timescale. The most important feature of Figure 3.5 and Figure 3.6 is that without magma replenishment, hydrothermal temperature decreases significantly on decadal time scales, regardless of the values of the parameters A_m and k, and regardless of which magma convection model is assumed. For the simple hydrothermal models used here, the hydrothermal temperatures are much higher than typical black smoker temperatures in the initial stages of magmatic heat transport (Figure 3.5 and Figure 3.6). This is a result of the starting conditions in the magma which result in an extremely high initial thermal gradient and heat transfer rate since the magma is assumed to be instantly emplaced at time $t = 0$. This initial singularity does not strongly affect the later behavior of the system.

Such a rapid decay of a seafloor hydrothermal system is not commonly observed in long-lived systems that are driven by basalt magmatic heat sources; instead, the heat transport from the magma chamber sustains relatively steady venting temperatures and heat output. The basic model presented here suggests that magma convection alone may not be sufficient to maintain the high hydrothermal temperature and heat output for decadal timescales. The inconsistency between the above simulation results and the observations provides motivation for the development of magma convection models with replenishment.

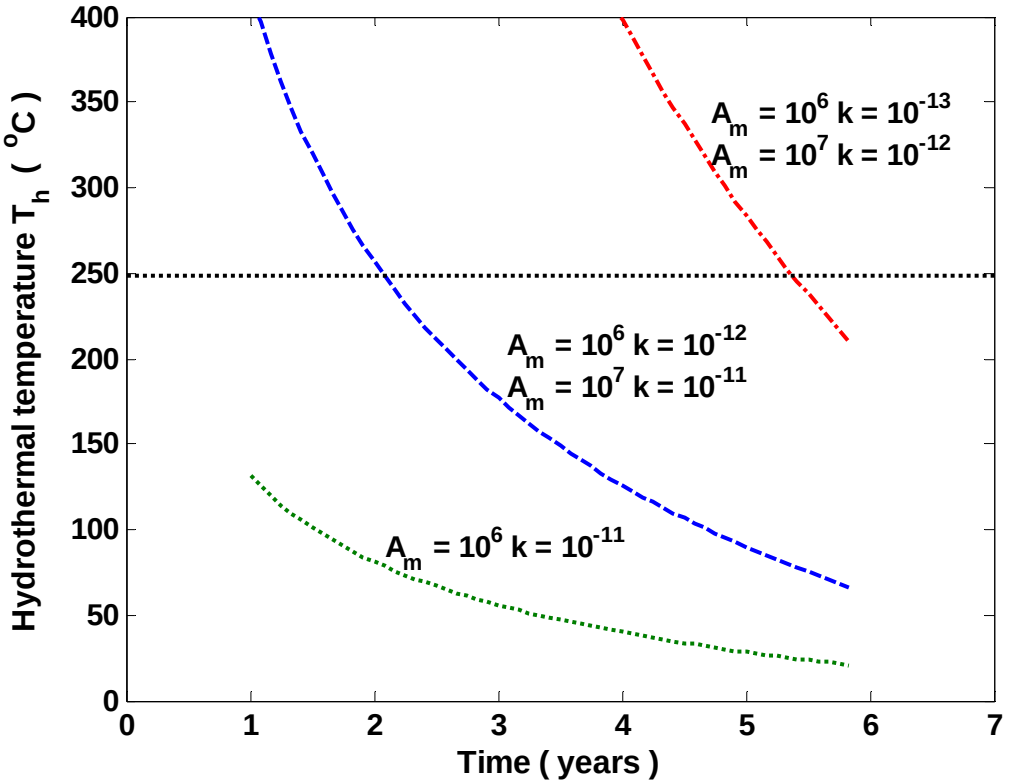

Figure 3.5 Hydrothermal temperatures as a function of time for the crystals suspended model for different values of permeability k and magma area A_m. The dotted line at T=250°C represents a lower limit for black-smoker venting.

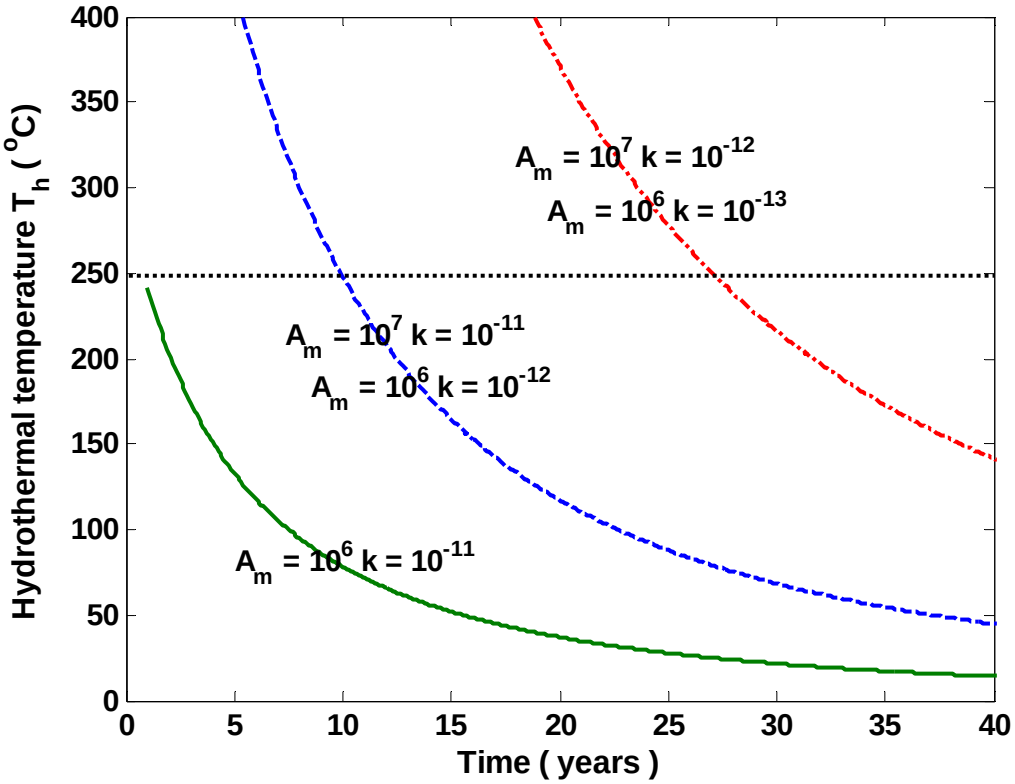

Figure 3.6 Same as Figure 3.5, except using the crystals settling model. Although magmatic convection lifetime is much longer, hydrothermal temperatures still decrease significantly on decadal timescales.

3.4.3 Magma replenishment

From the above simulations, we find that magmatic heat output decays significantly on decadal timescales. For the crystals settling model the rate of decay might not appear unreasonable, except that it is accompanied by a rapid decline in vent temperature as well. In the following subsections we investigate the effects of magma replenishment as a means of stabilizing magmatic and hydrothermal heat output.

3.4.3.1 Crystals suspended

First, we consider the case in which crystals are suspended in the crystallizing magma as described by equation (25). Figure 3.7 shows the total magmatic heat output over a range of replenishment velocities. The results show that for some range of replenishment velocity, magmatic heat output reaches an approximate steady state within the observed hydrothermal heat output limits. For these simulations, the magma area A_m = 10^6 m^2. Because the depth D_m is growing during replenishment, we stop the simulations when D_m doubles or when the heat output decreases to 10^7 Watts. For a velocity of 10^{-7} m/s, which is not shown, the depth of the magma chamber doubles within a few years. At a lower extreme (e.g. 10^{-9} m/s) heat output decreases below 10^7 Watts rather quickly.

The Appendix shows the analogous simulations when the depth of the magma chamber is held fixed and the area is assumed to increase as a result of replenishment. Figure A.1 shows that magmatic heat transfer is stabilized on decadal time scales for similar values of magma replenishment velocity. The lifetime of systems with area changing is shorter than for those in which the depth increases. This is because as the area increases the volume flux of magma increases with time (equations A.4 and A.6).

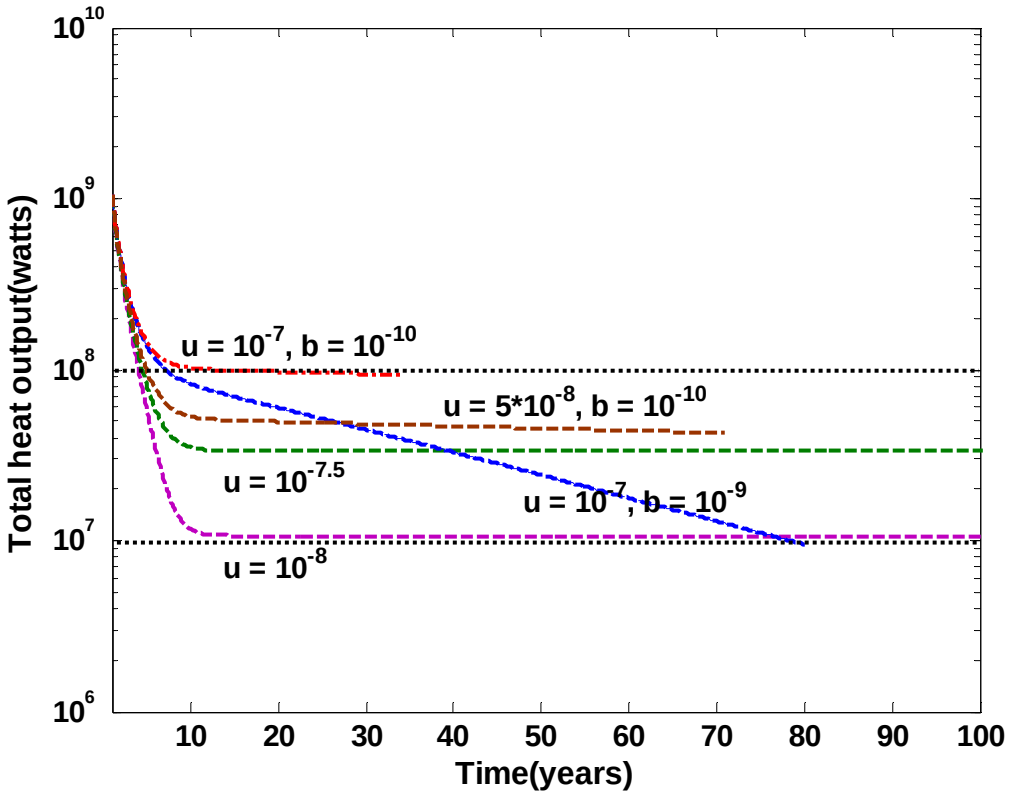

Figure 3.7 Total heat output as a function of time in the crystals suspended model for different values of constant or exponentially decaying magma replenishment velocity. Velocity u in m/s, b is the exponential factor. Simulations are run until magma depth D doubles from its initial value of 100 m, or until heat output decays to less than 10^7 Watts. Magma area is 10^6 m^2. Results show that u between 10^{-7} and 10^{-8} m/s tend to stabilize heat output on decadal timescales.

3.4.3.2 Crystals settling

Then we considered the case for crystals settling as described by equation (30), where $D(t)$ is given by (28a) and F_c is given by (16a). Figure 3.8 shows the total magmatic heat output for the same values of replenishment velocity shown in Figure 3.7. As in the case for crystals suspended, the heat output approaches steady state for certain

values of the replenishment velocity. In this model the area A_m is a constant value of 10^6 m^2. As for the prior case of crystals suspended, the simulations are run until the thickness $D(t)$ doubles or the heat output decreases to 10^7 Watts. As in the case for crystals suspended, replenishment velocities of ~ 10^{-7} – 10^{-8} m/s are needed to maintain quasi-steady state heat output on decadal time scales.

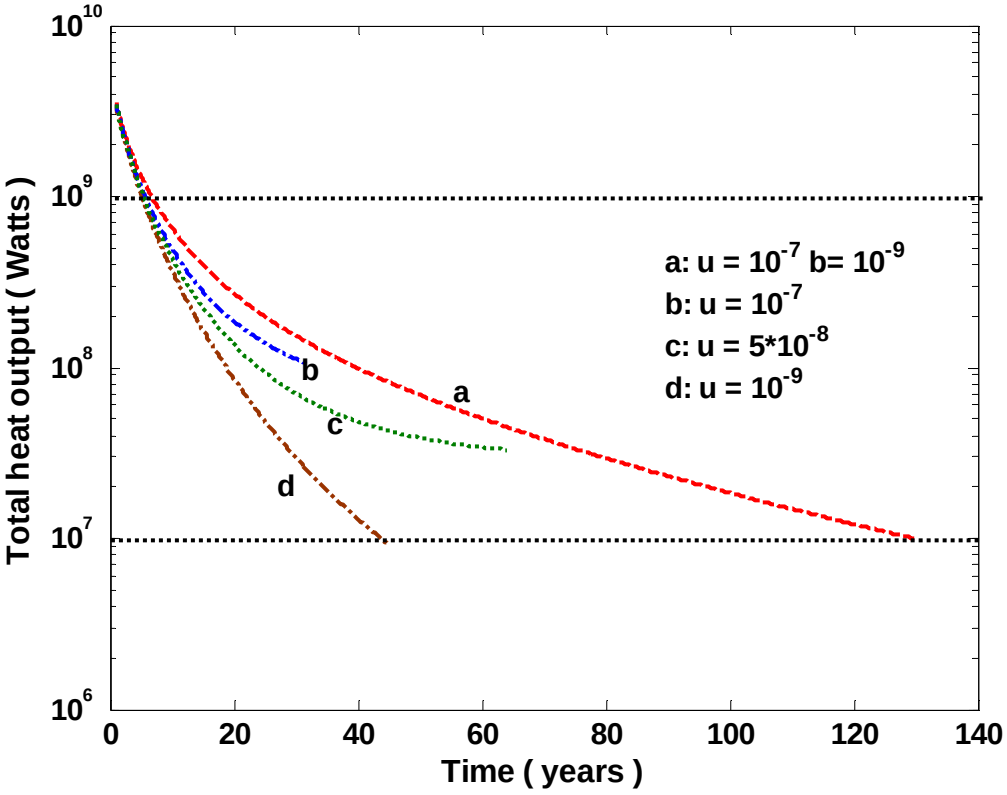

Figure 3.8 Total heat output as a function of time for the crystals settling model for a variety of magma replenishment velocities. As in Figure 3.7, simulations are run until the magma size doubles or heat output decreases to 10^7 W. Though heat output is decreasing, for u between 10^{-7} and 10^{-8} m/s, heat output is approximately constant on decadal timescales.

The Appendix shows the analogous simulations when the depth of the magma chamber is held fixed and the area is assumed to increase as a result of replenishment. Figure A.2 shows that magmatic heat transfer is stabilized on decadal time scales for similar values of magma replenishment velocity. Because the area increases in time (equations A.16 and A.17) in these simulations, the volume flux increases with time, resulting in a shorter doubling time than for cases in which the area is constant. .

3.5 Discussion

The results of the previous section show that heat output from a cooling, crystallizing, subaxial magma chamber undergoing vigorous convection at an ocean ridge axis decays on decadal timescales and is not able to maintain stable hydrothermal heat output and vent temperatures in the absence of replenishment. Models in which crystals grow on or rapidly settle to the floor giver more realistic results than models in which crystals stay suspended, however. After an initial transient period lasting a decade or more, models with magma replenishment yield quasi-steady state heat output on decadal timescales, provided the velocity of magma input is ~ 10^{-8} - 10^{-7} m/s.

The velocities needed to drive observed steady state hydrothermal heat fluxes correspond to magma volume fluxes ranging from 5 x 10^5 to 5 x 10^6 m^3/yr through an area of 1.5 km^2. The rates of magma replenishment at oceanic spreading centers are unknown, and magma replenishment rates in general volcanic settings are poorly constrained and vary widely [e.g. *Macleod and Tait*, 2000]. To place these fluxes in

perspective, however, consider that ~ 4 x 10^5 m^3/yr of magma is needed to produce 6 km of crust per km of ridge axis at a full spreading rate of 6 cm/yr; and ~10^8 m^3/yr of magma was supplied to Kilauea, Hawaii between 1956 and 1983 [*Dzurizin et al.*, 1984] and Krafla, Iceland between 1975 and 1981, respectively [see *Humphris and Cann*, 2000]. Hence the replenishment rates determined from the models presented here are similar to, or perhaps 10 times larger, than needed for crustal production, but are significantly smaller than occurs at some active volcanoes on decade time scales. Because crustal production rates are not expected to be steady on the time scales corresponding to changing occurring in the magma chamber, magma replenishment on decadal time scales at rates that are greater than needed for steady crustal production are not unreasonable. If the replenishment rates determined from our models are approximately correct, the lower values of replenishment to the magma lens are approximately the same as required for generation of the entire thickness of the oceanic crust. This result suggests that crustal formation under the gabbro glacier model [*Henstock et al.*, 1993; *Morgan and Chen*, 1993] is consistent with observed values of hydrothermal heat output. Further work is needed to confirm this idea, however.

Although the replenishment velocities needed to maintain stable heat output for the different models in Figure 3.7 and Figure 3.8, Figure 3.A.1, and Figure 3.A.2 are similar, there are several differences between the replenishment models in detail. In the models in which the magma surface area grows with time, the volumetric rate of magma replenishment increases with time and heat flux increases slightly with time (Figure 3.A.1

and Figure 3.A.2). In the models in which the surface area is fixed, heat output tends to decrease with time even with replenishment (Figure 3.7 and Figure 3.8). Moreover, because the volumetric magma flux is greater in models in which the area increases than in the models in which the depth increases, the time to doubling the magma volume is much shorter in the former case. Although heat output changes in time in all models shown in Figure 3.7, Figure 3.8, Figure 3.A.1 and Figure 3.A.2, changes occur on a long enough time scale that they might not be noticed with the present limited data from hydrothermal systems.

Although the replenishment velocities needed in the model to yield quasi-steady state heat output appear to be reasonable for decadal time scales, they cannot be maintained for geologic times. Because sections of ocean ridges axes are devoid of significant hydrothermal activity while other sections are active, even at fast spreading rates, the model results suggest that some regions of the ridge crest are undergoing more rapid rates of magma input than others. This result is consistent with recent seismic data suggesting that hydrothermal activity is associated with the most liquid regions of subsurface magma [*Singh et al.*, 1999; *Canales et al.*, 2006]. Given the rapid rate of crystallization shown by our calculations, this observation is consistent with frequent replenishment coupled with the crystals settling model during episodes of vigorous high-temperature hydrothermal circulation. Our results are also consistent with observations at EPR 9°50′N, which suggest magma replenishment occurred between the eruptive events of 1991 and 2005/2006 [*Von Damm*, 2004; *Scheirer et al.*, 2006]. Even at slow spreading

ridges, where magma supply is generally lower, high temperature, high heat output hydrothermal systems are likely driven by frequently replenished magma chambers [*Lowell*, 2008]. *Humphris and Cann* [2000] have also argued that the TAG hydrothermal system on the Mid-Atlantic Ridge is powered by a replenished magma chamber. If the TAG hydrothermal system is driven by magmatic heat, the magma chamber must lie deep in the crust or in the upper mantle, however [*Canales et al.*, 2007].

According to our models, magma chamber replenishment eventually yields quasi-steady state heat output in both the crystals suspended and the crystals settling models. Erupted lavas typically contain few phenocrysts [e.g., *Bryan*, 1983]; however, so from a petrological point of view, the crystals settling model appears to be more appropriate. Moreover, between the 1991/1992 and 2005/2006 eruption episodes, the magma chamber beneath EPR 9°50′ N cooled by approximately 30°C [*Soule et al.*, 2007]. Figure 3.9 and Figure 3.A.3 show that models with crystals suspended cool by approximately 30°C within the first few years, then maintain a nearly constant temperature. On the other hand, Figure 3.9 and Figure 3.A.3 show that a similar decrease in magma temperature also occurs in the crystals settling models but over 15-20 year time frames. Although both models show similar temperature decreases, we prefer the crystals settling model because we do not know at any one time where we are in the magma convection cycle. The crystals suspended model would require that we caught the initial temperature decrease that starts at time zero, whereas the crystals settling model gives reasonable results regardless of where we are in the system's history.

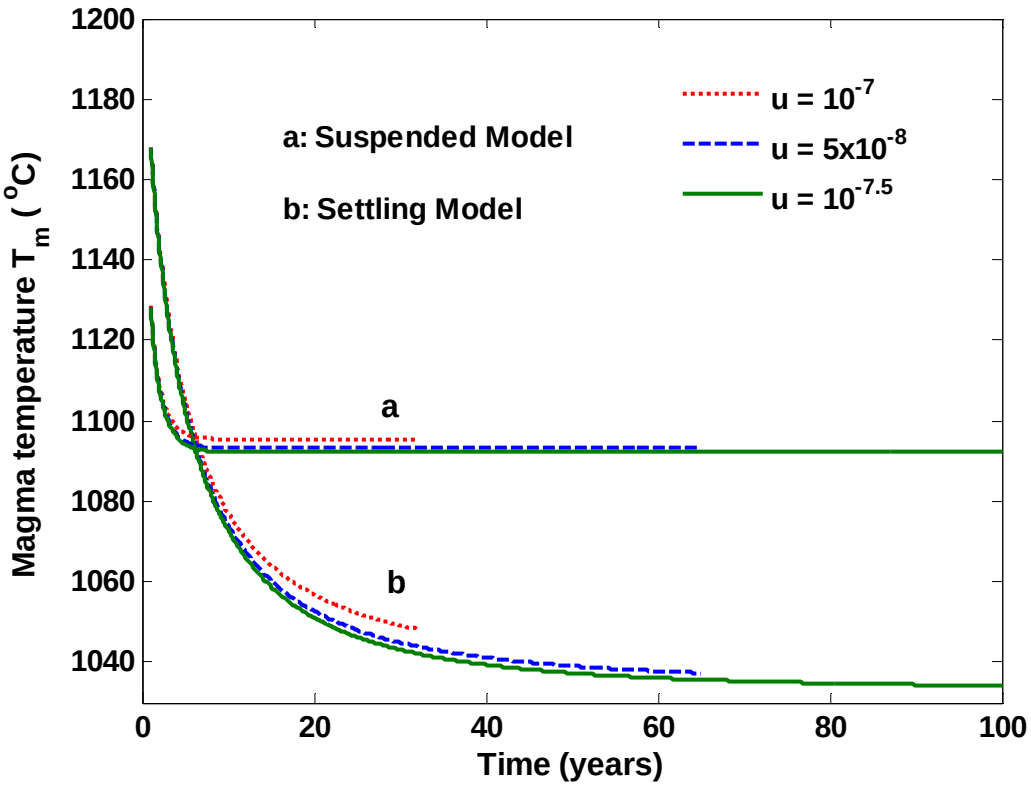

Figure 3.9 Magma temperature as a function of time for (a) crystals suspended and (b) crystals settling models for different values of constant magma replenishment velocity *u*. For (a) magma temperature approaches the value for which crystal content is 60%; for (b) the temperatures are significantly lower and decay by a few tens of degrees per decade. Curves ending at less than 100 years denote the time at which depth of the magma chamber doubles.

Although the model simulations suggest that magma replenishment coupled with magma chamber growth can help maintain a quasi steady-state hydrothermal system, the models employ a number of simplifications that need to be investigated further in order to make the simulations more robust. For example:

(1) In these models, rates of magma replenishment that satisfied observational constraints

were simply determined heuristically. Magma transport from the underlying mush zone to the magma chamber may not occur according to any simple mathematical function. To obtain a more realistic model of magma replenishment, our magmatic-hydrothermal models need to be linked to physical models of magma transport in upper mantle and lower crust.

(2) Magma chamber growth is greatly oversimplified. In these models, we simply assume that magma extends laterally or vertically as a result of replenishment. The stress field and the elastic response of the surrounding rock have been neglected. Magma chamber growth and pressurization of the magma cavity could lead to failure and magmatic eruptions [e.g., *Sim*, 2004]; however, so more realistic models of magma replenishment should be linked to deformation and possible eruption processes.

(3) Magma chamber dynamics and the effects of replenishment are greatly oversimplified. Even in the absence of magma replenishment, the models do not consider the dynamics of crystal settling and the effects of compositional convection. Attachment of crystals to the roof is also not considered. In models with magma replenishment, the new crystal-free magma imported into the magma chamber is assumed to mix with the magma in place instantaneously. However, the temperature, viscosity, and chemical composition of replenished magma may differ from the magma present in the chamber at any given time. Such differences may have a significant impact on magma crystallization and convection, and the composition at the time of an eruption.

3.6 Conclusions

This paper links heat transfer from a layer of vigorously convecting, crystallizing, and replenished magma chamber to an overlying high-temperature seafloor hydrothermal system. For magma chambers without replenishment, the results show that heat output decays on a decadal time scales, and for models in which crystals are assumed to be suspended in the melt convection is short-lived. These results are inconsistent with observed high-temperature hydrothermal systems that have maintained quasi-steady temperatures for decades. Magma convection models that include magma replenishment maintain nearly steady heat output on decadal time scales, while the magma body doubles its initial size. Magma replenishment rates for these cases appear to fall within a range between that required for long-term crustal generation and that observed at some volcanoes on decadal time scales. Models in which crystals either grow at or settle quickly to the floor of the magma chamber appear preferable for petrological reasons.

The magma convection, crystallization and replenishment models used here are oversimplified compared to real basaltic magma chambers at mid-ocean ridges. Future work will entail more complexity, including the mechanics of magma chamber growth, the mechanics of magma flow and replenishment from below, and magma chamber dynamics in a multi-component magma system.

3.7 Appendix: Magmatic Heat Flux Resulting from Replenishment when the Area of the Magma Chamber Increases with Time

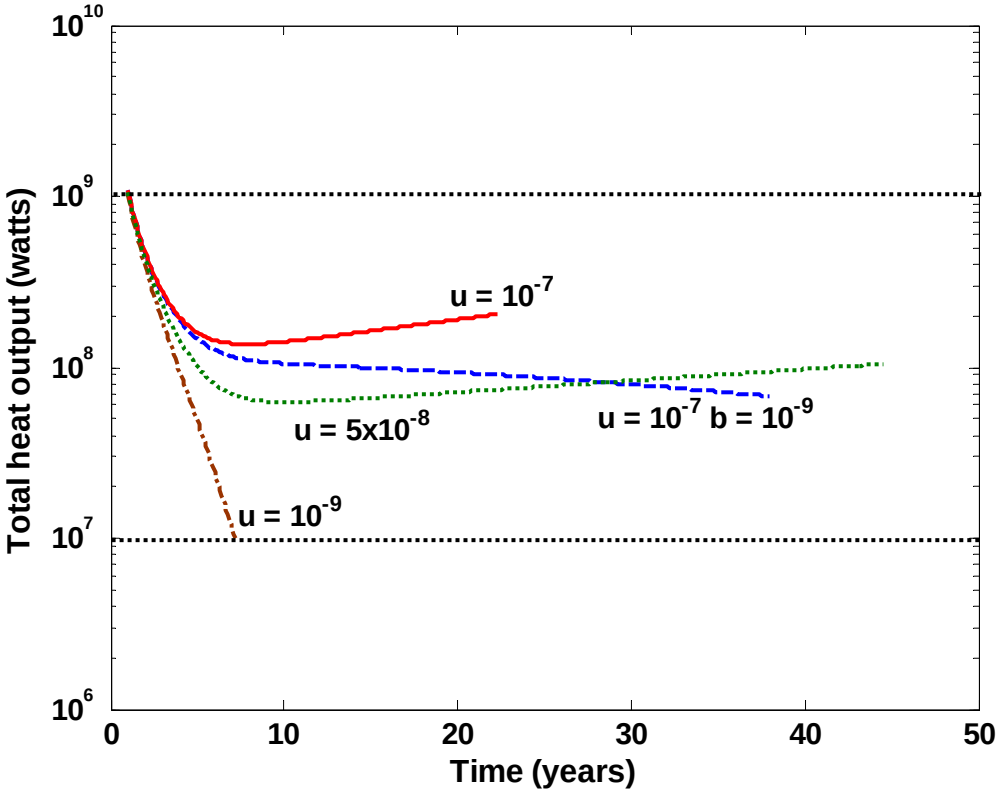

Figure 3.A.1 Total heat output as a function of time in the crystals suspended model for different values of constant or exponentially decaying magma replenishment velocity. Velocity u in m/s, b is the exponential factor. Simulations are run until magma area doubles from its initial value $A_{m0} = 10^6$ m^2, or until heat output decays to less than 10^7 Watts. Results show that u between 10^{-7} and 10^{-8} m/s tend to stabilize heat output on decadal timescales.

One can also consider the effects of magma replenishment on the heat output from the convecting, crystallizing magma chamber by keeping the depth of the magma

chamber fixed and allowing the area to increase with time. As before, the cases of crystals suspended and crystals settling are treated separately.

Crystals Suspended

As in section 3.3.4.1, we consider the change in volume $V(t)$ of the magma chamber with time as a result of replenishment. This is expressed by equation (18), which is rewritten below.

$$V(t) = V_0 + \int_0^t A_b(t')u(t')dt' \tag{A.1}$$

where V_0 is the initial volume, A_b is the area through which magma replenishment occurs, and $u(t)$ is the velocity of replenishment, respectively. Assuming that the depth of the magma chamber remains fixed and replenishment occurs over the entire area $A_m(t)$,

$$\frac{dV_m}{dt} = D_0 \frac{dA_m}{dt} = A_m(t)u(t) \tag{A.2}$$

We consider two different models of replenishment. In the first model, magma replenishment occurs at a constant velocity for a certain time period t_f, which corresponds to the time for the magma chamber to double in size or the magmatic heat flux to decay to less than 10^7 Watts

$$\begin{aligned} u(t) &= u_0 \qquad 0 \le \mathrm{t_f} \\ u(t) &= 0 \qquad \mathrm{t} > t_f . \end{aligned} \tag{A.3}$$

The area of the magma can be obtained by integrating equation (A.2) as follows:

$$A_m(t) = A_{m0} \exp(u_0 t / D) \tag{A.4}$$

where A_{m0} is the initial area of the magma chamber. In the second model, the velocity of

replenishment is assumed to decay exponentially

$$u(t) = u_0 e^{-bt} \tag{A.5}$$

where u_0 is the initial velocity. Similarly, the area of the magma is obtained as

$$A_m(t) = A_{m0} \exp(-u_0 \exp(-bt)/bD) \tag{A.6}$$

$$\frac{dT_m}{dt} = \frac{F_m(t) - \rho_m u(t)\left(c_m\left(T_L - T_m(t)\right) + \chi\left(T_m(t)\right)L\right)}{D_0 \rho_m \left(\chi'\left(T_m(t)\right)L - c_m\right)} \tag{A.7}$$

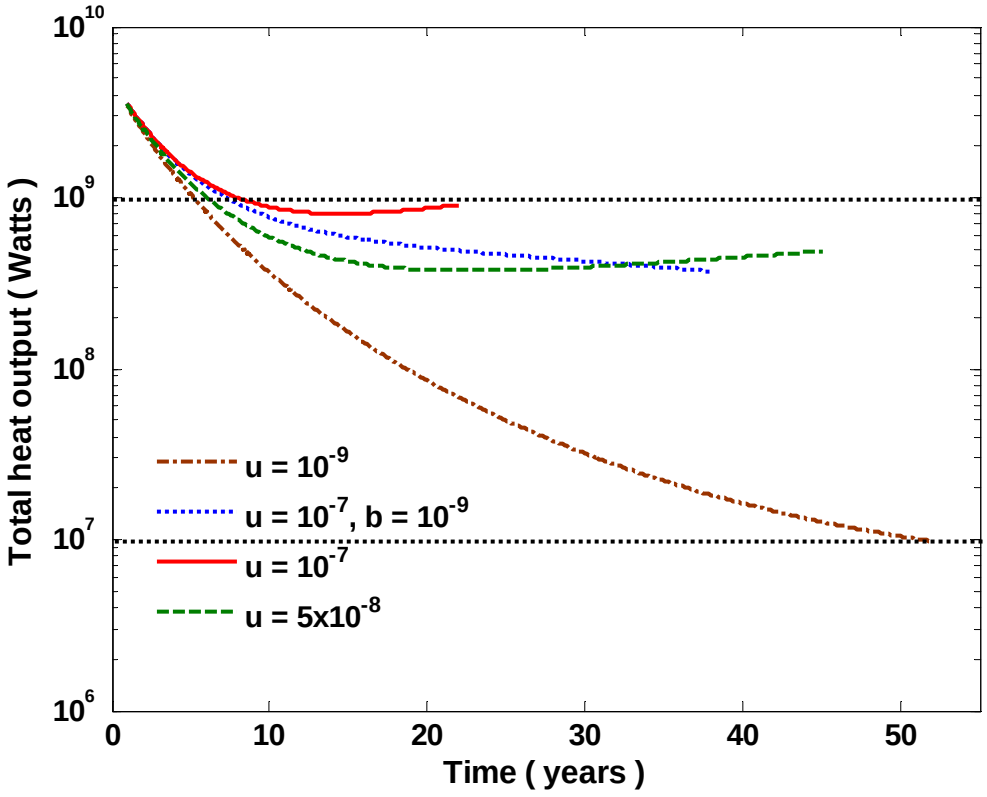

Figure 3.A.2 Total heat output as a function of time for the crystals settling model for a number of different replenishment velocities. Simulations cease when the magma chamber area doubles from its initial value of 10^6 m^2, or the heat flux decreases to 10^7 W.

Crrystals Settling

As in section 3.4.2, the volume of liquidus magma chamber is given by equation (26), which is reproduced here for convenience:

$$V_m(t) = V_0 - V_s + \int_0^t A_m(t')u(t')dt' \tag{A.8}$$

where the volume of crystals V_s is given by

$$V_s(t) = \frac{\chi}{1-\chi} V_m(t) \tag{A.9}$$

and

$$V_m(t) = D_0(1-\chi)A_m(t) \tag{A.10}$$

Equation (A.10) expresses the assumption that the area of magma chamber grows as a result of magma replenishment, while the thickness of magma chamber remains constant.

Substituting (A.9) into equation (A.8) yields

$$\frac{1}{1-\chi} V_m(t) = V_0 + \int_0^t A_m(t')u(t')dt' \tag{A.11}$$

Take the derivative of equation (A.11) with respect to time gives

$$\frac{dV_m(t)}{dt} = \frac{-\chi'}{1-\chi}\frac{dT_m}{dt} V_m(t) + (1-\chi)A_m(t)u(t) \tag{A.12}$$

In this case, because the depth of the magma chamber is constant, the rate of heat conduction from the crystal layer at the floor to the liquid magma above is given by

$$F_c(t) = \lambda \frac{T_L - T_m(t)}{\chi D_0} \tag{A.13}$$

To obtain the final equation for the temperature evolution in the liquid magma chamber, Equations (A.10), (A.12), (A.13), and (24) are substituted into equation (10). The result is:

$$\frac{dT_m}{dt} = \frac{F_m - A_m(t)\lambda\dfrac{T_L - T_m(t)}{D_0\chi} + \rho u(t)\left[(1-\chi)\left[CT_m(t) + (1-\chi(T_m(t))L\right] - (CT_L + L)\right]}{\rho D_0\chi'\left[CT_m(t) + (1-\chi(T_m(t))L\right] + D_0\rho(1-\chi)[L\chi' - C]} \tag{A.14}$$

In contrast to the situation in for crystals settling and in section 3.4.2 in which the magma area remains constant, equation (A.14) contains the magma area $A_m(t)$ explicitly. This expression of $A_m(t)$ can be obtained by substituting equation (A.10) into (A.11) and taking the derivative. The result is:

$$d \ln A_m(t) = \frac{u(t)}{D_0} dt \tag{A.15}$$

For $u(t) = u_0$, and constant, integration of equation (A.15) yields

$$A_m(t) = A_{m0} \exp(\frac{u_0}{D_0} t) \tag{A.16}$$

For $u(t) = u_0 e^{-bt}$, integration of equation (A.15) yields,

$$A_m(t) = A_0 \exp(\frac{u_0}{bD_0}) \exp(\frac{-u_0 e^{-bt}}{bD_0}) \tag{A.17}$$

Figure A.2 shows the magmatic heat output as a function of time for several rates of magma replenishment.

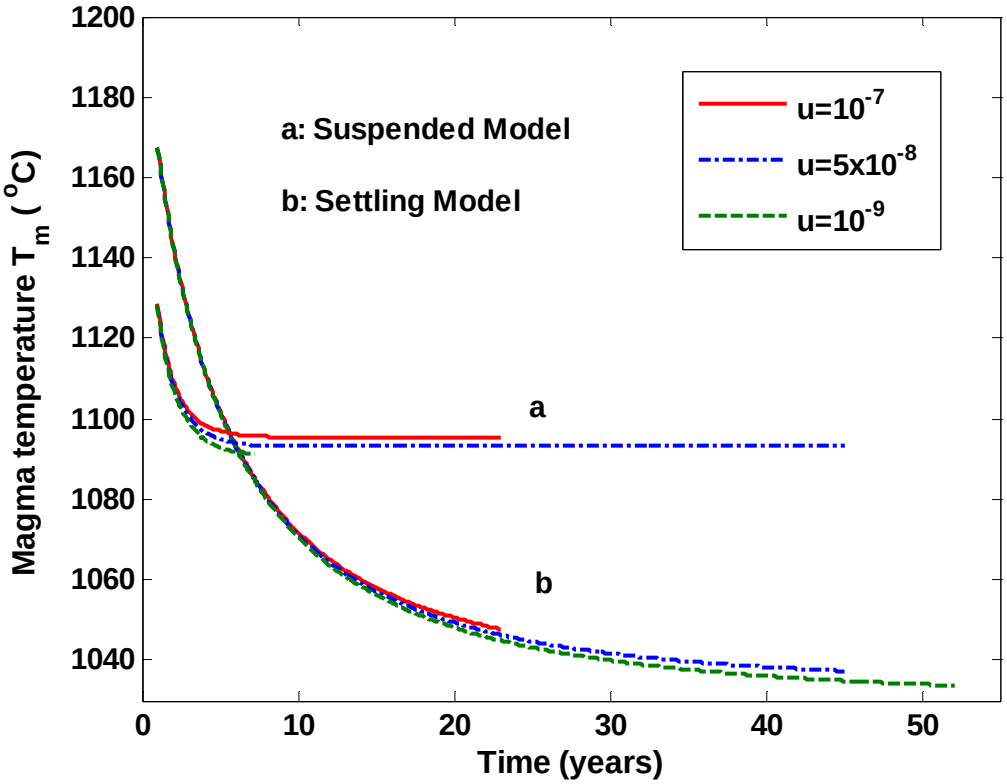

Figure 3.A.3 Magma temperature as a function of time for (a) crystals suspended and (b) crystals settling models for different values of constant magma replenishment velocity *u*. For (a) magma temperature approaches the value for which crystal content is 60%; for (b) the temperatures are significantly lower and decay by a few tens of degrees per decade. Curves end when the area of the magma chamber doubles.

Acknowledgments. We thank the reviewers Ed Baker and Adam Soule, and the Associate Editor Gary Massoth, for their thoughtful comments on the original version of this manuscript. This work was supported by NSF grant OCE 0527208 to RPL.

3.8 References

Asimow, P.D. and M.S. Ghiorso (1998), Algorithmic modifications extending MELTS to calculate subsolidus phase relations, *Amer. Mineral.*, *83*, 1127-1131.

Baker, E.T. (2007), Hydrothermal cooling of midocean ridge axes; do measured and modeled heat fluxes agree? *Earth Planet. Sci. Lett.*, *263*, 140-150.

Baker, E.T., H.N. Edmonds, P.J. Michael, W. Bach, H.J.B. Dick, J.E. Snow, S.L. Walker, N.R. Banerjee, and C.H. Langmuir (2004*a*), Hydrothermal venting in magma deserts: The ultraslow-spreading Gakkel and Southwest Indian ridges, *Geochem. Geophys. Geosyst.*, *5*(*8*) Q08002 doi: 10.1029/2004GC000712.

Baker, E. T., R.P. Lowell, J.A. Resing, R.A. Feely, R.W. Embley, G.J. Massoth, and S.L. Walker (2004*b*), Decay of hydrothermal output following the 1998 seafloor eruption at Axial Volcano: Observations and models, *J. Geophys. Res.*, *109*, B01205 doi: 10.1029/2003JB002618.

Batiza, R. and Y. Niu (1992), Petrology and magma chamber processes at the East Pacific Rise-9°30′N, *J. Geophys. Res.*, *97*, 6779-6797.

Bejan, A. (1995), *Convection Heat Transfer*, 2nd ed., John Wiley & Sons, New York, pp.623

Bryan, W.B. (1983), Systematics of modal phenocryst assemblages in submarine basalts; petrologic implications, *Contr. Mineral. Petrol.*, *83*, 62-74.

Brandeis G., and C. Jaupart (1986), On the interaction between convection and crystallization in cooling magma chambers, *Earth Planet. Sci. Lett.*, *77*, 345-361.

Campbell, A.C., T.S. Bowers, C.I. Measures, K.K. Falkner, M. Khadem, and J.M. Edmond (1988), A time series of vent fluid compositions from 21°N, East Pacific Rise (1979, 1981, 1985), and the Guaymas Basin, Gulf of California (1982, 1985), *J Geophys Res.*, *93*, 4537-4549.

Canales, J. P., S. C. Singh, R. S. Detrick, S. M. Carbotte, A. Harding, G. M. Kent, J. B. Diebold, J. Babcock, and M. R. Nedimovic (2006), Seismic evidence for variations in axial magma chamber properties along the southern Juan de Fuca Ridge, *Earth. Planet. Sci. Lett.*, *246*, 353-366.

Canales, J. P., R. A. Sohn, and B.J. deMartin, (2007),Crustal structure of the Trans-Atlantic Geotraverse (*TAG*) segment (Mid-Atlantic Ridge, 26 degrees 10'N); implications for the nature of hydrothermal circulation and detachment faulting at slow spreading ridges, *Geochem. Geophys. Geosyst.*, *8*(*8*), Q08004, doi:10.1029/2007GC001629.

Cann, J.R. and M.R. Strens, (1982), Black smokers fuelled by freezing magma, *Nature*, *298*, 147-149.

Collier, J. S., and M. C. Sinha (1990), Seismic images of a magma chamber beneath the Lau Basin back-arc spreading centre, *Nature*, *346*, 646-648.

Detrick, R. S., P. Buhl, E. Vera, J. Mutter, J. Orcutt, J. Madsen, and T. Brocher (1987), Multi-channel seismic imaging of a crustal magma chamber along the East Pacific Rise, *Nature*, *326*, 35-41.

Dzurizin, D., R.Y. Koyanagi, and T.T. English (1984), Magma supply and storage at Kilauea volcano, Hawaii, 1956-1983, *J. Volcanol. Geotherm. Res.*, *21*, 177-206.
Gente, P., J.M. Auzende, V.Renard, Y.Fouquet, and D.Bideau, (1986), Detailed geological mapping by submersible of the East Pacific Rise axial graben near 13° N, *Earth Planet. Sci. Lett.*, *78*, 224-236.

Germanovich, L.N., R.P. Lowell, and D.K. Astakhov (2000), Stress-dependent permeability and the formation of seafloor event plumes, *J. Geophys. Res.*, *105*, 8341-8354.

Germanovich, L.N., R.P. Lowell, and D.K. Astakhov (2001), Temperature-dependent permeability and bifurcations, in hydrothermal flow, *J. Geophys. Res.*, *106*, 473-495.

Ghiorso, M.S. and R.O. Sack (1995), Chemical mass transfer in magmatic processes. IV. A revised and internally consistent thermodynamic model for the interpolation and extrapolation of liquid-solid equilibria in magmatic systems at elevated temperatures and pressures. *Contr. Mineral. Petrol.*, *119*, 197-212.

Haymon, R. M., et al. (1993), Volcanic eruption of the mid-ocean ridge along the east Pacific Rise crest at 9°45´- 52´N: direct submersible observations of seafloor phenomena associated with an eruption event in April, 1991. *Earth Planet. Sci. Lett.*, *119*, 85–101.

Henstock, T.J., A.W. Woods, and R.S. White (1993), The accretion of oceanic crust by episodic sill intrusion, *J. Geophys. Res.*, *98*, 4143-4161.

Hort, M. (1997), Cooling and crystallization in sheet-like magma bodies revisited, *J. Volcanol. Geotherm. Res.*, *76*, 297-317.

Humphris, S. E., and J. R. Cann (2000). Constraints on the energy and chemical balances of the modern TAG and ancient Cyprus seafloor sulfide deposits, *J. Geophys. Res.*, *105*, 28,477-28,488.

Huppert, H. E., and R. S. J. Sparks (1981), The fluid dynamics of a basaltic magma chamber replenished by influx of hot, dense ultrabasic magma, *Contrib. Mineral. Petrol.*, *75*, 279-289.

Huppert, H. E., and R. S. J. Sparks (1988), The generation of granitic magmas by intrusion of basalt into continental crust, *J. Petrol.*, *29*, 599-624.

Huppert, H.E., R.S.J. Sparks, J.A. Whitehead, and M.A. Hallworth (1986), Replenishment of magma chambers by light inputs, *J. Geophys. Res.*, *91*, 6113-6122.

Huppert, H.E. and J. S. Turner (1991), Comments on "On convective style and vigor in sheet-like magma chambers" by Bruce D. Marsh, *J. Petrol.*, *32*, 851-854.

Irvine, T.N. (1980), Magmatic density currents and cumulus processes, *American J. Sci.*, *280*, 1-58.

Jaeger, J.C. (1968), Cooling and solidification of igneous rocks, In *Basalts vol 2*, edited by H.H. Hess and A. Poldervaart, 503-536, John Wiley, NY.

Jarvis, G.T., and W. R. Peltier (1989), Convection models and geophysical observations, in *Mantle Convection*: *Plate Tectonics and Global Dynamics*, ed. W. R. Peltier, Gordon and Breach Science Publishers, 479-595.

Jaupart, C., and S. Tait (1995), Dynamics of differentiation in magma reservoirs, *J. Geophys. Res.*, *100*, 17,615-17,636.

Jellinek, A.M., and R.C. Kerr (1999), Mixing and compositional stratification produced by natural convection. Part 2. Applications to the differentiation of basaltic and silicic magma chambers and komatiite lava flows, *J. Geophys. Res.*, *104*, 7203-7218.

Jellinek, A.M., R.C. Kerr, and R.W. Griffiths (1999), Mixing and compositional stratification produced by natural convection. Part 1. The experiments and their application to the Earth's core and mantle, *J. Geophys. Res.*, *104*, 7183-7201.

Jellinek, A M., and R.C. Kerr (2001), Magma dynamics, crystallization, and chemical differentiation of the 1959 Kilauea Iki lava lake, Hawaii, revisited, *J. Volcanol. Geotherm. Res.*, *110*, 235-263

Kelley, D. S., J. A. Baross, and J. R. Delaney (2002), Volcanoes, fluids, and life at mid-ocean ridge spreading centers, *Annu. Rev. Earth Planet. Sci*., *30*, 385-491.

Kent, G. M., A. J. Harding, and J. A. Orcutt (1990), Evidence for a smaller magma chamber beneath the East Pacific Rise at 9º30´N, *Nature*, *344*, 650-652.

Kerr, R.C. (1994). Melting driven by vigorous compositional convection. *J. Fluid Mech. 280*, 255–285.

Lejeune, A. M., and P. Richet, (1995), Rheology of crystal-bearing silicate melts: an experimental study at high viscosities, *J. Geophys. Res.*, *100*, 4215-4229.

Liu, L. (2007), The link between convection and crystallization in a sub-axial magma chamber and heat output in a seafloor hydrothermal system, *M.S. Thesis*, 74 p., Georgia Institute of Technology, Atlanta.

Lovering, T.S. (1955), Temperatures in and near intrusions, *Econ. Geol.*, *50*, 249-281.

Lowell, R. P. and D. K. Burnell (1991), A numerical model for magma-hydrothermal boundary layer heat transfer in the oceanic crust, *Earth Planet. Sci. Lett.*, *104*, 59-69.

Lowell, R.P., B.W. Crowell, K.C. Lewis, and L. Liu (2008), Modeling multiphase, multi-component processes at oceanic spreading centers, in *Magma to Microbe*: *Modeling Hydrothermal Processes at Oceanic Spreading Centers*, *Geophys. Monogr. Ser.*, v. *178*, ed. by R.P. Lowell, J.S. Seewald, A. Metaxas, and M.R. Perfit, p. 15-44, American Geophys. Union, Washington, DC.

Lowell, R. P. and L. N. Germanovich (1994), On the temporal evolution of high-temperature hydrothermal systems at ocean ridge crests, *J. Geophys. Res.*, *99*, 565-575.

Lowell, R. P. and L. N. Germanovich (2004), Seafloor hydrothermal processes: Results from scale analysis and single-Pass models, in *Mid-Ocean Ridges*: *Hydrothermal Interactions Between the Lithosphere and Oceans, Geophys. Monogr. Ser.*, *148*, ed. by C. R. German, J. Lin and L. M. Parson, pp. 219-244, Amer. Geophys. Union, Washington, D.C.

Lowell, R. P. and P. A. Rona (1985), Hydrothermal models for the generation of massive sulfide ore deposits, *J. Geophys. Res.*, *90*, 8769-8783.

MacLeod, C. J. and G. Yaouancq (2000), A fossil melt lens in the Oman ophiolite: Implications for magma chamber processes at fast spreading ridges, *Earth Planet. Sci. Lett.*, *176*, 357-373.

Marsh, B. D. (1981), On the crystallinity, probability of occurrence, and rheology of lava and magma, *Contrib. Mineral. Petrol.*, *78*, 85-98.

Marsh, B.D. (1989), On convective style and vigor in sheet-like magma chambers *J.Petrol.*, 30, 479-530.

Martin, D. (1990), Crystal settling and in situ crystallization in aqueous solutions and magma chambers, *Earth Planet. Sci. Lett.*, *96*, 336-348.

Martin, D., and R. Nokes (1988), Crystal settling in a vigorously convecting magma chamber, *Nature*, *332*, 534-536.

Martin, D., and R. Nokes (1989), A fluid dynamical study of crystal settling in convecting magmas, *J. Petrol.*, *30*, 1471-1500.

McBirney, A.R., and R.M. Noyes (1979), Crystallization and layering of the Skaergaard Intrusion, *J. Petrology*, *20*, 487-554.

Michael, P.J., et al. (2003), Magmatic and amagmatic seafloor generation at the ultraslow-spreading Gakkel Ridge, Arctic Ocean, *Nature*, 423, 956-961.

Morgan, J.P. and Y.J. Chen (1993), The genesis of oceanic crust: Magma injection, hydrothermal circulation, and crustal flow, *J. Geophys. Res.*, *98*, 6283-6297.

Perfit, M.R., D.J. Fornari, M.C. Smith, J.F. Bender, C.H. Langmuir, and R. M. Haymon (1994), Small-scale spatial and temporal variation in mid-ocean ridge crest magmatic processes, *Geology*, *22*, 375-379.

Ramondenc, P., L. N. Germanovich, K. L. Von Damm, and R. P. Lowell (2006), The first measurements of hydrothermal heat out at 9°50´N, East Pacific Rise, *Earth Planet. Sci. Lett.*, *245*, 487-497.

Ramondenc, P., L.N. Germanovich, and R.P. Lowell (2008), Modeling the hydrothermal response to earthquakes with application to the 1995 event at 9°50′ N, East Pacific Rise, in *Magma to Microbe*: *Modeling Hydrothermal Processes at Oceanic Spreading Centers*, *Geophys. Monogr. Ser.*, *178*, ed. by R.P. Lowell, J.S. Seewald, A. Metaxas, and M.R. Perfit, p. 97-122, American Geophys. Union, Washington, DC.

Roscoe, R. (1952), The viscosity of suspensions of rigid spheres. *British Journal of Applied Phys.*, *3*, 267-269.

Rubin, K. H., M. Perfit, D. J. Fornari, S. A. Soule, M. Tolstoy, and F. Waldhauser (2006), Geochronology and composition of the 2005-06 volcanic eruptions of the East Pacific Rise, 9°46'-56'N, *Eos Trans. AGU*, *87*(*52*), Fall Meet. Suppl., Abstract V23B-0602.

Scheirer, D.S., T.M. Shank, D.J. Fornari (2006), Temperature variations at diffuse and focused flow hydrothermal vent sites along the northern East Pacific Rise
Geochem. Geophys. Geosyst., 7, Q03002, doi: 10.1029/2005GC001094.

Shaw, H. R. (1980), The fracture mechanisms of magma transport from the mantle to the surface. In: *Physics of Magmatic Processes*, ed. by Hargraves, R. B., Princeton University Press, 201-264.

Sim, Y. (2004), Mechanics of complex hydraulic fractures in the Earth's crust, *Ph. D. Thesis*, 324 p. Georgia Institute of Technology, Atlanta.

Singh, S. C., J. S. Collier, A. J. Harding, G. M. Kent, and J. A. Orcutt (1999), Seismic evidence for a hydrothermal layer above the solid roof of the axial magma chamber at the southern East Pacific Rise, *Geology*, *27*, 219-222.

Singh, S. C., W. C. Crawford, H. Carton, T. Seher, V. Combier, M. Cannat, J. P. Canales,

D. Dusunur, J. Escartin, and J. M. Miranda (2006), Discovery of a magma chamber and faults beneath a Mid-Atlantic Ridge hydrothermal field, *Nature*, *442*, 1029-1032.

Sinton, J. M. and R. S. Detrick (1992), Mid-ocean ridge magma chambers, *J. Geophys. Res.*, *97*, 197-216.

Snyder, D. and S. Tait (1995), Replenishment of magma chambers: comparison of fluid dynamics experiments with field relations, *Contrib. Mineral. Petrol.*, *122*, 230-240.

Sohn, R.A., D.J.Fornari, K. L. Von Damm, J. A. Hildebrand, and S.C. Webb (1998), Seismic and hydrothermal evidence for a cracking event on the East Pacific Rise crest at 9°50'N, *Nature*, 396, 159-161.

Soule, S.A., D.J. Fornari, M.R. Perfit, K.H. Rubin (2007), New insights into mid-ocean ridge volcanic processes from the 2005-2006 eruption of the East Pacific Rise, 9°46'N-9° 56'N, *Geology, 35*, 1079-1082

Spera, F. J. (2000), Physical properties of magma, in *Encyclopedia of Volcanoes*, Academic Press, 171-190.

Trial, A.F., and F.J. Spera (1990), Mechanisms for the generation of compositional heterogeneities in magma chambers, *Geol. Soc. America Bul., 102*, 353-367

Turner, J. S. (1973), *Buoyancy effects in fluids*, Cambridge University Press, London.

Van Ark, E.M., R.S. Detrick, J.P. Canales, S.M. Carbotte, A.J. Harding, G..M. Kent, M.R. Nedimovic, W.S.D. Wilcock, J.B. Diebold, J.M. Babcock (2007), Seismic structure of the Endeavour Segment, Juan de Fuca Ridge; correlations with seismicity and hydrothermal activity, *J. Geophys. Res.*, *112*, B02401, doi: 10.1029/2005JB004210.

Von Damm, K. L., C. M. Parker, R. M. Gallant, and J. P. Loveless (2002), Chemical evolution of hydrothermal fluids from EPR 21°N: 23 years later in a phase separating world, *EOS Trans*., Amer. Geophys. Union, *83*, Suppl., 1421.

Von Damm K. L. (2004) Evolution of the hydrothermal system at East Pacific Rise 9˚50′N: Geochemical evidence for changes in the upper oceanic crust, in *Mid-Ocean Ridges: Hydrothermal Interactions Between the Lithosphere and Oceans, Geophys. Monogr. 148*, ed. by C.R. German, J. Lin, and L.M. Parson, pp. 285-304, Amer. Geophys. Union, Washington, D. C.

Worster, M. G., H. E. Huppert, and R. S. J. Sparks (1990), Convection and crystallization in magma cooled from above, *Earth Planet. Sci. Lett.*, *101*, 78-89.

CHAPTER 4. EFFECTS OF PERIODIC REPLENISHMENT AND INITIAL MAGMA SIZE[2]

Abstract

The temperature and heat output of hydrothermal systems play an important role in the thermal budget of the oceanic crust. In this paper, we investigate the time-varying heat transfer from a convecting, crystallizing, and replenished sub-axial magma chamber to the overlying hydrothermal system by considering the effects of initial magma chamber sill thickness and periodic replenishment rates. Both crystals suspended and crystals settling scenarios are considered. The initial rate of convective heat transfer is independent of the initial sill thickness; but without magma replenishment, the rate of decay of the heat output varies linearly with thickness, resulting a short convective lifetimes and decaying hydrothermal temperatures for sills up to ~ 100m thick. When magma replenishment is included in crystals settling scenarios at constant or exponentially decreasing rates of ~ 10^{-8} m/s to the base of the sill, growth of the sill results in stabilized heat output and hydrothermal temperature on decadal timescales and a relatively constant to increasing thickness of the liquid layer. Sills initially ~ 10 m thick can grow, in principal, to ~ 10 times there initial size with stable heat output and a final melt thickness less than 100m. These results suggest that magma replenishment might not be seismically detectable on decadal time scales. Periodic replenishment may also result

[2]The material is essentially reproduced from Liu, L. and R.P. Lowell (2010). Modeling heat transfer from a convecting, crystallizing, replenished magma chamber: Effects of initial magma chamber thickness and periodic replenishment, *Geophys. J. Int*. (submitted).

in quasi-stable heat output, but the magnitude of the heat output may vary considerably in crystals suspended models at low frequencies; compared to crystals settling models. In these models the direct coupling between magmatic and hydrothermal heat output would suggest that heat output fluctuations might be recorded in hydrothermal vents; but if the damping effects of the basal conductive boundary layer and the upflow zone are taken into account, it seems unlikely that heat output fluctuations on a time scale of years would be recorded in hydrothermal vent temperatures or heat output.

4.1 Introduction

Hydrothermal activity at mid-ocean ridges is closely linked to crustal magmatism. At nearly all sites of observed high-temperature venting, seismic reflection data has indicated the presence of shallow subaxial magma bodies beneath the active hydrothermal systems over a broad range of spreading rates. Examples include: the fast- and ultra-fast-spreading East Pacific Rise [*Detrick et al.*, 1987; 1993], the intermediate-spreading Valu Fa Ridge [*Collier and Sinha*, 1990] and Juan de Fuca Ridge [*Canales et al.*, 2006; *Van Ark et al.*, 2007], the slow-spreading Mid-Atlantic Ridge [*Singh et al.*, 2006], and the ultraslow-spreading Gakkel ridge in Arctic Ocean [*Jokat et al.*, 2003] and Southwest Indian Ridge [*Sauter et al.*, 2004]. Moreover, eruptions on the East Pacific Rise near 9°50′ N in 1991 and 1992 [*Haymon et al.*, 1993] have resulted in strong temporal changes in hydrothermal venting [e.g., *Von Damm*, 2004] that have persisted to the time of more recent eruptions in 2005/2006 [*Tolstoy et al.*, 2006; *Cowen et al.*, 2007; *Soule et al.,* 2007; *Lupton et al.*, 2006]. In between these two eruptive episodes, small non-eruptive diking events may have cause perturbations to the hydrothermal system [*Ramondenc et al.*, 2008; *Germanovich et al.*, 2010]. High temperature hydrothermal circulation within the permeable oceanic crust occurs as heat from the convecting, sub-axial magma chamber (AMC) is transferred by conduction across a thin thermal boundary layer between the top of magma chamber and the base of hydrothermal system based [e.g., *Lowell and Germanovich*, 1994; *Lowell et al.*, 2008; *Liu and Lowell*, 2009].

To better understand the evolution of the boundary layer and the linkages between heat flux from the convecting, crystallizing magma and hydrothermal heat transport, *Liu and Lowell* [2009] developed numerical models of magmatic heat flux. They investigated

two different crystallization scenarios, crystal-suspended and crystal-settling, and considered both un-replenished and replenished AMCs of basaltic composition. The models in [*Liu and Lowell*, 2009] showed that magma replenishment of ~ 10^{-7} to 10^{-8} m/s was needed to maintain quasi-steady heat output between 10^7 and 10^9 W over a time scale of decades. These results assumed an AMC with an initial thickness of 100 m and considered only constant or exponentially decreasing magma replenishment rates. Although the models presented in [*Liu and Lowell*, 2009] provide useful insights into the behavior of magma-hydrothermal systems at mid-ocean ridges, these models considered a very limited parameter space. Thus, we are motivated to investigate heat transfer from a convecting, crystallizing, replenished magma chamber from a parametric perspective.

Here, we investigate two factors that affect hydrothermal heat output: (a) initial magma chamber thickness and (b) a variable magma replenishment rate. Specifically, the magma convective lifetime and the evolution of magmatic heat flux are controlled by both the size and shape of the magma. Seismic imaging suggests that the AMC may range from as little as a few tens of meters [*Kent et al.,* 1990; *Singh et al.*, 1998; *Collier and Sinha*, 1990] to perhaps a few hundred meters thick [*Vera et al.,* 1990; *Sinha et al.*, 1998; *Navin et al.*, 1998]. Laterally, it may extend from as little as 500 m [*Babcock et al.*, 1998] to as much as 4 km across [*Sinha et al.,* 1998; *Vera et al.,* 1990; *Harding et al.,* 1989; *Detrick et al.,* 1987]; but typically it ranges between 1 and 2 km perpendicular to the ridge axis [*Detrick et al.*, 1993; *Kent et al.*, 1990; *collier and Sinha*, 1990; *Van ark et al.*, 2007]. The AMC may extend almost continuously along the ridge axis for 10s of km [*Burnett et al.,* 1989; *Detrick et al.,* 1987; *Babcock et al.,* 1998], but because several hydrothermal systems may lie along a given ridge segment [e.g. EPR [*Haymon et al.*,

1991; *Haymon and White*, 2004]; JDF [*Kelly et al.*, 2001]], we neglect the along axis variations in the AMC. Because the vertical thickness of the AMC appears to be relatively more variable than its lateral extent, we examine the effects of magma chamber thickness on the magmatic heat transfer rather than variations in its lateral extent. Magma replenishment rate also plays an important role in maintaining the heat flux and extending the magma convective lifetime.

The assumption of continuous a constant or exponentially decreasing rate of magma replenishment may be a significant over simplification. For example, interspersed between the magmatic eruptions on the East Pacific Rise near 9°50′ N in 1991 and 1992 [*Haymon et al.,* 1993] and again in 2005/ 2006 [*Soule et al.*, 2007;], there may have been non-eruptive magmatic events [*Ramondenc et al.*, 2008; *Germanovich et al.*, 2010]. The evidence for these comes from seismicity studies and observed changes in the temperature, fluid chemistry of some hydrothermal vents [*Sohn et al.*, 1998, *Baker et al.*, 1999; *Scheirer et al.*, 2006; *Tolstoy et al.*, 2008]. Here, we consider the effects of episodic replenishment by investigating the effects of sinusoidal replenishment rates. As in [*Liu and Lowell*, 2009], we consider both replenished and un-replenished AMCs; and in each case, we consider both crystals suspended and crystals settling scenarios.

The rest of the chapter is organized as follows. In section 4.2, we briefly review the mathematical models of magmatic heat transfer developed in [*Liu and Lowell*, 2009]. In section 4.3 we investigate the effects of magma chamber size on heat flux of hydrothermal systems. In section 4.4, we investigate the effects of episodic replenishment rates on hydrothermal heat flux. Section 4.5 discusses the implication of the model in

terms of the evolution of the magma chamber and the linkages between magmatic heat output and hydrothermal venting, followed by conclusions in section 4.6.

4.2 Mathematical Model of Magmatic Heat Transfer

Within the liquid magma body, thermal convection resulting from the temperature difference between hot magma and its cold upper boundary maintained by the overlying hydrothermal circulation is an efficient means of heat transfer. The basic equations governing the magma convection system, which are based on *Huppert and Sparks* [1988], are discussed in detail in [*Liu and Lowell*, 2009]. Here, only the key equations are reproduced to highlight the significant differences between the analyses in this chapter and those of [*Liu and Lowell*, 2009].

In a well-mixed sub-axial magma chamber, convection can be characterized by the Rayleigh number defined as

$$Ra = \frac{\alpha_m g D_0^{\,3} \Delta T}{a_m \nu_m} \tag{1}$$

where α_m is the coefficient of thermal expansion, g is the acceleration due to gravity, a_m is the thermal diffusivity, ν_m is the kinematic viscosity, D_0 is the initial thickness of the magma body, and ΔT is the difference between the mean magma temperature $T_m(t)$ and the solidus magma temperature T_s. The heat of magma crystallization is considered to be gradually released in the temperature interval 1200°C to 1030°C. The subscript m refers to the properties of the magma. Typical values of Ra in the AMC may range from ~ 10^6 to 10^{11} [*Liu and Lowell*, 2009] compared to the critical value is of ~ 10^3. For convection with large Ra, the heat transfer can be related to a Nusselt number Nu, which defines the ratio of convective heat flux to the heat flux due to conduction. With the assumption of

the classical relationship $Nu \sim Ra^{1/3}$ [e.g., *Jarvis and Peltier*, 1989], the heat flux $F_m(t)$ transferred from the top of the magma body is given by [*Turner*, 1973]

$$F_m(t) = 0.1\rho_m c_m (\alpha_m g a_m{}^2 / \nu_m)^{1/3} (T_m(t) - T_S)^{4/3} \tag{2}$$

where ρ_m is the magma density and c_m is the specific heat. Equation (2) shows that magma viscosity ν_m controls convective heat flux. In general, ν_m is a function of bulk composition, crystallinity, temperature, volatile content, and the magma temperature. During magma convection, cooling, crystallization and evolving volatile content results in a time-dependent magma viscosity. To characterize this time-varying magma viscosity, we consider two types of magma crystallization mechanisms: crystals suspended (all crystals remain suspended within the liquid magma) and crystals settling (all crystals occur at the floor of the magma chamber or rapidly settle there). Because mid-ocean ridge basaltic magmas contain few volatiles, we neglect the effect of volatiles on magma viscosity. For the crystals suspended model, we assume ν_m is only a function of crystal content $\chi(T_m(t))$, whereas for the crystals settling model, viscosity is a function of magma temperature. The resulting relationships from [*Liu and Lowell*, 2009] are, respectively,

$$\nu_m(t) = \nu_{m0}\left[1 - 1.67\chi(T_m(t)\right]^{-2.5} \tag{3}$$

$$\nu_m(t) = \nu_{m0}\left[\frac{T_L}{T_m(t)}\right]^{8.5} \tag{4}$$

where ν_{m0} is the initial viscosity, $\chi(T_m(t))$ is the crystal content as a function of magma temperature, and T_L denotes the liquidus magma temperature.

The crystal content χ relates to the magma temperature through the equation [*Huppert and Sparks*, 1988]

$$\chi(T_m(t)) = \frac{7200}{T_m(t)} - 6 \tag{5}$$

To solve for the magma temperature with and without magma replenishment, we equate the time derivative of the heat content in the magma body to the rate of heat loss through the top boundary and the magma replenishment rate from below the magma chamber. That is:

$$\frac{dH(t)}{dt} = -F_m(t)A_m(t) + F_r(t)A_m(t) \tag{6}$$

where $H(t)$ is the heat content in the magma chamber, $A_m(t)$ is the area of magma chamber, $F_r(t)$ is the heat replenishment rate due to the magma replenishment. For cases without magma replenishment, $F_r(t) = 0$.

For cases without magma replenishment, the magma temperature governing equation for crystal suspended and crystal settling models is given by [*Liu and Lowell*, 2009], respectively

$$\frac{dT_m(t)}{dt} = \frac{F_m(t)}{\rho_m D_0 L\chi'(T_m(t)) - \rho_m D_0 c_m} \tag{7}$$

$$\frac{dT_m(t)}{dt} = \frac{F_m(t) - F_c}{\rho_m D_0 \chi'(T_m(t))\left\{c_m T_m(t) + L\left[1-\chi(T_m(t))\right]\right\} + \rho_m D_0[1-\chi(T_m(t))]\left[\chi'(T_m(t))L - c_m\right]} \tag{8}$$

where χ' is the first order derivative of crystal content, and L is the latent heat, respectively. In the crystals settling model (equation (8)), F_c accounts for the rate of heat flux, that is conducted from the growing crystal layer to the remaining liquid magma.

With magma replenishment, new magma enters the magma chamber from the underlying mush zone. As a consequence, both the heat content and mass of magma

increase. The increase of heat content from mush zone contributed by magma replenishment is described by $F_r(t)$

$$F_r(t) = (\rho_m c_m T_L + \rho_m L)u(t) \tag{9}$$

where $V_m(t)$ is the volume of new magma that enters the convecting magma body. In [*Liu and Lowell*, 2009], two end-member scenarios of magma chamber growth upon replenishment were considered: (a) magma chamber thickness held constant while its area increased with respect to time; (b) magma chamber area held constant while its thickness increased with time. Here, we use model (b) and employ a time-varying magma thickness model for both the crystals suspended and crystal-settling scenarios. Denoting $u(t)$ as the magma replenishment velocity, the thickness of magma chamber is obtained from

$$D(t) = D_0 + \int_0^t u(s)ds \tag{10}$$

As in [*Liu and Lowell*, 2009], upon substituting equations (10) and (9) into equation (6), the temperature dependence for the convecting, replenished magma chambers for the crystals suspended and crystals settling models are given by, respectively,

$$\frac{dT_m(t)}{dt} = \frac{F_m(t) - \rho_m u(t)\{c_m[T_L - T_m(t)] + \chi(T_m(t))L\}}{\rho_m D(t)[\chi'(T_m(t))L - c_m]} \tag{11}$$

$$\frac{dT_m(t)}{dt} = \frac{F_m(t) - F_c + \Gamma_1(t)}{\Gamma_2(t)} \tag{12}$$

where

$$\Gamma_1(t) = \rho_m u(t)\left\{\left[1 - \chi\left(T_m(t)\right)\right]\left[c_m T_m(t) + \left(1 - \chi\left(T_m(t)\right)\right)L\right] - \left(c_m T_L + L\right)\right\} \tag{13}$$

$$\Gamma_2(t) = \rho_m D(t)\chi'\left(T_m(t)\right)\left\{c_m T_m(t) + L\left[1-\chi\left(T_m(t)\right)\right]\right\} + \rho_m D(t)\left(1-\chi\left(T_m(t)\right)\right)\left(\chi'\left(T_m(t)\right)L - c_m\right) \quad (14)$$

Combining equation (2), (7), (8), (11) and (12) respectively, we can obtain both magma temperature and heat flux. Although the $T_m(t)$ is a direct measure of the heat flux in equation (2), the primary observational link between heat transfer from the magma chamber and the overlying hydrothermal systems is best expressed in terms of total heat output $F_m(t)A_m$. The measured total heat output of hydrothermal systems at oceanic spreading center is typically between ~ 10^7 and 10^9 Watts [*Lowell and Germanovich*, 2004; *Ramondenc et al.*, 2006; *Baker*, 2007]. Thus, in our numerical analysis, the model parameters are tuned to provide an initial total heat output of ~ 10^9 W. In addition, heat output is a good indicator of the lifetime of a hydrothermal system. Therefore, to quantitatively examine the lifetime of a ridge-crest hydrothermal system, we define it based on either of two conditions: (1) when the crystal content in magma chamber approaches 60%, the viscosity of magma goes to infinity and no more heat transfer occurs by convection; or (2) when the total heat output is less than 10^7 Watts.

4.3 The Effect of Initial Intrusion Size

In [*Liu and Lowell*, 2009], we selected a single initial size of magma chamber thickness of 100 m for demonstration purposes. However, magma chambers in the earth can vary greatly in terms of shape and thickness. Here, we assume the magma chamber with a rectangular cross section of fixed area and study the effect of initial chamber thickness on magmatic heat flux. Seismic imaging suggests that magma sills at oceanic spreading centers range between a few tens and ~ 100 m [e.g., *Kent et al.*, 1990; *MacLeod and Yaoyancq*, 2000]. In continental settings, magma sills may be several

hundred meters to perhaps more than1 km thick [e.g., *Hogan and Gilbert*, 1995; *Auger et al.* 2001]; and similar melt thicknesses may result from impact events on Earth and other planets [e.g., *Rathbun and Squyres*, 2002]. Although the emphasis of this chapter is on the setting at oceanic spreading centers, where the AMC is typically ~ 100 thick or less, we consider sill-like magma chambers of different initial thicknesses ranging from 10 m to 1000 m.

To determine the magmatic heat flux for the different scenarios described in section 4.2, we solve equations (7), (8), (11) and (12) respectively in conjunction with equation (2). From these equations, the rate decay of the magma temperature with time varies inversely with the initial magma thickness D_0. Because the heat flux $F_m(t)$ also depends on mean magma temperature $T_m(t)$, its rate of decay also varies inversely with D_0. However, the initial heat flux $F_m(0)$ only depends on $T_m(0)$ (see equation (2)), which we assume to be a liquidus magma temperature T_L of 1200°C. Thus, $F_m(0)$ is independent of the initial thickness of magma chamber D_0.

4.3.1 Magmatic heat output for crystals suspended and crystals settling models without magma replenishment

In this part, we examine heat transfer from the magma chamber without magma replenishment as governed by equations (7) and (8). Both crystal-suspended and crystal-settling scenarios are considered. In both cases, the magma chamber starts at the liquidus temperature ($\chi = 0$). As in [*Liu and Lowell*, 2009] we assume magma surface area A_m to be 10^6 and 10^7 m^2. In the simulations, we calculate magmatic heat flux until either χ = 60% and the viscosity goes to infinity, or the total heat output drops below 10^7 W.

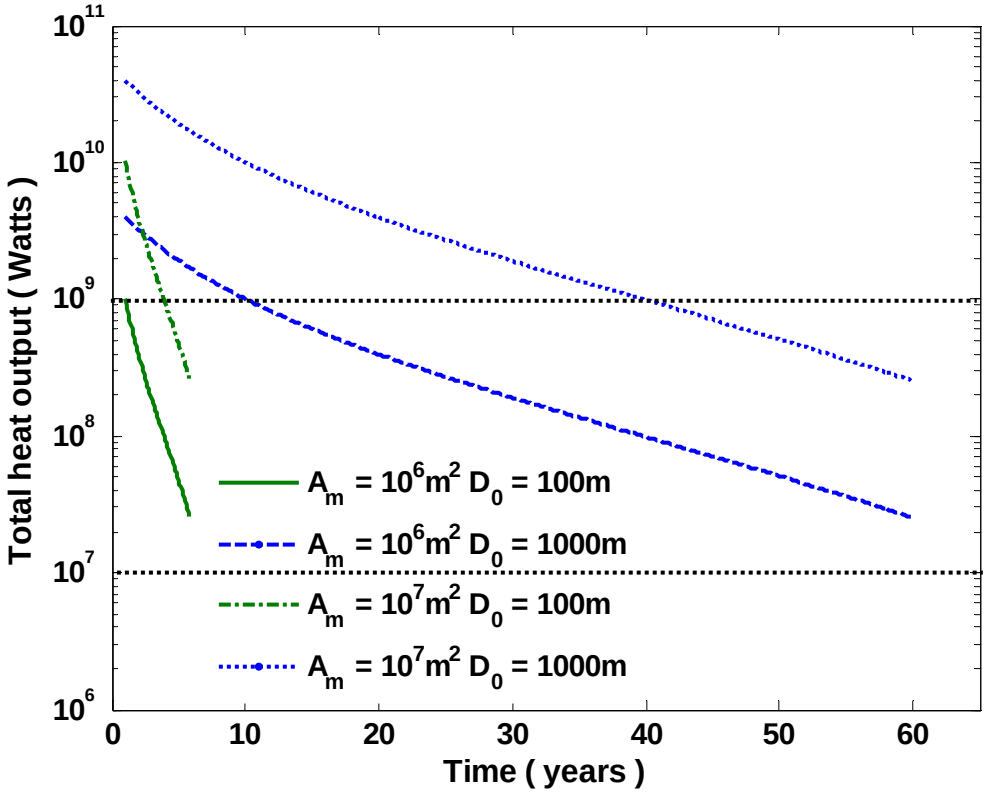

Figure 4.1 Total heat output as a function of time in the crystals suspended model without magma replenishment for two different initial thicknesses of magma chamber 100 m and 1000 m. A_m and D_0 denote the area and the initial thickness of magma chamber, respectively. A_m are 10^6 and 10^7 m^2. The magma area plays a role in determining the total heat output, but it has no influence on the lifetime of magma convection. The dashed horizontal lines located at 10^7 W and 10^9 W denote the approximate range of total hydrothermal heat output measured at oceanic spreading centers.

Figure 4.1 shows the total magmatic heat output as a function of time for the crystals suspended case for different initial thicknesses D_0. In these cases, convective magmatic heat flux stops because χ = 60%. The final total heat outputs are still greater than 10^7 W. As expected, the results in Figure 4.1 show that the larger the initial thickness the lower the rate of decay of magma heat output and the longer the convective lifetime. The lifetime is directly proportional to D_0. Note that because there is not enough

heat content in magma sill to keep the magmatic system last for 1 year, the heat output of the 10 m thick magma chamber is not shown in Figure 4.1. As noted earlier, the initial heat flux of 4.9×10^9 W is independent of the initial thickness of the magma chamber, but the initial total heat output is directly proportional to A_m.

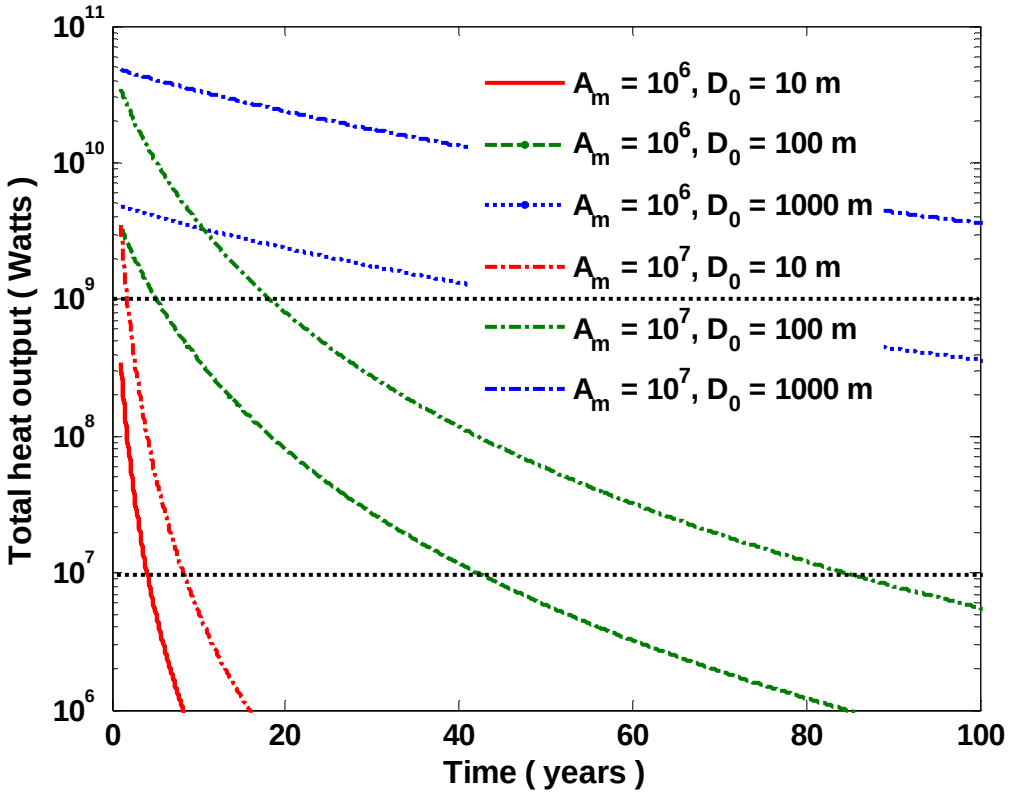

Figure 4.2 Same as Figure 4.1 except using the crystals settling model. The initial thicknesses of magma chamber are 10m, 100 m and 1000 m. In this case, the lifetime of magma convection increase significantly, although heat output gradually declines below 10^7 Watts.

Figure 4.2 shows the analogous results for the crystal settling model. As in the crystals suspended case, the rate of decay of magmatic heat output is inversely proportional to D_0. Similarly, the convective lifetime is directly proportional to D_0. In

contrast to the crystals suspended cases, however, the system lifetime is determined by the decay of the total heat output to below 10^7 Watts rather than by the crystallinity. Moreover, the comparison of Figure 4.1and Figure 4.2 shows that for a given value of D_0 and A_m, the heat flux decays more slowly in crystals-settling model than that in the crystals-suspended model. In contrast to the crystals-suspended case, the lifetime for even the D_0 = 10 m case is long enough to plot on the graph. The convective lifetime of the magma chamber with initial thickness of 1000 m and surface area of 10^6 m^2 is about 150 years, which is not shown entirely in the Figure 4.2 due to the scale of the figure. Note that precisely speaking, a magma chamber 1000 m thick with a surface area of 10^6 m^2 is a pluton, not a sill. To be considered a sill with this thickness its surface area would have to be ~10^8 m^2 or more. Moreover, such thick sills probably reflect multiple intrusion events. Here, we neglect the magma convection along the sides of pluton and assume that the rate of magma intrusion is fast compared to the cooling time so that the emplacement is effectively instantaneous.

The difference between Figures 4.1 and 4.2 results from the assumed end-member crystallization scenarios. In the crystals suspended case, the crystals mix well with the magma and the viscosity of the mixture increases rapidly as crystal content increases (equation (3)). From the equations (1) and (2), viscosity exerts a significant control on the Rayleigh number and hence on the rate of heat loss from magma chamber. In the crystals settling case, the viscosity of the magma is only a relatively weak function of temperature (equation (4)); and heat output decays mainly because $T_m(t)$ and the thickness of the liquid magma layer decrease with time.

4.3.2 Magmatic heat output for crystals suspended and crystals settling models with replenishment

[*Liu and Lowell*, 2009] showed that stable heat flux from a convecting AMC requires magma replenishment. Similar to the no-replenishment scenario, both crystals suspended and crystals settling cases are investigated. The magma chamber at its liquidus beneath a colder upper boundary represented by the hydrothermal system begins to crystallize and its volume shrinks. As the internal pressure in magma chamber declines new magma may be driven upward from the reservoir of relatively crystal-rich partial melt that occupies the lower crust [e.g., *Mainprice*, 1997; *Dunn et al.*, 2000]. Magmas from the mushy zone may also ascend because of the buoyancy that results from the density difference between melt and crystals in the mush zone either as porous flow [e.g., *McKenzie*, 1984] or as buoyant fluid-filled dikes [*Lister*, 1990]. When a new magma batch enters the chamber, we ignore the density differences that may be present and assume that the new magma mixes with the contents in chamber immediately. If the rate of magma replenishment is faster than the rate of volume loss resulting from crystallization, magma replenishment results in an increase of melt. We employ a numerical model to describe the magma chamber growth. Here, we assume that the surface area of the magma chamber remains fixed and the thickness of the magma body increases as new magma is added to the magma chamber (see equations (11) and (12)). We carry out simulations to examine the impact of initial thickness of magma chamber on the heat flux. Similar to the no-replenishment case, we choose the initial thickness to be 10, 100, and 1000 m, respectively. Based on the discussion in [*Liu and Lowell*, 2009], the velocity of magma replenishment between 10^{-7} and 10^{-8} m/s can yield quasi steady

state heat output on decadal timescales. In the simulations presented here we assumed a constant replenishment rate of 5×10^{-8} m/s. In our simulations for magmas initially 100 and 1000 m thick, we stop the simulations when the magma chamber grows to double its initial value. This limit is somewhat arbitrary, but at mid-ocean ridges seismic suggests that the magma chamber is typically not more than ~ 100 m thick [e.g., *Kent et al*., 1990; *MacLeod and Yaoyancq*, 2000]. For a 10 m initial size, we halt the simulation when it grows by a factor of 10.

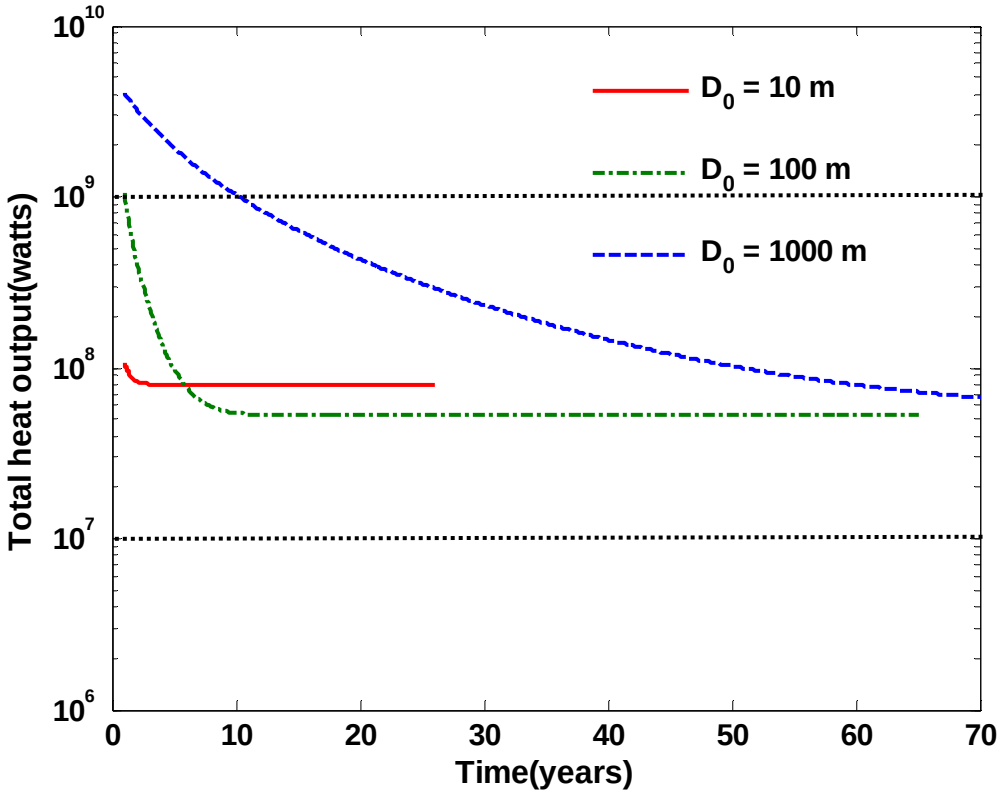

Figure 4.3 Total heat output as a function of time in the crystals suspended model for the different values of magma chamber thickness 10, 100, and 1000 m. The constant magma replenishment rate u_0 = 5×10^{-8} m/s, the area of magma chamber A_m = 10^6 m^2. The simulations are run until the magma thickness double. Except that the magma chamber with the thickness of 1000 m takes more than 600 years to double. It is not shown entirely due to the limited scale of the figure. Although the thicker magma body will last longer, the thinner one can undergo longer replenishment times. For a 10 m thick sill, the magmatic heat flux remains constant for 26 years as the sill thickness increases to 50 m.

Figure 4.3 and Figure 4.4 show the results of magmatic heat flux for crystals suspended and crystals settling models with magma replenishment, respectively. We define the doubling time as the time over which the initial thickness of magma chamber doubles. In each scenario the doubling time is proportional to the initial thickness of the magma. For example, with the same magma replenishment rate, the doubling time is 65 years for the magma with initial thickness of 100 m, while it is 6.5 years for the magma chamber with the initial thickness of 10 m and 650 years for an initial thickness of 1 km. Also as expected, the lifetimes of magmatic heat output are commonly extended by magma replenishment.

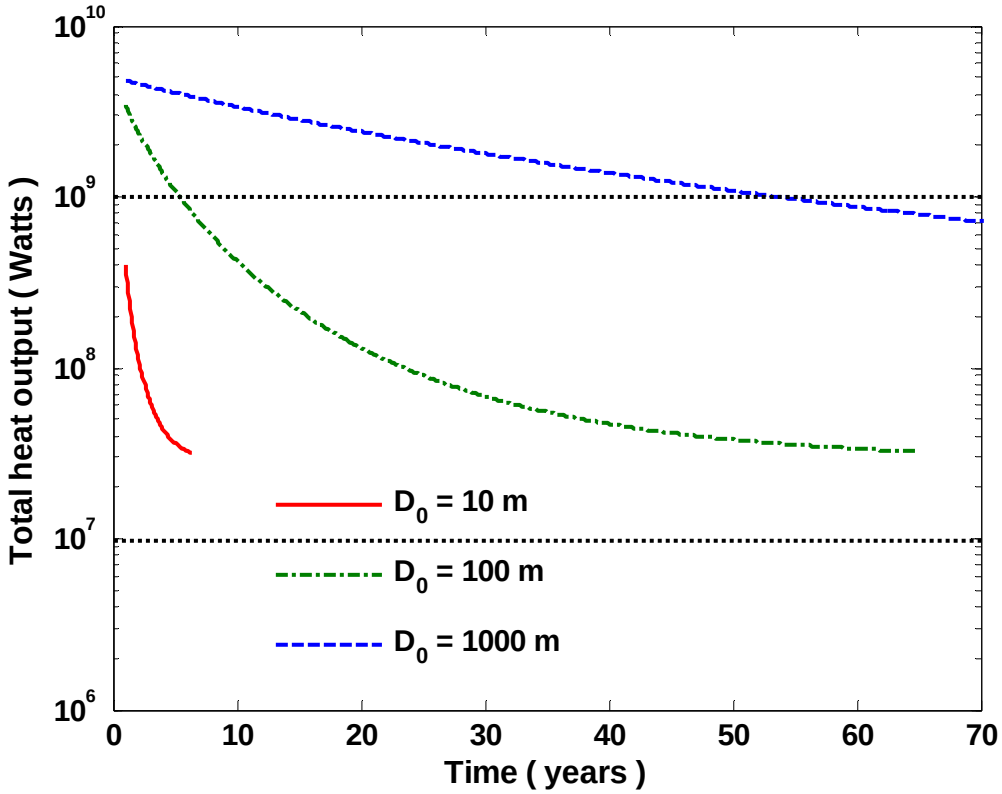

Figure 4.4 Same as Figure 4.3 except using the crystals settling model. As in Figure 4.3, simulations are run until the magma size doubles. Although heat output is decreasing, for $u_0 = 5\times10^{-8}$ m/s, heat output is approximately constant on decadal timescales.

Figure 4.5 implies that it takes less time for a thin magma body to double its thickness than for a thick one. Moreover, if a magma chamber starts with a thin size (10 m), it has the ability to grow to ten times the initial size rather than two times and still be within the MOR observational limits. For a magma chamber with small initial thickness (10 m), magma convection approaches a steady state after the magma thickness doubles, although it can grow up to 10 times the initial size to 100 m. Thus a small magma sill could achieve longer stable heat output by simply starting with a thinner initial magma body.

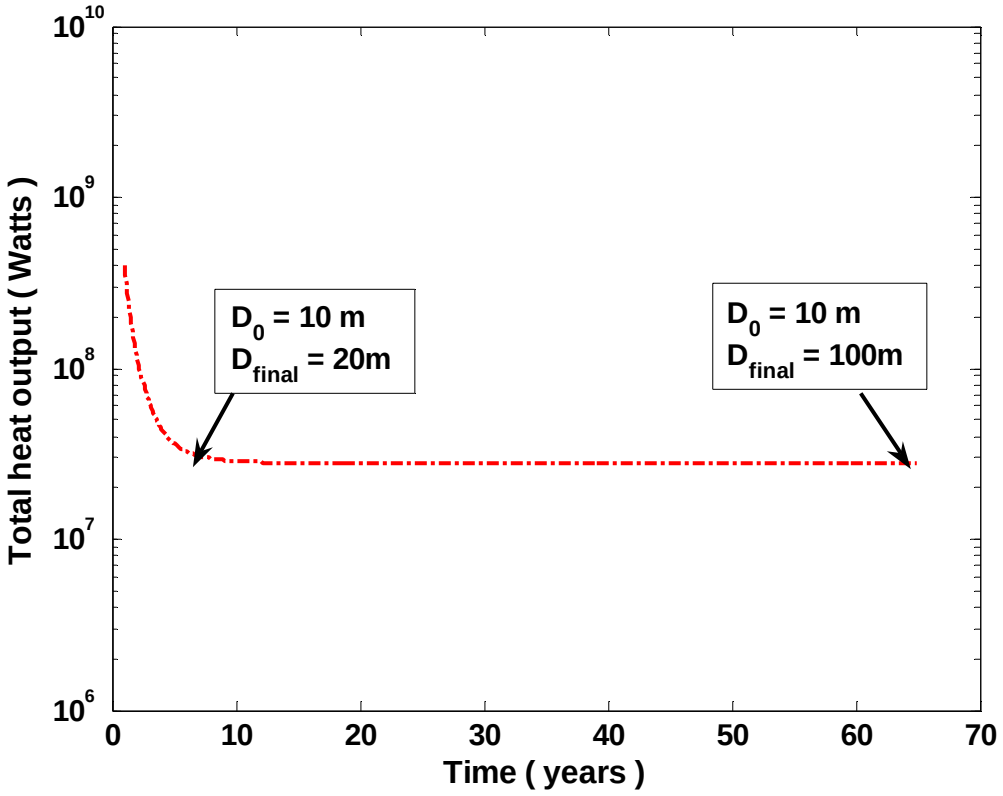

Figure 4.5 Compare the lifetime of magmatic heat transfer when the thickness of magma chamber increases two and ten times in crystals settling model at a constant magma replenishment rate. For the magma chamber 10m thick, the magma convection system enters a steady state after the magma thickness doubles. Thus, the small magma chamber could achieve longer stable heat output.

4.4 The Effect of Episodic Replenishment

The volume of incoming magma batches, their frequency, and the volume of the magma chamber play a critical part in heat transfer from magma systems. In section 4.3, we discussed the effect of the initial magma thickness on magmatic heat flux. In this section, we examine the effects of dynamically changing of magma volume by investigating the effects of episodic rates of magma replenishment.

High-temperature hydrothermal venting has shown marked stability in both composition and temperature at least on a decadal-scale [*Campbell et al.*, 1988; *Bowers et al.*, 1988; *Von Damm et al.*, 2002]**.** The analysis in [*Liu and Lowell*, 2009] and in the preceding section shows that magma replenishment is necessary to maintain a steady state hydrothermal system; but results were based on either a constant or exponentially decreasing replenishment rate. Although the results are instructive, there is little justification for such simplified replenishment scenarios. A more rigorous analysis of the replenishment rate is necessary for better understanding the effect of magma replenishment on hydrothermal heat output.

In this section, we incorporate episodic magma replenishment based on evidence for such replenishment in the literature. For example, the theoretical arguments in favor of episodic injection at all spreading rates have been advanced by *Lister* [1983b]. The seismic reflection by *Detrick et al.* [1987] suggests that the episodicity is important event along about 60% of the surveyed East Pacific Rise. Evidence of large-scale episodic venting of hydrothermal fluids was discovered at Juan de Fuca Ridge in 1986 [*Baker et al.*, 1989]. A detailed study of magnetization and morphology coupled with seismic reflection by *Collier and Sinha* [1992] has shown that magmatic processes on the Valu Fa

Ridge are episodic. In addition, there is evidence for episodic replenishment of the AMC at relatively high frequency, including eruption scenarios and non-eruptive diking events. For instance, the eruption cycle from 1991 to 2005/2006 near 9°50′ N on the EPR [*Haymon et al.*, 1993, *Soule et al*. 2007] provides direct evidence of replenishment at decadal timescales; and vent temperature excursions during this period [*Sohn et al.*, 1998; *Schierer et al*, 2006] may represent non-eruptive diking events [*Ramondenc et al.*, 2008; *Germanovich et al.*, 2010]. A non-eruptive diking event that affected vent temperature and chemistry has also been observed at Main Endeavour Field (MEF) on Juan de Fuca ridge (JDFR) [*Johnson et al.*, 2000, *Lilley et al.*, 2003]. Thus, we propose a new replenishment model to simulate a periodically replenished, continually cooled and fractionated magma chamber.

4.4.1 Sinusoidal magma replenishment rate

The characteristics of the hydrothermal system driven by the underlying magma chamber are closely coupled to the replenishment of the AMC process. For simplicity we assume that replenishment occurs over the entire base of the AMC and that the instantaneous rate of replenishment u is only a function of time. Based on the Fourier analysis, any periodic function $u(t)$ can be decomposed into a sum of simple oscillating functions, namely sines and cosines [*Oppenheim et al.*, 1996].

$$u(t) = a_0 + \sum_{n=1}^{\infty} a_n \sin(nwt) + b_n \cos(nwt) \tag{15}$$

For simplicity, we model the rate of magma replenishment as a sinusoid function

$$u(t) = u_0 + u_0 \sin(wt) \tag{16}$$

where u_0 is the initial replenishment rate, w is the injection frequency of magma refilled from mushy zone, and the corresponding replenishment period is $P = 2\pi/w$. As a consequence of the principle of superposition, once the behavior of the hydrothermal system subject to equation (16) is well understood, one can obtain the response to any other periodic function by utilizing the Fourier expansion in equation (15). Combining equations (10) and (16), the thickness of magma chamber is expressed in terms of the replenishment rate by:

$$D(t) = u_0 t + D_0 + \frac{u_0}{w}(1 - \cos(wt)) \tag{17}$$

Note that with a constant magma replenishment $u(t) = u_0$, the thickness of magma chamber is expressed by [*Liu and Lowell*, 2009]

$$D(t) = u_0 t + D_0 \tag{18}$$

Comparing equations (17) and (18), we see that when the magma replenishment period is infinite (frequency is zero), equation (17) reduces to equation (18). Thus, with the replenishment rate model of equation (16), a broader range of situations are covered. Moreover, with non-zero replenishment frequency, the periodic replenishment rate is always greater than the constant rate. Thus, the time to double the thickness of the magma chamber is less in the case with periodic supply than in the case of constant replenishment. The doubling time also depends upon the replenishment period because the period affects the rate of temporal variation of the total heat output. If the replenished period is 1 year, the equation (17) is nearly the same as equation (18), which means, that the overall trend of total heat output doesn't change with time. Over the same length of time, however, for a larger replenishment period, the total heat output exhibits much greater fluctuations with time.

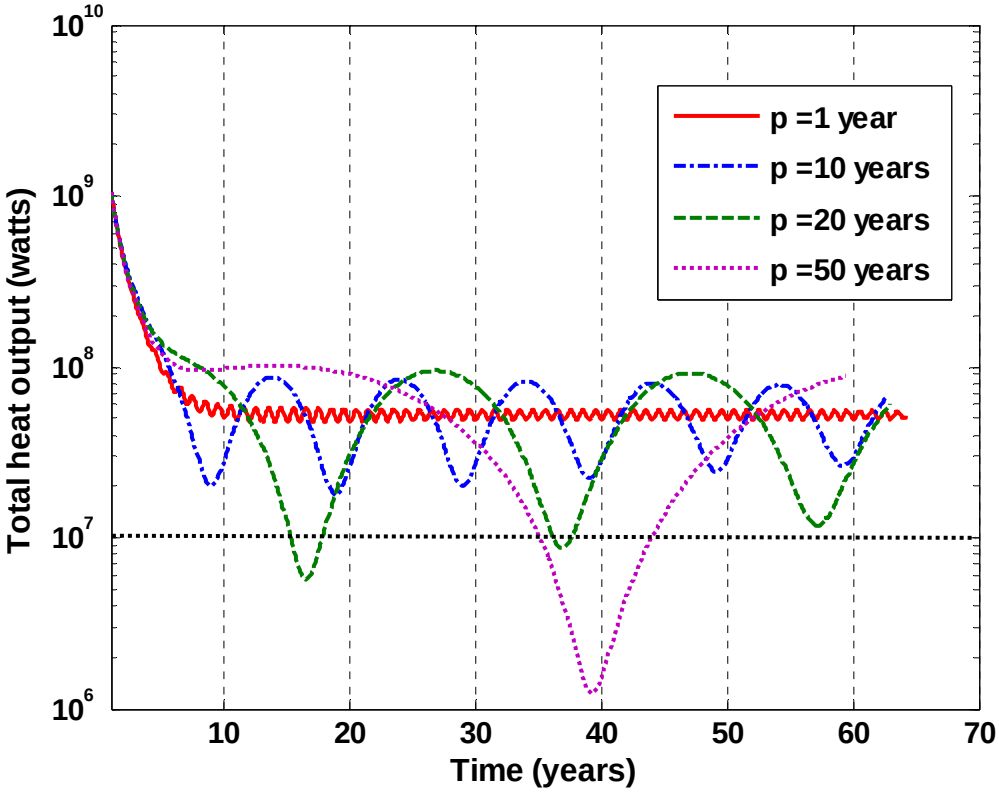

Figure 4.6 Total heat output as a function of time in the crystals suspended model with magma replenishment at four different periodic intrusion rates for 1, 10, 20, and 50 years. *P* denotes the magma replenishment period. The magma replenishment rate is sinusoidal with initial rate $u_0 = 5\times10^{-8}$ m/s. Simulations are run until the thickness of magma chamber doubles.

In the following, we simulate the magmatic heat output with periodic replenishment considering both the crystals suspended and the crystals settling models. Similar to the section 4.3.2, $u_0 = 5\times10^{-8}$ m/s in each case and the thickness of magma chamber is 100 meters. For the crystal-suspended model we choose replenishment periods of 1, 10, 20 and 50 years, whereas for the crystals-settling case we use 1, 10, 50 and 100 years, respectively. For the latter case, we choose the longer replenishment period because the relatively low magma viscosity results in vigorous convection within the magma chamber. As a result, higher heat flux can be maintained. For the crystal

suspended model quasi-stable heat output requires a greater frequency of magma replenishment. Figure 4.6 shows the heat output characteristics in the crystal suspended case. Replenishment periods of 1 and 10 years keep the total heat output within the observational range of 10^7 to 10^9 Watts. At longer replenishment periods, the heat loss from magma chamber is greater than the rate of magma heat flux into magma chamber. As a result, the total heat output may at times drop below the observational lower boundary 10^7 Watts.. For example, the total heat output drops below 10^7 Watts after around forty years when the replenishment period increases to 50 years and remains there for nearly a decade. To keep the total heat output within the observed range, our results show that the replenishment period must be less than 15 years. Moreover, we notice that the hydrothermal activity reaches its lifetime because crystal content in magma chamber approaches 60%. The crystallinity does not go rapidly up to 60% and shut the system down in a few years as it does in the no-replenishment case [*Liu and Lowell*, 2009]. This can be explained through a close look at the changes of Rayleigh number with and without magma replenishment. With magma replenishment, the Rayleigh number is 9.6×10^7 after six years; whereas, the Rayleigh number is 3×10^6 at the same time in the non-replenishment case. As a result of the high Rayleigh number, convection is maintained within the magma chamber. In addition, at longer replenishment periods, the heat output exhibits large fluctuations on decadal timescales. The fluctuations of heat output are not symmetric, because cooling initially affects the heat loss in the convecting magma system more rapidly than the increasing heat flux that accompanies magma replenishment. Consequently, the total heat output exhibits non-symmetric variation,

which is shown as a sharper drop and slower increase. As the rate of heat loss from cooling decreases, the temporal evolution of the heat flux becomes more symmetric.

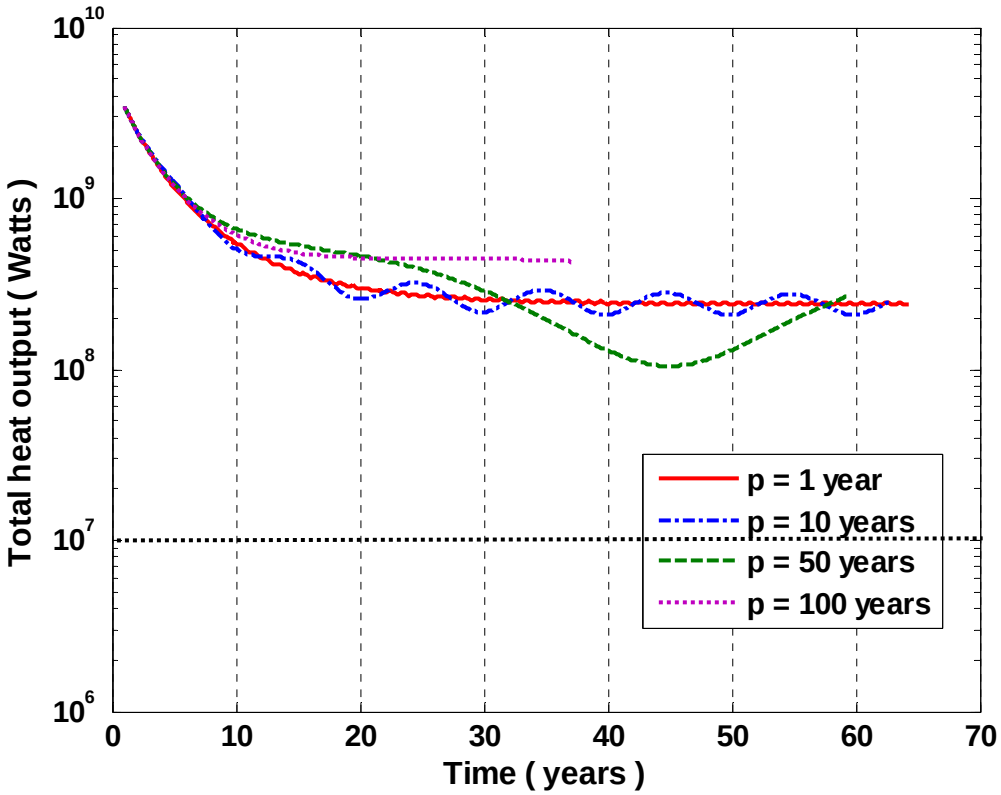

Figure 4.7 Total heat output as a function of time in the crystals settling model with magma replenishment at four different periodic intrusion rates for 1, 10, 50, and 100 years. *P* denotes the magma replenishment period. The magma replenishment rate is sinusoidal with initial rate $u_0 = 5\times10^{-8}$ m/s. Simulations are run until the thickness of magma chamber doubles. The growth of magma chamber thickness is a function of magma replenishment rate and period. At the same magma replenishment rate, the magma chamber with a large replenishment period doubles first.

Figure 4.7 shows the heat output in the crystals settling case. It can be seen that the periodic variation of total heat output is not as large as in the crystals suspended case. Moreover, the magmatic heat output is within the range between 10^7 to 10^9 Watts for all

replenishment periods. Figure 4.7 shows that convective heat output is longer-lived and more stable in the case of crystals settling than in the case of crystals suspended (Figure 4.6). This is primarily a result of the relatively slow rate of change of magma viscosity in the crystals settling regime. Because the heat output is maintained above 10^7 W, the crystal settling model does not have a critical requirement for the period of magma replenishment.

4.4.2 Exponential sinusoidal magma replenishment rate

In the previous section we considered simple sinusoidal replenishment. Because gradual depletion of the underlying mush zone may result in a declining replenishment rate, we also consider a periodic rate of magma replenishment with an exponential decay envelope:

$$u(t) = u_0 + u_0 e^{-bt} \sin(wt) \tag{19}$$

In this case, substituting equation (19) into (10), the time dependent magma chamber thickness is given by

$$D(t) = D_0 + u_o t + u_0 \beta(t) \tag{20}$$

Where

$$\beta(t) = \frac{w - w\cos(wt)e^{-bt} - b\sin(wt) + e^{-bt}}{b^2 + w^2} \tag{21}$$

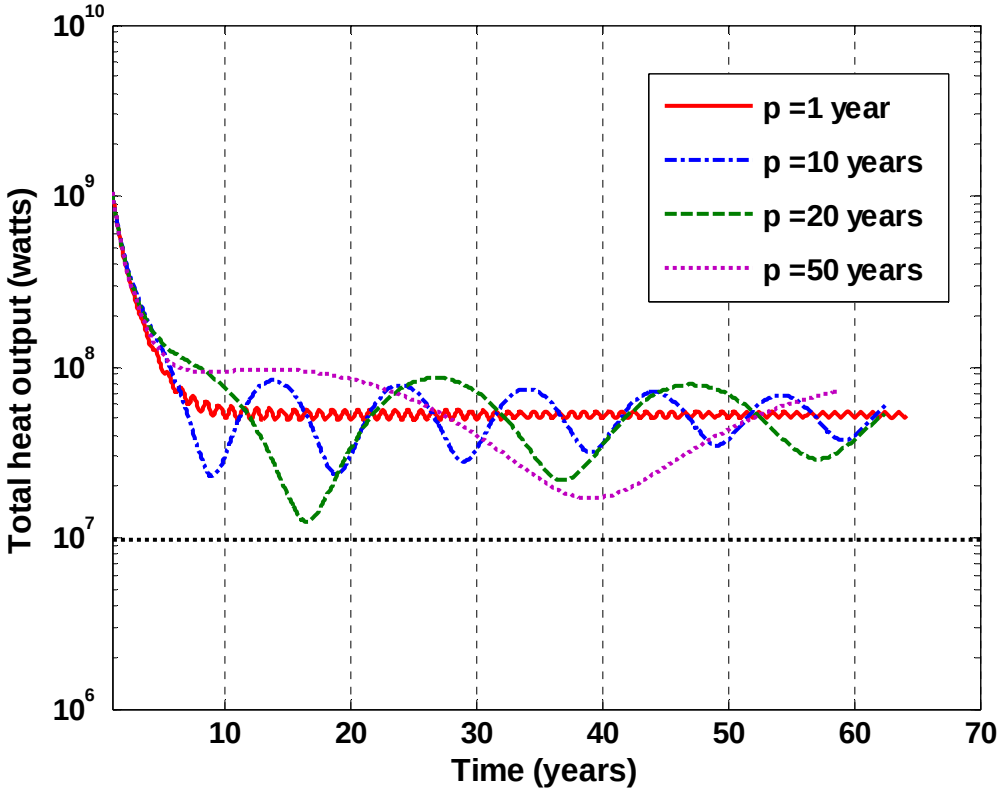

Figure 4.8 Total heat output as a function of time in the crystals suspended model with episodic magma replenishment for different periods of 1, 10, 20, and 50 years. The magma replenishment rate is exponential sinusoidal with initial rate $u_0 = 5\times10^{-8}$ m/s, the exponential factor $b = 3\times10^{-10}$. Simulations are run until the thickness of magma chamber doubles.

Figure 4.8 and Figure 4.9 show the heat output of crystals suspended and crystals settling magma system, respectively. With different replenishment periods, an initial rate of replenishment $u_0 = 5\times10^{-8}$ m/s, and constant value b of 3×10^{-10}. The selection of the replenishment period is the same as in section 4.1. Comparing the exponential decaying sinusoid with simple sinusoid replenishment rate, we observed that in the crystals suspended system, even large replenishment period, for instance, 50 years, still maintains the system total heat output between 10^7 W to 10^9 W (see Figure 4.6 and Figure 4.8).

Similarly, in the crystals settling system, the total heat output with exponential sinusoid magma replenishment rate are higher than that with simple sinusoid magma replenishment for the same period (see Figure 4.7 and Figure 4.9). Based on the exponential decaying replenishment model, the magmatic heat transfer is also maintained steady for a long period. Thus, the conclusion in [*Liu and Lowell*, 2009] that quasi-steady magmatic heat output can be maintained for long periods of time by magma replenishment can be drawn in a broader sense.

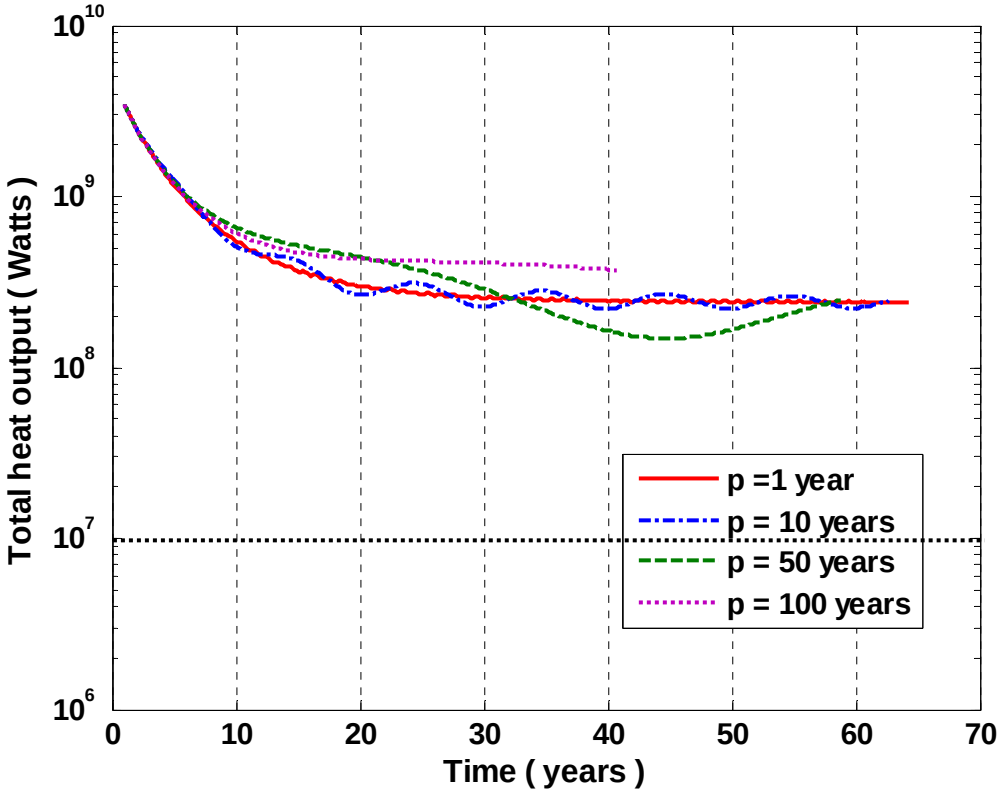

Figure 4.9 Total heat output as a function of time in the crystals settling model with episodic magma replenishment for different periods at 1, 10, 50, and 100 years. The magma replenishment rate is exponential sinusoidal with initial rate $u_0 = 5\times10^{-8}$ m/s, the exponential factor $b = 3\times10^{-10}$. Simulations are run until the thickness of magma chamber doubles.

4.5 Discussion

This chapter has linked heat transfer from a vigorously convecting, crystallizing, and replenished sill-like magma chamber to an overlying hydrothermal system using a parameterized convection model to describe the dynamic behavior of the magma chamber. We have considered both crystals suspended and crystals settling models to describe the evolution of the magma body. We have assumed, for simplicity that the magma replenishment results only in increasing the thickness of the magma, while the surface area remains constant, though the latter case has been discussed by *Liu and Lowell* [2009]. We have investigated the effect of the initial magma chamber size by considering initial thickness ranging from 10 m to 1000 m. We have also investigated the effects of a periodic replenishment rate on magmatic heat output, but for these models we have assumed an initial sill thickness of 100 m. Our simulations were not designed with any particular spreading center in mind, but in the discussion below we describe how the model might apply to the East Pacific Rise (EPR) near 9°50′ N, which has undergone a full eruptive cycle between 1991/1992 and 2005/2006. In the following subsections, we discuss the implications of the model in terms of internal properties of the magma chamber over time and the linkages between modeled magmatic heat output and hydrothermal venting.

4.5.1 Implications for evolution of the AMC

4.5.1.1 Magma temperature

Figure 4.10 shows the effects of different magma replenishment rates on evolution of magma temperature for a sill initially 100 m thick; and Figure 4.11 shows

the effects of initial magma chamber thickness on the evolution of magma temperature for a fixed replenishment rate $u_0 = 10^{-8}$ m/s. In both cases mean magma temperature drops rapidly and then stabilizes as magma replenishment stabilizes the heat output. Figure 4.10 shows that the greater the replenishment rate and the higher the equilibrium heat flux, the higher the resulting magma temperature. This result follows directly from equation (2). Similarly Figure 4.11 shows that the smaller the initial thickness of the magma chamber the faster the magma temperature drops. This is consistent with the fact that because of their smaller Rayleigh number, the initial rate of decay of the magmatic heat flux is greater for thinner sills than for thicker sills. However, once replenishment stabilizes the heat flux, the steady magma temperature is nearly the same regardless of the initial thickness.

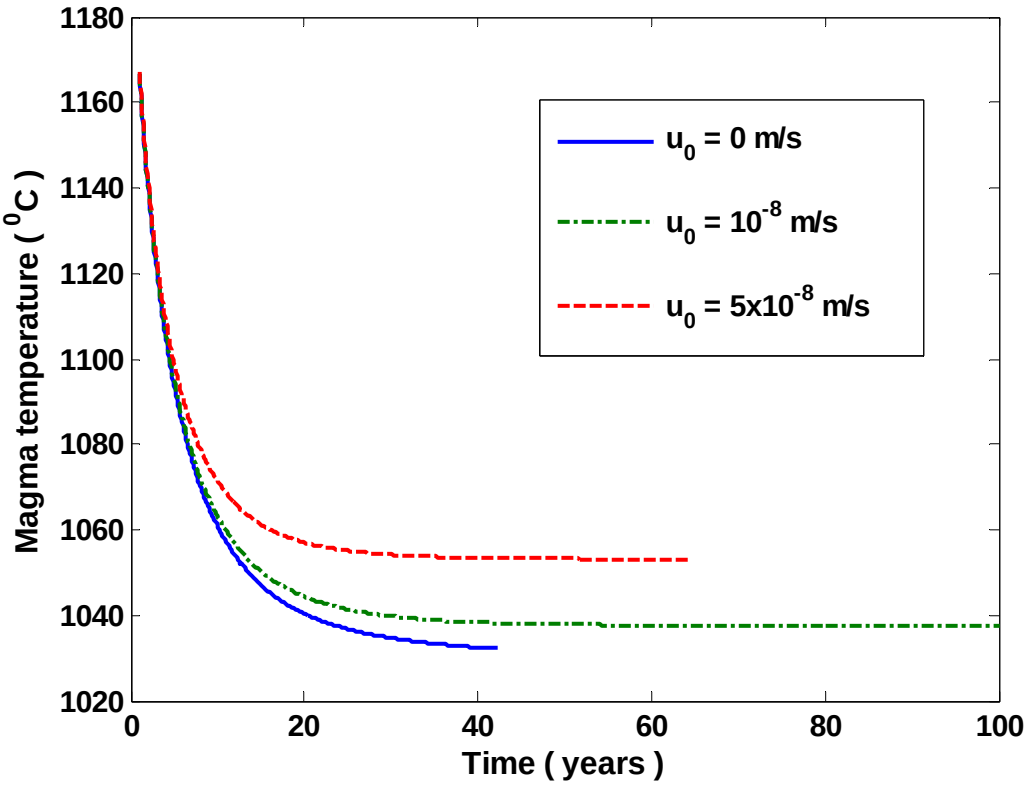

Figure 4.10 Magma temperatures as a function of time for the crystals settling case without and with magma replenishment. u_0 denotes the initial magma replenishment velocity, and $u_0 = 0$ denotes the case without magma replenishment. The initial thickness of magma sill is 100 m.

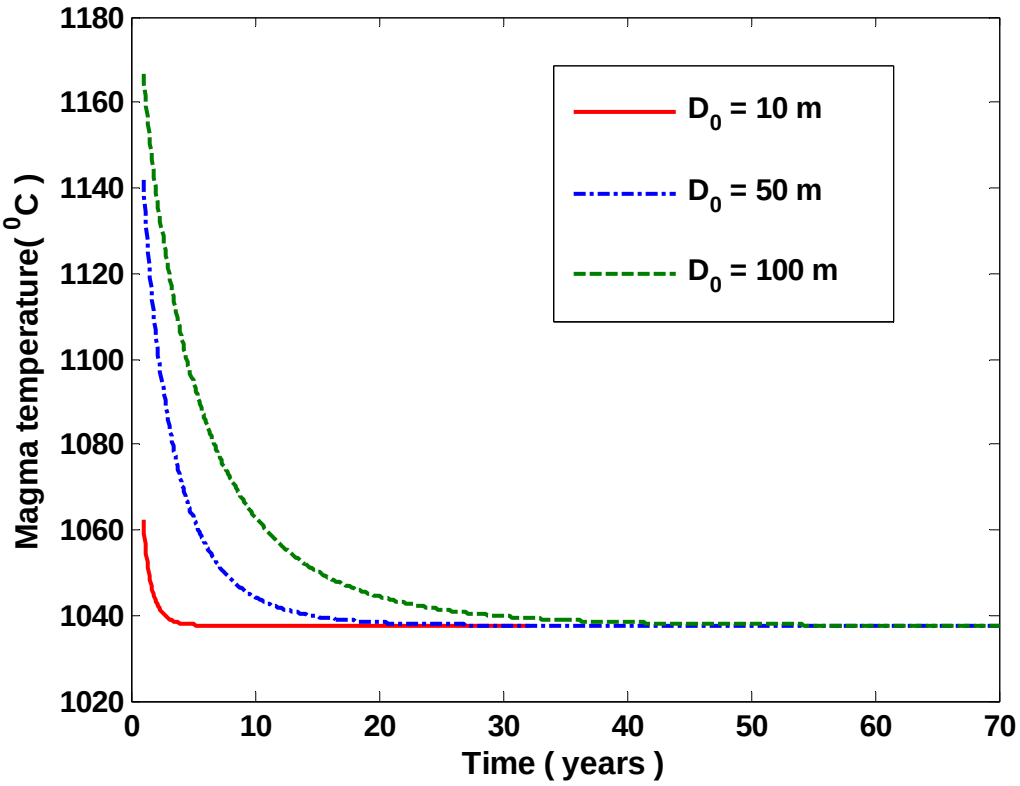

Figure 4.11 Magma temperatures as a function of time for the crystals settling case with magma replenishment at 10^{-8} m/s for different magma thicknesses. D_0 denotes that the initial thickness of magma chamber.

Figure 4.12 and Figure 4.13 depict the evolution of magma chamber temperatures for an initial 100 m thick sill and periodic magma replenishment for the crystals suspended and crystals settling cases, respectively. Figure 4.13 shows that with the exception of the periodic fluctuations the temperature evolution is similar to that in Figure 4.12. For the crystals settling cases, which are most appropriate for mid-ocean ridge settings, the results suggest that even with magma replenishment at a rate to eventually stabilize the heat flux, that magma temperature may drop or fluctuate as the heat balance between cooling and replenishment fluctuates.

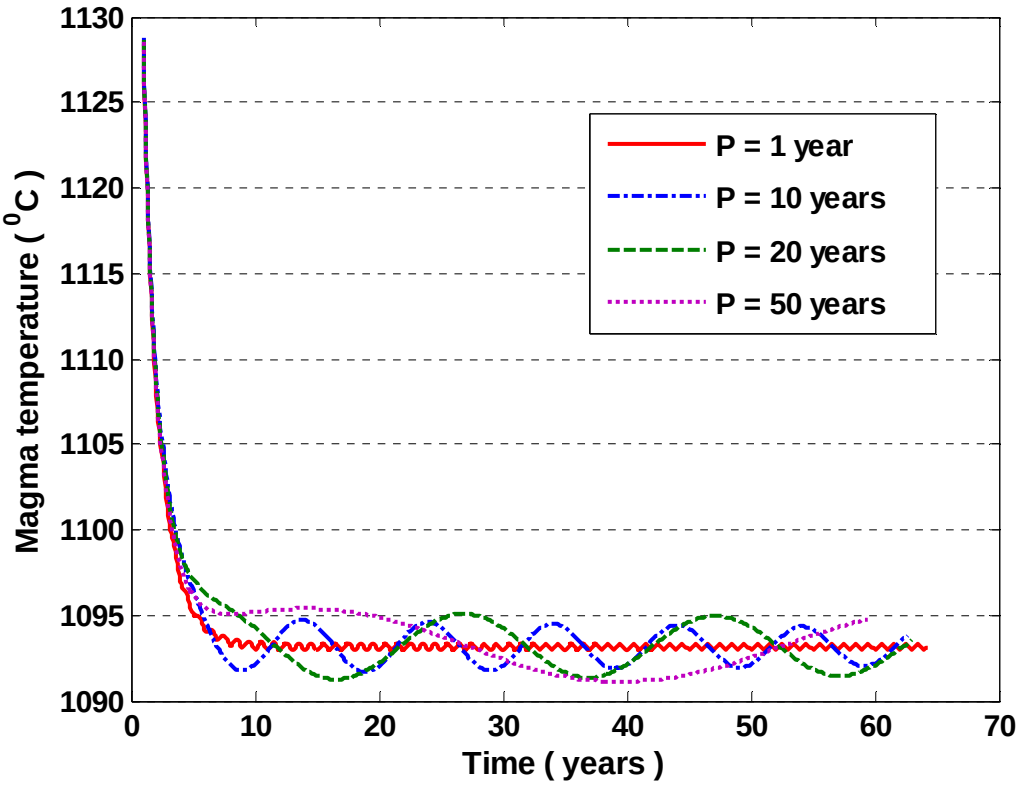

Figure 4.12 Magma temperatures as a function of time for the crystals suspended case with magma replenishment at 5×10^{-8} m/s. Curves end when the thickness of magma chamber doubles.

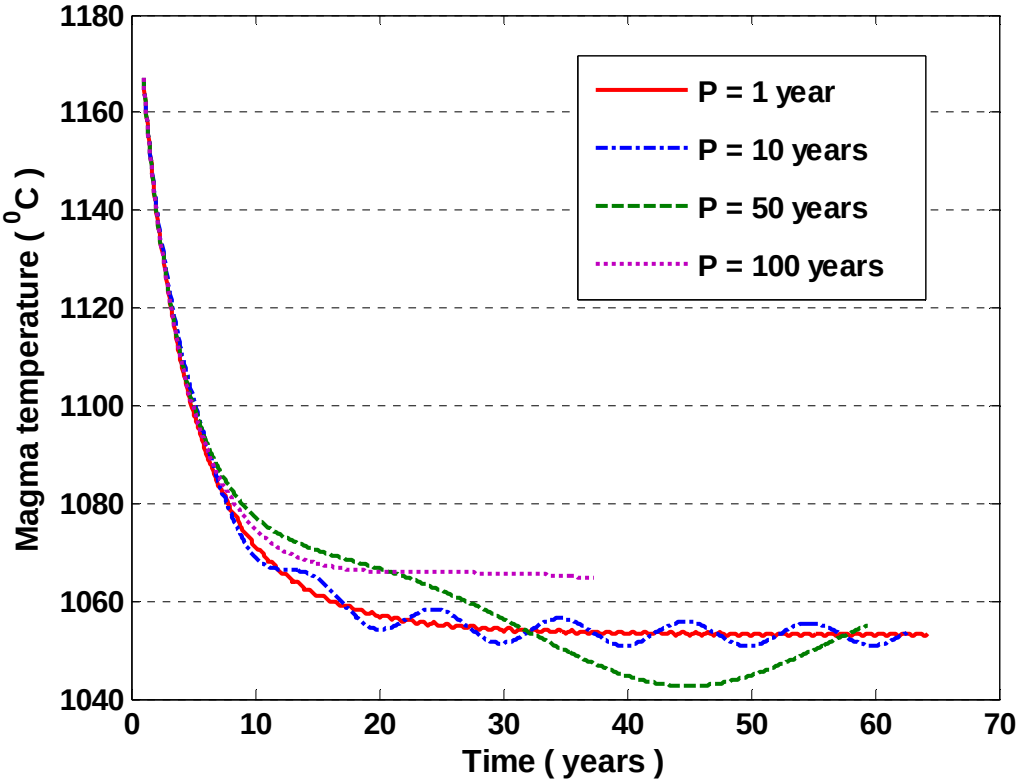

Figure 4.13 Magma temperatures as a function of time for the crystals settling case with magma replenishment at 5×10^{-8} m/s.

The magma temperatures produced here are significantly less than is typically estimated for MORB lavas. This result may be partly a result of the viscosity models used in the simulations. The value ν_{m0} = 0.1 m^2/s chosen is for a crystal free basalt, however, the presence of micro-crystals in the lava may increase this value by orders of magnitude [*Lejeune and Richet,* 1995]. Even for crystals settling models, the effect of micro-crystallinity on the viscosity within the cooling basalt may need to be considered to obtain more accurate magma temperatures. The assumption of instantaneous mixing with replenished magma is also somewhat simplistic. The overall trends of magma temperature evolution should remain unchanged, however.

4.5.1.2 Melt thickness

Along with the evolution of magma temperature, we also explore the evolution of liquid part of the magma chamber as replenishment occurs. The thickness represented by equation (10) is the thickness of original liquid magma chamber plus the thickness resulting from replenishment. For the crystal suspended case, the thickness of liquid magma chamber is the same as that of magma chamber since crystals are not separated. For the crystal settling case, the thickness of liquid magma chamber depends on both the magma chamber thickness and crystal content, which can be represented by

$$D_m(t) = [1 - \chi(t)]D(t) \tag{22}$$

Where $D_m(t)$ is the thickness of liquid magma, and $\chi(t)$ from equation (5) denotes the crystal content, which varies with time as the magma system evolves.

Figure 4.14 and Figure 4.15 depict the liquid magma thickness growth with respect to time for the magma chamber with thickness of 100 m and 10 m, respectively, for a replenishment rate of 5×10^{-8} m/s and different periodic replenishment frequencies. Although magma replenishment is included, Figure 4.14 shows that the thickness of liquid magma layer decreases rapidly during the first decades of magma chamber cooling and crystallization because convective heat loss initially exceeds the rate of heat input from replenishment. After the heat flux from magma replenishment balances the convective heat loss, the thickness of liquid magma increases slowly with time. Figure 4.15 shows that convective heat loss has a relatively greater effect on reducing the melt thickness of a thinner magma chamber in the early stages of cooling. Figure 4.15 shows that a 10 m thick melt lens will shrink to 4 m after 1 year (60%) whereas a 100 m thick melt lens thins to 85 m (15%) in the same time frame in Figure 4.14.

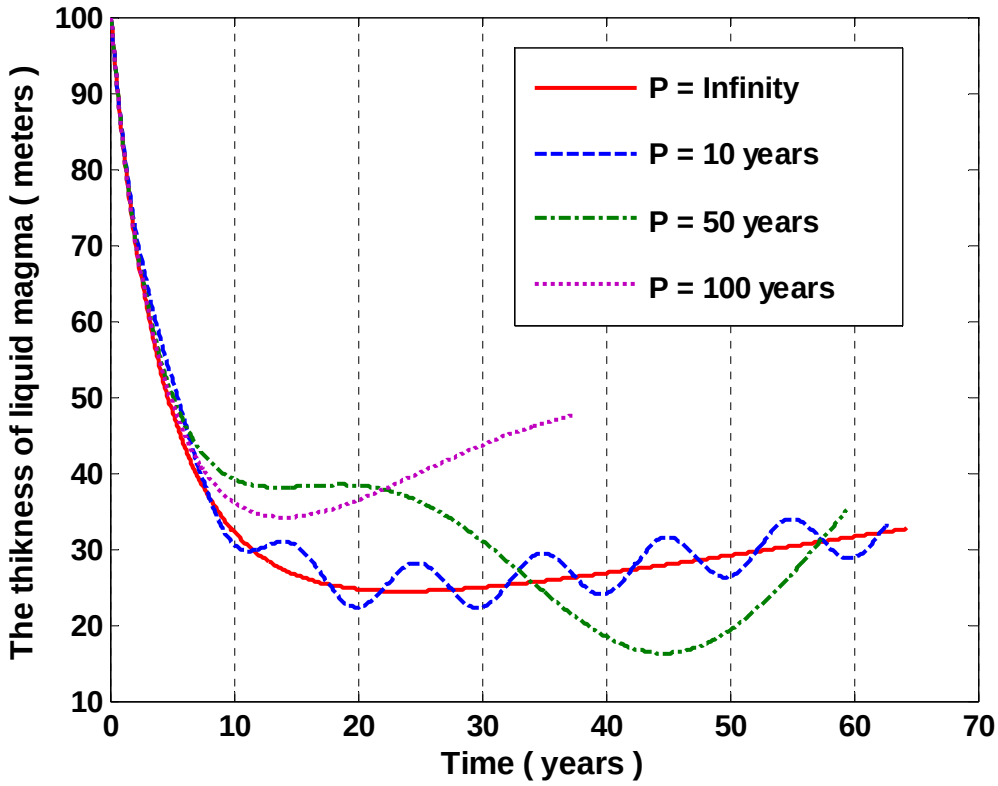

Figure 4.14 The time-varying of the thickness of liquid magma layers. The magma chamber with the initial thickness of 100 m grows with magma replenishment at 5×10^{-8} m/s for the crystals settling case. Magma chambers doubles for different values of magma replenishment period. *P* = infinity denotes the constant magma replenishment case.

Small essentially liquid-filled melt bodies, which are frequently present at the fast spreading ridges [*Detrick et al*., 1987; *Detrick et al*., 1993], are more sensitive to small frequent changes in thermal conditions because of the more tenuous balance between melt supply and convective heat loss. When replenishment balances convective loss at a given replenishment rate, the thickness of liquid magma layer increases relatively faster for a magma chamber with smaller initial thickness than for a thicker one. This occurs because at a given replenishment rate, the relative rate of volume increase is greater for a

thinner magma chamber than for a thicker one. Thus, one might anticipate that smaller melt lenses require lower replenishment rates to avoid freezing entirely.

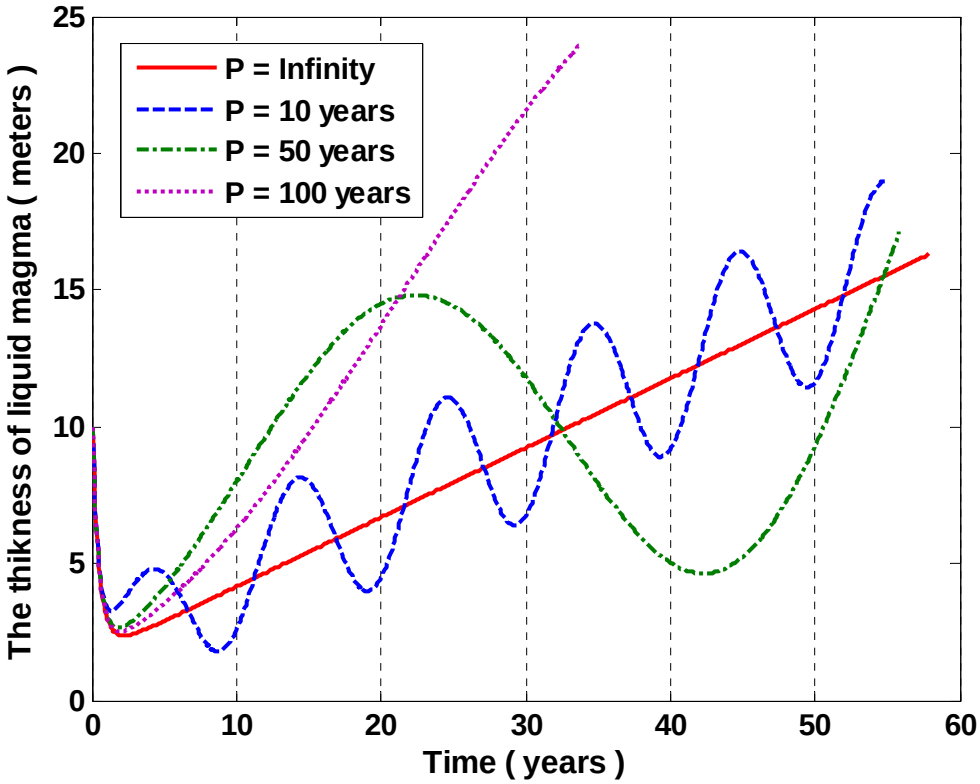

Figure 4.15 The time-varying of the thickness of liquid magma layers. The magma chamber with the initial thickness of 10 m grows with magma replenishment at 5×10^{-8} m/s for the crystals settling case. Magma chambers grow up to 10 times at different values of magma replenishment period.

Different magma replenishment rates might have different effects on the liquid magma chamber thickness and heat flux. At the beginning phase, when magma cooling and crystallization outweighs the effect of magma replenishment, both the liquid magma thickness and the convective heat flux drop sharply. When cooling weakens and magma replenishment dominates the magma chamber heat output, whether the liquid magma

thickness and the heat flux increase or decrease depends on the replenishment rates. In our example, the replenishment rate is high enough to increase the liquid magma thickness (see Figure 4.14); however, it is not so high that the heat output increases with time (see Figure 4.7).

In these simulations, even though the magma chamber may double or more in thickness, the thickness of the melt layer itself remains quite thin, and its position in space may not change dramatically. This result is consistent with recent 3-D seismic results from the EPR 9°50′N area, which suggest that the AMC is located in essentially the same place as in the 1985 survey of *Detrick et al*. [1987] [*Carbotte et al*., 2008].

4.5.1.3 Effect of magma replenishment temperature

Analysis of the lavas from the 2005/2006 eruptions at EPR suggests that the replenishment occurred, at least in part, with more evolved and cooler magma [*Goss et al*., 2010]. We assumed that the replenished magma at temperature of T_{in} which is less than the liquidus temperature T_L, and there has already been a certain amount of latent heat removed from the incoming melts. Assuming the latent heat is released uniformly between the liquidus (with temperature of 1200°C) and solidus (with temperature of 1030°C), the crystal content of the added magma is linearly proportional to its temperature, which can be obtained from equation (4) by replacing T_m with T_{in}. In addition, the latent heat left linearly depends on the liquid magma portion out of the refilled magma, i.e., $L(1-\chi_{in})$, where χ_{in} is the crystal content for added magma. Therefore, the heat flux corresponds to the magma replenishment in equation (9) is rewritten as

$$F_r(t) = \left[\rho_m c_m T_{in} + \rho_m L(1-\chi_{in})\right]u(t) \tag{23}$$

Correspondingly, the magma temperature for the crystals suspended and crystals settling model are written as, respectively

$$\frac{dT_m(t)}{dt} = \frac{F_m(t) - \rho_m u(t)\{c_m[T_{in} - T_m(t)] + [\chi(T_m(t)) - \chi_{in}]L\}}{D(t)\rho_m[\chi'(T_m(t))L - c_m]} \tag{24}$$

$$\frac{dT_m(t)}{dt} = \frac{F_m(t) - F_c + \Gamma_1(t)}{\Gamma_2(t)} \tag{25}$$

where

$$\Gamma_1(t) = \rho_m u(t)\left\{\left(1-\chi\left(T_m(t)\right)\right)\left[c_m T_m(t) + \left(1-\chi\left(T_m(t)\right)\right)L\right] - \left[c_m T_{in} + L(1-\chi_{in})\right]\right\} \tag{26}$$

$$\begin{aligned}\Gamma_2(t) = {} & D(t)\rho_m \chi'\left(T_m(t)\right)\left[c_m T_m(t) + L\left(1-\chi\left(T_m(t)\right)\right)\right] \\ & + D(t)\rho_m\left(1-\chi\left(T_m(t)\right)\right)\left(\chi'\left(T_m(t)\right)L - c_m\right)\end{aligned} \tag{27}$$

Figure 4.16 and Figure 4.17 show the effect of the replenished magma temperature T_{in} on total magmatic heat output for crystals suspended and crystals settling, respectively. We observed that the temperature of added magma T_{in} has slight effects on the total heat output at the earlier several years, i.e., it does not change the total heat output decay rate significantly, because during this period, the heat loss due to the convection dominates the total heat loss. When the replenishment process balances convection, added magma with higher temperature leads to greater heat transfer from the convecting magma chamber to the hydrothermal system.

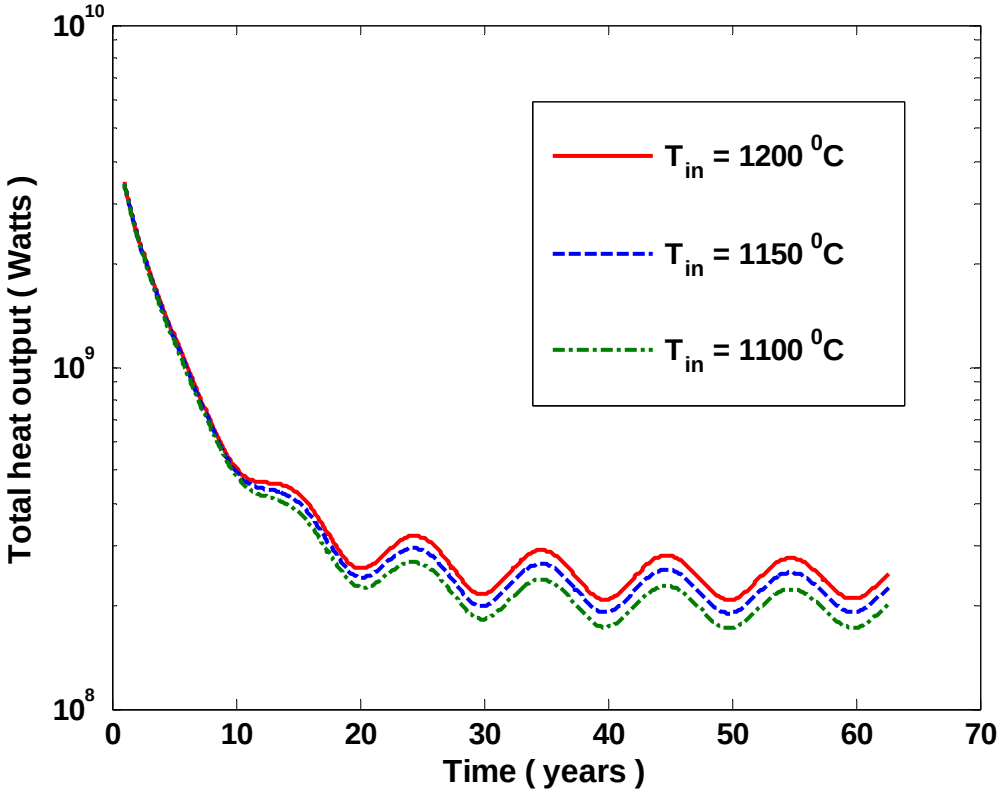

Figure 4.16 Total heat output as a function of time for the crystals settling model with magma replenishment period of 10 years at a constant rate 5×10^{-8} m/s for different magma temperatures T_{in}.

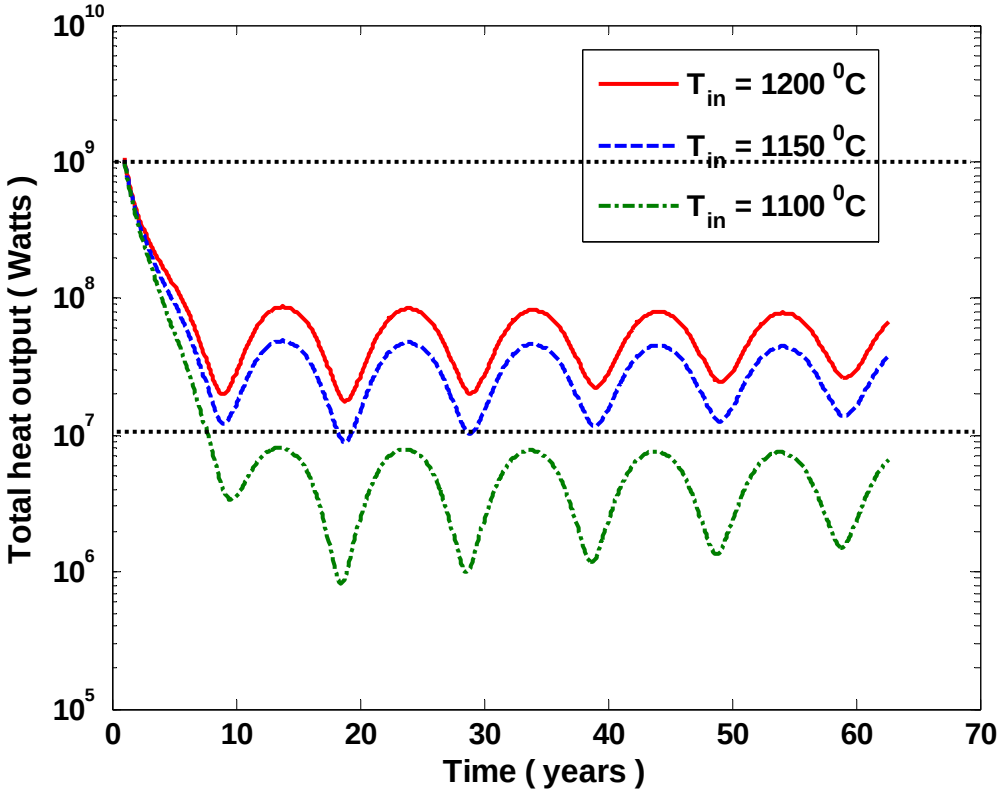

Figure 4.17 Total heat output as a function of time for the crystals suspended model with magma replenishment period of 10 years at a constant rate 5×10^{-8} m/s for different magma temperatures T_{in}.

4.5.2 Implications for hydrothermal systems

4.5.2.1 Hydrothermal vent temperature

Time-series observation and theoretical studies of hydrothermal vents along mid-ocean ridges reveal a close coupling between magma supply and hydrothermal fluxes. The magmatic heat supply exerts a primary control on hydrothermal processes. *Liu and Lowell* [2009] discuss the link between magmatic and hydrothermal heat flux. Here we employ the same relationships to investigate this link as a function of the parameters explored in this chapter. We assume that the heat transfer between the magma and

hydrothermal fluid is instantaneous, and that the variation of hydrothermal temperature T_h and heat flux F_h instantly reflect that in the magma chamber. Thus, assuming that no heat loss occurs during the heat transfer from the magma chamber to the overlying hydrothermal system, we have

$$F_h(t)A_d = F_m(t)A_m(t) \tag{28}$$

where A_d is the area of hydrothermal discharge zone. For a hydrothermal system venting at temperature $T_h(t)$, the heat flux of the hydrothermal venting is

$$F_h(t) = \rho_f c_f u_d(t) T_h(t) \tag{29}$$

where ρ_f is the density of hydrothermal fluid, c_f is the specific heat of the fluid, and $u_d(t)$ is the Darcian upflow velocity. Assuming that $u_d(t)$ results from the thermal buoyancy difference between the recharge and discharge limbs of the hydrothermal convection cell, and that the flow resistance occurs mainly in the discharge limb,

$$u_d(t) = \frac{\alpha_f g k T_h(t)}{v_f} \tag{30}$$

where v_f is the kinematic viscosity of thermal fluid, k is the permeability, α_f is the coefficient of the thermal expansion of thermal fluid in the discharge zone, respectively. Combining equations (28), (29), and (30), we obtain the temperature of hydrothermal venting as

$$T_h(t) = \left(\frac{F_m(t)A_m v_f}{A_d \rho_f c_f \alpha_f g k} \right)^{1/2} \tag{31}$$

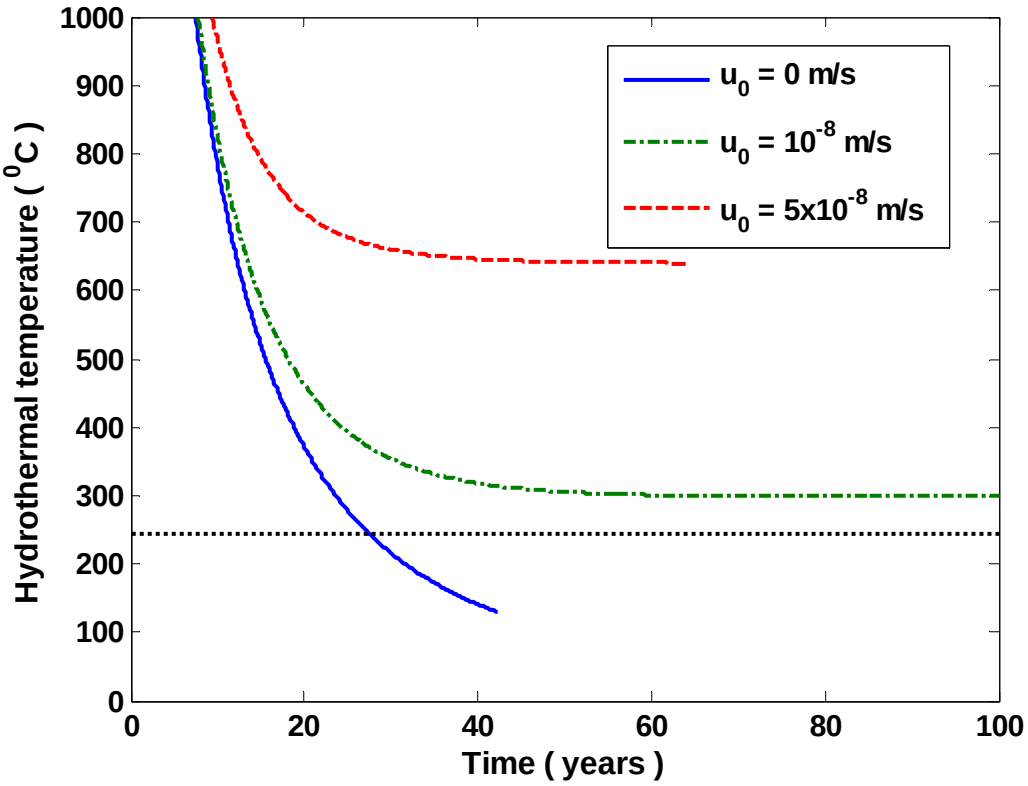

Figure 4.18 The temperatures of hydrothermal venting in response to the magmatic heat flux for the crystals settling case without and with magma replenishment. The horizontal dash line at 250°C is the lower limit for observed black smoker vent temperatures.

The hydrothermal temperatures of magmatic heat supply from a 100 m thick sill with different constant rates of replenishment are shown in Figure 4.18. The typical value of permeability k and the area of discharge zone A_d used to calculate the hydrothermal temperature are 10^{-13} m^2 and 10^4 m^2, respectively. Figure 4.18 shows that the temperature of hydrothermal system is controlled by the magmatic heat flux from below. Hydrothermal temperatures decrease significantly on decadal timescales during the initial cooling phase of magmatic heat transport but stabilize as the heat input from magma replenishment balances the convective heat loss. In the initial stages of magmatic heat transport, hydrothermal temperatures are unrealistically high. This is a result of the

assumed initial conditions of the simulations. The quasi-steady equilibrium temperature differs as a function of replenishment rate. The curve for zero-replenishment rate drops quickly and is cut off when the magmatic heat output is below 10^7 W. In this case, the temperature drops below 250 °C, which we assume is the minimum temperature that characterizes a black smoker vent. Such a rapid decay of a hydrothermal system is not commonly observed among the long-lived seafloor systems. This result suggests that magma convection alone is not sufficient to maintain a high temperature hydrothermal system for decadal time scales and therefore supports the need for magma replenishment on relatively rapid timescales. The dot-dash curve corresponds to the case of magma replenishment with a moderate rate. It shows that the hydrothermal temperature maintains ~ 300 °C for decadal times, which is consistent with the thermal measurement of high temperature of seafloor hydrothermal systems. The dot curve shows the estimated hydrothermal temperature resulting from a 100 m thick sill with higher magma replenishment rate. This relatively high temperature is not realistic but could be reduced by considering a thinner sill to begin with or changing the hydrothermal parameters used in equation (31). For example, Figure 4.19 shows the resulting hydrothermal temperature as a function of initial sill thickness for replenishment at the rate of 10^{-8} m/s and the same hydrothermal parameters as Figure 4.18. The results show that for a typical magma body thicknesses ranging from a few tens of meters to ~ 100 m hydrothermal temperatures are maintained at ~300 °C for decadal timescales following the initial decline. For a thinner initial magma lens, the hydrothermal temperature initially decays more rapidly than for a thicker initial magma lens because, as discussed previously, convective heat loss at early times has a greater effect on the smaller magma sills.

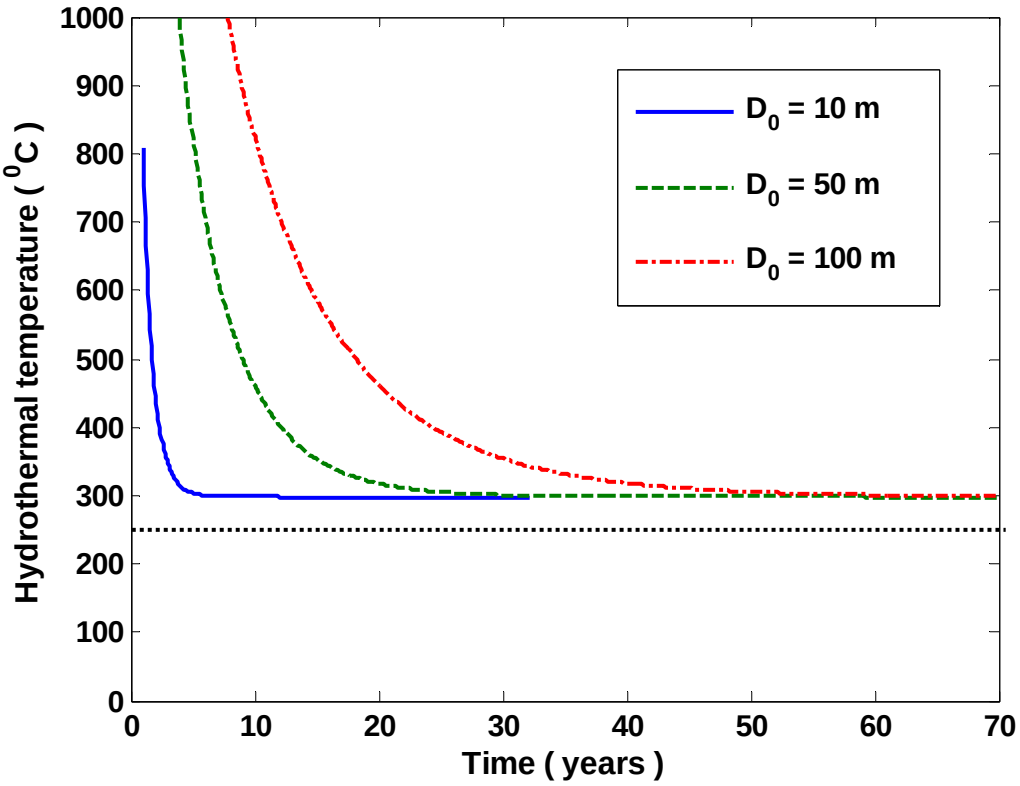

Figure 4.19 Hydrothermal temperatures as a function of time for the crystals settling case with magma replenishment at 10^{-8} m/s for different magma initial thicknesses.

Figure 4.20 shows that permeability strongly affects the evolution of hydrothermal temperature. With high permeability, the hydrothermal temperature drops below 250°C within a few years after its initial rapid decline. As permeability decreases, the hydrothermal temperatures increase in both initial and the steady states. Note that both the initial thickness of magma chamber and the permeability affect the evolution of hydrothermal system; however, they influence temperature evolution in different ways. The initial thickness affects the decay rate of hydrothermal temperatures, while permeability affects the equilibrium hydrothermal temperatures. In general it appears that convecting, crystallizing thin magmatic sills with magma replenishment rates ranging

between ~10^{-7}-10^{-8} m/s may maintain the hydrothermal heat output and high-temperature venting for decadal time scales in a manner that represents observed hydrothermal systems at oceanic spreading centers.

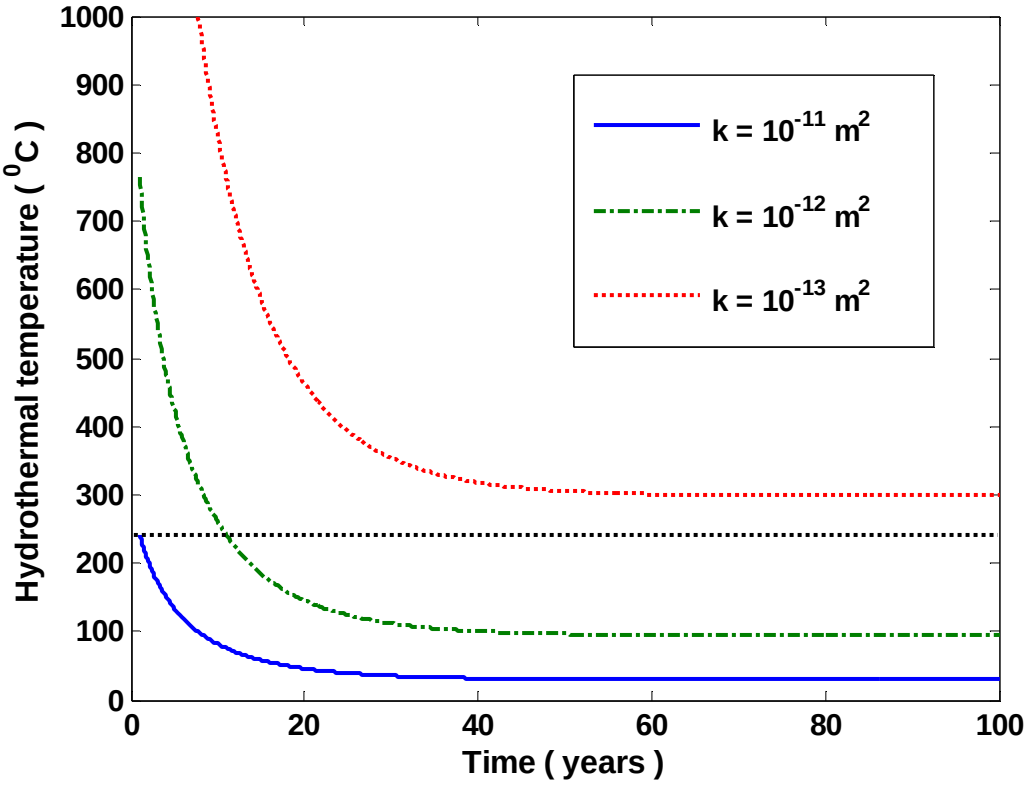

Figure 4.20 Hydrothermal temperatures as a function of time for a 100 m thick magma chamber with magma replenishment at 10^{-8} m/s with permabilities in the range 10^{-11} ~10^{-13} m^2. *k* denotes the permeability of discharge zone in equation (31).

4.5.2.2 Hydrothermal response to episodic heat input

Simulations involving periodic magma replenishment show that the magmatic heat output will vary periodically, depending upon the replenishment period (see Figure 4.6, Figure 4.7, Figure 4.8, and Figure 4.9). As we discussed before, the total magmatic

heat output exhibits different characteristics for crystals suspended and crystals settling cases. The relatively smaller magma viscosity in crystal settling case results in the more vigorous convection. Thus, with the same strength of cooling from the overlying hydrothermal system, the total heat output decays slower and maintains a relatively higher equilibrium level in crystals settling than that in the crystals suspended case. In this part, we focus on the hydrothermal response to the magma heat output and we consider only the crystal settling case, since the same mechanism plays the role in both of the cases.

Hydrothermal vents on mid-ocean ridges reflect the rate of heat transfer from the convecting, cooling, replenished underlying AMC. One way to study the evolution of the AMC is by measurements of temperature and heat output as a function of time. Heat output measurements are relatively rare and time series measurements do not exist; however good temperature records exist for the hydrothermal vents near 9°50'N on EPR [*Von Damm*, 2000, 2004; *Schierer et al*., 2006] over a full eruption cycle between 1991/1992 [*Haymon et al*., 1993] and 2005/2006 [*Soule et al*., 2007]. Several T excursions at Bio (both positive and negative) have been measured in later years [*Schierer et al*., 2006]. Some of the positive excursions [e.g., March 1995, November 1997, and November 2003] have been correlated with seismic swarms [*Sohn et al*., 1998; *Tolstoy et al*., 2008] whereas the negative excursions may be associated with periods of declining heat flux. The seismic swarm hydrothermal temperature excursion in March 1995 may have been associated with a non-eruptive diking event [*Germanovich et al*., 2010], suggesting the magma chamber may have been gradually inflating and creating pressure at tip of magma lens. Similarly, the November 2003 events may also have been

linked with a non-eruptive diking event. Continued magma input then presumably led to the eruptions in 2005/2006.

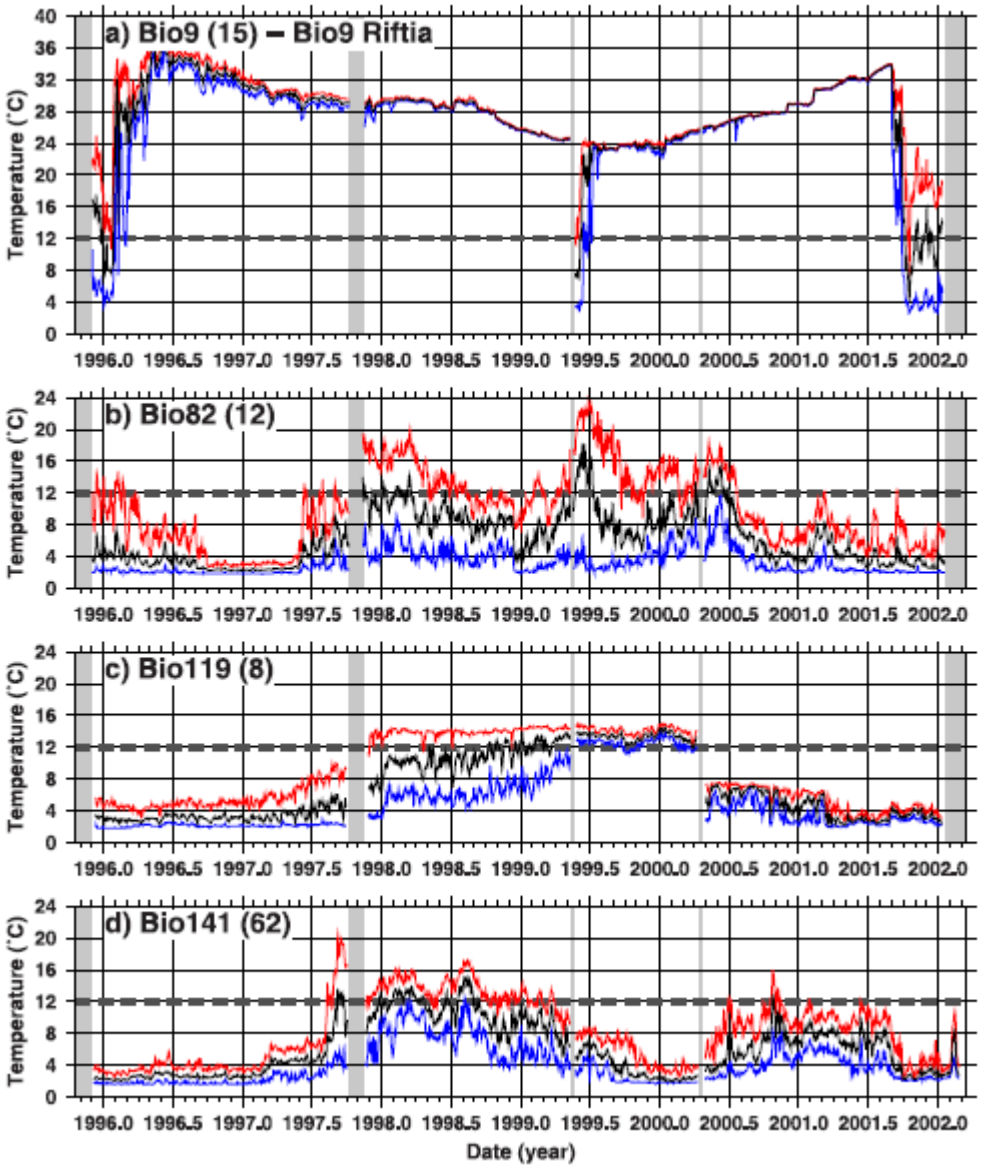

Figure 4.21 Temperature records from 1996 through 2001 at the four diffuse flow vent sites at the EPR near 9°50'N. Black, red, and blue lines display daily mean, maximum, and minimum temperatures, respectively. All of the vent temperatures vary significantly over timescales of 0.5-2.0 years [*Scheirer et al.*, 2006].

As an example of the hydrothermal response to the periodic magma replenishment with our numerical method, we consider the magma chamber at EPR, where positive T excursions occur every few years (see Figure 4.21). Based on the on-site measurement evidences, the overall heat flux is around 160 MW [*Ramondenc et al*., 2006]. The temperature fluctuation in Bio82 from 1997-2000 is between 5 and 20°C [*Sheirer et al*., 2006]. Assuming that the magmatic replenishment period is 3 years, our model for the crystal settling case indicates the vent temperature variations of 10 °C and heat flux changing from 160 MW to 154 MW. It is seen that the simulation result is consistent with the observed T fluctuation magnitudes, but see the additional discussion below concerning the phase lags in the system.

4.5.2.3 The magma-hydrothermal boundary layer and response of hydrothermal systems

The response of the hydrothermal system to the changes of basal heat flux is assumed to be instantaneous in this chapter and [*Liu and Lowell*, 2009]; however, this assumption is not very realistic. There is a time lag as a result of finite time required for heat to be conducted across the thermal boundary layers between the convecting magma sill and the overlying hydrothermal system. The second lag time results from the finite residence time of the hydrothermal fluid circulation in the crust. In addition, in cases of periodic heat flux changes, the thermal perturbations are damped as they traverse the boundary layer and the upflow zone of the hydrothermal system.

To determine to the lag time resulting from the conductive boundary layers, we first determine their thicknesses. The boundary layer thickness $d(t)$ consists of two parts.

$$d(t) = \delta_1(t) + \delta_2(t) \tag{32}$$

where $\delta_1(t)$ is the boundary layer between the convecting liquid magma and the solidus temperature at the top of the magma chamber and $\delta_2(t)$ is the boundary layer between the solidus temperature T_s and the hydrothermal system at $T_h(t)$:

$$\delta_1(t) = \frac{\lambda(T_m(t) - T_s)}{F_m(t)} \tag{33}$$

$$\delta_2(t) = \frac{\lambda(T_s - T_h(t))}{F_m(t)} \tag{34}$$

Equation (33) will give a unique solution for the evolution of $\delta_1(t)$ by substituting equation (2) for $F_m(t)$ and equation (7), (8), (11), or (12) for $T_m(t)$ into equation (33). We also have a unique solution for $\delta_2(t)$ by substituting equation (31) for T_h(t) and (2) into equation (34). Note that although T_s is a constant, the location of T_s is not fixed in space. We can determine the movement of T_s in space with respect to time during the magma cooling and replenishment. Assuming that the position of the bottom of magma chamber is the reference point, the position of T_s can be calculated by $D_{Ts}(t) = D(t) + \delta_1(t)$. Substitution of equation (2) into equation (33), we obtain the boundary layer thickness $\delta_1(t) \sim (T_m(t) - T_s)^{-1/3}$. For both without and with magma replenishment cases, magma temperature always decreases with time during magma cooling and crystallizing. Therefore, $\delta_1(t)$ increases with time for both cases.

Figure 4.22 illustrates the time-varying $\delta_1(t)$ for both without and with magma replenishment with different replenishment rates in crystals settling case. The increasing rate of $\delta_1(t)$ depends upon the decreasing rate of magma temperature. Without magma replenishment, the temperature of magma decreases more rapidly, resulting in a faster increase of $\delta_1(t)$ with time. Combining equations (29) and (34), we obtain $\delta_2(t) \sim (T_s -$

$T_h(t))/T_h^2(t)$, i.e., $\delta_2(t)$ increases with time as the hydrothermal temperature decreases. However, the hydrothermal temperatures at the early stages represent an "initial condition" that is not highly realistic (Figure 4.18, Figure 4.19, and Figure 4.20), since we assume that the heat transferred from magma to hydrothermal system is instantaneous. Thus, the negative $\delta_2(t)$ results at the first decades, which means that the rock above the "supposed magma chamber" would actually undergo some partial melting (see Figure 4.23).

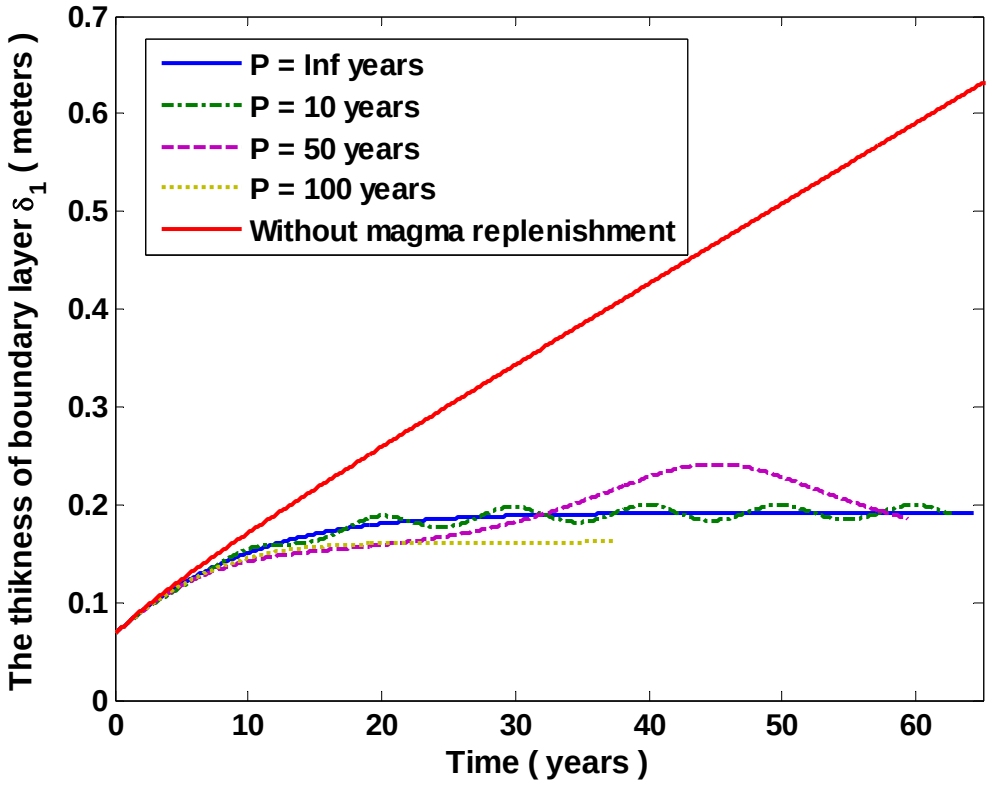

Figure 4.22 The boundary layers between the convecting liquid magma and the solidus temperature at the top of the magma chamber as a function of time for the crystals settling model without and with magma replenishment at 5×10^{-8} m/s.

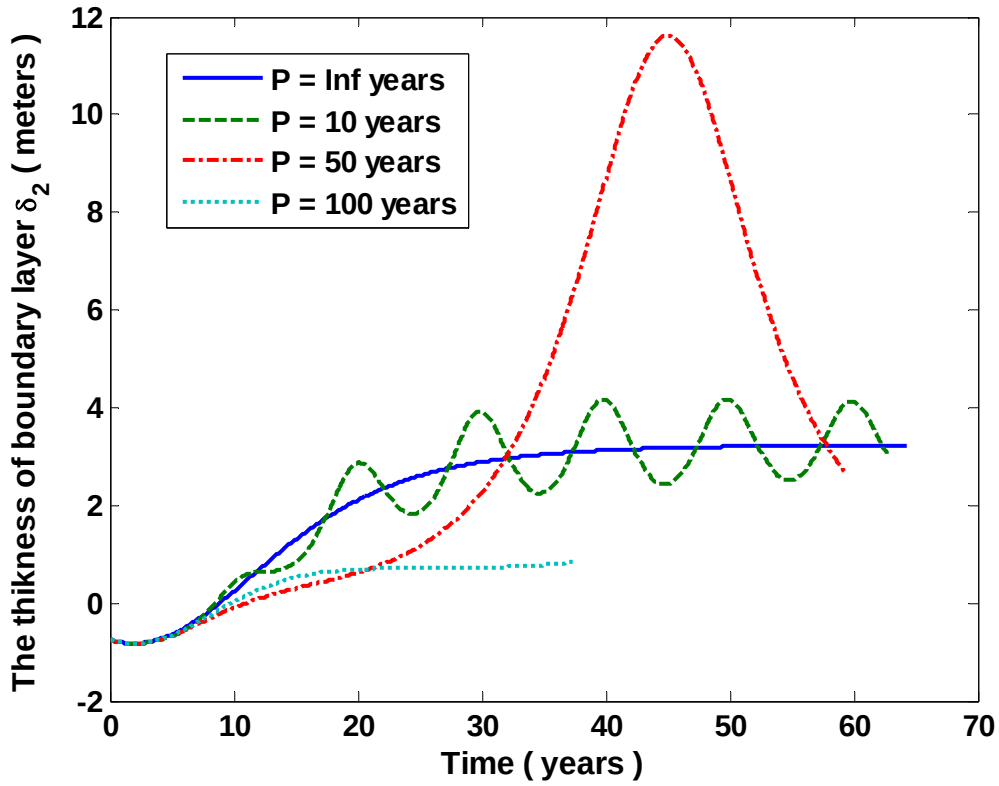

Figure 4.23 The boundary layers between the solidus temperature and the hydrothermal system as a function of time for the crystals settling model with magma replenishment at 5×10^{-8} m/s.

The time scale for heat conduction is given by

$$t =\sim \frac{d^2}{a_m} \tag{35}$$

For a replenishment rate of 5×10^{-8} m/s with frequency of 50 years, the thickness of boundary layer ranges between ≈ 3 to 10 m. Hence, the heat conduction time through the boundary layer ranges between ≈ 10^7 to 10^8 s. In a system with continuously varying heat flux, the time to propagate the thermal perturbation across the boundary layer may not be an issue after an initial delay, but with periodic changes in heat flux, the rate of transport and amount of damping can be calculated. Based on the half space heat conduction

analysis in [*Carslaw and Jaeger*, 1959], the damping factor is $(w/2a_m)^{1/2}$ and the amplitude of the heat flux oscillation diminishes as $\exp[-x(w/2a_m)^{1/2}]$. For x = 10 m, the amplitude of the heat flux oscillation is 0.6, for P = 50 year, and 0.15 for P = 3 years. Thus, the amplitude of the heat flux oscillations from the magma chamber is significantly attenuated after passing through the boundary layer with thickness of ~ 10m, particularly for relatively short periods.

The second lag time results from the residence time–as the hydrothermal fluid rises to the seafloor through the upflow zone. The fluid residence time through the discharge zone is in the wide range from hours and days to months and years. The observation of thermal perturbations at Bio9 vent following a seismic swarm on the EPR at 9°50′ N has been used to argue that the fluid residence in the discharge zone is approximately four days [*Fornari et al*., 1998b; *Sohn et al*., 1998; *Sohn et al*., 1999]. On the other hands *Pascoe and Cann* [1995]; *Lowell and Germanovich* [2004], and *Germanovich et al*. [2010] argue that the fluid residence time within the hydrothermal system in the discharge zone is months to years. Based on the study of $^{228}Ra/^{226}Ra$ ratio of hydrothermal fluids on the Endeavour segment of the Juan de Fuca Ridge, [*Kadko and Butterfield*, 1998] suggests that the fluid residence time from the onset of high-temperature reaction is less than 3 years. Both the time lags delay the hydrothermal response to the periodic variations in the magmatic heat flux, and the hydrothermal temperature oscillation will be out of phase with the oscillating magmatic heat output. In addition, the damping diminishes the hydrothermal response to the periodic changes of heat flux. The higher the frequency of the heat flux variation, the greater the resultant damping of hydrothermal response.

4.6 Conclusions

In this chapter, we have examined the time-varying heat flux transfer from a convecting, crystallizing, and replenished magma chamber to an overlying hydrothermal system. In particular we investigated the role of initial sill size and episodic magma replenishment on the heat output. We considered both crystals suspended and crystals settling scenarios and a constant area/increasing magma thickness model during replenishment. The initial heat flux from the magma chamber is independent of the thickness of magma chamber, but the decay rate of heat flux is inversely proportional to the initial thickness of magma chamber. When replenishment is included in the crystals settling model, we find that hydrothermal heat output and hydrothermal vent temperature are stabilized for replenishment rates of ~ 10^{-8} – 10^{-7} m/s, regardless of initial thickness. We further find that even though considerable magma replenishment occurs, up to ten times the initial thickness for an initially thin sill, the thickness of the liquid layer remains much less than 100 m thick. This result suggests that changes in the AMC resulting from magma replenishment may not be detectable by seismic reflection methods. With episodic magma replenishment rates, magmatic heat output remains relatively unchanged except for oscillations related to the frequency of replenishment; this result is especially true for crystals settling models. Assuming instantaneous hydrothermal responses, hydrothermal temperature oscillates in phase with the oscillating magmatic heat output. For a replenishment period of ~ 3 years as may occur at EPR 9°50′ [*Scheirer et al.*, 2006], the model predicts temperature fluctuation of a few °C. This is similar to observations; however, this result must be viewed with caution. The assumption of instantaneous hydrothermal response essentially neglects the time for heat to be

conducted through the thin boundary layers at the top of the magma chamber and at the base of the hydrothermal system. The boundary layer at the top of the magma chamber is negligible, but the other one is ~ 10-20 m. The thermal conduction time for this layer is weeks and months and one would expect significant damping of the oscillations as they cross this layer [*Carlsaw and Jaeger*, 1959]. Moreover, one must consider the time required for hydrothermal fluid to flow through the upflow zone. This time is few days to years, and additional damping will occur [e.g., *Wilcoc*k, 2004; *Ramondenc et al.*, 2008].These two factors introduce delay and damping to the hydrothermal system response, suggesting that hydrothermal responses resulting from periodic changes in magmatic supply might not be observed in the seafloor vents.

4.7 References

Auger, E., P. Gasparini, J. Virieux, and A. Zollo (2001). Seismic evidence of an extended magmatic sill under Mt. Vesuvius, *Science*, vol.294, no.5546, pp.1510-1512, 16

Babcock, J. M., A. J. Harding, G. M. Kent, and J. A. Orcutt (1998). An examination of along-axis variation of magma chamber width and crustal structure on the East Pacific Rise between 13°30'N and 12°20'N, *J. Geophys. Res.*, 103(B12), 30451-30467.

Baker, E.T., J. W. Lavelle, R. A. Feely, G. J. Massoth, S. L. Walker and J. E. Lupton (1989). Episodic venting of hydrothermal fluids from the Juan de Fuca Ridge, *J. Geophys. Res. 94,* 9237-9250.

Baker, E.T., C.G. Fox, J.P. Cowen (1999). In situ observations of the onset of hydrothermal discharge during the 1998 submarine eruption of Axial Volcano, Juan de Fuca Ridge, *Geophys. Res.Lett.*, vol. 26, no. 23, pp.3445-3448

Baker E.T. (2007). Hydrothermal cooling of midocean ridge axes: Do measured and modeled heat fluxes agree?, *Earth Planet. Sci. Lett.*, 263, 140-150.

Bowers, T.S., A.C. Campbell, C.I. Measures, A.J. Spivack, M. Khadem, and J.M. Edmond (1988). Chemical controls on the composition of vent fluids at 13°-11°N and 21°N, East Pacific Rise, *J. Geophys. Res., 93*, 4522-4536.

Burnett, M.S., D.W. Caress, and J.A. Orcutt (1989). Tomographic image of the magma chamber at 12°50' on the East Pacific Rise, *Nature*, *339*, 206-208.

Campbell, A.C., T.S. Bowers, C.I. Measures, K.K. Falkner, M. Khadem, and E.M. Edmond (1988). A time series of vent fluid composition from 21°N, East Pacific Rise (1979, 1981, 1985) and the Guaymas Basin, Gulf of California (1982, 1985), *J. Geophys. Res., 93*, 4537-4550.

Canales, J.P., S.C. Singh, R.S. Detrick, S.M. Carbotte, A. Harding, G.M. Kent, J.B. Diebold, J. Babcock, and M.R. Nedimovic (2006). Seismic evidence for variations in axial magma chamber properties along the southern Juan de Fuca Ridge, *Earth. Planet. Sci. Lett.*, *246*, 353-366.

Carbotte, S.M., J.C. Mutter, J.P. Canales, M.R. Nedimovi´c, H. Carton, M. Xu, K.R. Newman, M. Marjanovic, O. Aghaei, and L. Stowe (2008). New observations of the magmatic segmentation of the East Pacific Rise from Siquieros to Clipperton from a multi-streamer seismic reflection imaging study, *EOS Trans.* AGU 89(53). Fall Meet. Suppl., Abstract B21A-0320.

Collier, J.S. and M.C. Sinha (1990). Seismic images of a magma chamber beneath the Lau Basin back-arc spreading centre, *Nature*, *346*, 646-648.

Collier, J.S. and M.C. Sinha, (1992). Seismic mapping of a magma chamber beneath the Valu Fa Ridge, Lau Basin, *J. Geophys. Res.*, vol. *97*, no. B10, pp.14,031-14,053

Cowen, J.P., D.J. Fornari, T.M. Shank, B. Love, B. Glazer, A. Treusch, R.C. Holmes, S.A. Soule, E.T. Baker, M. Tolstoy, and K.R. Pomranig (2007). Volcanic Eruptions at East Pacific Rise Near 9°50'N, *EOS*, *Trans.*, AGU, *88*, NO. 7, doi:10.1029/2007EO070001

Detrick, R.S., P. Buhl, E. Vera, J. Mutter, J. Orcutt, J. Madsen, and T. Brocher (1987). Multi-channel seismic imaging of a crustal magma chamber along the East Pacific Rise, *Nature*, *326*, 35-41.

Detrick, R.S., A.J. Harding, G.M. Kent, J.A. Orcutt, J.C. Mutter, and P. Buhl, (1993). Seismic structure of the southern East Pacific Rise, *Science*, *259*, no.5094, pp.499-503.

Dunn, R.A., D.R. Toomey, and S.C. Solomon (2000). Three-dimensional seismic structure and physical properties of the crust and shallow mantle beneath the East Pacific Rise at 9 degrees 30'N, *J. Geophys. Res.*, *105*, no. B10, pp.23,537-23,555.

Fornari, D.J., T. Shank, K.L. Von Damm, T.K.P. Gregg, M. Lilley, G. Levai, A. Bray, R.M. Haymon, M.R. Perfit, and R. Lutz (1998). Time-series temperature measurements at high-temperature hydrothermal vents, East Pacific Rise 9°49'-51'N: evidence for monitoring a crustal cracking event, *Earth Planet. Sci. Lett.*, *160*, 419-431.

Germanovich, L.N., R.P. Lowell, and P. Ramondenc (2010). Hydrothermal response to the earthquake swarm at 9°50 N, East Pacific Rise: Magmatic origin and constraints from heat flow and geochemical data, *J. Geophys Res.* (in press).

Harding, A. J., J. A. Orcutt, M. E. Kappus, E. E. Vera, J. C. Mutter, P. Buhl, R. S. Detrick, and T. M. Brocher (1989). Structure of young oceanic crust at 13°N on the East Pacific Rise from expanding spread profiles, *J. Geophys. Res.*, 94(B9). 12163-12196.

Haymon, R. M., D. J. Fornari, M. H. Edwards, S. Carbotte, D. Wright, and K. C. Macdonald, (1991). Hydrothermal vent distribution along the East Pacific Rise Crest (9°09'-54'N) and its relationship to magmatic and tectonic processes on fast-spreading mid-ocean ridges, *Earth Planet. Sci. Lett.*, 104, 513-534.

Haymon, R. M., D. J. Fornari, K. L. Von Damm, M. D. Lilley, M. R. Perfit, J. M. Edmond, W. C. Shanks, R. A.Lutz, J. M. Grebmeier, S. Carbotte, D. Wright, E. McLaughlin, M. Smith, N. Beedle, and E. Olson (1993). Volcanic eruption of the mid-ocean ridge along the East Pacific Rise crest at 9°45–52'N: Direct submersible observations of seafloor phenomena associated with an eruption event in April, 1991, *Earth Planet. Sci.Lett.*, 119, 85–101.

Haymon, R. M. and S. M. White, (2004). Fine scale segmentation of volcanic/hydrothermal systems along fast-spreading ridge crests, *Earth Planet. Sci.Lett.*, vol.226, no.3-4, pp.367-382

Hogan, J. P. and Gilbert, M. C. (1995). The A-type Mount Scott Granite sheet: importance of crustal magma traps. *J. Geophys. Res.*, 100, 15 779–15 792.
Huppert, H. E. and R. S. J. Sparks (1988). The generation of granitic magmas by intrusion of basalt into continental crust, *J. Petrol.*, *29*, 599-624.

Jarvis, G. T. and W. R. Peltier (1989), Convection models and geophysical observations, in *Mantle Convection: Plate Tectonics and Global Dynamics*, ed. W.R. Peltier, Gordon and Breach Science Publishers, 479-595.

Johnson, H. P., M. Hutnak, R. P. Dziak, C. G. Fox, I. Urcuyo, J. P. Cowen, J. Nabelek, and C. Fisher (2000), Earthquake-induced changes in a hydrothermal system on the Juan de Fuca mid-ocean ridge, *Nature*, *407*, 174-177.

Jokat, W., O. Ritzmann, M. C. Schmidt-Aursch, S. Drachev, S. Gauger, and J. Snow, (2003). Geophysical evidence for reduced melt production on the Arctic ultraslow Gakkel mid-ocean ridge, *Nature*, *vol.*423, no.6943, pp.962-965

Kadko, D. and D. A. Butterfield (1998). The relationship of hydrothermal field composition and crustal residence time to maturity of vent fields on the Juan de Fuca Ridge, *Geochimica et Cosmochimica Acta*, vol.62, no.9, pp.1521-1533,

Kent, G. M., A. J. Harding, and J. A. Orcutt (1990). Evidence for a smaller magma chamber beneath the East Pacific Rise at 9º30´N, *Nature*, *344*, 650-652.

Lejeune, A.M., Richet, P., 1995. Rheology of crystal-bearing silicate melts - an experimental study at high viscosities. J. Geophys. Res.-Solid Earth, 100, 4215-4229.

Lilley, M. D., D. A. Butterfield, J. E. Lupton, and E. J. Olson (2003). Magmatic events can produce rapid changes in hydrothermal vent chemistry, *Nature*, *422*, 878-881, doi:10.1038/nature01569.

Lister, C. R. B., (1983). On the intermittency and crystallization mechanisms of sub-seafloor magma chambers, *Geophysical Journal of the Royal Astronomical Society*, vol.73, no.2, pp.351-365.

Lister, J.R. (1990). Buoyancy-driven fluid fracture: similarity solutions for the horizontal and vertical propagation of fluid-filled cracks. *J. Fluid Mech.*, 217, 213-239.

Liu, L. and P. R. Lowell, (2009). Models of hydrothermal heat output from a convecting, crystallizing, replenished magma chamber beneath an oceanic spreading center, *J. Geophys. Res.*, *114*, B02102, doi:10.1029/2008JB005846.

Lowell, R. P. and L. N. Germanovich (1994). On the temporal evolution of high-temperature systems at ocean ridge crests, *J. Geophys. Res., 99*, 565-575.

Lowell, R. P. and L. N. Germanovich (2004). Seafloor hydrothermal processes: Results from scale analysis and single-Pass models, in Mid-Ocean Ridges: Hydrothermal Interactions Between the Lithosphere and Oceans, *Geophys. Monogr. Ser., 148*, ed. By C. R. German, J. Lin and L. M. Parson, pp.219-244, Amer. Geophys. Union, Washington, D.C.

Lowell, R. P., B. W. Crowell, K. C. Lewis, and L. Liu, (2008). Modeling multiphase, multicomponent processes at oceanic spreading centers, *Geophys. Monogr. Ser., 178*, pp.15-44 American Geophys. Union, Washington, DC.

Lupton, J. E., M. Lilley, D. A. Butterfield, J. Cowen, K. L. von Damm, E. T. Baker, J. A. Resing, R. W. Embley, W.W. Chadwick, B. Love, R. R. Greene, and L. J. Evans, (2006). Changes in hydrothermal gas chemistry associated with deep-sea eruptive events, *Eos, Trans.,* AGU, vol.87, Fall Meeting Supplement, Abstract V13C-08

MacLeod, C. J. and G. Yaouancq (2000). A fossil melt lens in the Oman ophiolite: Implications for magma chamber processes at fast spreading ridges, *Earth Planet. Sci. Lett.*, *176*, 357-373.

Mainprice, D., (1997). Modelling the anisotropic seismic properties of partially molten rocks found at mid-ocean ridges, *Tectonophysics*, vol.279, no.1-4, pp.161-179

McKenzie, D. (1984). The generation and compaction of partially molten rocks. *Journal of Petrology* 25, 713-765.

Navin, D.A., C. Peirce, and M.C. Sinha (1998). The RAMESSES experiment-II. Evidence for accumulated melt beneath a slow spreading ridge from wide-angle refraction and multichannel reflection seismic profiles, *Geophys. J. Int.*, *135*, 746-772.

Oppenheim, A. V., A. S. Willsky, and S. Hamid, (1996). *Signals and Systems*, Prentice Hall, Inc., Englewood Cliffs, NJ.

Pascoe, A. R., and J. R. Cann (1995), Modeling diffuse hydrothermal flow in black smoker vent fields, in *Hydrothermal Vents and Processes*, *Geological Society Special Publication*, vol. 87, edited by L. M. Parson, et al., pp. 159-173, The Geological Society, London, UK.

Ramondenc, P., L.N. Germanovich, K. L. Von Damm, and R. P. Lowell (2006). The first measurements of hydrothermal heat out at 9°50´N, East Pacific Rise, *Earth Planet. Sci. Lett.*, 245, 487-497.

Ramondenc. P, L. Germanovich, and R. P. Lowell (2008). Modeling Hydrothermal Response to Earthquakes at Oceanic Spreading Centers, *Geophys. Monogr. Ser., 178*, American Geophys. Union, Washington, DC.

Rathbun, J. A., S. W. Squyres (2002). Hydrothermal systems associated with Martian impact craters, *Icarus*, vol. 157, no. 2, pp.362-372.

Sauter, Daniel; Mendel, Veronique; Rommevaux-Jestin, Celine; Parson, Lindsay M; Fujimoto, Hiromi; Mevel, Catherine; Cannat, Mathilde; Tamaki, Kensaku (2004). Focused magmatism versus amagmatic spreading along the ultra-slow spreading Southwest Indian Ridge; evidence from TOBI side scan sonar imagery, *Geochemistry, Geophysics, Geosystem*s, *vol.*5, no.10, 20 pp.

Scheirer, D. S., T. M. Shank, and D. J. Fornari. (2006). Temperature variations at diffuse and focused flow hydrothermal vent sites along the northern East Pacific Rise, *Geochem. Geophys. Geosys* 7:1–23.

Sinha, M.C., S.C. Contable, C. Peirce, A. White, G. Heinson, L.M. MacGregor and D.A. Navin (1998). Magmatic processes at slow spreading ridges: implications of the RAMESSES experiment at 57°45'N on the Mid-Atlantic Ridge, *Geophysical Journal International*, 135, 731-745.

Singh, S.C., G.M. Kent, J.S. Collier, A.J. Harding, and J.A. Orcutt (1998). Melt to mush variations in crustal magma properties along the ridge crust at the sourthern East Pacific Rise, *Nature*, 394, 874-878.

Singh, S. C., W. C. Crawford, H. Carton, T. Seher, V. Combier, M. Cannat, J. P. Canales, D. Dusunur, J. Escartin, and J. M. Miranda (2006). Discovery of a magma chamber and faults beneath a Mid-Atlantic Ridge hydrothermal field, *Nature*, *442*, 1029-1032.

Sinton, J. M., and R. S. Detrick (1992). Mid-ocean ridge magma chambers, *J. Geophys. Res.*, 97, 197-216.

Sohn, R., D. J. Fornari, K. Von Damm, S. Webb, and J. Hildebrand (1998). Seismic and hydrothermal evidence for a propagating cracking event on the East Pacific Rise crest at 9°50'N, *Nature*, *396*, 159–161.

Sohn, R. A., J. A. Hildebrand, and S. C. Webb (1999). A microearthquake survey of the high-temperature vent fields on the volcanically active East Pacific Rise (9°50'N). *J. Geophys. Res.*, *104*(B11). 25,367-25,377.

Soule, S. A., D. J. Fornari, M. R. Perfit, and K. H. Rubin (2007). New insights into mid-ocean ridge volcanic processes from the 2005-2006 eruption of the East Pacific Rise, 9 degrees 46'N-9 degrees 56'N, *Geology*, vol. 35, no. 12, pp.1079-1082

Tolstoy, M., J. P. Cowen, E. T. Baker, D. J. Fornari, K. H. Rubin, T. M. Shank, F. Waldhauser, D. R. Bohnenstiehl, D. W. Forsyth, R. C. Holmes, B. Love, M. R. Perfit, R. T. Weekly, S. A. Soule, and B. Glazer (2006). A Seafloor Spreading Event Captured by Seismometers, *Science, 314*, Issue 5807, pp. 1920-1922

Tolstoy, M., F. Waldhauser, D. R. Bohnenstiehl, R. T. Weekly, and W. Y. Kim (2008). Seismic identification of along-axis hydrothermal flow on the East Pacific Rise, *Nature* 451, pp.181-184

Tolstoy, M. (2008). Seismological constraints on hydrothermal processes at mid-ocean ridges. *Eos, Transactions*, American Geophysical Union, vol. 89, no. 53, Suppl., Abstract V51B-2025

Turner, J. S. (1973). *Buoyancy effects in fluids*, Cambridge University Press, London.

Van Ark, E., R. S. Detrick, J. P. Canales, S. M. Carbotte, J. Diebold, G. Kent, A. Harding, Wilcock, W. S. (2004). Seismic characterization of crustal magma bodies at the Endeavour Segment, Juan de Fuca Ridge, *Eos, Trans*, AGU, vol. 85, no. 47, Suppl., Abstract B13A-0181.

Van Ark, E.M., R.S. Detrick, J.P. Canales, S.M. Carbotte, A.J. Harding, G.M. Kent, M.R. Nedimovic, W.S.D. Wilcock, J.B. Diebold, J.M. Babcock (2007). Seismic structure of the Endeavour Segment, Juan de Fuca Ridge; correlations with seismicity and hydrothermal activity, *J. Geophys. Res.*, *112*, B02401, doi: 10.1029/2005JB004210.

Vera, E.E., J.C. Mutter, P. Buhl, J.A. Orcutt, A.J. Harding, M.E. Kappus, R.S. Detrick, and T.M. Brocher (1990). The structure of 0- to 0.2-m.y.-old oceanic crust at 9°N on the East Pacific Rise from expanded spreading profiles, *J. Geophys. Res.*, 95(B10), 15529-15556.

Von Damm, K. L. (2000). Chemistry of hydrothermal vent fluids from 9-10°N, East Pacific Rise: "Time zero" the immediate post-eruptive period, *J. Geophys. Res.*, 105, 11,203-11,222.

Von Damm, K. L., C. M. Parker, R. M. Gallant, and J. P. Loveless (2002). Chemical evolution of hydrothermal fluids from EPR 21°N: 23 years later in a phase separating world, *EOS Trans.* AGU, 83(47). Fall Meet. Suppl., Abstract V61B-1365

Von Damm, K. L. (2004). Evolution of the hydrothermal system at East Pacific Rise 9 degrees 50'N; geochemical evidence for changes in the upper oceanic crust, *Geophys. Monogr. Ser., 148*, pp.285-304, American Geophys. Union, Washington, DC.

Wilcock, W. S. D. (2004). Physical response of mid-ocean ridge hydrothermal systems to local earthquakes, *Geochem. Geophys. Geosyst.*, *5*, Q11009.

CHAPTER 5. MODELING MAGMA-HYDROTHERMAL HEAT TRANSFER FROM A CONVECTING, CRYSTALLIZING, REPLENISHED DIOPSIDE-ANORTHITE MAGMA SILL[3]

Abstract

This work aims to determine the effect of magma chemical composition on the dynamic characteristics of convective heat transfer from a crystallizing, replenished, two-component magma chamber at an oceanic spreading center overlain by a hydrothermal circulation system. We focus on the Di-An system as an analogue for basalt because most hydrothermal systems at mid-ocean ridges are driven by basalts. We assume that crystals settle rapidly to the floor of magma chambers and consider cases both without and with magma replenishment. We model melt temperature and viscosity as a function of Di concentration, and incorporate these relations in modeling of the heat flux. Simulations comparing the effects of different initial Di concentrations indicate that magmas with higher initial Di concentration convect more vigorously, which results in faster heat transfer, more rapid removal of Di from the melt, and growth of crystals on the floor. With magma replenishment, we assume that the magma chamber grows either horizontally or vertically. In either case magma replenishment at a constant rate of ~ 10^{-8} m/s can maintain relatively stable heat output between ~ 10^{7}-10^{9} Watts and reasonable hydrothermal vent temperatures for decades. The final stabilized heat flux increases with increasing Di contents of the added magma, and periodic replenishment with a 10 year period results in temperature perturbations within the magma that also increase as a

[3] The material is essentially reproduced from Liu, L. and R.P. Lowell (2010). Modeling magma-hydrothermal heat transfer from a convecting, crystallizing, replenished Di-An magma sill (to be submitted).

function of increasing Di. With the simple magma model used here, one can not discern conclusively whether the decrease in magma temperature between the 1991/1992 and the 2005/2006 eruptions at EPR 9°50′ involved replenishment with more or less evolved magmas.

5.1 Introduction

When a fluid layer is cooled from above, thermal instabilities result in fluid motion in form of convection. The vigor of convection is determined by the Rayleigh number [*Turner et al.*, 1986]. Such thermally driven convection is expected to occur when magma is emplaced into Earth's crust. One of the earliest studies of convective heat transfer in magmatic systems was conducted by *Shaw* [1965]. Since then, heat transfer from a convecting magma chamber has been considered by numerous researchers [e.g., *Spera*, 1979; *Brandeis and Jaupart*, 1986; *Huppert and Sparks*, 1988; *Marsh*, 1989; *Hort et al.*, 1999] who assumed that the magma could be described as a simple one-component convecting crystallizing body cooled from above by the surrounding rocks.

In reality, magmas are multi-component fluids. Convection is complicated because magma convection with cooling and crystallization is a two-phase, multi-component system consisting of both crystals and melt. The density difference between crystals and melt results in both their mechanical separation and in chemical fractionation as crystals and melt are typically of different composition [*McBirney and Noyes* 1979, *Sparks et al.*, 1984, *Turner and Campbell*, 1986; *Martin et al.*, 1987; *Jellinek et al.*, 1999].

Real magmas have a large number of chemical constituents, so considerable emphasis has been placed on more simplified binary systems such as albite-anorthite [e.g., *Koyaguchi and Kaneko*, 1999; *Maaloe*, 1984]; forsterite-fayalite [*Bowen and Schairer*, 1935; *Bradley*, 1962; *Wood and Kleppa*, 1981]; dioside-anorthite [*Bowen*, 1915], or ternary systems such as diopside-anorthite-forserite [*Yoder*, 1976]. Among different binary systems, a particular example that is useful for studying basalt-like silicate melts is the system $CaMgSi_2O_6$ (diopside)- $CaAl_2Si_2O_8$ (anorthite) (Di-An) system, which has

been extensively studied in the literature [e.g., *Bowen*, 1915; *Osborn and Tait*, 1952; *Schairer and Yoder*, 1960; *Kushiro*, 1973; *Weill et al.*, 1980; *Navrotsky et al.*, 1989]. For example, *Ridgen et al.* [1988] use the magma with a certain silicate liquid composition, which consists of 64 mol% diopside and 36mol% anorthite, as a simplified analogue to basalt.

From the perspective of magma convection, experimental investigations addressed the influence of convection on solidification of binary systems cooled from above. A pioneering work of *Turner et al.* [1986] describes a number of laboratory experiments and theoretical analyses of a cooling eutectic melt. Since then, magma convection in a two-component melt have greatly been extended by [*Kerr et al*, 1990; *Kerr et al*, 1990; *Kerr et al*, 1990; *Worster*, 1990; *Huppert and Worster*, 1991; *Huppert and Worster*, 1992].

The studies on magma convection discussed above have been focused on sub-continental magma chambers, where magma chambers are cooled predominantly from above by conduction through solid roof rocks [*Worster*, 1990; *Huppert and Worster*, 1991]. In this paper, however, we focus on heat transfer from magma bodies beneath the axes of ocean spreading centers, where seismic reflection data reveals the presence of sills at depths of ~ 1-3 km beneath the seafloor that are ~ 10s to 100 m thick, ~ 1-3 km across the ridge axis, and at least several kilometers in extent along axis [*Detrick et al.*, 1987; *Kent et al*., 1990; S*ingh et al.*, 1999; *Sinha* 1995; *Canales et al.*, 2006; *Singh et al.*, 2006]. In contrast to most sub-continental magma chambers, sub-axial magma chambers are closely linked to an overlying hydrothermal convection system [*Haymon et al*. 1996; *Embley et al*. 1995; *Haymon and White,* 2004; *MacLennan,* 2008]. It is well recognized

that seafloor hydrothermal venting is driven by heat transfer from the underlying melt lens at mid-ocean ridges [*Cann and Strens*, 1982; *Lowell and Rona,* 1985; *Lowell*, 2010].

In this paper, we study how heat transfer from a convecting, crystallizing, replenished two-component Di-An magma chamber affects the evolution of hydrothermal systems on mid-ocean ridges. We characterize different dynamic features of the system, including heat flux, crystal content, etc., by connecting them to the time-varying Di concentration. The approach taken here differs from previous modeling of convection in Di-An magma bodies [*Lowell*, 1985; *Worster et al.*, 1990] in three significant ways. In constrast to *Lowell*. [1985], we consider convection in a sill-like magma body and hence neglect vertical boundary layer flow near the side margins. Then, we assume that convective heat transfer from the magma is coupled to an overlying hydrothermal circulation system at mid-ocean ridges rather than to a conductive thermal regime in the surrounding continental rocks as in *Worster et al.* [1990]. As a result we focus on the evolution of heat flux and hydrothermal temperature as these are observables in the hydrothermal system. We focus on the Di rich side of the Di-An systems since it provides an analogue to basalt magma system, which drives most of hydrothermal systems in mid-ocean ridges [*Fornari and Embley*, 1995; *Langmuir et al.* 1997]. Finally, we consider magma replenishment for the Di-An system as a mechanism to maintain the hydrothermal system active for a reasonable lifetime and include the affects of magma replenishment on the evolution of the convective heat flux and chemistry of the system. This work complements the previous paper of *Liu and Lowell* [2009], which considered a one-component magma system. By comparing the results in this paper with those for a one-component system we can better understand the effects of chemical fractionation on

heat transfer. Moreover, we will gain insight into the chemical evolution of a sub-axial magma chamber that might be useful for interpreting chemical heterogeneity in erupted lavas over time at mid-ocean ridges.

The rest of the paper is organized as follows. In section 5.2, we review the Di-An phase diagram and the fundamentals of binary eutectic melts. In section 5.3, we model the dependence of physical properties of the systems on the chemical composition. The heat transfer model from Di-An chamber to the overlying hydrothermal system is developed in section 5.4. The magma replenishment effects on the heat transfer process are examined in section 5.5. Section 5.6 discusses the implications of the modeling results, and Section 5.7 concludes the paper.

5.2 Diopside - Anorthite Binary System

For multi-component magmas, the phase diagram is a well known tool for studying melt evolution and crystallization processes as a function of temperature and pressure. The temperature-composition (T-X) phase diagram describing the crystallization pathway in Di-An system at a pressure of 1 bar is shown in Figure 5.1(a), where $CaMgSi_2O_6$ represents the mineral diopside and $CaAl_2Si_2O_8$ represents the mineral anorthite. If the temperature is high enough, a binary mixture melts completely produce a single melt phase. The pure anorthite melts to liquidus at 1553°C. The melting point for the pure diopside is 1391°C.

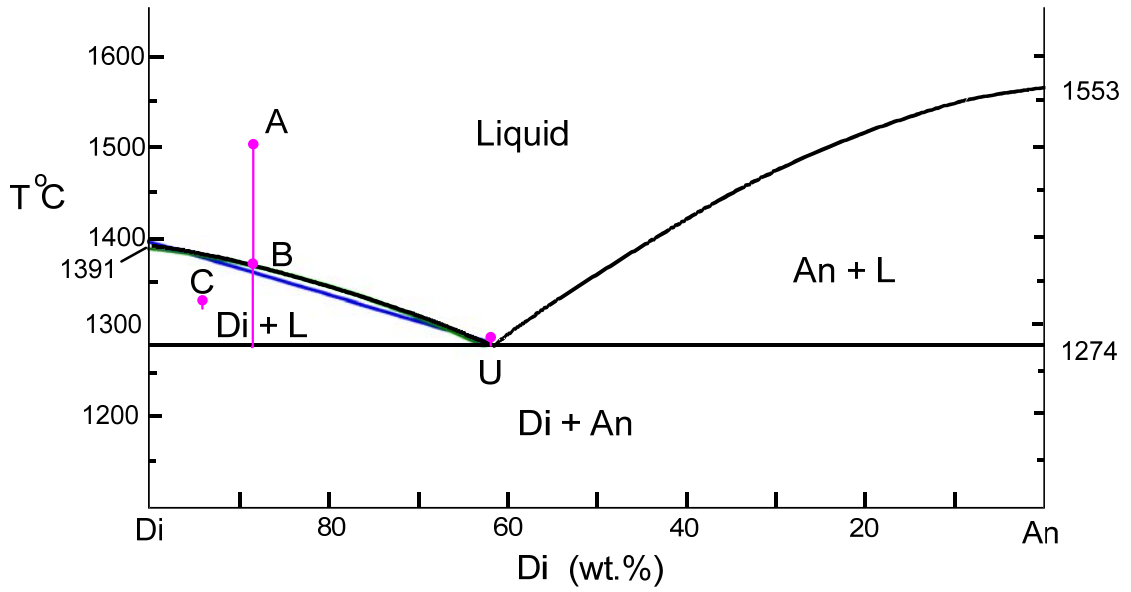

Figure 5.1 (a) Phase diagram for the diopside-anorthite system by assuming magma crystallize under constant pressure at atmospheric pressure (1bar). Diagram is modified from [*Yoder*, 1976]. Di = diopside, An = anorthite, L = liquid. The linear and polynomial relationship between magma temperature and Di concentration for Di-rich side are shown in blue and green line, respectively.

For any rocks consisting of a mixture of diopside and anorthite with any proportions, the curves in Figure 5.1(a) define the liquidus temperature, below which crystals appear. The liquidus boundary temperature depends on the bulk composition. The intersection of the two liquidus curves, which is called the eutectic temperature, the mixture has the lowest melt temperature of 1275°C [*Bowen*, 1915; *Scarfe et al.*, 1983; *Richard,* 1922]. At the eutectic composition with 58 wt.% diopside and 42 wt.% anorthite, the solidus and liquidus temperatures coincide and as further crystallization occurs, melt and crystals will both have this composition. In addition, the phase diagram describes the evolution of chemical composition during the changes of the temperature for other bulk compositons. For example, the crystallization pathway for a Di-An system with composition of 90% Di and 10% An is shown in Figure 5.1(a) as temperature decreases

from around 1500°C (point A). Above the liquidus line at point B, the material is completely molten.. When the temperature drops further, Di starts to crystallize and correspondingly the chemical composition of the melt changes with respect to temperature along the liquidus boundary temperature curve until the temperature reaches the eutectic point U. At the eutectic point, An begins to crystallize, and Di and An crystallize out together at the eutectic composition until all melt is gone. C is in the liquid and Di crystal region. The chemical composition in a Di-An system varies with the different initial combination of Di and An components. Table 5.1 shows the chemical composition in a Di-An system with different compositions of Di and An, where Di_bAn_a denotes a Di-An system with the composition of b% Di and a% An, respectively. Table 5.1 shows that the content of MgO increases as the increase of Di component. Thus, the Di-An system with Di content more than 58% represents more chemical analogues to basaltic melts. In the rest of the paper, we focus the Di-rich side, where the Di content is greater than 58% (see Figure 5.1(a)).

Table 5.1 The chemical composition of magma with different compositions in $CaMgSi_2O_6$ (diopside) - $CaAl_2Si_2O_8$ (anorthite) system [*Knoche*, 1992]

Sample	Di_{100}	$Di_{90}An_{10}$	$Di_{80}An_{20}$	$Di_{58}An_{42}$	$Di_{30}An_{70}$	$Di_{10}An_{90}$	An_{100}
SiO_2 (%)	56.2	55.6	52.3	49.60	46.3	44.60	43
Al_2O_3	0.19	4.47	8.7	17.2	26.5	32.4	35.1
MgO (%)	17.3	14.6	14.1	9.75	4.77	1.43	0.1
CaO (%)	25.9	24.7	24.3	22.7	21.3	20.5	20.5

5.3 Modeling Physical Properties of Diopside-Anorthite System

In order to model convective heat transfer from the Di-An binary melt system, a number of important physical properties are needed, among which the melt temperature and viscosity the most critical ones. In the following, we discuss modeling both of these parameters as a function of Di composition.

6.3.1 Temperature of silicate melts

As shown in the phase diagram in Figure 5.1(a), the liquidus temperature depends on the bulk magma composition in a Di-An system. We derive the expression between magma temperature and composition by fitting a curve to the graphical data of [*Yoder*, 1976]. Focusing on the Di-rich side, we employ polynomial to model the relationship between the temperature and Di content. First, the temperature is modeled as a linear function of the Di composition for the Di-rich side up to the eutectic point. The least square based curve fitting results in

$$T_m(C) = 291 \times C + 1111.5 \tag{1}$$

where 58% < C <100% is the weight fraction of the Di in the system, and T_m denotes the temperature of the melt at its liquidus. Here we model the temperature as a function of Di concentration, since the melt composition is constrained by the liquidus temperature even though the mean temperature of the melt drops crystal-liquid region of the phase diagram. An alternative way to model the relationship between the temperature of melt and Di composition is using a higher-order polynomial function. With a quadratic function, the temperature and Di composition is related by

$$T_m(C) = -410C^2 + 930C + 870.87 \tag{2}$$

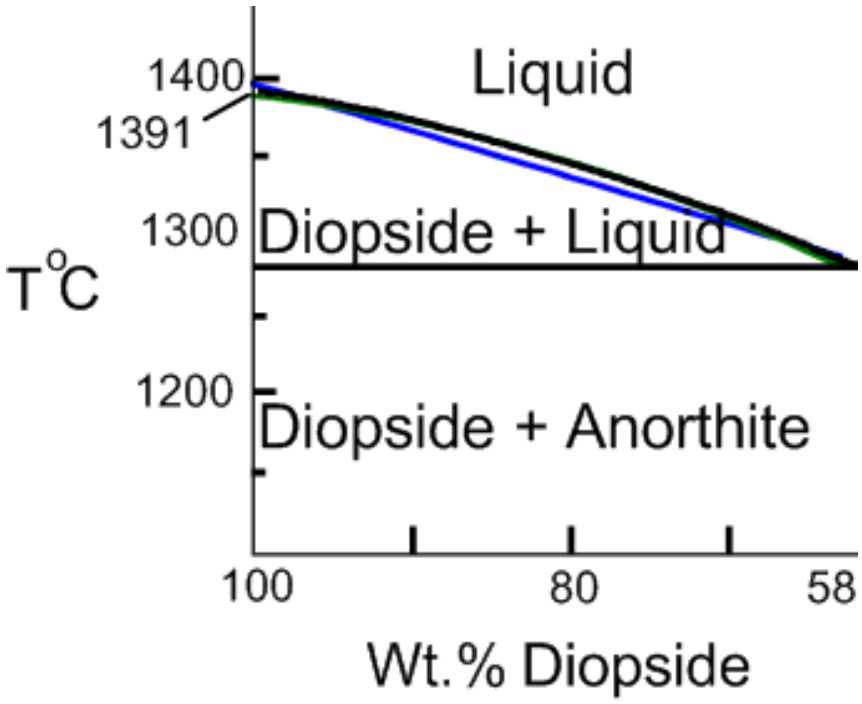

Figure 5.1(b) Zoom in the Di-rich side of diagram in Figure 5.1(a). The quadratic fitting curve is best matched with the original curve.

Figure 5.1(b) shows that the zoom-in part of the comparison of both fitting curves and the graphical data of [*Yoder*, 1976]. In addition both of the modeling results are shown in Figure 5.2. It is seen that the linear model tracks the trend of the temperature variation with respect to Di composition. In contrast, quadratic fitting provides a more accurate result in terms of curvature and smoothness.

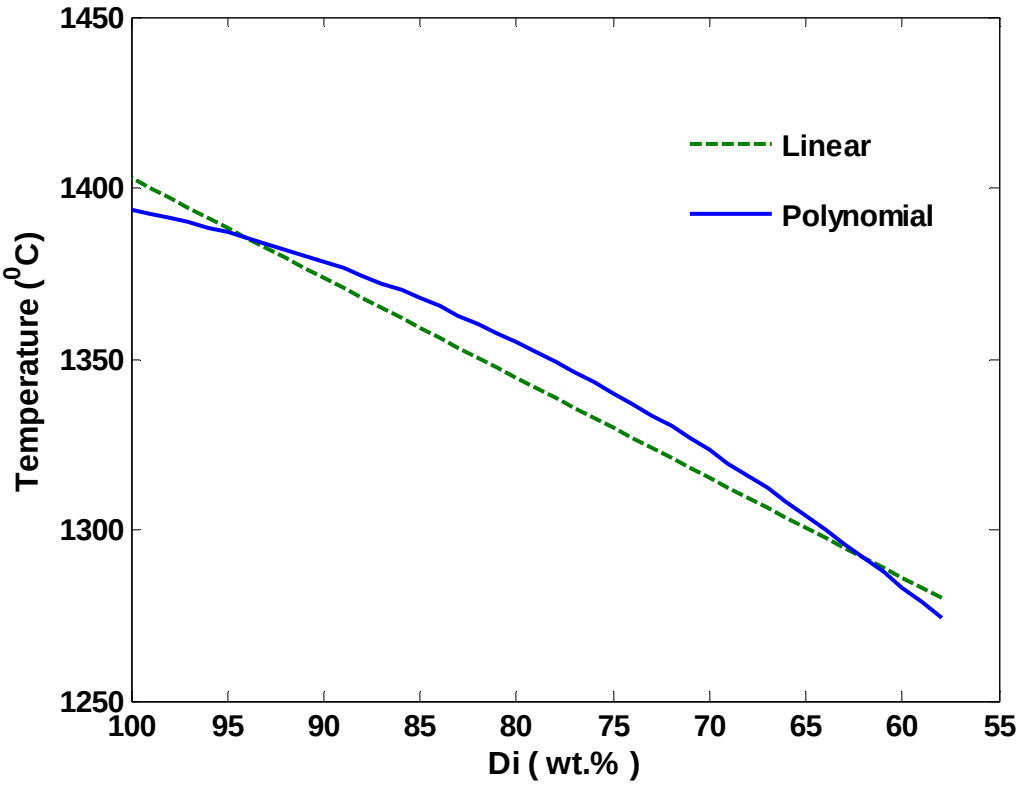

Figure 5.2 Magma temperature as a function of diopside composition in Di-rich side of Di-An system. The range of diopside composition is from 100% to 58% wt.%. The range of temperature is from 1391 to 1275°C. The linear relationship is in green dash and the polynomial relationship is in blue line, respectively.

5.3.2 Viscosity of silicate melts

The viscosity is one of the most important physical properties of silicate melts because it controls magma transport and eruption styles [*Sparks and Aspinall*, 2004; *Dingwell*, 2006]. The studies of natural silicate magmas have shown that the viscosity can span many orders of magnitude from 10^{-1} to 10^{14} Pa s [*Dingwell*, 1996; *Russell and Giordano*, 2005; *Giordano et al.*, 2006; *Hui and Zhang*, 2007]. Experimental studies together with theoretical analyses suggest that during convection in the crystallizing systems, crystals often separate from the liquid and fall to the floor because of their

negative buoyancy [e.g., *Nilson and Baer,* 1982]. As a result of fractionation, the chemical composition of the residual melt changes along with its temperature and its viscosity. During cooling and crystallization, magma viscosity always increases and crystallization leads to bulk composition variations of the residual liquid, which in turn affects magma viscosity. It has been shown that the viscosity of magma depends on both the magma's chemical composition and temperature. The prediction of viscosity in silicate melts remains a challenging task in earth sciences. The first model predicting the viscosity of silicate melts as a function of melt composition and temperature was developed in [*Shaw*, 1972] and [*Bottinga and Weill*, 1972]. To model the viscosity dependence on the chemical composition, assuming that all crystals instantly settle on the floor of magma chamber, we adopt the relationship between viscosity and magma temperature in [*Liu and Lowell*, 2009] that is derived from fitting the data in *Spera* [2000]:

$$\nu_m = v_0 \times (T_L / T_m)^{8.5} \tag{3}$$

where v_0 is the initial viscosity of magma, T_L is the liquidus temperature of the two-component system, T_m denotes the magma temperature. Substitution of equations (1) or (2) into equation (3) results in a relationship between viscosity and Di composition, respectively:

$$\nu_m(C) = v_0 \left(\frac{T_L}{291 \times C + 1111.5} \right)^{8.5} \tag{4}$$

and

$$\nu_m(C) = v_0 \left(\frac{T_L}{-410C^2 + 930C + 870.87} \right)^{8.5} \tag{5}$$

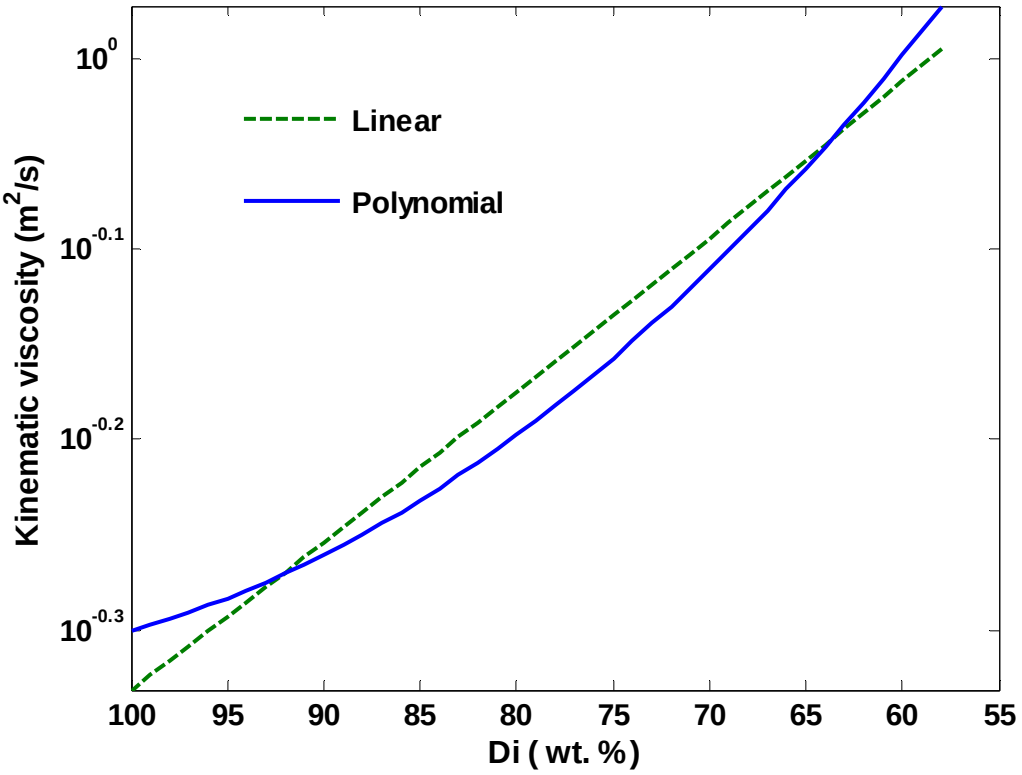

Figure 5.3 The variation of the melts viscosity corresponds to diopside composition for linear and polynomial relationships in green dash and blue line, respectively.

The relationship between magma viscosity and Di composition is depicted in Figure 5.3 for both linear and quadratic approximations of the liquidus–temperature-Di composition relation. The viscosity order increases about 0.3 with Di composition changing from the pure Di (Di_{100}) to the eutectic composition ($Di_{58}An_{42}$). In addition, based on the Di composition-magma viscosity relationship (Figure 5.3) and the Di component–temperature relationship (Figure 5.2), the melt temperature decreases as magma viscosity increases, and the viscosity has sharper variations at lower temperature than at higher temperature for the quadratic model. Thus, the melt composition variation during crystallization affects both the liquid viscosity and temperature. In a Di-An system,

melts with higher temperature and higher concentration of diopside have lower viscosity. At the temperature of 1391°C, the system is composed of 100% Di, and the viscosity of liquid diopside is 0.5 m^2/s. With decreasing Di content, the viscosity increases. At the eutectic temperature of 1275°C, the Di content reaches its lower bound of 58%, and the corresponding viscosity of the Di-An eutectic liquid is 1 m^2/s. Other properties of the Di-An system, such as the coefficient of thermal expansion, the latent heat of crystallization of diopside and anorthite are defined in Table 5.2. In the rest of the chapter, we adopt the quadratic relationship between the liquidus temperature and the Di content due to its better fit to the phase boundary.

5.4 Two-Component Magma Convection System without Replenishment

5.4.1 Mathematical formulation

Within the liquid magma body, thermal convection resulting from the temperature difference between hot magma and the cold upper boundary maintained by the overlying hydrothermal circulation is an efficient means of heat transfer. The basic mechanisms governing the magma convection system, which are based on *Huppert and Sparks* [1988], are discussed in detail in [*Liu and Lowell*, 2009]. Conservation of energy in the binary system is similar to the single component system. Thus, some of the analysis from [*Liu and Lowell*, 2009] are adopted and some key results are reviewed (refer to Chapter 2 and 3 for details).

In a well-mixed sub-axial magma chamber, the heat content of magma chamber is expressed as

$$H(t) = V_m(t)\left[\rho_m c_m T_m(t) + \rho_m (1 - \chi(t)) L(t)\right] \tag{6}$$

where ρ_m is the density of magma, $V_m(t)$ is the volume of liquid magma, c_m is the specific heat of magma, $\chi(t)$ is the crystal content, $L(t)$ is the latent heat of magma crystallization. The first term on the right hand side of equation (6) is related to the specific heat capacity of magma, and the second term represents the latent heat released by crystallization. Energy conservation in a vigorously convecting magma body with magma replenishment is given by

$$\frac{dH(t)}{dt} = -F_m(t)A_m(t) + F_r(t)A_m(t) \tag{7}$$

where $F_m(t)$ is the convective heat transfer of the magma system, $F_r(t)$ is the heat replenishment rate due to the magma replenishment, and $A_m(t)$ denotes the magma area. Substituting equation (6) into equation (7) yields

$$\begin{aligned} &\frac{dV_m(t)}{dt}[\rho_m c_m T_m(t) + \rho_m(1-\chi(t)L(t)] + V_m(t)\rho_m c_m \frac{dT_m(t)}{dt} \\ &+ \rho_m V_m(t)\frac{dL(t)}{dt} - \rho_m V_m(t)\frac{d\chi(t)L(t)}{dt} = -F_m(t)A_m(t) + F_r(t)A_m(t) \end{aligned} \tag{8}$$

In the two-component Di-An eutectic system, it is convenient to replace the quantity $T_m(t)$ with the concentration of diopside $C(t)$ since they are related to each other through equation (1) or (2). In the following analysis, we first consider the cases without magma replenishment, i.e. $F_r(t) = 0$. We analyze the dependence of the heat flux $F_m(t)$, latent heat $L(t)$, crystal content $\chi(t)$, and the volume of liquid magma V_m(t) on the Di concentration $C(t)$.

To develop the relationship between F_m, L, χ, V and C, respectively, we ignore the time dependence for simplicity of expression. Then, the time-dependent nature of these quantities is added through the time-varying Di concentration $C(t)$ when the heat conservation equation is solved. In addition, due to the closeness of diopside and

anorthite densities, we assume the magma density is constant, although its composition is time varying.

5.4.1.1 Heat flux F_m

Seismic imaging at oceanic spreading centers [e.g. *Singh et al.*, 2006; *Van Ark et al.*, 2007] and observations of high-temperature hydrothermal vents on the seafloor [e.g., *Haymon et al.*, 1991; *Fouquet et al.*, 1991; *Baker et al.*, 1994] indicate a close correlation between hydrothermal systems and axial magma chambers. The heat flux transferred as a result of high Rayleigh and Nusselt number convection in the magma chamber is given by [*Turner*, 1973]:

$$F_m(C) = 0.1\rho_m c_m(\alpha_m g a_m{}^2 / v_m)^{1/3}(T_m(C) - T_e)^{4/3} \tag{9}$$

where α_m is the coefficient of thermal expansion, a_m is the thermal diffusivity, g is the acceleration due to the gravity, v_m is the kinematic viscosity of the magma (given by equation (5)), and T_e is the eutectic temperature of melts. Recall that the temperature T_m depends of Di concentration C in equation (1) or (2), thus, equation (9) indicates an indirect relation between the heat flux F_m and Di concentration C bridged by temperature T_m.

5.4.1.2 Latent heat L

In the Di-An system, latent heat is a function of the composition of the different components. Denote L_{di} and L_{an} as the latent heat of crystallization of the liquid diopside and anorthite, respectively. Based on the assumption that the density difference between diopside and anorthite is negligible, the latent heat of the two-component magma is

linearly dependent on each component's concentration. Thus, it is written as a linear combination of the latent heat of pure Di and An weighted by their concentrations:

$$L(C) = L_{di} \times C + L_{an} \times (1 - C) \tag{10}$$

5.4.1.3 Crystal content χ

Based on the assumption that the local composition of the solid does not change after it is formed, and the concentration of the liquid is uniform during the solidification process, the Scheil equation [*Scheil*, 1942] can be used to calculate the eutectic composition at the end of single-phase solidification. The formation of the multi-component Scheil equation incorporates the composition of $C(t)$ and fraction solid $\chi(t)$ through the conservation of mass in the melt [*Petrakis et. al, 1981*]

$$(1 - \chi)\frac{dC}{dt} = (C - 1)\frac{d\chi}{dt} \tag{11}$$

Solving equation (11) results in

$$(1 - \chi)(C - 1) = const \tag{12}$$

where *const* denotes a constant. Define C_0 to be the initial composition of liquid diopside in the magma system. With the boundary condition $\chi = 1, C = C_0$, the volume fraction of crystals $\chi(C)$ is related to the liquid diopside concentration by

$$\chi(C) = \frac{C_0 - C}{1 - C} \tag{13}$$

The value C_0 = 100% for a pure melt of diopside, and we consider C_0 ranging between 58% and 100%. In this paper, we consider four silicate melts with different initial composition of diopside: $Di_{90}An_{10}$, $Di_{80}An_{20}$, $Di_{70}An_{30}$, and $Di_{60}An_{40}$.

5.4.1.4 Liquid magma volume V_m

In the process of magma crystallization, we assume that all the crystals are immediately removed or fractionated from the residual melts and settle on the floor of magma chamber so that no further reactions can occur within the magma chamber. In addition, we assume that any change in the horizontal area of magma chamber A_m upon crystal solidification can be neglected, i.e., the area of magma remains constant $A_m=A_{m0}$. Thus, as the crystal layer grows on the magma chamber floor, the thickness of crystal and remaining melt layers are time variant and given by, respectively,

$$\begin{aligned} D_s(C) &= D_0 \times \chi(C) \\ D_m(C) &= D_0 \times (1-\chi(C)) \end{aligned} \tag{14}$$

where D_0 is the initial thickness of magma chamber, $D_s(C)$ denotes the depth of the crystals growing on the floor, and $D_m(C)$ is the depth of the liquid magma. As crystals settle on the floor of the magma chamber, the thickness of melt in magma chamber decreases. Correspondingly, the liquid magma volume $V_m(C)$ is

$$V_m(C) = A_{m0}D_0(1-\chi(C)) \tag{15}$$

5.4.1.5 Dynamic characterization of Di-An systems

With the expression (2), (10), (13), (14), and (15) we take the appropriate derivatives and substitute them into equations (8) and (9) to obtain a differential equation for the concentration $C(t)$. Recall that the goal of this work is to model the dynamic heat flux $F_m(t)$. Based on equation (9), the calculation $F_m(t)$ is straightforward once the time-varying $C(t)$ is solved. In the following, we derive $C(t)$ through the energy conservation as shown in equation (8). First, we rewrite the variables $\frac{dV_m(t)}{dt}$, $\frac{dT_m(t)}{dt}$, $\frac{dL(t)}{dt}$, and

$\frac{d\chi(t)L(t)}{dt}$ in equation (8) in terms of the Di concentration C. Taking derivative of equations (15), (2), and (10) with respect to time, respectively, results in

$$\frac{dV_m(t)}{dt} = -A_{m0}D_0\chi_c'(t)\frac{dC(t)}{dt} \tag{16}$$

$$\frac{dT_m(t)}{dt} = (-820C(t) + 930)\frac{dC(t)}{dt} \tag{17}$$

$$\frac{dL(t)}{dt} = L_c'(t)\frac{dC(t)}{dt} \tag{18}$$

where the derivative of the crystal content and the latent heat with respect to Di concentration are calculated based on equations (13) and (10), respectively

$$\chi_c' = \frac{d\chi}{dC} = \frac{C_0 - 1}{(C-1)^2} \tag{19}$$

$$L_c' = \frac{dL}{dC} = L_{di} - L_{an} \tag{20}$$

In addition, it is straightforward to obtain

$$\frac{d\chi(t)L(t)}{dt} = [\chi(C)L_c' + L(C)\chi_c']\frac{dC(t)}{dt} \tag{21}$$

Substituting equations (16), (17), (18), and (21) into (8), we obtain the governing equation of the Di concentration as

$$\frac{dC(t)}{dt} = \frac{F_m(C)}{\Gamma_1(C)} \tag{22}$$

where the variable $\Gamma_1(t)$ is defined as

$$\Gamma_1(C) = \rho D_0 \chi_c' \left[c_m \left(-410C^2 + 930C + 870.87 \right) + L(C)\left(1 - \chi(C)\right) \right] - \rho D_m(C) \left[c_m (-820C + 930) + L_c' - \chi(C) L_c' - L(C) \chi_c' \right] \quad (23)$$

Although the close-form solution of equation (22) is difficult to obtain, it is solved numerically. Once $C(t)$ is solved, the heat flux $F_m(t)$ is straightforward to obtain using equation (9).

5.4.2 Results

In our simulations, we consider a magma chamber with the initial thickness D = 100 m and area $A_{m0} = 10^6$ m^2. Different initial chemical compositions of Di (C_0) for the sample melts are used, including $Di_{90}An_{10}$, $Di_{80}An_{20}$, $Di_{70}An_{30}$, and $Di_{60}An_{40}$.

Figure 5.4 shows the total heat output $F_m(t)A_m$ of the Di-An system with different initial Di compositions. Because we wish to connect magmatic heat output with observed seafloor hydrothermal systems, we show the horizontal line representing total heat output of 10^7 Watts. This value is the lower boundary of the measured heat output from seafloor hydrothermal systems which typically ranges between 10^7 and 10^9 Watts [*Lowell and Germanovich*, 2004; *Ramondenc et al.*, 2006; *Baker*, 2007]. As expected, for the given Di concentration, the higher initial diopside composition gives rise to a larger the initial total heat output. Moreover, the larger the initial total heat output results in faster decay of the heat output. In addition, the life time of the overlying hydrothermal system (i.e., the time period for total heat output to reach 10^7 Watts) driven by four magmas is around 32, 50, 60, and 30 years, respectively. The $Di_{70}An_{30}$ system has the longest lifetime because the lifetime is determined by both of the initial heat output and the decay rate.

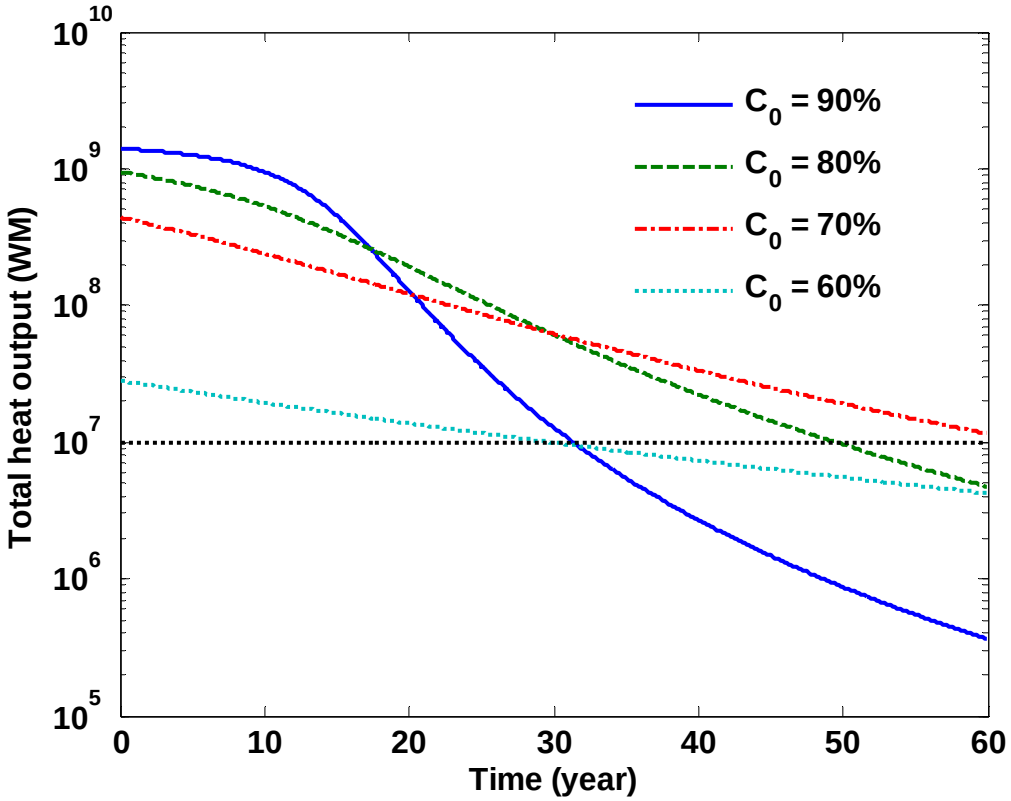

Figure 5.4 Total heat output as a function of time for different initial compositions of diopside without magma replenishment. The horizontal dash line located at 10^7 Watts denotes the lower limit of total hydrothermal heat output measured at oceanic spreading centers. C_0 denotes the initial diopside concentration.

Figure 5.5 shows the thickness of crystal layer growing during magma cooling for magma chambers with different diopside composition. The larger initial diopside composition leads to faster growth of the crystal layer thickness, which is consistent with decay rate of the total heat output shown in Figure 5.4. That is, the rate of crystal layer grows depends on the rate of heat output from the magma chamber. The thickness of the crystal layer approaches a constant as there is less and less Di content left in the melt. Thus, the system with larger initial diopside composition creates a thicker layer of crystals.

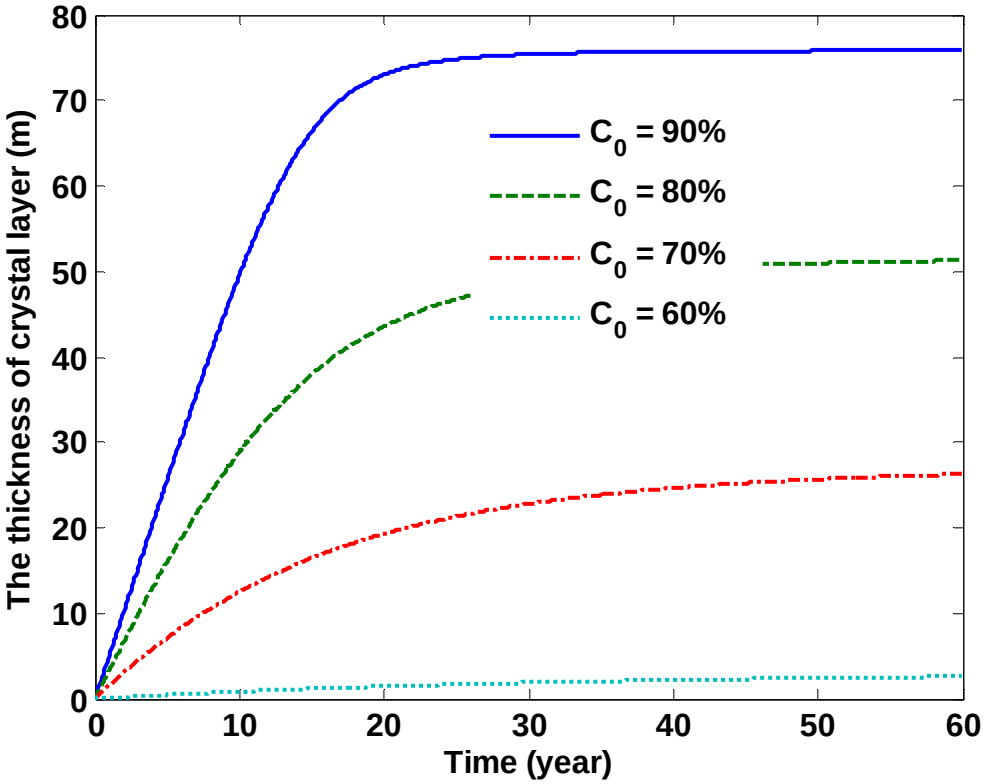

Figure 5.5 The thickness of crystals layer as a function of time for different initial diopside compositions without magma replenishment. The crystals settle on the floor of magma chamber and grow with respect to time.

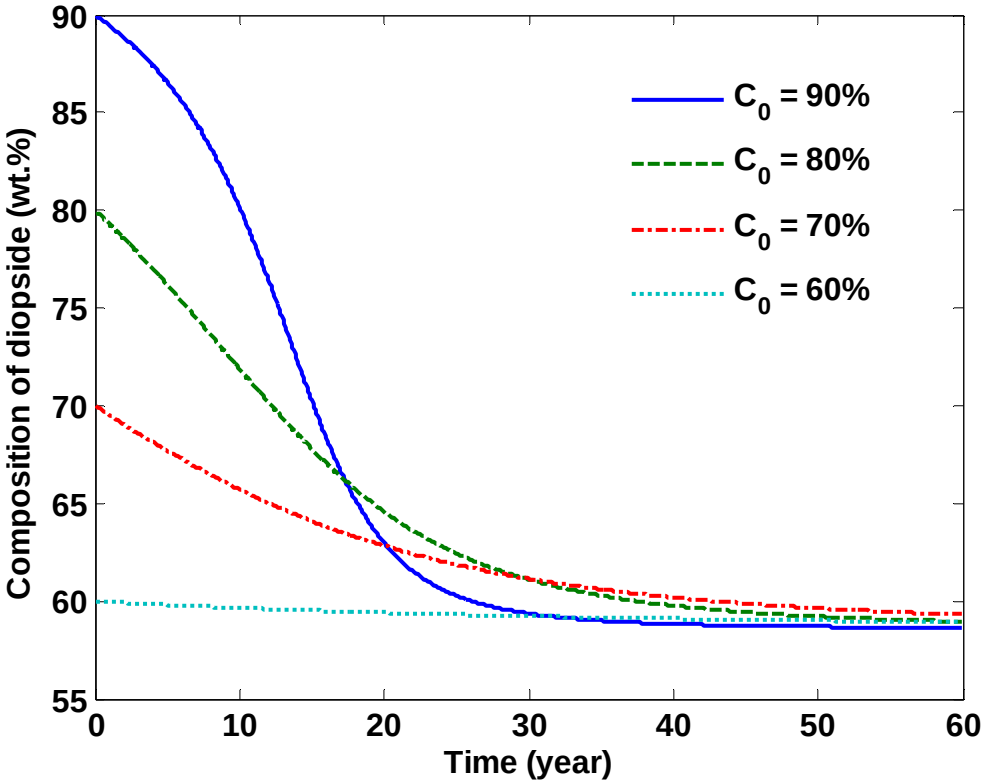

Figure 5.6 The time-varying composition of diopside for different initial diopside compositions without magma replenishment.

Figure 5.6 shows the instantaneous diopside concentration with different initial diopside compositions. The system with $Di_{90}An_{10}$ demonstrates fast decay to the eutectic composition for the first decade and the rapid decrease in Di composition because of the high crystallization rate. For the Di composition close to the eutectic composition (Di_{58}), the silicate melt with $Di_{60}An_{40}$ has lower liquidus temperature due to the lower Di concentration so that Di composition changes very slowly with respect to time, which results in a stable melt system for a relatively long time.

5.5 Two-Component Magma System with Replenishment

In this section, we analyze the effect of magma replenishment on the Di-An system. There are a number of mechanisms by which melt might be extracted from its source host and added to the sub-axial magma chamber. One of them could be the decreasing internal pressure in magma chamber caused by the shrinking of magma volume during magma cooling and crystallization. The resulting pressure gradient would then drive new magma from the underlying mush zone into the magma chamber. Others could be buoyant porous flow through the mush zone as a result of compaction [*McKenzie*, 1984; *McKenzie*, 1985], buoyant crack propagation [*Shaw*, 1985; *Lister*, 1990; *Lister and Kerr*, 1991], or dike propagation from a deeper lying magma body [*Sim*, 2004]. Since we do not incorporate any physical mechanism in these models, we simply assume that the magma replenishment is controlled by a replenishment velocity. With additional magma added into the magma chamber, both magma mass and heat content increase. We incorporate magma replenishment and analyze the resulting heat flux in the similar manner described in section 5.4, except that now $F_r(t)$ is included.

5.5.1 Numerical modeling

The heat flux $F_r(t)$ resulting from replenishment is given by [*Liu and Lowell*, 2010]:

$$F_r(t) = (\rho c_m T_{in} + \rho L(t)(1 - \chi_{in})) \times u(t) \tag{24}$$

where $u(t)$ denotes the rate of magma replenishment, T_{in} is the temperature of replenished magma, and χ_{in} is the crystal content of input magma. Here, we assume that the added magma is also Di-An magma, but it may have a composition other than the initial Di

composition in the magma chamber. Thus, the temperature T_{in} of the added magma depends on its Di concentration (see equation (2))

$$T_{in} = -410C_{in}^2 + 930C_{in} + 870.87 \tag{25}$$

where C_{in} denotes the Di concentration of the magma being added. The crystal content of input magma is modeled as

$$\chi_{in} = \frac{1 - C_{in}}{1 - C_e} \tag{26}$$

where C_e denotes the eutectic composition of Di (C_e = 58%).

We assume that the added magma is rapidly mixed after it enters the magma chamber. The bulk composition $C_b(t)$ is then given by

$$C_b(t) = (1 - \phi(t))C_0 + \phi(t)C_{in} \tag{27}$$

where $\phi(t)$ is determined by the ratio of the volumes between the added magma and the total magma in the magma chamber

$$\phi(t) = \frac{V_{in}(t)}{V_{total}(t)} \tag{28}$$

With magma replenishment, the crystal content $\chi(t)$ in equation (13) is rewritten by considering the time-varying bulk composition

$$\chi(t) = \frac{C_b(t) - C(t)}{1 - C(t)} \tag{29}$$

Taking derivative of equation (29), we obtain

$$\frac{d\chi(t)}{dt} = w(t)\frac{dC(t)}{dt} + r(t)C_b'(t) \tag{30}$$

where the quantities $r(t)$ are $w(t)$ are defined as

$$r(t) = \frac{1}{1 - C(t)} \tag{31}$$

$$w(t) = \left[C_b(t) - 1\right] r^2(t) \tag{32}$$

and $C_b'(t)$ denotes the derivative of bulk composition with respect to time and is calculated from equation (27) as

$$C_b'(t) = \frac{dC_b(t)}{dt} = (C_{in} - C_0)\frac{d\phi(t)}{dt} \tag{33}$$

In the magma replenishment case, conservation of energy is still governed by equation (7); but in contrast to the case without replenishment, the heat flux $F_r(t)$ corresponding to magma replenishment is incorporated. To solve the heat flux from the magma chamber, we start by solving the quantities in equation (8). Combining equations (10) and (29), we obtain

$$\frac{d\chi(t)L(t)}{dt} = \left[\chi(t)L_c'(t) + L(t)w(t)\right]\frac{dC(t)}{dt} + L(t)C_b'(t)r(t) \tag{34}$$

To calculate the magmatic heat output with magma replenishment, we consider the magma chamber growth in two directions, both vertically and horizontally.

5.5.1.1 Time-varying magma chamber thickness

Assume that as the new magma enters the magma chamber, the thickness of magma chamber grows. Then the total magma chamber thickness is expressed by

$$D(t) = D_0 + D_{in}(t) \tag{35}$$

where $D_{in}(t)$ denotes the thickness contributed by the additional magma and can be calculated from the magma replenishment rate. That is,

$$D_{in}(t) = \int_0^t u(s)ds \tag{36}$$

and $u(t)$ denotes the magma replenishment rate. Because the magma chamber area remains constant, equation (28) is reduced to

$$\phi(t) = \frac{D_{in}(t)}{D(t)} \tag{37}$$

Taking derivative of equation (37) and combining (36) results in

$$\frac{d\phi(t)}{dt} = \frac{D_0 u(t)}{D^2(t)} \tag{38}$$

With the time-varying magma chamber thickness, the thickness and volume of the liquid magma are given by, respectively

$$D_m(t) = (1 - \chi(t))D(t) \tag{39}$$

$$V_m(t) = A_{m0} D_m(t) = A_{m0}(1 - \chi(t))D(t) \tag{40}$$

Taking derivative of equation (40) and combining equation (30) results in

$$\frac{dV_m(t)}{dt} = -A_{m0} D(t) w(t) \frac{dC(t)}{dt} + A_{m0}[u(t)(1 - \chi(t)) - D(t)C_b'(t)r(t)] \tag{41}$$

Substitution of equations (17), (18), (34), and (41) into equation (8) leads to the governing equation of Di content in the magma replenishment case

$$\frac{dC(t)}{dt} = \frac{F_m(t) - F_r(t) + p(t)}{\Gamma_2(t)} \tag{42}$$

where

$$\begin{aligned} p(t) = \rho[u(t)(1-\chi) - D(t)C_b'(t)r(t)][c_m\left(-410C^2(t) + 930C(t) + 870.87\right) \\ + (1-\chi)L(t)] - \rho D_m(t)L(t)C_b'(t)r(t) \end{aligned} \tag{43}$$

$$\Gamma_2(t) = \rho D(t) w(t)\left[c_m\left(-410C^2(t) + 930C(t) + 870.87\right) + L(t)\left(1 - \chi(t)\right)\right] \\ - \rho D_m(t)\left[c_m(-820C(t) + 930) + L_c'(t) - \chi(t)L_c'(t) - L(t)w(t)\right] \tag{44}$$

Eventually, given the magma replenishment rate $u(t)$, the Di concentration $C(t)$ can be solved numerically from equation (42). From this solution, other quantities such as heat flux $F_m(t)$, temperature of magma chamber $T_m(t)$, etc can be obtained..

In our computation, we employ two models for the magma replenishment rate. For simplicity, the magma replenishment rate $u(t)$ is first modeled as constant, i.e.,

$$u(t) = u_0 \tag{45}$$

Another way is to model the rate of magma replenishment as a sinusoid function, which is capable of modeling the periodic behavior of the replenishment. For simplicity we incorporate episodic magma replenishment as a simple sinusoid. Hence

$$u(t) = u_0 + u_0 \sin(wt) \tag{46}$$

where w denotes the angular frequency. Correspondingly, the thicknesses of the replenished magma based on the two replenishment rate models are given by, respectively

$$D_{in}(t) = u_0 t \tag{47}$$

$$D_{in}(t) = u_0 t + \frac{u_0}{w}(1 - \cos(wt)) \tag{48}$$

5.5.1.2 Time-varying magma chamber area

In this part, we assume that the magma chamber grows horizontally as new magma is added, i.e., the magma chamber area is time-varying while its thickness remains constant. Based on the analysis in [*Liu and Lowell, 2009*], the magma chamber area grows according to

$$D_0 \frac{dA_m(t)}{dt} = A_m(t)u(t) \tag{49}$$

Solving equation (49) results in

$$A_m(t) = A_{m0} \exp\left(\frac{\int_0^t u(s)ds}{D_0} \right) \tag{50}$$

Thus, the volume of the added magma and total magma chamber can be written as, respectively

$$V_{in}(t) = \int_0^t A_m(s)u(s)ds = D_0(A_m(t) - A_{m0}) \tag{51}$$

$$V_{total}(t) = D_0 A_m(t) \tag{52}$$

Substitution of equations (51) and (52) into equation (28) leads to

$$\phi(t) = \frac{\int_0^t A_m(s)u(s)ds}{D_0 A_m(t)} = \frac{A_m(t) - A_{m0}}{A_m(t)} \tag{53}$$

Taking derivative of equation (53) and combining equation (49), we obtain

$$\frac{d\phi(t)}{dt} = \frac{u(t)A_{m0}}{D_0 A_m(t)} \tag{54}$$

Although the thickness of the magma chamber remains constant, the thickness of the liquid magma still varies with time as a result of crystal settling. The liquid magma chamber volume is expressed as

$$V_m(t) = D_0(1 - \chi(t))A_m(t) \tag{55}$$

Combining equations (29), (49), and (55), we obtain the time dependence of the magma chamber volume as

$$\frac{dV_m(t)}{dt} = -D_0 A_m(t)w(t)\frac{dC(t)}{dt} + A_m(t)\left[u(t)(1 - \chi(t)) - D_0 r(t)C_b'(t)\right] \tag{56}$$

Substituting of equations (17), (18), (34), and (56) into (8), we obtain the governing equation of Di content for the time-varying area case in the same form as the time-varying thickness case in equation (42), with $D(t)$ replaced by D_0, and $C_b'(t)$ is computed using equation (54) instead of equation (38). Thus, the Di concentration $C(t)$ can be solved numerically, along with the heat flux and temperature of the magma chamber.

5.5.2 Results

In this part, numerical results show how magmatic heat output evolves as a function of magma replenishment rate, initial Di composition, and the composition of the added magma. We assume that the hydrothermal system is not active any more when either the total heat output is below the minimum observation value of 10^7 Watts or the magma chamber volume doubles.

5.5.2.1 Time-varying magma thickness.

First, the simulation results for the time-varying magma chamber thickness case are demonstrated. Figure 5.7 shows the total heat output from the magma chamber as a function of different constant magma replenishment rates of 10^{-7}, 10^{-8}, and 10^{-9} m/s, respectively. The initial Di concentration C_0 in the magma chamber is set to be 90%. The added magma has Di concentration C_{in} of 80%. With the fast replenishment rate of 10^{-7} m/s, the thickness of magma chamber doubles after 32 years. With the moderate replenishment rate of 10^{-8} m/s, the system reaches a quasi-steady heat output for several decades before the magma chamber doubles its size. For a replenishment rate of 10^{-9} m/s, replenishment has little effect on counteracting the intrinsic heat flux decay. The system heat output falls to 10^7 Watts in about 32 years.

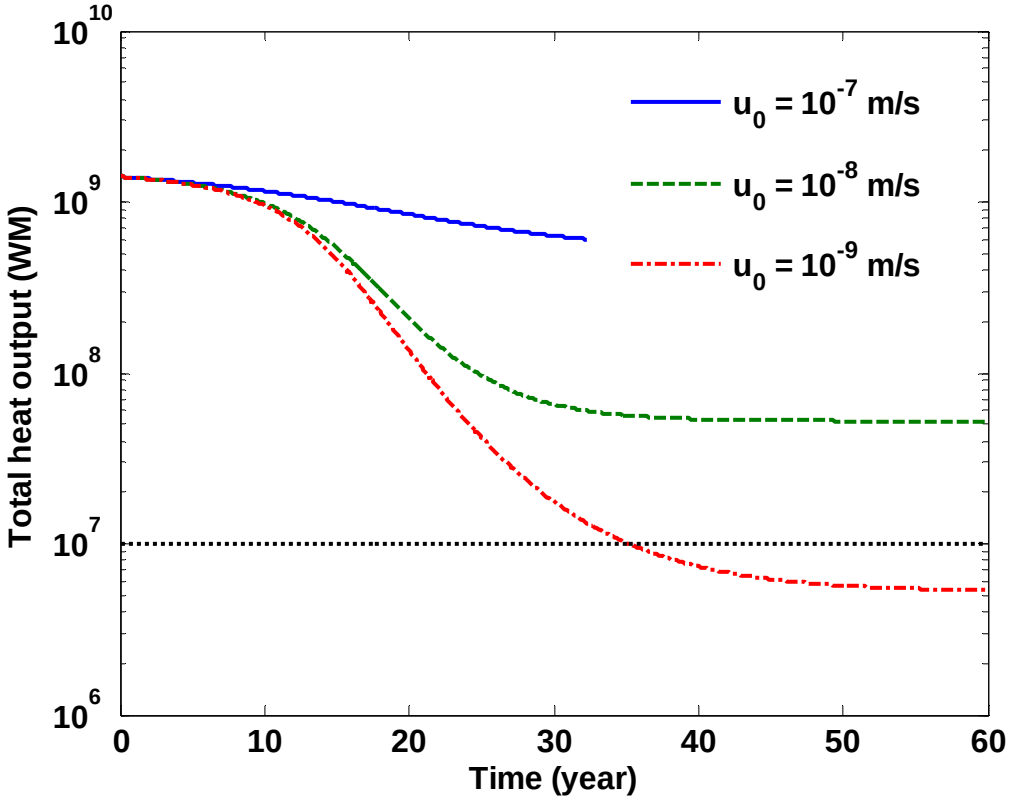

Figure 5.7 Total heat output as a function of time for a variety of constant magma replenishment rates in Di-An system with the initial Di concentration of 90% and replenished Di concentration of 90%. u_0 denotes the initial magma replenishment rate. Simulations run until magma thickness D doubles from its initial value of 100 m. Results show that u_0 between 10^{-7} and 10^{-8} m/s tends to stabilize heat output on decadal timescales and keep them within the range of total hydrothermal heat output measurements from 10^7 to 10^9 W.

Figure 5.8 shows the total heat output for different sets of initial and added Di compositions at the constant replenishment rate of 10^{-8} m/s. The Figure shows that the initial composition C_0 determines the initial total heat output, i.e., the larger C_0 results in larger total heat output initially. The composition C_{in} of the added magma affects heat flux decay rate of the magma chamber in the presence of cooling and replenishment. Magma replenishment with the higher C_{in} introduces more heat into the magma chamber and thus slows down the decay of total magma chamber heat output.

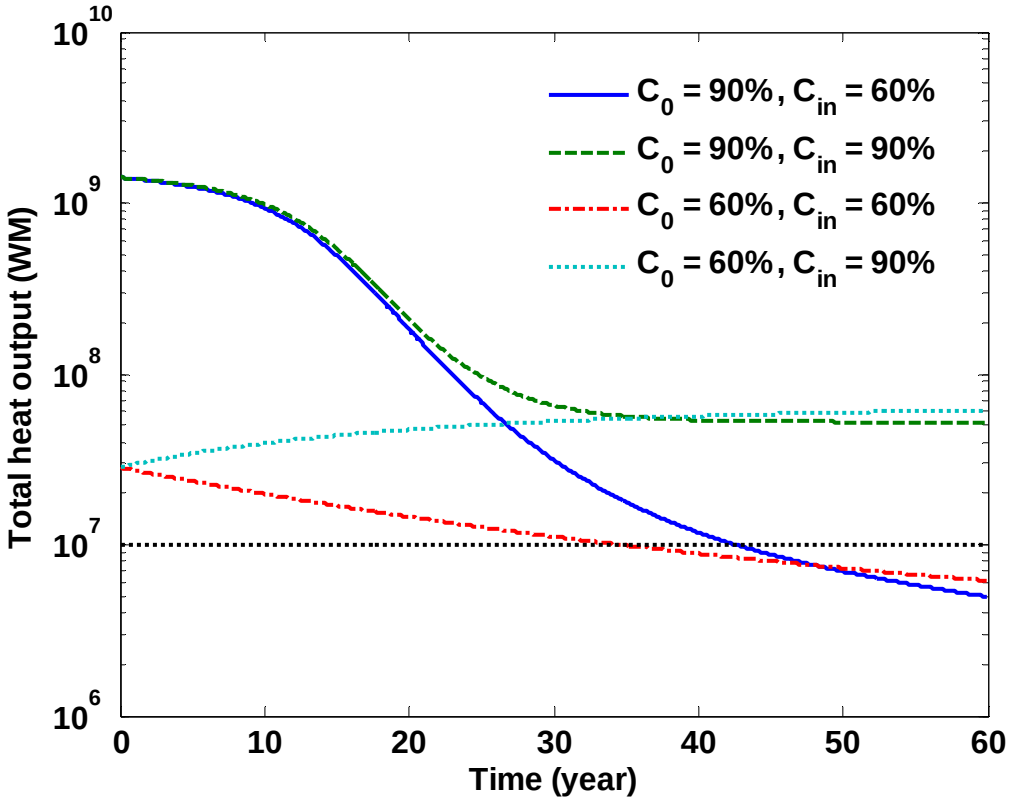

Figure 5.8 Total heat output as a function of time for different values of initial and input Di concentration with magma replenishment at a constant rate of 10^{-8} m/s. C_0 and C_{in} denote the initial Di and replenished Di concentration, respectively. Results show that C_0 determine the initial total heat output from magma chambers and C_{in} control the decay rate of total heat output.

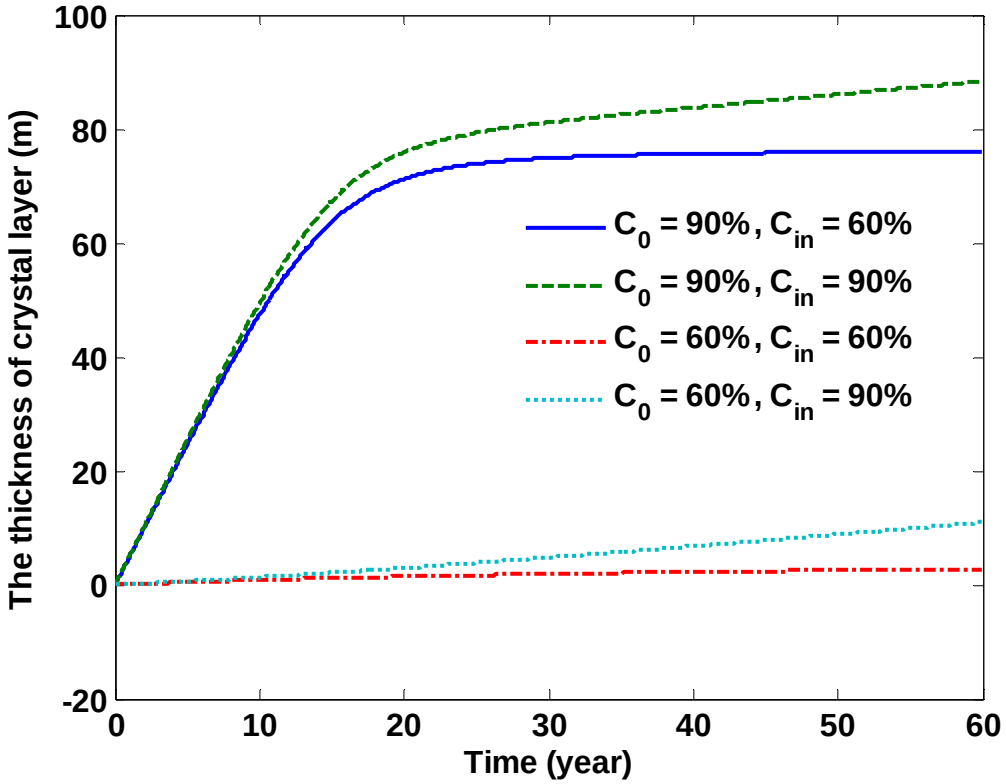

Figure 5.9 The thickness of crystal layer growing at the floor of magma chamber as a function of time with different sets of initial and input Di concentrations with magma replenishment at a constant rate of 10^{-8} m/s. The area of magma chamber keeps constant during magma replenishment. Results show that more crystals settle on the floor of magma chamber with increasing initial Di concentration in magma.

Figure 5.9 and Figure 5.10 depict the time-varying thickness of the crystal layer and Di composition during the magma chamber convection, respectively. We choose different sets of initial and input Di compositions and set the constant replenishment rate to be 10^{-8} m/s. In this case the crystal thickness grows in two stages that result from the combination effects of both the cooling and replenishment. In the first stage, the system cooling dominates the magma evolution. Thus, the thickness of the crystal layer has a sharp initial growth rate due to the crystallization. In the second stage, the magma cooling weakens and the magma replenishment becomes the dominant process. Correspondingly,

the crystal thickness either grows slowly (C_{in} = 90%) or extremely slow (C_{in} = 60%) depending on the Di composition of the replenished magma. In addition, replenishment makes the crystal layer thickness grow differently than in the case of without replenishment, where the crystal thickness remains nearly constant after the cooling process slows down. In a consistent manner, the time-varying Di concentration $C(t)$ demonstrates similar dynamic trend (Figure 5.10), where the two-stage variation in Di content is more obvious when the magma chamber has the bigger initial Di content (90%).

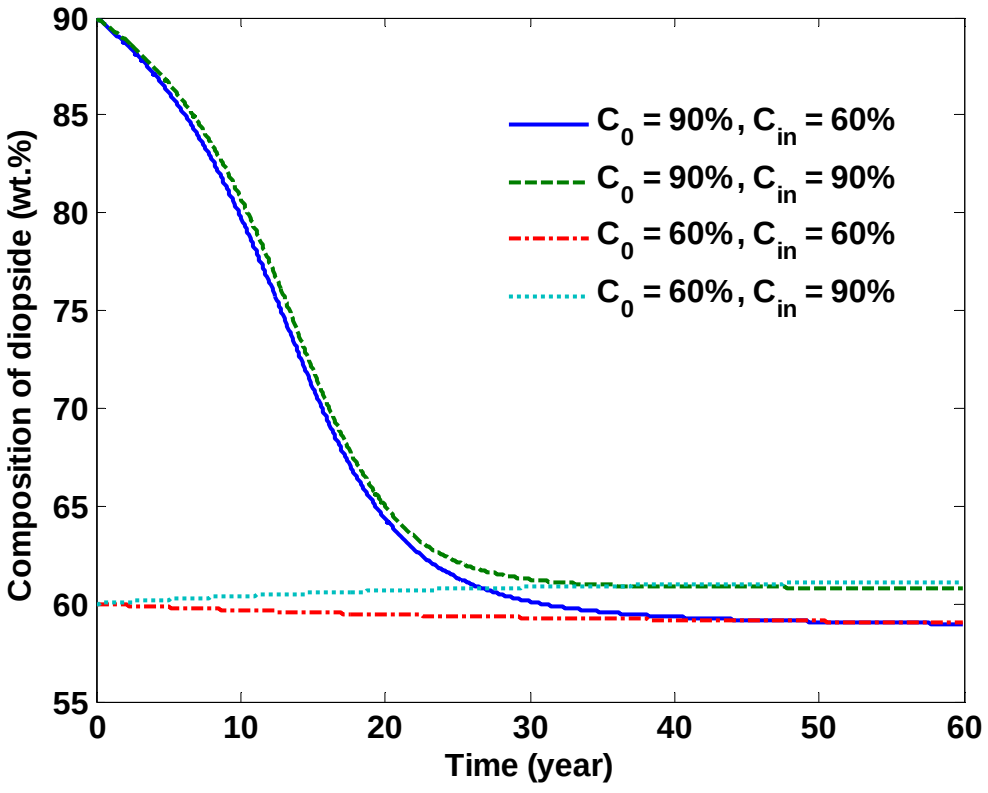

Figure 5.10 The time-varying diopside composition of magma with different sets of initial and input Di concentrations with magma replenishment at a constant replenishment rate of 10^{-8} m/s. The variation of diopside composition is more obvious for the magma with high initial Di concentration during magma cooling and crystallization.

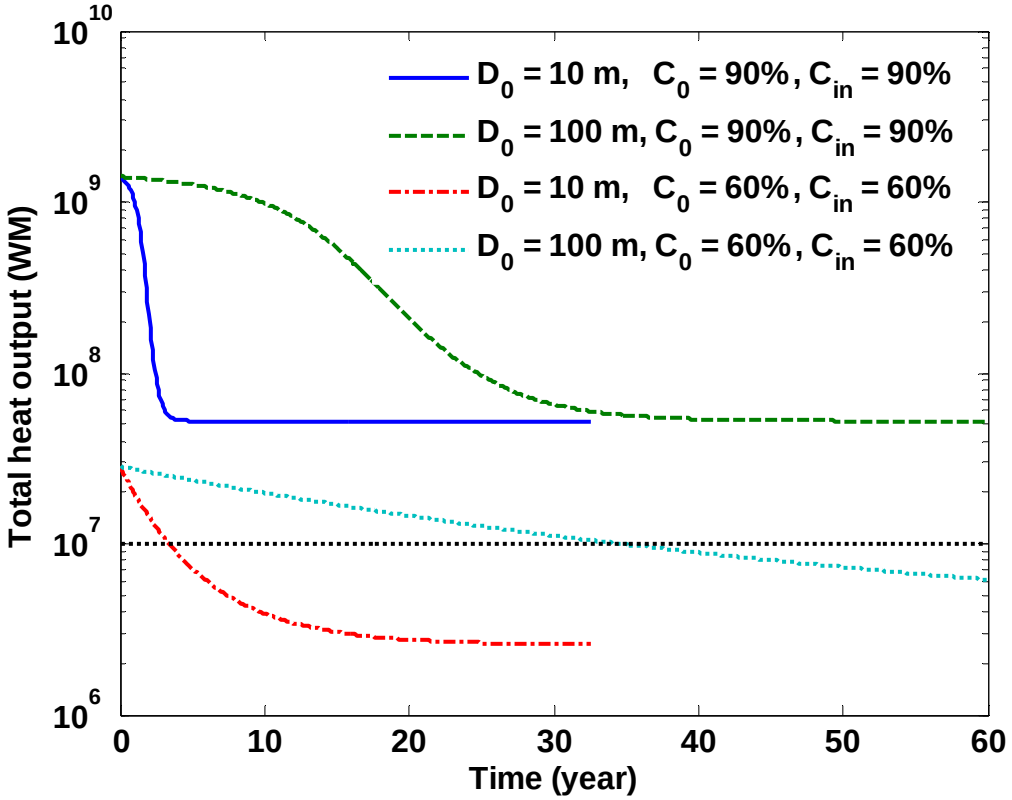

Figure 5.11 Total heat output as a function of time for a variety of initial and input Di concentrations with magma replenishment at a constant rate of 10^{-8} m/s. Results show the effect of different thicknesses of magma chambers (D = 100 and 10 m) on the total heat output. The thinner magma chambers have rapid decay rates of total heat output at first few years. However, with high initial and replenished Di concentration, a thinner magma chamber enables to stabilize heat output above 10^7 W on decadal timescales.

Seismic evidence suggests that the magma lens along the oceanic spreading centers ranges between a few tens meters to around one hundred meters [*Kent et al.* 1990; *MacLeod and Yaoyancq*, 2000]. To illustrate the effect of the magma chamber thickness on its heat output, Figure 5.11 plots the total heat output of two magma chambers with the thickness of 10 and 100 m, respectively. We choose different initial Di contents of 90% and 60%. The replenished magma is at a constant rate of 10^{-8} m/s and with different Di contents of 90% and 60%. Figure 5.11 shows that for the given initial and added Di

concentration, magma with an initial thickness of 10 m has faster rate of heat output decline than the one with an initial thickness of 100 m. The reason is twofold. First, the thinner magma chamber has smaller Rayleigh number and less vigorous convection. Second, the rate of crystallization is faster for a smaller magma chamber than for a larger magma chamber although the initial heat flux is independent of magma chamber thickness.

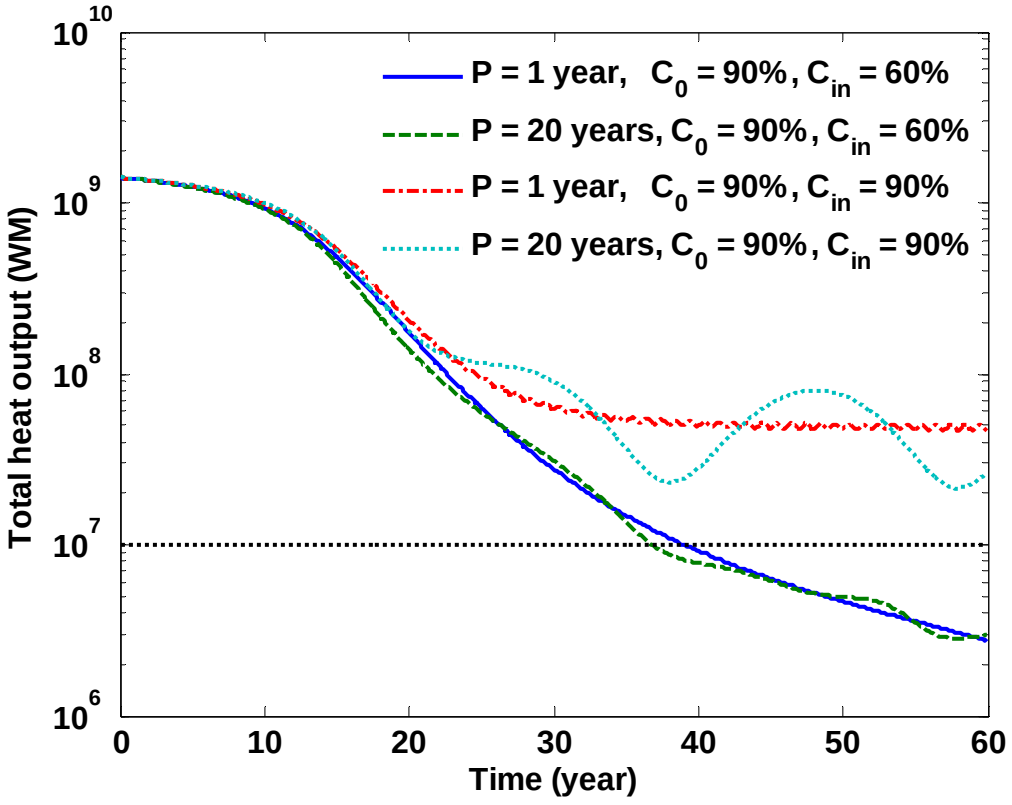

Figure 5.12 Total heat output as a function of time for a variety of initial and input Di concentrations with a constant magma replenishment rate of 10^{-8} m/s for a different replenishment period (1 and 20 years). *P* denotes the period of magma replenishment.

Figure 5.12 shows the total heat output from the magma chamber with periodic magma replenishment. The initial Di concentration C_0 in the magma chamber is set to be 90%. The replenishment has period of 1 and 20 years, and the replenished magma has Di concentration C_{in} of either 90% or 60%. Similar to the case of constant replenishment rate, magma replenishment with a higher C_{in} introduces more heat into the magma chamber and thus keeps the magma heat output at a steady state for decadal time scales. In the first 25 years, the heat flux decays rapidly because of strong heat transfer from magma convection. During this period, magma cooling and crystallization dominates magma chamber evolution, thus the periodic behavior cannot be observed. After the cooling weakens and magma replenishment dominates the rate of heat flux, heat output exhibits periodic behavior in accord with the periodic replenishment rate.

5.5.2.2 Time-varying magma area

Second, we show the simulation results for the case of the time-varying magma chamber area. Figure 5.13 shows the total heat outputs with different sets of initial and input Di compositions at the constant replenishment rate of 10^{-8} m/s. In this simulation, we choose the same parameters as in section 5.5.2.1. Similar to the variation of heat flux in the case in which the chamber thickness grows, the initial composition C_0 determines the initial total heat output, and the composition C_{in} of the added magma dominates the heat flux decay rate of the magma chamber in the presence of cooling and replenishment. Although the replenishment velocities needed to maintain stable heat output for time-varying thickness and area models are similar, the volumetric rate of magma replenishment are different in the area-growth model than that in the thickness-growth model.

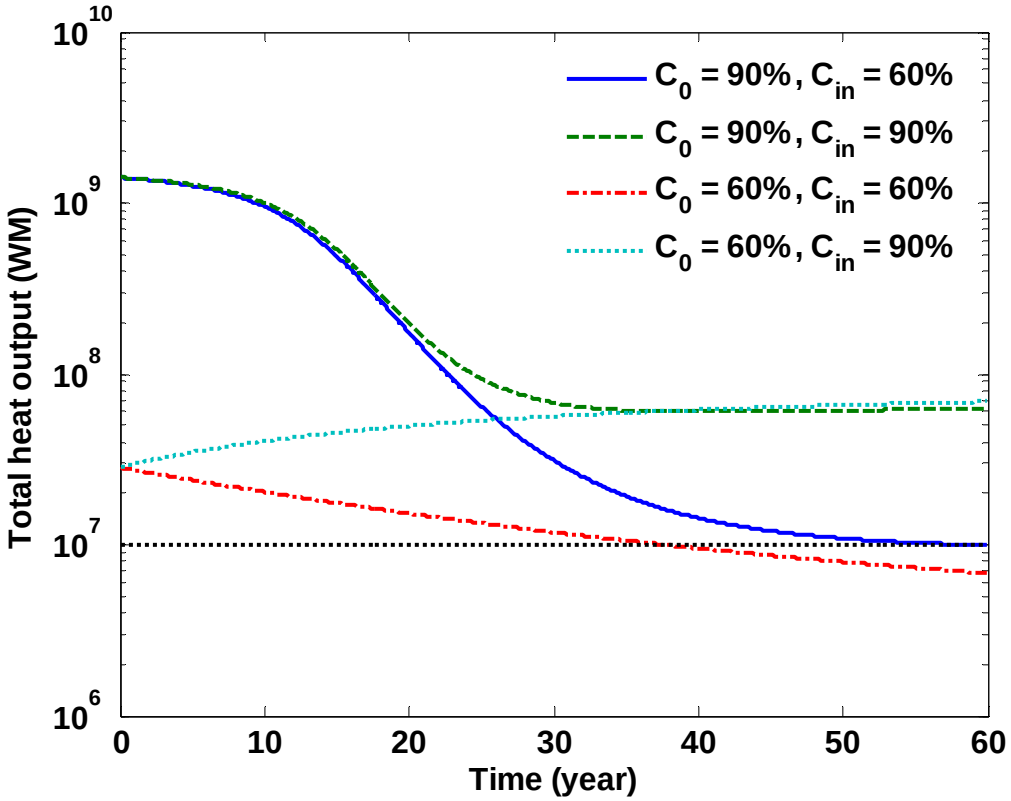

Figure 5.13 Total heat output as a function of time for different initial and input compositions with magma replenishment at 10^{-8} m/s. The thickness of magma chamber is fixed and the area of magma grows during magma replenishment.

Based on equations (35), (36), and (49), the volumetric rates of magma replenishment are obtained as

$$\frac{dV_{in}(t)}{dt} = A_{m0}\frac{dD_{in}}{dt} = A_{m0}u(t) \tag{57}$$

$$\frac{dV_{in}(t)}{dt} = D_0\frac{dA_{in}(t)}{dt} = A_m(t)u(t) \tag{58}$$

for thickness-growth and area-growth cases, respectively. Comparing equations (57) and (58), we can see that the area-growth case has larger volumetric rate of magma replenishment. Thus, the heat flux decays slightly slower in the area-growth model.

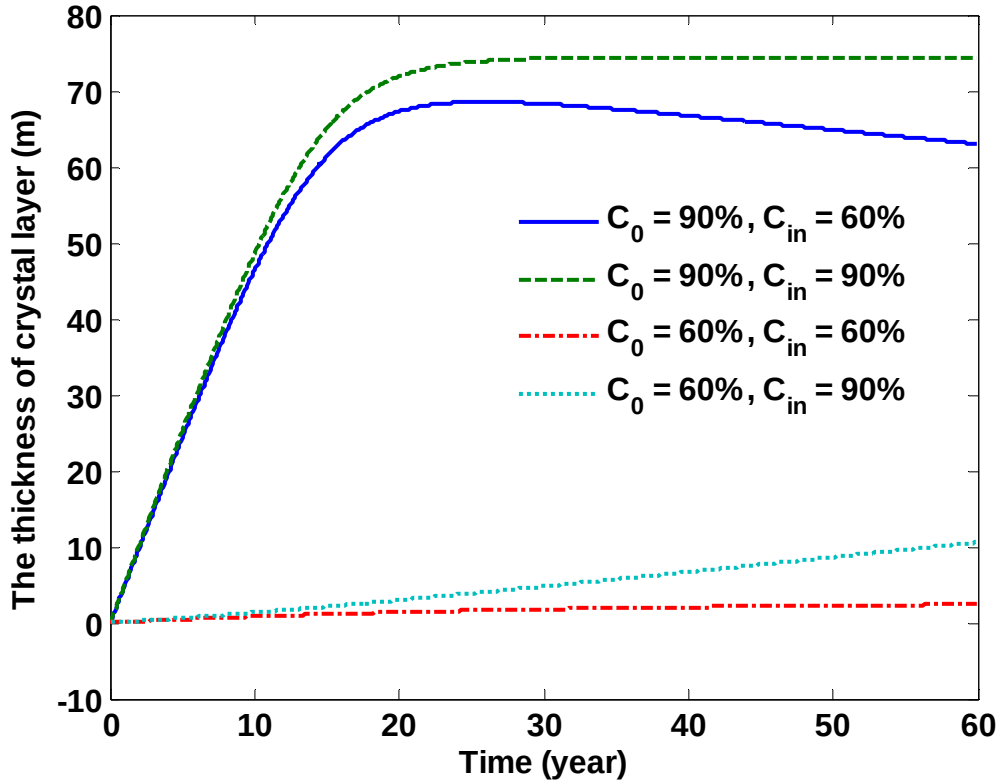

Figure 5.14 The thickness of crystal layer as a function of time for different initial and input compositions with magma replenishment at 10^{-8} m/s. The thickness of magma chamber is fixed and the area of magma grows during magma replenishment.

Figure 5.14 and Figure 5.15 depict the time-varying thickness of the crystal layer and Di composition during the magma chamber evolution, respectively. Similarly to the magma chamber thickness-growth case the crystal thickness grows in two stages that result from the combination effects of both the cooling and replenishment. In the first stage, the system cooling dominates the magma evolution. Thus, the thickness of the crystal layer has the sharp initial growth rate due to the crystallization. In the second stage, the magma cooling weakens and the magma replenishment becomes the dominant process. Different from the magma chamber thickness growth case, the crystal growth in the second stage exhibits different patterns, e.g., the growth in the thickness of the crystal

layer is not observable for the case with C_0 = 60% and C_{in} = 60%, and the thickness of the crystal layer even decreases for the case C_0 = 60% and C_{in} = 90%. This result occurs because as the volume of the crystals accumulates, the crystallization occurs over an increasing area. Figure 5.15 demonstrates the evolution of Di composition. The Di content with greater initial Di content (90%) has greater decay rate at the beginning due to the dominant cooling in the magma chamber. In addition, the steady-state Di composition is determined by the Di content of the added magma since after the original magma crystallizes, the added magma is the dominant crystal source.

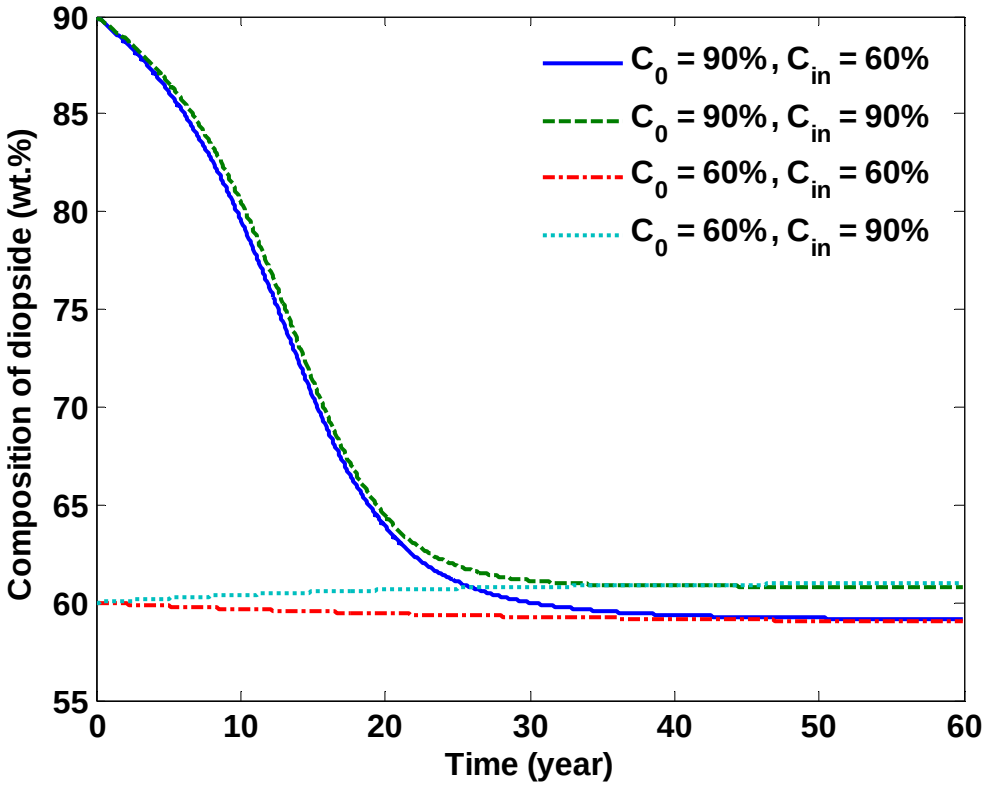

Figure 5.15 The composition of diopside as a function of time for different initial and input compositions with magma replenishment at 10^{-8} m/s. The thickness of magma chamber is fixed and the area of magma grows during magma replenishment.

5.6 Discussion

5.6.1 Rayleigh Number

The vigor of convection in a magma chamber can be expressed by the Rayleigh number *Ra*, which is a dimensionless parameter defined as

$$Ra = \frac{\alpha_m g D_0^{\,3} \Delta T}{a_m \nu_m} \tag{59}$$

where $\Delta T = T_m\,(t)\text{-}T_e$ is the difference between the average temperature of the convecting magma $T_m(t)$ and the eutectic temperature T_e and other parameters have been defined previously. The larger the Rayleigh number, the more vigorous the convection and the greater the convective heat transfer from the magma chamber. The Rayleigh number will decrease as crystallization proceeds, as a result of the combined effects of the increasing viscosity, decreasing temperature and decreasing chamber size. Thus, the heat output results described in previous sections can be understood by plotting the evolution of the Rayleigh number with time as crystallization and cooling proceeds for different initial compositions. The temporal evolution of *Ra* as a function of initial Di composition C_0 is depicted in Figure 5.16. The initial value of C_0 has a significant effect on the evolution of the Rayleigh number. Magmas with larger C_0 have a larger initial value of Rayleigh number. Small differences in C_0 (only a few tenths of mole) give rise to large differences in the initial value of *Ra*. Thus, because of the initially rapid rate of heat transfer from magma with higher C_0, these magmas exhibit a more rapid decay rate of *Ra*, and correspondingly the higher the initial value of C_0, the shorter convective life time before the temperature approaches eutectic temperature. The Rayleigh number decreases rapidly due to the vigorous convection at the beginning. Then, magma temperature and Rayleigh

number R_a drop very slowly as the magma system approaches the eutectic temperature T_e. When R_a drops below the critical value, magma convection stops. In this paper, we do not consider the situation when the magma temperature reaches at the eutectic temperature because the Raleigh number based on ΔT will be zero at this point. [*Worster et al.*, 1990] showed that anorthite begin crystallizing in addition to the diopside crystals already formed once magma temperature approaches the eutectic value. While the interior magma temperature remains fixed, the increased crystallization release appropriate latent heat maintain slight convection. The Rayleigh number decreases progressively and drop sharply to zero (fig6(c) in *Worster et al.* [1990].

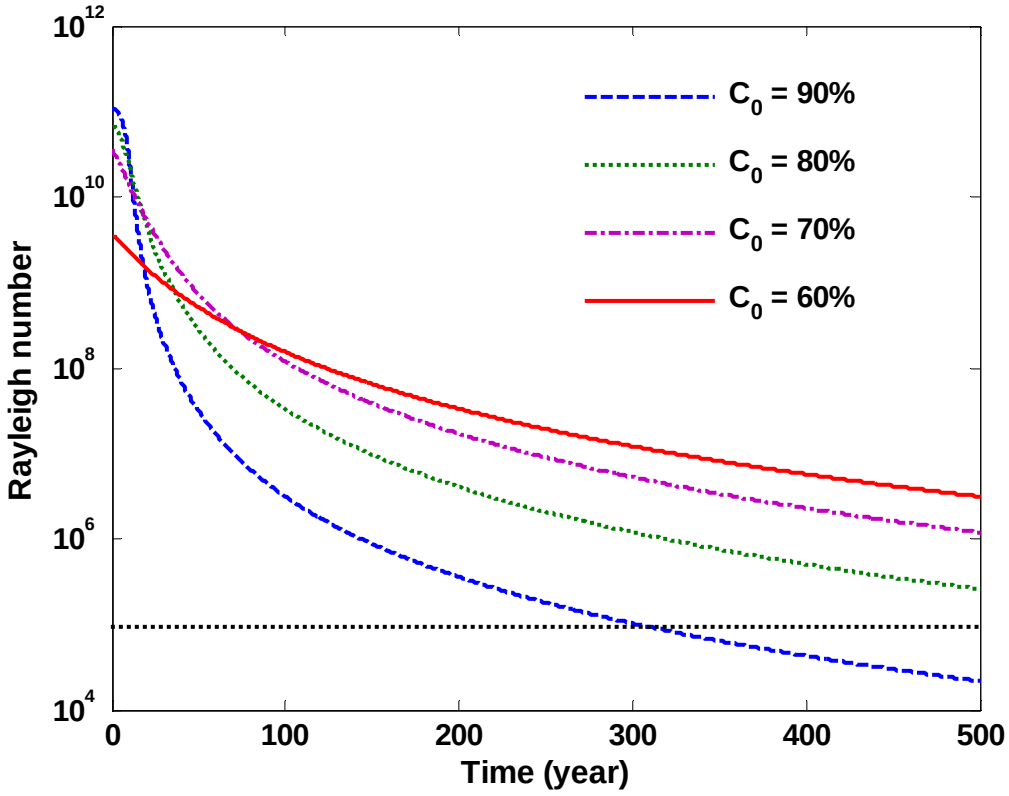

Figure 5.16 Raleigh number as a function of time for different initial diopside compositions. The horizontal dash line located at Raleigh number at 10^5 denotes the convection in magma chamber effectively stops.

5.6.2 Magma temperature

Hydrothermal venting has shown remarkable stability in both composition and temperature at least on a decadal-scale [*Bowers et al.*, 1988; *Campbell et al.*, 1988; *Von Damm et al.*, 2002]. The analysis in [*Liu and Lowell*, 2009] suggests that the magma replenishment rate plays an important role in the maintaining the heat flux and extending magma convective lifetime for a one-component magma system, and is also confirmed in this paper for two-component magmas. However, seismicity studies and observed changes in the temperature and chemistry of some hydrothermal vents [*Sohn et al.*, 1998, *Baker et al.*, 1999; *Scheirer et al.*, 2006; *Tolstoy et al.*, 2008] indicate the evidence of the interruption of the steady state of the hydrothermal venting due to magmatic activity. For example, magmatic eruptions on the East Pacific Rise near 9°50'N in 1991 and 1992 [*Haymon et al.*, 1993], again in 2005/2006 [*Soule et al.*, 2007], and some non-eruptive magmatic events [*Ramondenc et al*., 2008; *Germanovich et al.*, 2010] have disturbed the hydrothermal system.

To show the fluctuation of magmatic activity, we model magma replenishment with period of 10 years. We consider the magma chamber thickness growth case and the initial Di composition is set to be 90 wt.%. Figure 5.17 shows the magma temperature with different replenished Di composition, i.e, C_{in} = 60%, 75%, 90%. It is seen that the period replenishment results in the fluctuation of the characteristics of magma temperature. The evolution of magma temperature varies depending upon the composition of replenished magmas. The higher replenished Di composition gives rise to larger fluctuations, because the richer crystal content generates stronger cooling and makes it difficult to cooling and replenishment. More significantly, when the composition

of the added magma is close to the eutectic, most of the chamber has a near-eutectic composition magma temperature exhibits insignificant fluctuations. The magma temperature shows greater fluctuations for primary magmas (high-Di) than evolved magmas (low-Di).

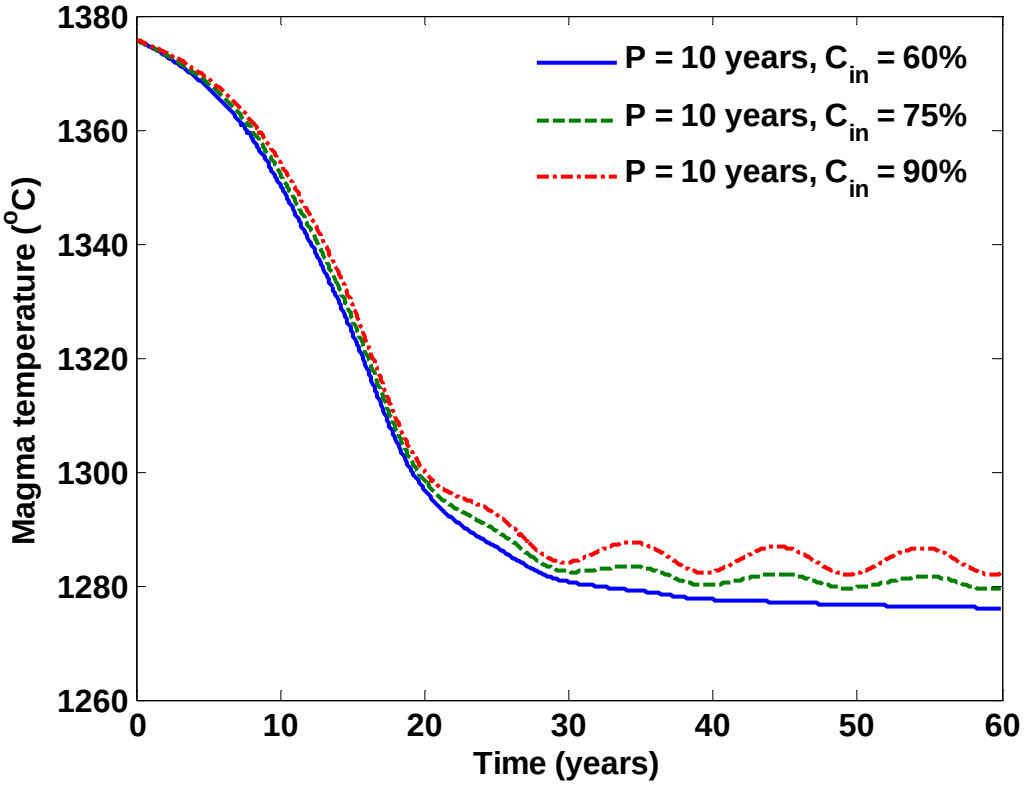

Figure 5.17 The magma temperature as a function of time with different input Di compositions with the same magma replenishment period of 10 years at a constant rate 10^{-8} m/s. Results show that the period replenishment results in the fluctuation of the characteristics of magma temperature. The higher initial Di composition gives rise to the larger fluctuation of magma temperature.

Figure 5.18 depicts the corresponding evolution of diopside concentrations in the magma chamber. Its variation is consistent to the magma temperature, which is described

by equation (2). The Di composition drops rapidly at early years for magma replenishment due to the stronger cooling and crystallization. Then, it stabilizes as magma replenishment stabilizes the heat output. The periodic fluctuations of composition are due to the periodic magma replenishment and are more significant for the magma replenishment with higher Di composition.

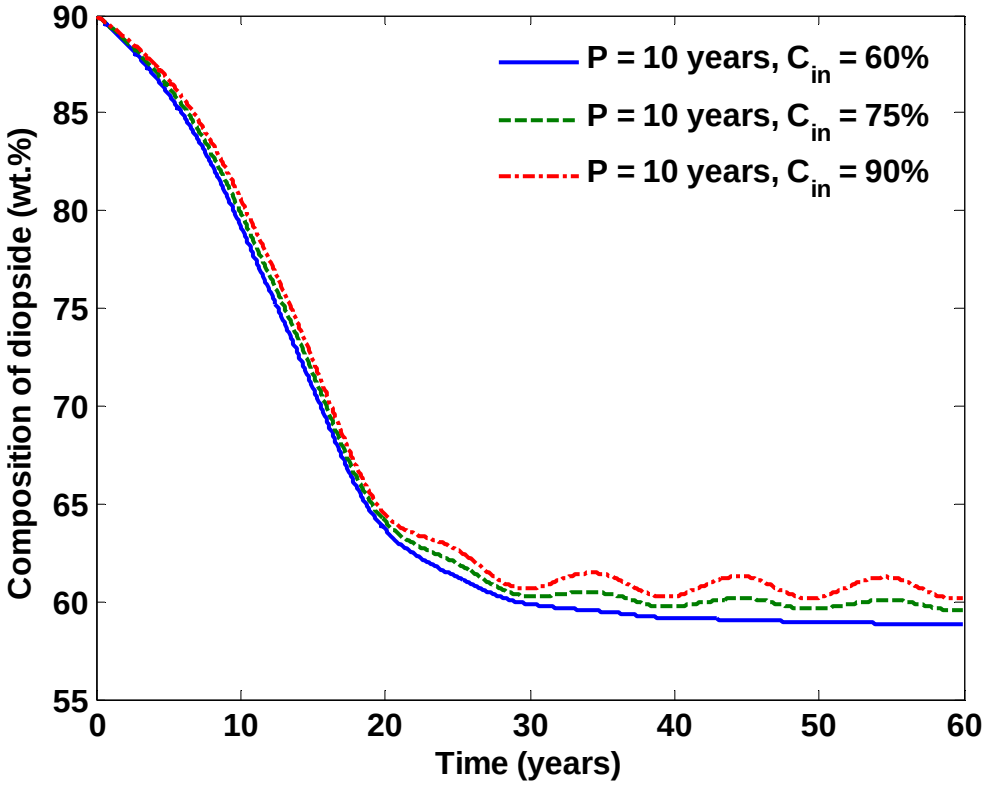

Figure 5.18 The composition of diopside as a function of time with different input Di compositions with the same magma replenishment period of 10 years at a constant rate 10^{-8} m/s. Results show that the periodic fluctuations of composition are due to the periodic magma replenishment and are more significant for the magma replenishment with higher Di composition.

With episodic magma replenishment rates, magma temperature remains relatively unchanged except for oscillations related to the frequency of replenishment. Hydrothermal responses resulting from periodic changes in magmatic supply might not be observed in the seafloor vents because of two factors related to time delay: the time for heat to be conducted through the thin boundary layers at the top of the magma chamber and at the base of the hydrothermal system (see more details in Chapter 6).

At the EPR at 9°50′ N, lava chemistry suggests both magma cooling and replenishment between the eruption episodes of 1991/1992 and 2005/2006 [*Goss et al.*, 2010]. The models shown here for Di-An analogues of basaltic magma with cooling and replenishment show secular cooling with slight temperature fluctuations that might result from periodic replenishment on a decadal time scale. Although periodic replenishment with more primitive (i.e., higher Di) magmas give rise to greater thermal fluctuations than replenishment with more evolved magmas, the results shown here do not allow us to speculate on whether replenishment with more or less primitive magma might be representative of the magma replenishment patterns at EPR.

5.7 Conclusion

This paper investigates convective heat output for a two-component Di-An, crystallizing, replenished magma sill as an analogue to basaltic AMCs at oceanic spreading centers. In un-replenished magma chambers in which crystals are assumed to settle quickly to the floor, the results show that the higher initial Di concentration results in higher initial heat output and faster decay rate of heat output, leading to correspondingly shorter lifetimes of magma convection, based on a heat output cut-off of 10^7 Watts for the hydrothermal system.

With magma replenishment, simulations with magma replenishment at a velocity of ~ 10^{-8} m/s stabilize heat output at a value greater than the cut-off cutoff of 10^7 Watts for decadal time scales. The stabilized heat output varies depending on both the Di concentration and the initial magma chamber thickness. Numerical simulations of convection and crystallization in a ~ 100 m thick sill show that a 90% Di content of added magma maintains a stable heat output of ~ 4 x 10^7 Watts whereas replenishment with 60% Di magma has a heat output ~ 1 x 10^7 Watts. In a thinner sill of ~ 10 m the initially high convective heat loss results in faster decay and a lower stable value of heat flux. Simulations with the periodic replenishment give rise to magma temperature fluctuations that increase as the Di concentration of the added magma increases. Whether this model can be used to discern episodic events at EPR over an eruption cycle requires further investigation.

Table 5.2 Values of the physical parameters for Di-An System

Physical meaning	Parameter	Value	Units
Thermal diffusivity of magma	a_m	8×10^{-7}	m^2/s
Horizontal magma area in chamber	A_m	10^6	m^2
Magma specific heat	c_m	1400	J/kg ºC
Diopside concentration	C		
Eutectic concentration	C_e	58%	
Di concentration of the added magma	C_{in}	variable	
The total thickness of magma chamber	D		
The initial thickness of magma chamber	D_0	100	m
The thickness of added magma	D_{in}		
The thickness of liquid magma	D_m		
The thickness of crystals layer	D_s		
Magmatic heat flux	F_m		W/m^2
Magma replenishment heat flux	F_r		W/m^2
Acceleration due to gravity	g	9.81	m/s^2
Latent heat of solid anorthite	L_{an}	3.9×10^5	J/kg
Latent heat of solid diopside	L_{di}	6.6×10^5	J/kg
Mass of magma	M		kg
Rayleigh number	Ra		-
Anothrite liquidus temperature	T_{anL}	1553	ºC
Diopside liquidus temperature	T_{diL}	1391	ºC
Eutectic temperature	T_e	1275	ºC
The temperature of replenished magma	T_{in}		ºC
Replenishment rate	u		m/s
Initial replenishment rate	u_0		m/s
Magma replenishment frequency	w		$year^{-1}$
Thermal expansion coefficient	α_m	5×10^{-5}	$ºC^{-1}$
Density of magma	ρ_m	2.7×10^3	kg/m^3
Magma kinematic viscosity	v_m	variable	m^2/s
Volume fraction of crystals	χ		-
The crystal content of input magma	χ_{in}		-
The ratio of magma volumes	ϕ		-

5.8 References

Baker, E.T. (2007). Hydrothermal cooling of midocean ridge axes; do measured and modeled heat fluxes agree? *Earth Planet. Sci. Lett.*, *263*, 140-150.

Baker, E.T., R.A. Feely, M.J. Mottl, F.J. Sansone, C.G. Wheat, J.A. Resing, and J.E. Lupton (1994). Hydrothermal plumes along the East Pacific Rise, 8°40 to 11°50N: Plume distribution and relationship to the apparent magmatic budget, *Earth Planet. Sci. Lett., 128*, 1–17

Baker, E.T., C.G. Fox, and J.P. Cowen (1999). In situ observations of the onset of hydrothermal discharge during the 1998 submarine eruption of Axial Volcano, Juan de Fuca Ridge, *Geophys. Res. Lett.*, *26*, no. 23, pp.3445-3448

Bottinga Y. and D.F. Weill (1970). Densities of liquid silicate systems calculated from partial molar volumes of oxide components. *Am. J. Sci.*, *269*: 169-182.

Bottinga Y. and D. Weill (1972). The viscosity of magmatic silicate liquids: a model for calculation. *Am. J. Sci.*, *272*, 438–475.

Bowen, N.L. (1915). The crystallization of Haplobasaltic, Haplodioritic and related magmas, *Amer. J. Sci. 40*, p. 161-185.

Bowen, N.L. and J.F. Schairer (1935). The system MgO-FeO-SiO_2. *Am. J. Sci. 29*:151-217

Bowers, T.S., A.C. Campbell, C.I. Measures, A.J. Spivack, M. Khadem, and J.M. Edmond (1988). Chemical controls on the composition of vent fluids at 13°-11°N and 21°N, East Pacific Rise, *J. Geophys. Res., 93*, 4522-4536.

Bradley, R.S. (1962). Thermodynamic calculations on phase equilibria involving fused slats. Part II: Solid solutions and applications to the olivines. *Am. J. Sci. 260*:550-554

Brandeis, G. and C. Jaupart (1986). On the interaction between convection and crystallization in cooling magma chambers. *Earth Planet. Sci. Lett. 77*: 345-61

Campbell, A.C., T.S. Bowers, C.I. Measures, K.K. Falkner, M. Khadem, and E.M. Edmond (1988). A time series of vent fluid composition from 21°N, East Pacific Rise (1979, 1981, 1985) and the Guaymas Basin, Gulf of California (1982, 1985), *J. Geophys. Res., 93*, 4537-4550.

Canales, J.P., S.C. Singh, R.S. Detrick, S.M. Carbotte, A. Harding, G.M. Kent, J.B. Diebold, J. Babcock, and M.R. Nedimovic (2006). Seismic evidence for variations in axial magma chamber properties along the southern Juan de Fuca Ridge, *Earth. Planet. Sci. Lett.*, *246*, 353-366.

Cann, J.R. and M.R. Strens (1982). Black smokers fuelled by freezing magma, *Nature*, *298*, 147-149.

Carslaw, H.S. and J.C Jaeger (1959). *Conduction of heat in solids*. Oxford, Clarendon Press

Cukierman, M. and D.R. Uhlmann (1973). Viscosity of Liquid Anorthite, *J. Geophys. Res.*, *78*, no.23, pp.4920-4923

Dingwell, D.B. (2006). Transport properties of magmas: Diffusion and rheology. *Elements*, *2*, no. 5, pp.281-286.

Elderfield, H. and A. Schultz (1996). Mid-ocean ridge hydrothermal fluxes and the chemical composition of the ocean. *Annual Review of Earth and Planetary Sciences*, *24*, pp.191-224, 1996

Embley, R.W, W.W. Chadwick, Jr., I.R. Jonasson, D.A. Butterfield, and E.T. Baker (1995). Initial results of the rapid response to the 1993 CoAxial event: relationships between hydrothermal and volcanic process, *Geophys. Res. Lett*., *22*, 143-146.

Fornari, D.J. and R.W. Embley (1995), in Seafloor Hydrothermal Systems, Physical, Chemical, Biological, and Geological Interactions, eds Humphris, S.E., R.A. Zierenberg, S. Mullineaux, and R.E. Thomson, Monograph *91*,1-26, AGU Washington DC.

Fouquet, Y., U. Von Stackelberg, J.L. Charlou, J.P. Donval, J. Erzinger, J.P. Foucher, P. Herzig, R.K. Muehe, S. Soakai, M. Wiedicke, and H. Whitechurch (1991), Hydrothermal activity and metallogenesis in the Lau back-arc basin, *Nature*, *349*, 778-781.

Germanovich, L.N., R.P. Lowell, and P. Ramondenc, (2010). Hydrothermal response to the earthquake swarm at 9°50 N, East Pacific Rise: Magmatic origin and constraints from heat flow and geochemical data, *J. Geophys Res.* (in press).

Giordano, D., A. Mangicapra, M. Potuzak, J.K. Russell, C. Romano, D.B. Dingwell, and A. Di Muro, (2006). An expanded non-Arrhenian model for silicate melt viscosity: A treatment for metaluminous, peraluminous and peralkaline liquids. *Chem. Geol*., 229, 42–56.

Giordano, D., M. Potuzak, C. Romano, D.B. Dingwell, and M. Nowak (2008). Viscosity and glass transition temperature of hydrous melts in the system $CaAl_2Si_2O_8$-$CaMgSi_2O_6$, *Chem. Geol*., *256*, no. 3-4, pp.203-215, 15

Goss, A.R., M.R. Perfit, W.I. Ridley, K.H. Rubin, G.D. Kamenov, S.A. Soule, A. Fundis, and D.J. Fornari (2010). Geochemistry of lavas from the 2005–2006 eruption at the East Pacific Rise, 9°46′N–9°56′N: Implications for ridge crest plumbing and decadal changes in magma chamber compositions, *Geochem. Geophys. Geosyst.*, 11, Q05T09, doi:10.1029/2009GC002977.

Hannington, M.D., C.E.J. de Ronde, and S. Petersen. (2005). Sea-floor tectonics and submarine hydrothermal systems. Pp. 111–141 in 100th *Anniversary Volume of Economic Geology*. J. Hedenquist et al., eds, Society of Economic Geologists, Littleton, Colorado.

Haymon, R.M. (1996). The response of ridge-crest hydrothermal systems to segmented, episodic magma supply, *Geological Society Special Publication*, *118*, 157-168.

Haymon, R.M. and M. Kastner. (1981). Hot spring deposits on the East Pacific Rise at 21°N: Preliminary description of mineralogy and genesis. *Earth and Planetary Science Letters*. *53*:363–381.

Haymon, R.M. and S.M. White, (2004). Fine scale segmentation of volcanic-hydrothermal systems along fast-spreading ridge crests, *Earth Planet. Sci.Lett.*, *226*, no.3-4, pp.367-382

Haymon, R.M., D.J. Fornari, M.H. Edwards, S.M. Carbotte, D. Wright, and K.C. MacDonald (1991). Hydrothermal vent distribution along the East Pacific Rise crest (9°09'–54'N) and its relationship to magmatic and tectonic processes on fast-spreading mid-ocean ridges, *Earth. Planet. Sci. Lett.*, vol.104, no.2-4, pp.513-534

Haymon, R.M., D.J. Fornari, K.L. Von Damm, M.D. Lilley, M.R. Perfit, J.M. Edmond, W.C. Shanks, R.A. Lutz, J.M. Grebmeier, S. Carbotte, D. Wright, E. McLaughlin, M. Smith, N. Beedle, and E. Olson, (1993). Volcanic eruption of the mid-ocean ridge along the East Pacific Rise crest at 9°45–52'N: Direct submersible observations of seafloor phenomena associated with an eruption event in April, 1991, *Earth Planet. Sci.Lett.*, *119*, 85–101.

Hort, M., B.D. Marsh, R.G. Resmini, and M.K. Smith (1999). Convection of crystallization in a liquid cooled from above; an experimental and theoretical study, *J. Petrol.*, *40*, no.8, pp.1271-1300

Hui, H. and Y. Zhang, (2007). Toward a general viscosity equation for natural anhydrous and hydrous silicate melts. *Geochim. Cosmochim. Acta*. *71*, 403–416.

Huppert, H.E. and Sparks, R.S.J. (1988). The generation of granitic magmas by intrusion of basalt into continental crust. *J. Petrol.*, *29*, 599–642.

Huppert, H.E., M.G. Worster (1991). Vigorous motions in magma chambers and lava lakes, The IMA Volumes in *Mathematics and its Applications*, vol.41, pp.141-173

Jellinek, A.M., R.C. Kerr, and R.W. Griffiths (1999). Mixing and compositional stratification produced by natural convection: 1. Experiments and their applications to Earth's core and mantle. *J. Geophys. Res. 104*:7183- 7201

Kerr, R.C., A.W. Woods, M.G. Worster, and H. E. Huppert, (1990). Solidification of an alloy cooled from above: Part 1. Equilibrium growth, *J. Fluid Mech*, vol. 216, pp. 323-342

Kerr, R.C., A.W. Woods, M.G. Worster, and H. E. Huppert, (1990). Solidification of an alloy cooled from above: Part 2. Non-equilibrium interfacial kinetics, *J. Fluid Mech*, vol. 217 : 331-348

Kerr, R.C., A.W. Woods, M.G. Worster, and H. E. Huppert, (1990). Solidification of an alloy cooled from above. Part 3. Compositional stratification within the solid, *J. Fluid Mech*, vol. 218, pp. 337-354

Kent, G.M., A.J. Harding, and J.A. Orcutt (1990). Evidence for a smaller magma chamber beneath the East Pacific Rise at 9º30´N, *Nature*, *344*, 650-652.

Knoche, R., D.B. Dingwell, and S.L. Webb, (1992). Temperature-dependent thermal expansivities of silicate melts; the system anorthite-diopside, *Geochimica et Cosmochimica Acta*, vol.56, no.2, pp.689-699

Koyaguchi, T. and K. Kaneko (1999). A two-stage thermal evolution model of magmas in continental crust, *J. Petrol.*, *4*0, no.2, pp.241-254

Kushiro, I. (1973). The system diopside-anorthite-albite: determination of compositions of coexisting phases, *Carnegie Inst. Washington Year Book 72*, pp. 502–507.

Lister, J.R. (1990). Buoyancy-driven fluid fracture: the effects of material toughness and of low-viscosity precursors, *J. Fluid Mech.*, *210*, 263–280.

Lister, J.R. and R.C. Kerr (1991). Fluid-mechanical models of crack propagation and their application to magma transport in dikes, *J. Geophys. Res.*, *96*, 10,049–10,077.

Liu, L. and P.R. Lowell (2009). Models of hydrothermal heat output from a convecting, crystallizing, replenished magma chamber beneath an oceanic spreading center, *J. Geophys. Res.*, *114*, B02102, doi:10.1029/2008JB005846.

Lowell, R.P. (1985). Double-diffusive convection in partially molten silicate systems: Its role during magma production and in magma chambers, *Journal of Volcanology and Geothermal Research*, Volume 26, Issues 1-2, October 1985, Pages 1-24

Lowell, R.P. and P.A. Rona (1985). Hydrothermal models for the generation of massive sulfide ore deposits, *J. Geophys. Res.*, *90*, 8769-8783.

Lowell, R.P. (2010). Hydrothermal circulation at slow spreading ridges: analysis of heat sources and heat transfer processes, in *Diversity of Hydrothermal Systems on Slow Spreading Ocean Ridges*. *Geophysical Monograph Series 188*, AGU

Maaloe S. (1984). Fractional crystallization and melting within binary systems with solid solution, *Am. J. sci.*, *284*. 272-287

Maclennan, J. (2008). Concurrent mixing and cooling of melts under Iceland. *J. Petrol.* 49, pp.1930-1953.

Marsh, B.D. (1989). Magma chambers. *Annual Review of Earth and Planetary Sciences* 17, 439–474.

Martin, D., R.W. Griffiths, and I.H. Campbell (1987). Composition and thermal convection in magma chambers. *Contrib. Mineral. Petrol. 96*, 465-4

McBirney, A.R. and R.M. Noyes (1979). Crystallization and layering of the Skaergaard intrusion. *J. Petrol. 20*, 487-554.

McKenzie, D. (1984). The generation and compaction of partially molten rock. *J. Petrol. 25*, 713-765.

McKenzie, D. (1985). The extraction of magma from the crust and mantle. *Earth. Planet. Sci. Lett.* 74, 81-91.

Morey, G.W. and C.N. Fenner (1917). The ternary system H_2O-K_2SiO_3-SiO_2. *Journal of the American Chemical Society*, 39, 1173–1229.

Navrotsky A., D. Ziegler, R. Oestrike and P. Maniar, (1989). Calorimetry of silicate melts at 1773 K: measurement of enthalpies of fusion and mixing in the systems diopside-anorthite-albite and anorthite-forsterite, *Contrib. Mineral. Petrol. 101*, pp. 122–130.

Nilson, R.H. and M.R. Baer (1982). Double-diffusive counterbuoyant boundary layer in laminar natural convection. *Int. J. Heat Mass Transfer*, *25*: 285--287.

Osborn, E.F., and D.B. Tait (1952). The system diopside-forsterite-anorthite. *Am. J. Sci.*, 250A, 413-433.

Petrakis, D., M.C. Flemings, and D. R. Poirier (1981). *Modeling of Casting and Welding Processes* (edited by Brody, H.D. and D. Arpetian), The Metallurgical Society of American Institute of Mining, Metallurgical and Petroleum Engineering, Warrendale, PA, pp. 313-332.

Richard G. (1922). *a dictionary of applied physics*, London, Macmillan.

Rigden, S.M., T.J. Ahrens, and E.M. Stolper (1988). Shock compression of molten silicate - results for a model basaltic composition. *J. Geophys. Res.,* 93(B1): p. 367-382.

Ramondenc, P., L.N. Germanovich, and R.P. Lowell (2008). Modeling Hydrothermal Response to Earthquakes at Oceanic Spreading Centers, *Geophys. Monogr. Ser., 178*, American Geophys. Union, Washington, DC.

Russell, J.K. and D. Giordano (2005). A model for silicate melt viscosity in the System $CaMgSi_2O_6$–$CaAl_2Si_2O_8$–$NaAlSi_3O_8$. *Geochim. Cosmochim. Acta* 69, 5333–5349.

Scarfe, C.M., D.J. Cronin, J.T. Wenzel, and D.A. Kauffman (1983). Viscosity-temperature relationships at 1 atm in the system diopside-anorthite, *American Mineralogist*, vol.68, no.11-12, pp.1083-1088

Schairer J.F. and H.S. Yoder Jr., (1960). The nature of residual liquids from crystallization, with data on the system nepheline-diopside-silica, *Am. J. Sci.*, *258A*, pp. 273–283.

Scheirer, D.S., T.M. Shank, and D.J. Fornari (2006). Temperature variations at diffuse and focused flow hydrothermal vent sites along the northern East Pacific Rise, *Geochem. Geophys. Geosys* 7:1–23.

Scheil, E. (1942). Retrograde saturation curves, *Z. Metallk, 34*, p.70.

Shaw, H.R. (1965). Comments on viscosity, crystal settling, and convection in granitic magmas. *Am. J. Sci.*, 263, 120–152.

Shaw, H.R. (1972). Viscosities of magmatic silicate liquids: An empirical model of prediction. *Am. J. Sci.*, 272, 438–475.

Shaw, H.R. (1980). The fracture mechanisms of magma transport from the mantle to the surface, in *Physics of Magmatic Processes*, edited by R.B. Hargraves, pp. 201– 264, Princeton Univ. Press, Princeton, N. J..

Singh, S.C., J.S. Collier, A.J. Harding, G.M. Kent, and J.A. Orcutt (1999). Seismic evidence for a hydrothermal layer above the solid roof of the axial magma chamber at the southern East Pacific Rise, *Geology*, *27*, 219-222.

Singh, S.C., W.C. Crawford, H. Carton, T. Seher, V. Combier, M. Cannat, J.P. Canales, D. Dusunur, J. Escartin, and J. M. Miranda (2006). Discovery of a magma chamber and faults beneath a Mid-Atlantic Ridge hydrothermal field, *Nature*, *442*, 1029-1032.

Sinha, M.C. (1995). Segmentation and rift propagation at the Valu Fa Ridge, Lau Basin; evidence from gravity data, *J. Geophys. Res.*, vol. 100, no. B8, pp.15,025-15,043

Sohn, R., D.J. Fornari, K. Von Damm, S.Webb, and J. Hildebrand (1998). Seismic and hydrothermal evidence for a propagating cracking event on the East Pacific Rise crest at 9°50'N, *Nature*, *396*, 159–161.

Soule, S.A., D.J. Fornari, M.R.Perfit, and K.H. Rubin, (2007). New insights into mid-ocean ridge volcanic processes from the 2005-2006 eruption of the East Pacific Rise, 9°46'N-9°56'N, *Geology*, vol. 35, no. 12, pp.1079-1082

Sparks, R.S.J., H.E. Huppert, J.S. Turner (1984). The fluid dynamics of evolving magma chambers, Philosophical Transactions of the Royal Society of London, Series A: *Mathematical and Physical Sciences*, vol.310, no.1514, pp.511-534

Sparks R.S.J. and W.P. Aspinall (2004). Volcanic activity: Frontiers and challenges in forecasting, prediction and risk assessment. State Planet.: *Front. Challenges Geophys*. 150, 359–373.

Sparks, R.S.J. (2004). Dynamics of magma degassing. Volcanic degassing. *Geol. Soc. Lond.* Spec. Pub. 213, 5–22

Spera, F. J. (1979). Thermal evolution of plutons: a parameterized approach. *Science, 297*, 299–301.

Tolstoy, M., Waldhauser, F., Bohnenstiehl, D.R., Weekly, R.T., and Kim, W.Y., (2008). Seismic identification of along-axis hydrothermal flow on the East Pacific Rise, *Nature* 451, pp.181-184

Turner, J. S. and I. H. Campbell, (1986). Convection and mixing in magma chambers. *Earth Sci. Rev.* 23, 255-352.

Turner, J. S., H. E. Huppert, and R. S. J. Sparks (1986). Komatiites II: Experimental and theoretical investigation of post-emplacement cooling and crystallization. *J. Petrol.*, 27, 397-437.

Turner, I. M., C. Peirce, M. C. Sinha (1999). Seismic imaging of the axial region of the Valu Fa Ridge, Lau Basin; the accretionary processes of an intermediate back-arc spreading ridge, *Geophysical Journal International*, vol.138, no.2, pp.495-519

Van Ark, E.M., R.S. Detrick, J.P. Canales, S.M. Carbotte, A.J. Harding, G.M. Kent, M.R. Nedimovic, W.S.D. Wilcock, J.B. Diebold, and J.M. Babcock (2007). Seismic structure of the Endeavour Segment, Juan de Fuca Ridge; correlations with seismicity and hydrothermal activity, *J. Geophys. Res.*, *112*, B02401, doi: 10.1029/2005JB004210.

Von Damm, K.L., C.M. Parker, R.M. Gallant, and J.P. Loveless (2002). Chemical evolution of hydrothermal fluids from EPR 21°N: 23 years later in a phase separating world, *EOS Trans.* AGU, 83(47), Fall Meet. Suppl., Abstract V61B-1365

Webb, S. and R. Knoche (1996). The glass-transition, structural relaxation and shear viscosity of silicate melts, *Chemical Geology*, vol.128, no.1-4, pp.165-183

Weill D.F., R. Hon, and A. Navrotsky (1980). The igneous system $CaMgSi_2O_6$-$CaAl_2Si_2O_6$-$NaAlSi_3O_8$: Variations on a classic theme by Bowen. In *Physics of Magmatic Processes* (ed. R. B. Hargraves), pp. 49-92. Princeton Univ. Press.

Wood, B.J., and O.J. Kleppa (1981). Thermochemistry of forsterite–fayalite olivine solid solutions. *Geochim Cosmochim Acta 45*: 529–534

Worster, M.G., H.E. Huppert, R.S.J. Sparks (1990). Convection and crystallization in magma cooled from above, *Earth. Planet. Sci. Lett.*, vol.101, no.1, pp.78-89

Yoder, H.S., Jr., (1976). Generation of basaltic magma: Washington, D.C., *National Academy of Sciences*, 265 p.

CHAPTER 6. MODELING HEAT TRANSFER FROM A CONVECTING, CRYSTALLIZING, REPLENISHED SILICIC MAGMA CHAMBER AT AN OCEANIC SPREADING CENTER[4]

Abstract

Although most hydrothermal systems at oceanic spreading centers are driven by convective heat transport from axial magma chambers of basaltic composition, some are driven by magmas with higher silica composition such as andesite or dacite. The different viscosity of the latter magmas that results from their higher SiO_2 content, lower liquidus and solidus temperatures, and water contents likely affects the rate of heat transport from these magmas, and hence affects the behavior of the overlying hydrothermal system. We construct viscosity models for andesite and dacite melts as a function of temperature and water content and incorporate these expressions into a numerical model of thermal convective heat transport from a high Rayleigh number, well-mixed, crystallizing and replenished magma sill beneath a hydrothermal circulation system. Simulations comparing the time dependent heat flux from basalt, 0.1wt.% andesite, 3wt.% andesite, and 4wt.% dacite, indicate that higher viscosity magmas convect less vigorously, which results in lower heat transport, possibly lower vent temperatures, and in a slower decay rate of the heat flux. Consequently, hydrothermal systems driven by unreplenished high-silica melts tend to have a slightly longer lifetime than those driven by basalts; however,

[4] The material is essentially reproduced from Liu, L. and R.P. Lowell (2010). Modeling heat transfer from a convecting, crystallizing, replenished silicic magma chamber at an oceanic spreading center (to be submitted)

vent temperatures and heat output decay on decadal time scales. ,. As in the basaltic case, magma replenishment at a rate of ~ 10^{-8} – 10^{-7} m/s can maintain relatively stable heat output between ~ 10^{7}-10^{9} Watts and hydrothermal vent temperatures for decades. Such a replenishment rate is not likely to result from buoyancy driven melt transport by porous flow through the lower crust, especially for high-viscosity magmas such as andesite and dacite. Long term stability of hydrothermal systems driven by these magmas requires an alternate means of magma replenishment.

6.1 Introduction

Hydrothermal systems at oceanic spreading centers play an important role in the composition of seawater, the formation of ore deposits, the support of microbial and macrofaunal ecosystems, and even for the development of life on early earth. As our understanding of hydrothermal processes at oceanic spreading centers has advanced over the last 30 years, the substrate composition, permeability of the oceanic crust, and the nature of the underlying heat source have become recognized as important factors influencing fluid-rock interactions [*Hajash and Chandler,* 1981; *Fouquet et al.*, 1993a; *Wetzel and Shock*, 2000], hydrothermal vent chemistry [*Von Damm et al.*, 1985; *Von Damm*, 1995], and the attendant microbial and macrofauna ecosystems [*Tunnicliffe and Fowler*, 1996; *Juniper and Tunnicliffe*, 1997; *Kelley et al*, 2002]. Axial magma chambers have now been found along the fast spreading East Pacific Rise [*Detrick et al.*, 1987; 1993], the intermediate-spreading Valu Fa Ridge [*Collier and Sinha*, 1990] and Juan de Fuca Ridge [*Canales et al.*, 2006; *Van Ark et al.*, 2007], the slow-spreading Mid-Atlantic Ridge [*Singh et al.*, 2006], and the ultraslow-spreading Gakkel ridge in the Arctic Ocean [*Jokat et al.*, 2003] and Southwest Indian Ridge [*Sauter et al.*, 2004] in areas of active hydrothermal venting. Seismic reflection data thus reveals a close spatial association between hydrothermal venting and an underling relatively thin sub-axial magma chamber (AMC) at nearly all the high-temperature vent sites for which seismic imaging experiments exist. It is now generally accepted that the AMC represents the heat source that drives the hydrothermal circulation [e.g., *Kelley et al.*, 2002; *Maclennan*, 2008; *Lowell* et al., 2008, 2010].

Since most vent fields are hosted by basalts, the detailed experimental, theoretical, and field studies have been carried out on the basaltic magma-hosted hydrothermal activity. However, vigorous hydrothermal systems are hosted by a broad range of rock types. For example, the Rainbow vent field and others on the Mid-Atlantic Ridge are hosted by peridotite [*Kelley et al.*, 2001; *Allan and Seyfried*, 2003]. Pacmanus hydrothermal systems are hosted by dacitic volcanoes in the Eastern Manus back-arc basin [*Binns and Scott,* 1993; *Binns*, 2003]. Some vent fields on the Eastern Lau Spreading Center (ELSC) (e.g., Valu Fa Ridge [*Fouquet et al.*, 1993]) and other back arc basins (e.g., Manus Basin) [*Sinton et al.*, 2003] are hosted by andesitic rocks. Moreover, the occurrence of high-silica andesitic and dacitic rocks near the 9°03′ N over-lapper on the East Pacific rise and at other sites along the mid-ocean ridge system is reported in [*Wanless et al.*, 2010].

The characteristics of hydrothermal activity (alteration mineralogy, chemistry of fluid etc.) vary depending on the composition of host rocks. Thus, hydrothermal venting driven by andesite and dacite found in back arc basins is quite different from most mid-ocean ridge vent fields which are hosted within basalts. The Lau Basin is a typical example of an active back-arc basin with active spreading ridges and seamount volcanoes associated with a wide variety of hydrothermal deposits, located between the active Tofua volcanic arc and a remnant Lau ridge (see Figure 6.1).

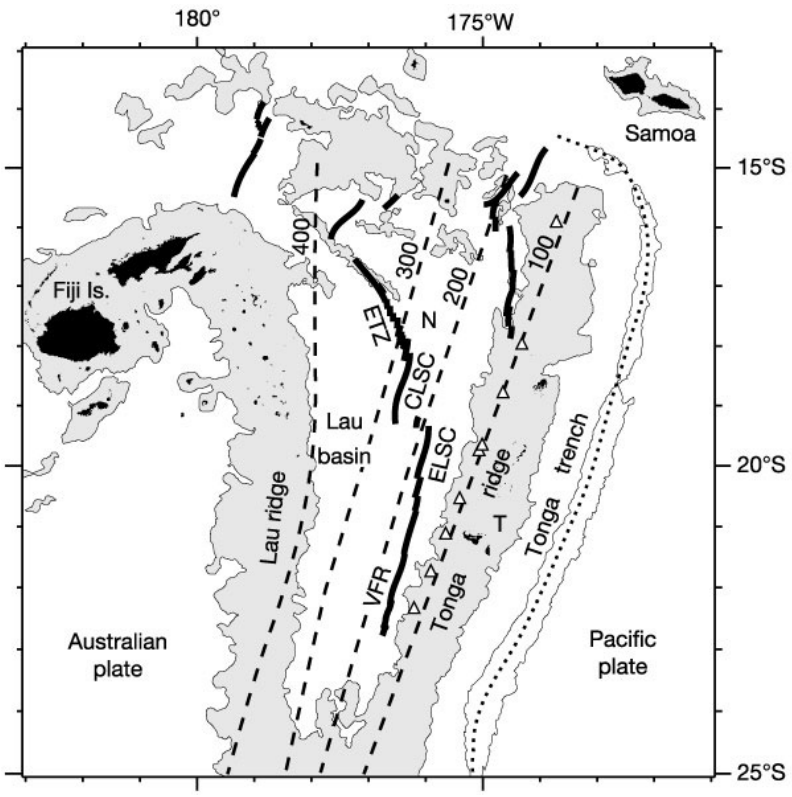

Figure 6.1 Location map of the Lau Basin showing the back-arc spreading centers (heavy lines), trench axis (dotted line) and contours of the subducted slab (dashed lines). [from *Fernando and Taylor*, 2002]

It has been found that andesitic rocks prevail at the southern Lau Basin and the Valu Fa Ridge [*Fouquet et al.*, 1993]. High-temperature hydrothermal fields were discovered and sampled by submersible in the Valu Fa Ridge of the Lau back-arc basin during the *Nautilau* cruise in 1989 [*Fouquet et al.*, 1991]. Their characteristics contrast strongly with those of the hydrothermal fields found at normal mid-ocean ridges, which is mainly composed of basalts. The primary differences between the hydrothermal vents driven by andesites and basalts include the acidity, chemistry and temperature (up to 400 °C) of the hydrothermal fluids, the composition of the ore deposits, and the volcanic and tectonic environments. For example, in some back-arc and arc systems where magma is

more siliceous and richer in H_2O, very-low-PH fluids are observed [*Gamo et al.*, 1997]. Also, it is found that the fluids sampled at vent fields hosted in andesite have very high concentrations of trace metals (e.g., Zn, Cd, Pb, As), and primary gold is present in the accompanying mineral deposits [*Fouquet et al.*, 1993]. Recent detailed exploration of Eastern Lau Spreading Center has discovered a number of other sites (i.e., ABE, Tu'i Malila, and Mariner) hosted on andesite [*Tivey et al.*, 2005; *Lau Workshop Report,* 2006; *Resing et al.*, 2008], and underlain by a magma chamber [*Jacobs et al.* 2007].

The physical and geochemical properties of andesite and other high-silica magmas are different from those of basalt. For example, compared to basaltic magma, high-silica magmas have lower liquidus and solidus temperatures [*Spera*, 2000]. Moreover, high-silica magmas have greater viscosity and lower density due to their higher water and SiO_2 content [*Spera*, 2000]. These features affect the convective properties of the magma and correspondingly influence the magma heat output into the overlaying hydrothermal system.

Since few studies have been conducted regarding the high-silica substrates, an analysis of hydrothermal systems driven by high-silica magma chambers is needed. In this chapter, we investigate high silica andesite and dacite-hosted magma chambers and their effects on the hydrothermal activity. Specifically, both the andesitic and dacitic magma properties are parameterized and the convective heat output and the convective lifetime are quantitatively characterized based on these properties. In addition, we develop numerical models to describe hydrothermal activity that may be associated with the magma system. The rest of the chapter is organized as follows. In section 6.2, we discuss the different physical properties that affect the magma viscosity and propose new

magma viscosity models for both andesite and dacite magmas. In section 6.3, we develop the mathematical models of magmatic heat transfer based on the proposed magma viscosity model. In section 6.4, we extend the results in section 6.3 by considering the magmatic heat flux with magma replenishment. Section 6.5 discusses the evolution of the magma chamber, the temperature of hydrothermal and magma systems, and magma replenishment mechanisms. Section 6.6 concludes the paper.

6.2 Magma Viscosity Modeling

Magma viscosity can vary by many orders of magnitude within a single environment, and it is very sensitive to a variety of factors such as chemical composition [*Liebske*, 2003], temperature [*Bottinga and Weill*, 1972; *Shaw*, 1972], pressure [*Kushiro et al.*, 1976; *Scarfe et al.*, 1987], volatile content (mainly H_2O) [*Richet et al.*, 1995; *Whittington et al.,* 2000], and crystal content [*Marsh*, 1981; *Lejeune and Richet*, 1995]. It has been shown that the viscosity of naturally-occurring silicate melts varies from 10^{-1} Pa s to 10^{14} Pa s in response to changes of magma temperature and melt composition [*Dingwell*, 1996; *Giordano et al.*, 2004; *Giordano et al.*, 2008]. Because the viscosity of magma exerts a fundamental control over many geological processes, including the segregation of melt from source regions, ascent and emplacement of magma, mixing in magma chambers, and eruption styles, magma chambers hosted by different magmas exhibit different rates of convective heat transfer and temporal evolution, and thus affect the overlying hydrothermal system in different ways. In the following, we quantify the effects of each of these factors on the viscosity and propose a new viscosity model for conducting the numerical analysis of magma convection and heat transfer. We incorporate

the dominant factors into the viscosity model and disregard those that have negligible effects.

6.2.1 Pressure

The studies of the viscosity of both anhydrous and hydrous andesitic melts using parallel plate viscometry in [*Liebske*, 2003] combined with the experimental results in [*Richet et al.*, 1996] indicate that the viscosity of water-free andesitic melts are independent of pressure, whereas the viscosity of water-bearing melts slightly increases with the increasing pressure. The results in [*Liebske*, 2003] show that the viscosity increases by up to a factor of 5 for andesitic melts containing H_2O (1-2 wt.%) with increasing pressure from 0.1 to 300 MPa. For more water-rich hydrous andesitic melts (2.3-5.6 wt%), it is found that the viscosity has a minor dependence on pressure ranging from 0.1 to 500 MPa [*Vetere et al.*, 2006]. Thus, we consider the effect of pressure to be minor and neglect its effect on the magma viscosity in our analysis. In addition, the magma chambers being considered here are relatively thin and occur over a small range of pressure. Typically, the estimated ranges are between 53MPa and 110MPa for the magmas below the seafloor about 1-3 km.

6.2.2 Water content

Evidence shows that andesitic and dacitic magmas with high SiO_2 content can have water content as high as 10 wt.%. For example, [*Eggler*, 1972] found that H_2O contents of 2 wt.% - 10 wt.% is in the Paricutin Volcano andesite at the pressure of 1000 MPa. The petrological data from *Rutherford and Devine* [1988] and *Rutherford et al.* [1985] indicate that the Mount St. Helens, Mount Unzen, and Soufriere Hills magmas

have water contents in the range of approximately 4 wt.% - 5 wt.%. The dacites in the eruptions of Mount St. Helens Volcano from 1980 to1986 have a wide range of water contents (3.5 wt.% - 5.7 wt.%) [*Blundy and Cashman*, 2001]. Water content has a significant effect on the high-silica magmas viscosity [*Shaw*, 1963, *Kohn*, 2000; *Giordano et al.*, 2004]. Even a few percent of water may decrease the viscosity of high-silica magmas by several orders of magnitude [*Lejeune et al.,* 1994]. In contrast, the mid-ocean ridge basalts are typically relatively dry with H_2O contents ranging between 0.1 and 0.5 wt.% [*Johnson et al.*, 1994], and the small amount of water in basalts at mid-ocean ridges makes its effect on viscosity small enough to be neglected.

The dependence of viscosity on water content has been investigated through laboratory experiments for different high-silica magmas. Viscosity can be measured directly by experimental techniques. For example, the concentric cylinder viscometer [*Dingwell*, 1986] and the falling sphere technique [*Shaw*, 1963] can be used for the low viscosity range. The micropenetration method [*Hummel and Arndt,* 1985] and parallel plate viscometer [*Liebske*, 2003] can be employed over a high viscosity range. Based on the experimental data, *Vetere* [2006] proposed an empirical model to predict the viscosity of andesitic melts as a function of water content and magma temperature:

$$\log_{10} v_{a0} = \left[-4.86 + \frac{8198}{(T_m - 257)} - \frac{6060}{(T_m - 300)} \times \frac{w}{(w^{1.1673} - 1.1952 + 0.0056 \times T_m)} \right] - \log_{10} \rho_a \qquad (1)$$

where v_{a0} denotes the kinematic viscosity of andesite, w is the water content represented in the form of wt.%, T_m is the magma temperature in °C, ρ_a is the density of andesite (kg/m^3). Similarly, the viscosity of dacite melts is connected to water content and magma temperature in *Whittington* [2009]:

$$\log_{10} v_{d0} = \left[-4.43 + \frac{7618.3 - 17.25\log_{10}(w + 0.26)}{T_m - 679.1 + 292.6\log_{10}(w + 0.26)} \right] - \log_{10} \rho_d \qquad (2)$$

Where v_{d0} *and* ρ_d denote the kinematic viscosity and density of dacite, respectively.

6.2.3 Chemical composition

Equations (1) and (2), show that the viscosity depends not only on water content, but also on magma density and temperature. We will discuss these dependences in this and next subsections. The magma density is determined by its chemical composition, mainly the SiO_2 or silica content. Because silica forms chains that link together and hinder the movement of magma [*Kawaguchi et al.*, 1996], magma viscosity increases with silica content. The silica content in crustal igneous rocks exhibits a considerable range spanning from 45-55 % in basalt to 65-75 % in rhyolite. Typically, andesites have 55-60 % and dacites have 60-65 % SiO_2 contents, respectively. In this chapter, we consider andesite and dacite. Thus, the viscosity is between that of basalt and rhyolite. The effect of Si concentration on the viscosity has been implicitly considered in both equations (1) and (2).

6.2.4 Magma temperature

Viscosity is dependent on magma temperature in two different ways. First, as shown in equations (1) or (2), both *Vetere* [2006] and *Whittington* [2009] have captured the relationship between viscosity and magma temperature T_m. Generally, higher temperature results in lower viscosity based on the historical viscosity-temperature model [e.g., *Vogel*, 1921; *Fulcher*, 1992]. Second, an indirect connection between magma temperature and viscosity exists through their common relation to crystal content. In the

absence of a more precise formulation, we follow [*Hort*, 1997] and assume that the crystal content χ variation is linearly related to magma temperature, i.e.,

$$\chi(T_m(t)) = \frac{T_L - T_m(t)}{T_L - T_s} \tag{3}$$

where T_L and T_s denote the liquidus and solidus temperature, respectively. Note that the two effects of the temperature on viscosity are different. The relation in equations (1) or (2) is static, while the equation (3) captures the relation in a more dynamic way.

6.2.5 Crystal content

During magma convection, magma cools and crystallizes. When the magma temperature drops below the liquidus temperature, crystals nucleate and grow inside the magma chamber, potentially resulting in a significant increase of magma viscosity. The effective viscosity of crystal-rich magmas is often estimated from the Einstein-Roscoe equation [*Roscoe*, 1952]:

$$v_m = v_{m0}(1 - \chi / \chi_c)^{-n} \tag{4}$$

Where v_m denotes the effective viscosity of mixture magma, χ denotes the volume fraction of crystals, χ_c is critical fraction value at which crystals effectively solidify the suspension, resulting in ν_m approaching infinity, v_{m0} denotes the viscosity of the liquid magma, and n is an adjustable constant exponent, with the range from 1.5 to 5. Based on the experimental and empirical evidence in [*Marsh,* 1981], the parameters χ_c = 60% and n = 2.5 are widely adopted as typical values [*Shaw*, 1980, *Marsh*, 1981]. Correspondingly, the magma viscosity in equation (4) is reduced to

$$v_m = v_{m0}(1 - 1.67\chi)^{-2.5} \tag{5}$$

In this case, viscosity becomes infinite as χ approaches 60%. In this expression, the density difference between crystals and melts and variations in the chemical composition of the residual melts are neglected.

6.2.6 Proposed magma viscosity model

As discussed above, the viscosity of high-silica magma depends on water content, crystal content, and temperature. However, the existing models only capture partial dependence of all these factors. The models in equations (1) and (2) relate the viscosity to temperature and water content. The model in equation (5) links the viscosity and crystal content, which is indirectly related to the magma temperature through equation (3). The viscosity gradually increases as the temperature decreases due to the cooling and crystallization of the magma body. Therefore, it is necessary to have a universal viscosity model that can capture its dependence on the magma temperature, water content, and crystal content simultaneously. To achieve this, we propose a new viscosity model as a function of temperature, the crystal content and the water content by combining equations (1), (2), and (5)

$$v_c(T_m(t)) = v_{c0}(1-1.67\chi(T_m(t))^{-2.5} \tag{6}$$

Where *c* is either "*a*" or "*d*", denoting andesite or dacite.

For demonstration purposes, we show the relationship between magma viscosity and crystal content, water content, and temperature, respectively. Four different magmas are taken into account based on their water content, including basaltic magma, 0.1 wt.% H_2O andesitic magma, 3 wt.% H_2O andesitic magma, and 4 wt.% dacitic magma. The solidus temperature T_S and the liquidus temperature T_L are selected to be 1030°C and 1200 °C for basaltic magma, 970°C and 1100 °C for 0.1 wt.% H_2O andesitic magma (dry

andesitic magma), 900°C and 1010 °C for 3 wt.% H_2O andesitic magma, and 800°C and 950°C for 3 wt.% dacitic magma, respectively. First, we show the relationship between magma viscosity and crystal content in Figure 6.2.

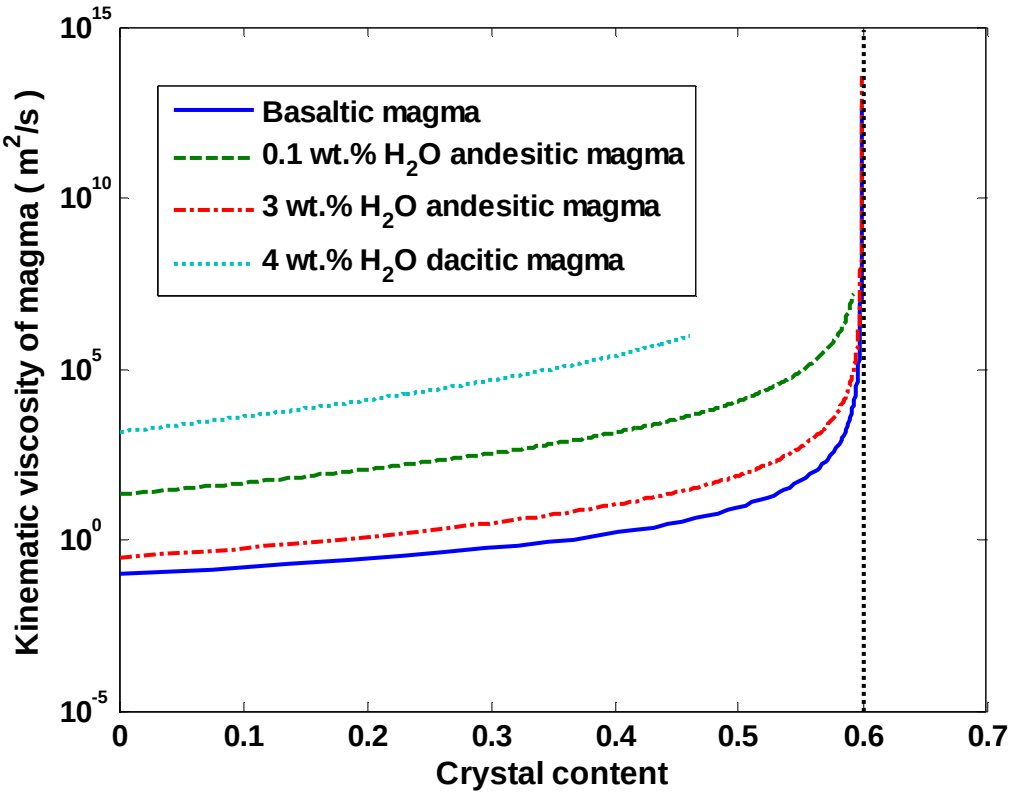

Figure 6.2 The relationship between magma viscosity and crystal content in crystals suspended case for different magmas. The vertical dashed line at 60% shows the viscosity becomes infinite.

Figure 6.2 shows that the viscosity monotonically increases as a function of crystallinity for all types of magma. For the same crystal content, dacitic magma has the highest viscosity, and both andesitic and dacitic magmas have the higher viscosity than the basalts due to the higher silica content. Moreover, viscosity increases non-linearly

with increasing crystal content,especially when the crystal content approaches the critical value of 60 %. Magma convection stops when the crystal content approaches 60%.

The viscosity dependence on water content is shown in Figure 6.3 for different andesite and dacite.

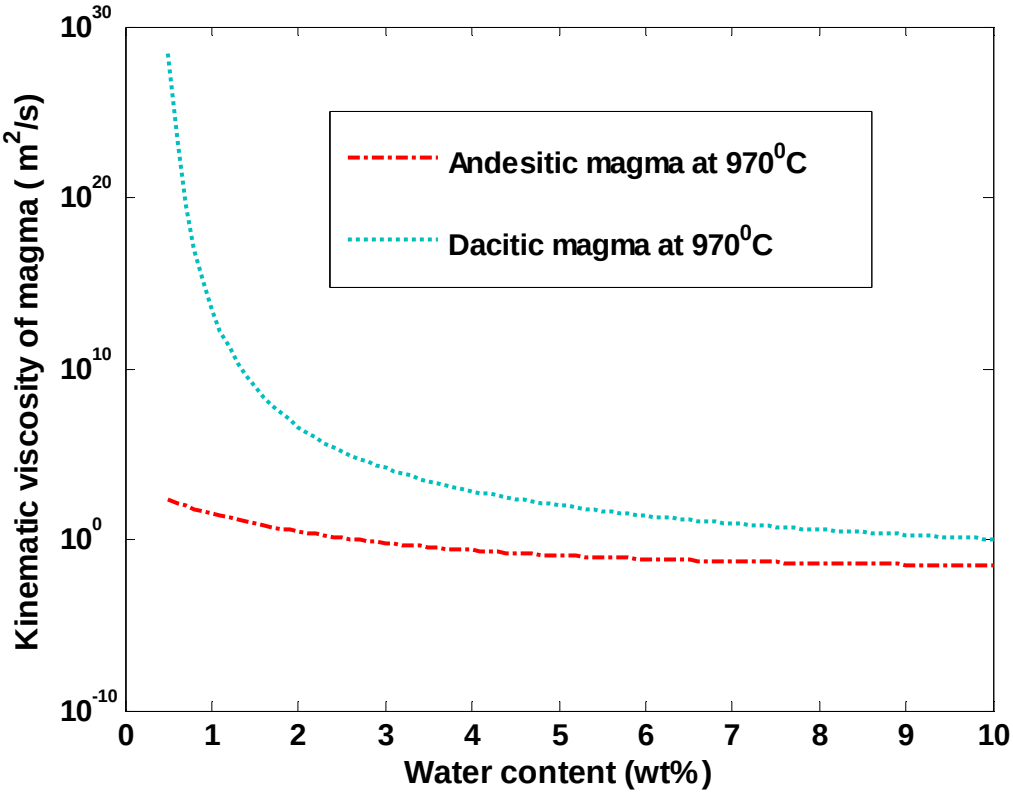

Figure 6.3 The effect of water content on the viscosity of andesitic and dacitic magma at a fixed magma temperature 970°C. Water content has a greater effect on the decrease of magma viscosity on higher silica magma, especially when water content less than 3 wt.%

Figure 6.3 shows that water content has a significant effect on viscosity and that the higher the silica content, the greater the effect of small changes in water content on the viscosity, i.e., water decreases the viscosity of the dacitic magma more than for

andesites. Therefore, the determination of the water content of magma is vital to understanding the dynamic behavior of melts. In addition, Figure 6.3 shows that viscosity increases sharply for dacites when water content is below 3 wt. % and that a further increase in the amount of water above 3 wt.% has a little influence on the viscosity (see equations (1) and (2)).

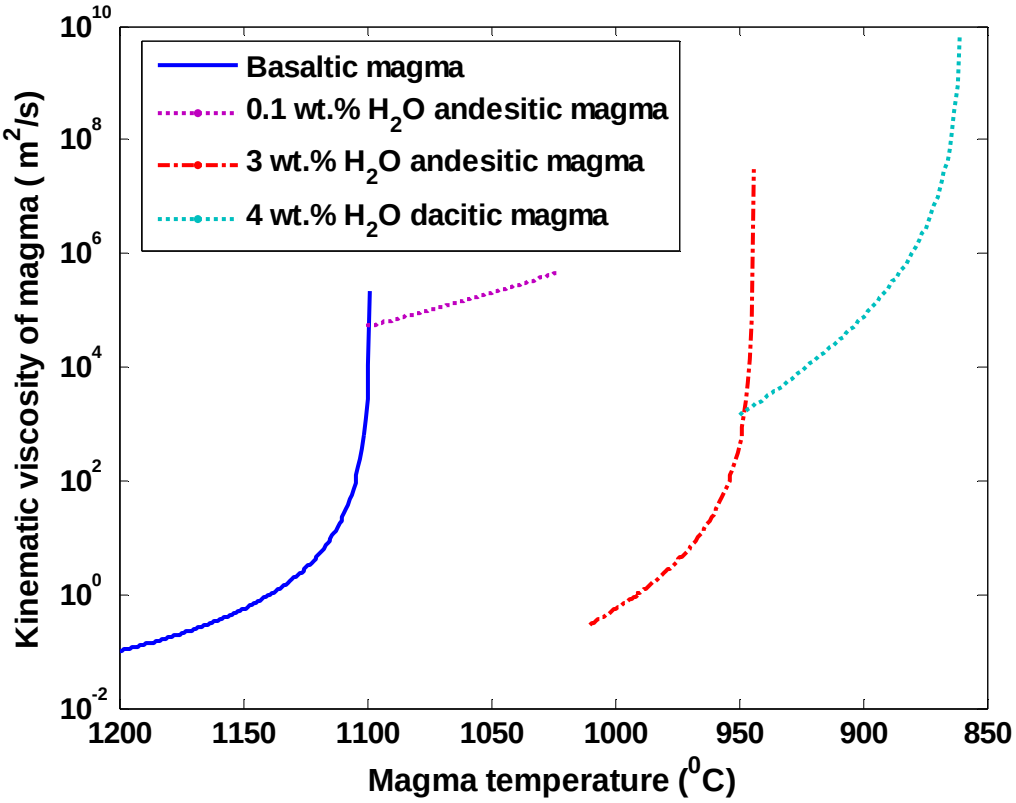

Figure 6.4 Viscosity versus magma temperature with varying water content (wt.%) for basaltic, anhydrous and 3 wt.% andesitic, and 4 wt.% dacitic magmas in crystals suspended case. The temperature affects the melt viscosity significantly, especially at low temperatures.

Lastly, the relation between the magma viscosity and temperature is shown in Figure 6.4 for different magmas. Although different magmas have different temperature ranges during convection, the viscosity increases with a decrease of magma temperature between their respective liquidus and solidus temperatures, because cooling generates more and more crystals and correspondingly increases viscosity. Also, we observe that the range of viscosity of andesites and dacites are greater than that of basalts due to the high SiO_2 content. In the following sections, we will discuss heat transfer from a magma chamber based on the proposed viscosity models.

6.3 Heat Transfer from High-Silica Magmas without Magma Replenishment

To better understand the evolution of heat flux from the convecting, crystallizing magma to hydrothermal system, *Liu and Lowell* [2009], adapted an approach by *Huppert and Sparks* [1988] and developed numerical models of magmatic heat flux for basaltic magma. In this section, we extend this work to the investigation of the hydrothermal system behavior driven by the high-silica magma. Moreover, we compare the characteristics of different hydrothermal systems driven by basalt, andesite and dacite with different water content.

Despite the wide range in spreading rates, depths, substrate compositions, and geometries or even types of heat source along mid-ocean ridge and back-arc basin spreading center, there are strong similarities among all seafloor vent fields in terms of the processes of heat and mass transfer. Within the liquid magma body, thermal convection resulting from the temperature difference between the hot magma and the cold upper boundary maintained by the overlying hydrothermal circulation is an efficient mechanism of heat transfer. Considering a hydrothermal system circulation driven by the

underlying magma system, the heat flux transferred from a vigorously convecting magma chamber is expressed as [*Turner*, 1973]:

$$F_m(t) = 0.1\rho_m c_m(\alpha_m g a_m{}^2 / \nu_m(t))^{1/3}(T_m(t) - T_S)^{4/3} \tag{7}$$

where ρ_m is the magma density, c_m is the magma specific heat, α_m is the coefficient of thermal expansion, g is the gravity acceleration, a_m is the thermal diffusivity, and ν_m(t) is the kinematic viscosity. In our analysis, ν_m(t) is modeled in equation (6), representing either andesites or dacites. Correspondingly, the total magmatic heat output transferred cross the entire area of the magma chamber is obtained as:

$$G_m(t) = F_m(t)A_m \tag{8}$$

where A_m is the surface area of magma chamber. According to [*Liu and Lowell* 2009], the heat content of the magma chamber is calculated by:

$$H(t) = D_m(t)A_m[\rho_m c_m T_m(t) + \rho_m(1 - \chi(T_m(t))L] \tag{9}$$

where $D_m(t)$ is the thickness of liquidus magma, $\chi(T_m(t))$ is the volume fraction of crystal content at the temperature $T_m(t)$, and L is the latent heat of the crystallization of the magma. The first term on the right-hand side of equation (8) represents the sensible heat per unit volume of magma, and the second term represents the latent heat yet to be released as crystallization occurs.

Energy conservation in the magma convection system is determined by equating the time derivative of the heat content in the magma body to the rate of heat loss through the top boundary

$$\frac{dH(t)}{dt} = -F_m(t)A_m \tag{10}$$

To further solve equation (10), we consider two end-member scenarios depending on how the crystals reside in the magma chamber. One is crystals suspended [*Sparks et al.*, 1984; *Solomatov and Stevenson*, 1993], where crystals remain suspended and well mixed with the liquid magma as they crystallize. The other is crystals settling, where crystals instantly settle down to the floor of the magma chamber during cooling [e.g., *Martin*, 1990; *Martin and Nokes*, 1988; *Worster et al.*, 1990; *Liu and Lowell*, 2009].

6.3.1 Crystals suspended

In the crystal-suspended scenario, the crystals are well mixed with liquid magma during cooling and crystallization. The thickness of the liquidus magma remains invariant as the thickness of the magma chamber. Denote D_0 to be the initial thickness of magma chamber. Thus, the liquidus magma thickness is $D_m(t) = D_0$. Substitution of equation (9) into (10) leads to

$$\rho_m c_m D_0 \frac{dT_m(t)}{dt} - \rho_m L D_0 \chi'\left(T_m(t)\right)\frac{dT_m(t)}{dt} = -F_m(t) \tag{11}$$

By combining equations (7) and (11), both the magma temperature $T_{\mathrm{m}}(t)$ and heat flux $F_{\mathrm{m}}(t)$ can be solved numerically. Therefore, the total magmatic heat output for the crystals suspended scenario is obtained as

$$\frac{dT_m(t)}{dt} = \frac{F_m(t)}{\rho_m L D_0 \chi'(T_m(t) - \rho_m c_m D_0} \tag{12}$$

6.3.2 Crystals settling

As the magma chamber cools and crystals settle to the chamber floor, the liquid magma thickness $D_m(t)$ decreases as more and more magma crystallizes. The thickness of the liquidus magma depends on the crystal content as

$$D_m(t) = D_0\left[1 - \chi(T_m(t))\right] \tag{13}$$

Combining equations (9) and (13), we rewire equation (10) for the crystals settling case:

$$\begin{aligned}&\rho_m D\left[\chi(T_m(t)) - 1\right]\left[\chi'(T_m(t)) - c_m\right]\frac{dT_m}{dt} \\ &- \rho_m D\chi'(T_m(t))\left[c_m T_m(t) + L(1 - \chi(T_m(t))\right]\frac{dT_m}{dt} = -F_m(t)\end{aligned} \tag{14}$$

where $\chi'(T_m(t))$ denotes the derivative of χ with respect to T_m. Thus, $T_m(t)$ and $F_m(t)$ can be numerically solved by combining equations (7) and (14). Correspondingly, the total magmatic heat outputs for the crystals settling model is obtained as

$$\frac{dT_m(t)}{dt} = \frac{F_m(t)}{\rho_m D_0 \chi'(T_m(t))\left[c_m T_m(t) + L(1 - \chi(T_m(t))\right] + D_0 \rho_m [1 - \chi(T_m(t))](\chi'(T_m(t))L - c_m)} \tag{15}$$

As we have discussed previously, magma viscosity affects the heat flux from a convecting magma chamber and hence magma composition affects the evolution of the overlying hydrothermal system. To demonstrate this idea, we compare the heat flux from convecting, crystallizing dacitic, andesitic and basalt magmas. Here, we consider both the crystals suspended and crystals settling cases. The viscosity is modeled by equations (5) for basalts and (6) for andesites and dacites, respectively. For andesitic and dacitic magmas, we consider the range of initial water contents from 0.1 to 4 wt.%. The total heat flux of different magmas for crystals suspended and settling cases are shown in Figure 6.5 and Figure 6.6, respectively.

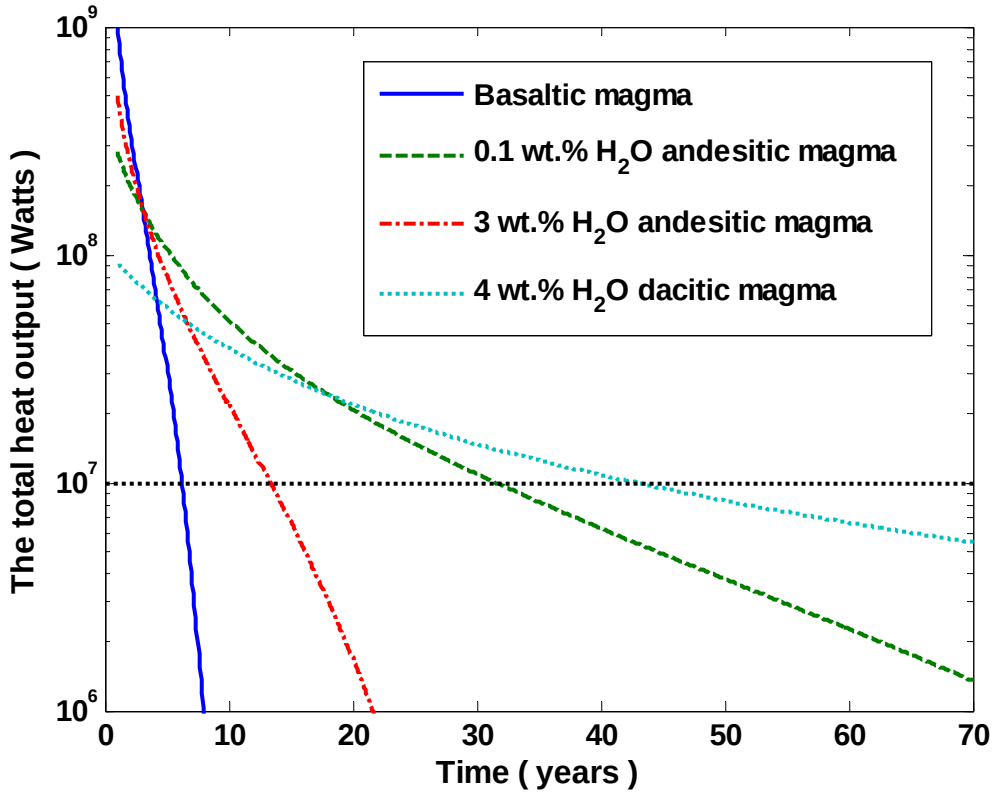

Figure 6.5 Comparison of the total heat output from basaltic, andesitic and dacitic magma without magma replenishment in crystals suspended case.

We assume that the heat transferred from magma chamber is carried solely by hydrothermal convection, i.e., no heat loss through surrounding rock by conduction occurs. The estimated range of the integrated heat fluxes in hydrothermal vents at oceanic spreading centers is between 10^7 and 10^9 Watts [*Baker*, 2007; *Ramondenc et al.*, 2008]. The horizontal line at 10^7 Watts denotes the minimum value of total hydrothermal heat output. We assume that the hydrothermal circulation effectively stops when the magmatic heat output drops below 10^7 Watts. Figure 6.5 shows that basaltic magma has the highest initial total heat output as a result of its low viscosity and high initial temperature (see equation (7)). In addition, the viscosity has a significant effect on both the decay rate of

total heat output and on the lifetime of hydrothermal system through the modeling dependence of the water content.

Figure 6.5 shows that dacitic magmas have the lowest decay rate followed by andesites and basalts, because dacites have the highest SiO_2 content and the correspondingly highest viscosity. For the same type of magma, for example andesite in Figure 6.5, the one with water content 3 wt.% has a faster decay rate than the one with water content 0.1 wt.%, since lower water content results in the higher viscosity. In terms of lifetime, a hydrothermal system driven by 0.1 wt.% andesitic magma lasts for 30 years before the total heat output drops below 10^7 watts. A hydrothermal system driven by dacitic magma lasts a litter longer. Although andesitic magma bodies have lower initial heat flux than basaltic ones as a result of their large viscosity, the heat output decays more slowly than the basaltic one. Therefore, for a given magma chamber geometry, with the same properties except for viscosity, and latent heat, the andesitic-driven hydrothermal systems have longer lifetimes than basaltic ones.

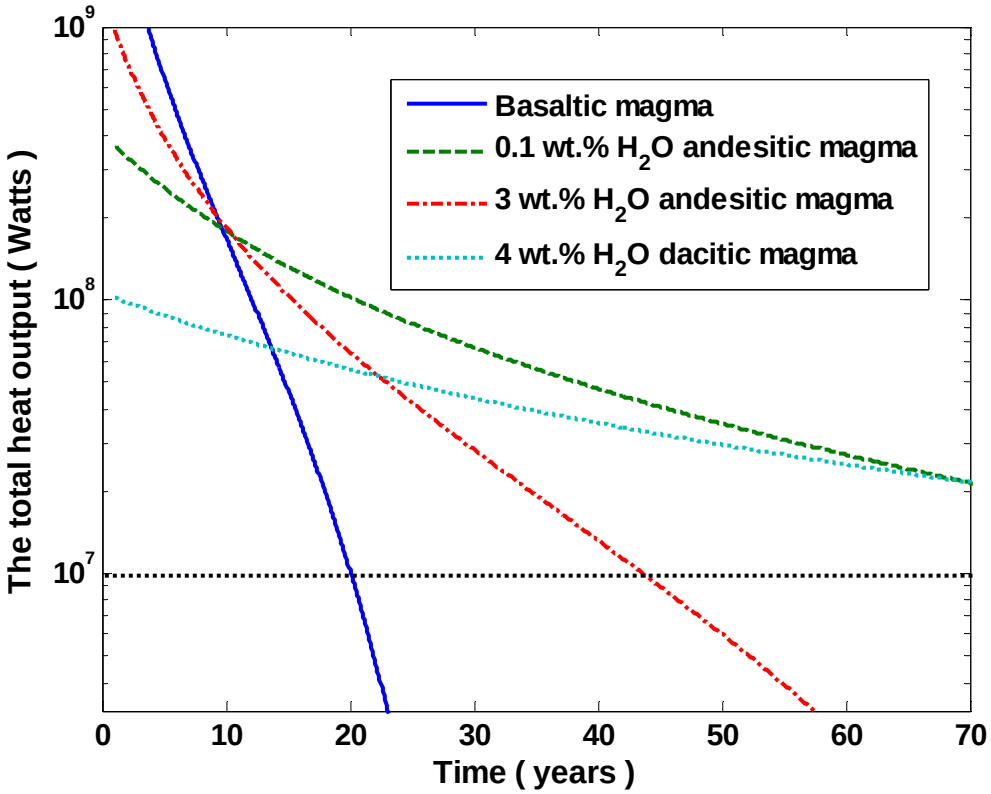

Figure 6.6 Comparison of the total heat output from basaltic, andesitic (anhydrous and with 3 wt.%), and dacitic (with 4 wt.%) magmas without magma replenishment in crystals settling case.

Comparing Figure 6.6 and Figure 6.5, it is observed that under similar conditions, the total heat output for all types of magmas have longer lifetime for crystals settling than crystals suspended model. This occurs because of the rapid increase in viscosity and decrease in Rayleigh number when crystals are suspended. Even for the basaltic magma, the lifetime lasts for about 20 years before the total heat output drops below 10^7 watts. On the other hand, systems with higher initial viscosity and lower initial heat output such as the 4 wt.% dacitic magma it has the longest lifetime and lowest decay rate of the total heat output. Thus occurs because the lower the initial heat output, the lower the overall

rate of decay. For the crystal-suspended case, an alternative way to determine the termination of the hydrothermal activity is based on crystal content. As discussed in equations (5) and (6), the crystal content can not exceed 60%. Figure 6.7 depicts the crystal content variation with respect to time for different magmas. It is seen that basalt has the shortest magma convection time, followed by the 3 wt.% andesite and 0.1 wt.% andesite, and 4 wt.% dacite takes almost 200 years till convection stops. Magmas with higher viscosity have longer convectiive lifetime due to their slower heat flux, and correspondingly have longer lifetimes in terms of the crystal content approaching 60%.

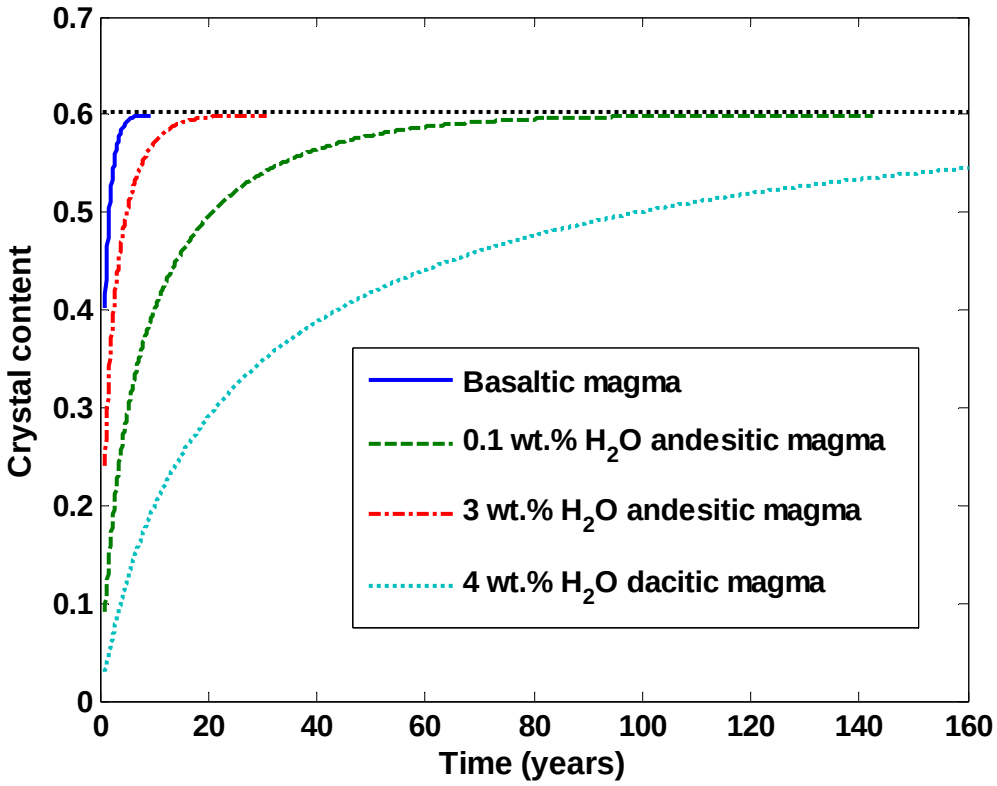

Figure 6.7 The growth of crystals as a function of time for different magmas when the crystal content approaches to 60% in crystals suspended case.

6.4 Heat Transfer from High-Silica Magmas with Magma Replenishment

Liu and Lowell [2009] show that heat transfer from a convecting, cooling, replenished basaltic magma chamber can maintain seafloor hydrothermal systems on decadal timescales. The results in the previous section show that for high-silica magmas heat output decays on decadal timescales in both cases of crystals settling and suspended. Thus, by adopting the methodology in *Liu and Lowell* [2009], we investigate whether heat transfer from high-silica magmas can also sustain themselves with reasonable rates of replenishment from the underlying mush zone.

Denote $u(t)$ to be the velocity of magma replenishment. Then the rate of heat replenishment $F_r(t)$ is expressed by

$$F_r(t) = (\rho_m c_m T_{in} + \rho_m L(1-\chi_{in})u(t) \tag{16}$$

where T_{in} denotes the replenished magma temperature, and χ_{in} is the corresponding crystal content which can be obtained from equation (3) with $T_m(t)$ replaced by T_{in}. In addition, the latent heat remaining in the newly added magma depends linearly on the fraction of liquid magma being added, i.e., $L(1-\chi_{in})$.

In contrast with the no-replenishment case, the magma chamber size grows with added magma. We assume, for simplicity that the andesitic and dacitic magma chambers grow vertically rather than laterally during the intrusion of new magma, i.e., the area of the magma chamber remains constant, while its thickness grows with time [see Liu and Lowell 2009 for discussion of the case in which area grows and thickness remains constant]. To model the time-varying thickness of magma chamber, we neglect any density difference between the replenished magma and the crystal-melts mixture in the magma chamber. Mass conservation of the magma then requires

$$\frac{dD(t)}{dt} = u(t) \tag{17}$$

To solve the thickness of the magma chamber, we consider two models of the magma replenishment rate, constant velocity and exponentially decay rate, which are given by, respectively

$$\begin{aligned} u(t) &= u_0 \\ u(t) &= u_0 e^{-bt} \end{aligned} \tag{18}$$

where u_0 is the initial rate of the replenishment; b is a constant determining the exponential decay rate. Substitution of equation (17) into equation (18) results in the expression of time-varying magma chamber thickness for different replenishment rates, respectively

$$\begin{aligned} D(t) &= D(0) + u_0 t \\ D(t) &= D(0) - \frac{u_0 e^{-bt}}{b} + u_0 b \end{aligned} \tag{19}$$

With the magma replenishment, the magma volume changes with time, so the heat content in equation (9) is rewritten as

$$H(t) = D_m(t) A_m [\rho_m c_m T_m(t) + \rho_m (1 - \chi(T_m(t)) L] \tag{20}$$

With new heat flux into the hydrothermal system, the energy conservation in equation (10) is extended to

$$\frac{dH(t)}{dt} = -F_m(t) A_m + F_r(t) A_m \tag{21}$$

In the following, we develop the heat flux model for a magma chamber with replenishment. Both magma cooling and crystallizing models of crystals suspended and crystals settling are considered.

6.4.1 Crystals suspended

In the crystals suspended case, we assume that the crystals are well mixed in the magma. Thus, the liquidus magma thickness is the same as the magma chamber thickness, i.e., $D_m(t) = D(t)$. Combining equations (16), (17), (20), and (21), we obtain

$$\frac{dT_m(t)}{dt} = \frac{F_m(t) - \rho_m u(t)\left(c_m\left(T_{in} - T_m(t)\right) + \left(\chi\left(T_m(t)\right) - \chi_{in}\right)L\right)}{D(t)\rho_m\left(\chi'\left(T_m(t)\right)L - c_m\right)} \tag{22}$$

Thus, by combining equations (7), (19) and (22) both the magma temperature $T_m(t)$ and heat flux $F_m(t)$ can be solved numerically. The total magmatic heat output can then be obtained from equation (8). Comparing equations (12) and (22) for systems with and without magma replenishment, respectively, the second term in the numerator of equation (22) is generated by the addition of new magma into the chamber. For the special case of zero-rate replenishment, equation (22) is reduced to equation (12), with $D(t) = D_0$, which shows the consistency of our analysis.

6.4.2 Crystals settling

For the crystals settling model with replenishment, assuming that during the crystallization, crystals form on or instantly settle to the floor of the magma chamber, the thickness of the liquid magma can be expressed as

$$D_m(t) = \left[1 - \chi(T_m(t)\right]D(t) \tag{23}$$

Correspondingly, the rate of magma chamber growth is

$$\frac{dV_m(t)}{dt} = A_m \frac{dD_m(t)}{dt} = A_m\left[-D(t)\chi'(T_m(t)\frac{dT_m}{dt} + (1 - \chi(T_m(t))u(t)\right] \tag{24}$$

Combining equations (16), (20), (21), and (24), the magma temperature $T_m(t)$ can be expressed as

$$\frac{dT_m(t)}{dt} = \frac{F_m(t) - F_c + \rho_m u(t)\left[\left(1-\chi(T_m(t))\right)\left(c_m T_m(t) + \left(1-\chi(T_m(t))\right)L\right) - \left(c_m T_{in} + L(1-\chi_{in})\right)\right]}{D(t)\rho_m \chi'(T_m(t))\left(c_m T_m(t) + L\left(1-\chi(T_m(t))\right)\right) + D(t)\rho_m\left(1-\chi(T_m(t))\right)\left(\chi'(T_m(t))L - c_m\right)} \quad (25)$$

With equations (7), (19), and (25), both the magma temperature $T_m(t)$ and heat flux $F_m(t)$ can be solved numerically, and the magmatic heat output is obtained from equation (8).

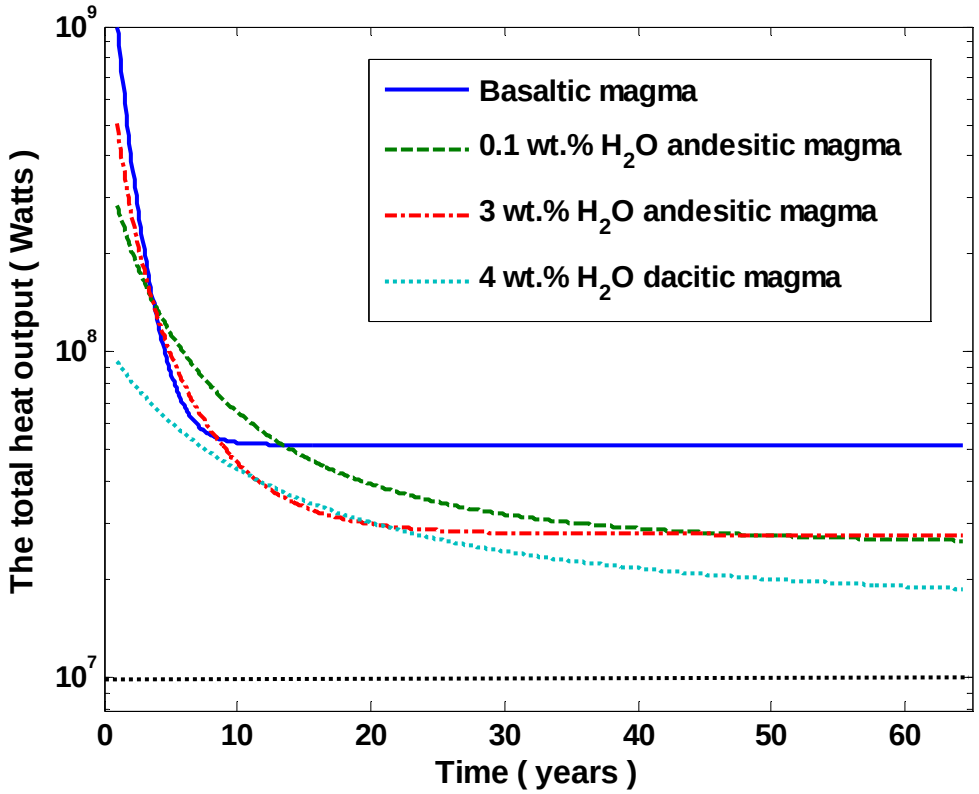

Figure 6.8 Total heat output as a function of time for four types of magma convection systems with a constant magma replenishment rate at 5×10^{-8} m/s when the thickness of magma chamber doubles in crystals suspended case.

In the following, we provide some simulation results to demonstrate our analysis.

In the simulations, the initial thickness of magma is set to 100 meters, and the magma thickness grows during replenishment as in equation (19). Based on seismic evidence, the thickness of magma lens in mid-ocean ridges is less than a few hundred meters. Thus, we run the simulations until the thickness of the magma chamber doubles. Figure 6.8 shows the total magmatic heat output in crystals suspended case with the constant replenishment rate of 5×10^{-8} m/s for four different magmas, including basalt, 0.1 wt.% and 3 wt.% andesite, and 4 wt.% dacitic magma. Figure 6.8 shows that with magma replenishment, the magma chamber size doubles after 65 years and the total heat output reaches a quasi-steady state between 10^7 and 10^9 W. With the same initial chamber size and constant rate of replenishment, the high-silica magmas have slower decay rate of heat output compared to the basaltic magma. As in the case of without replenishment, this occurs because the high-silica magmas have higher viscosity (see Figure 6.9), which results in the lower Rayleigh numbers. Thus, convection in high-silica magmas is less vigorous, and provides less heat output than in basaltic magma. In addition, the steady-state magmatic heat outputs of high-silica magmas drop below that of basaltic magma. Because the faster decay heat flux of basalts results in faster rate of crystallization which makes replenishment significant in the balance between magma convection and replenishment. The basaltic magmas reach equilibrium earlier than high-silica magmas. In contrast, high-silica magma heat flux decays slowly and the long period of decay leads the steady-stage heat flux below that of the basalts.

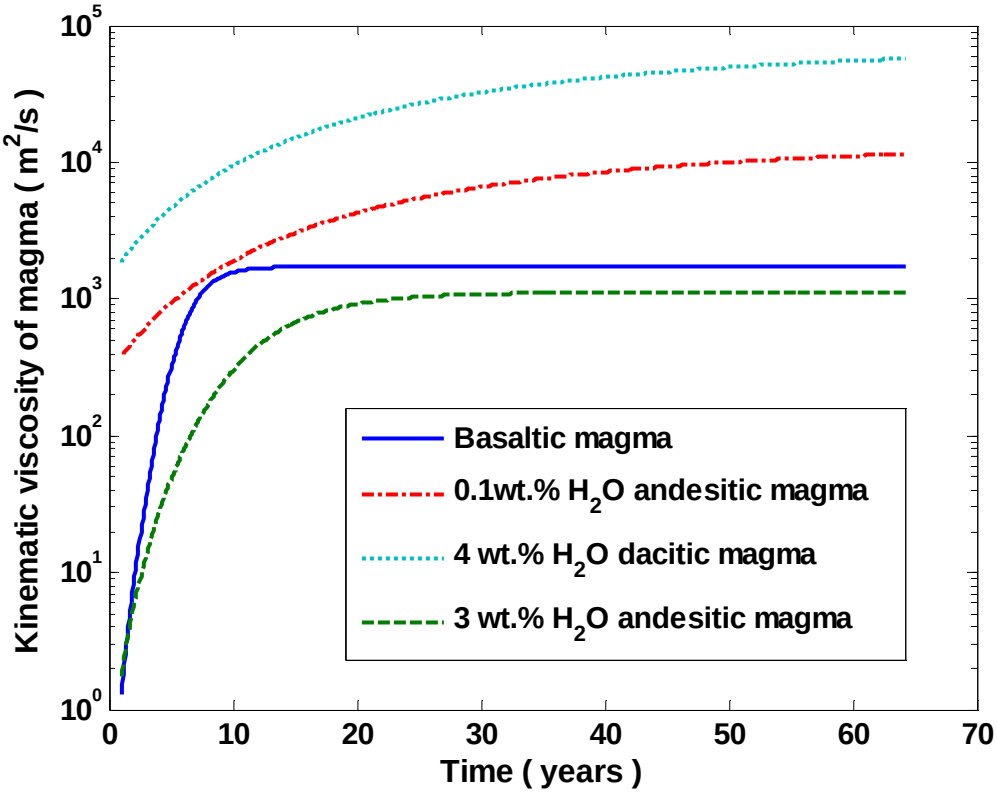

Figure 6.9 Magma viscosity as a function of time for different magma in crystal suspended case with magma replenishment at 5×10^{-8} m/s.

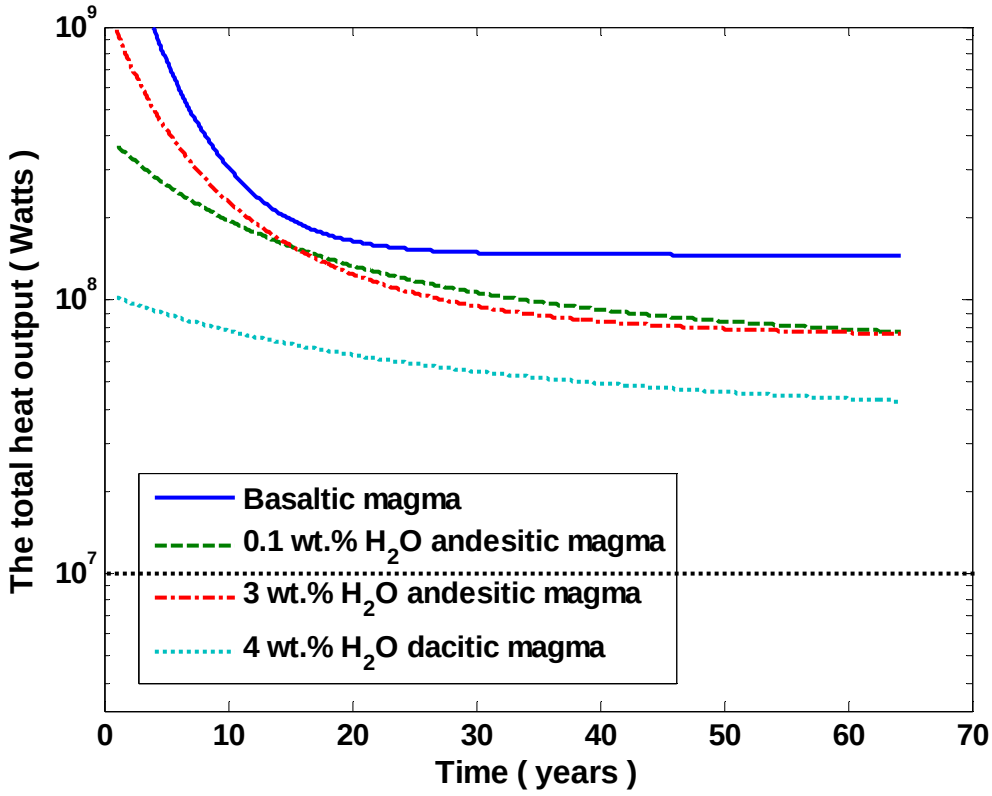

Figure 6.10 Total heat output as a function of time for three types of magma convection systems with a constant magma replenishment rate at 5×10^{-8} m/s when the thickness of magma chamber doubles in crystals settling case.

With the same simulation setups as in Figure 6.8 and Figure 6.9, Figure 6.10 and Figure 6.11 show the total heat outputs and the corresponding viscosities for different magmas in the crystals settling case. Similar to the crystals suspended case, the thickness of all the magma chambers doubles after 65 years, because the growth of magma thickness depends only on the magma replenishment rate. Also, each type of magma has slower heat flux decay rate compared to the counterpart in the crystals suspended case (see Figure 6.8 and Figure 6.10), because the viscosity in the crystals settling case is lower than that in the crystals suspended case (see Figure 6.9 and Figure 6.11). With

crystals settling, the magma temperature decreases more slowly than in the crystals suspended case. As a result, in conjunction with the absences of crystals in the magma, the viscosity increases more slowly than in the crystals suspended case.

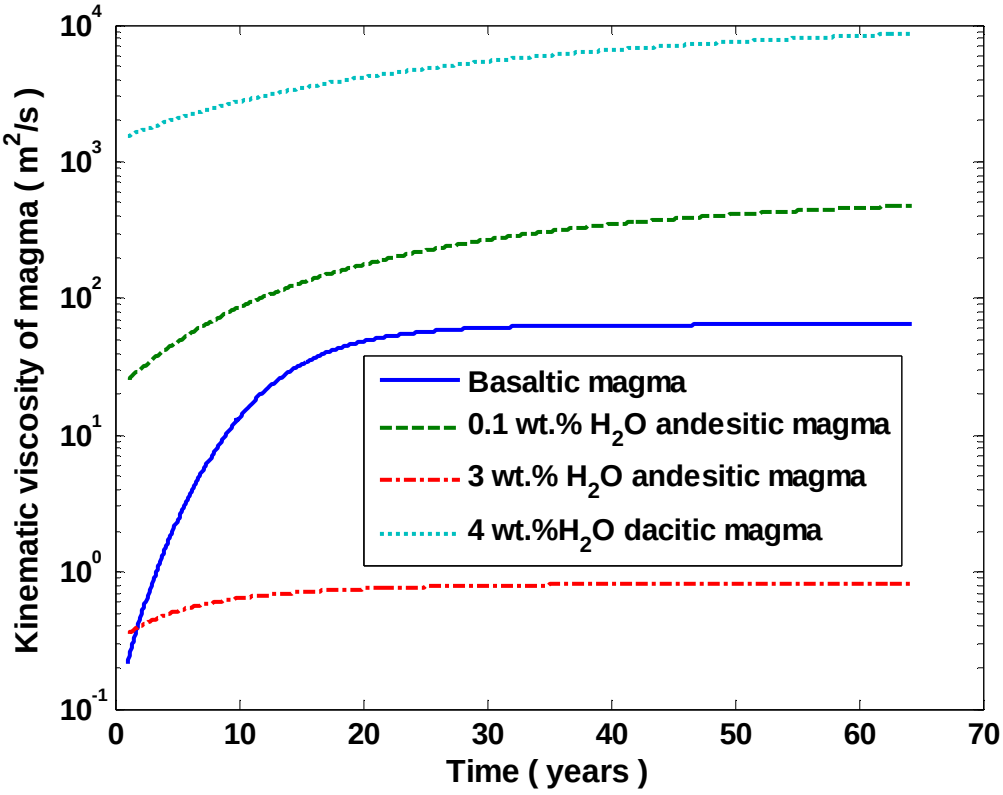

Figure 6.11 Magma viscosity for different magmas in crystals settling case with magma replenishment at 5×10^{-8} m/s.

In addition, we investigated magma replenishment with an exponential decay rate (equation (18)). As an example, Figure 6.12 shows the heat output of different magmas in crystals settling model with the magma replenishment at an exponentially decay rate. Magma supply is slower in this replenishment rate model than the constant rate (see

Figure 6.10). Thus, it takes longer time for the magma chamber to double its size, and correspondingly the effective lifetime increases to 100 years for all magmas.

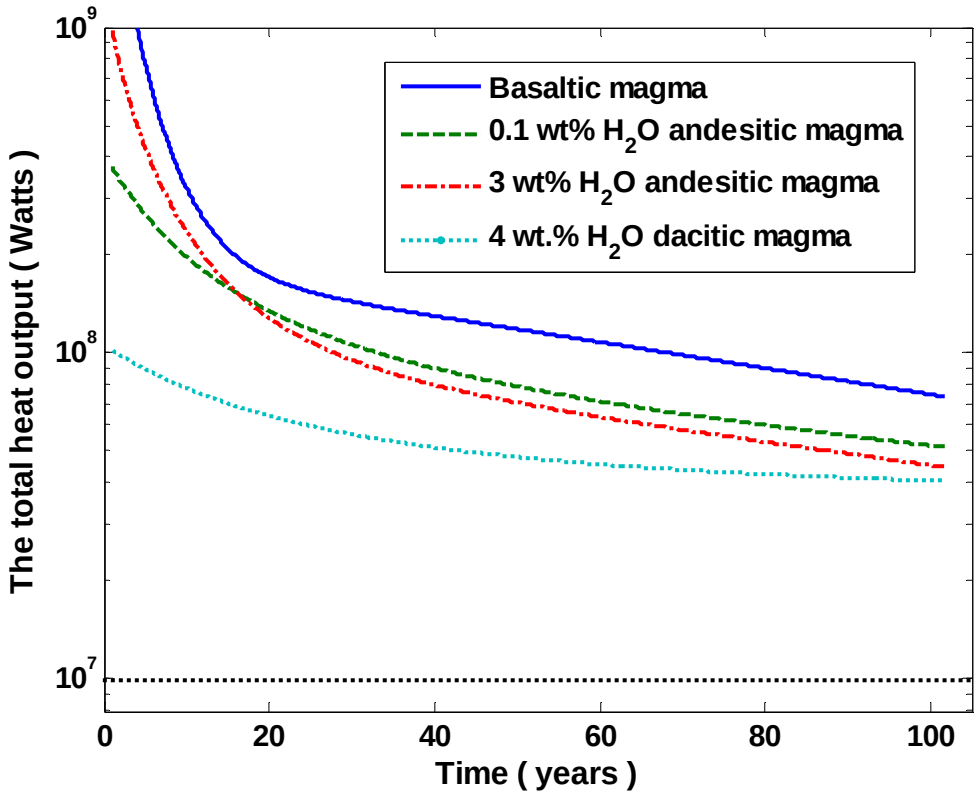

Figure 6.12 The total heat output as a function of time for four types of magma with magma replenishment at a certain exponential decay rate, u_0 at 5×10^{-8} m/s and b at 10^{-9}.

Finally, to investigate the effect of replenishment rate, Figure 6.13 shows the magmatic heat output of 0.1 wt.% andesitic magma chamber in crystals settling model with the magma chamber being refilled with different initial replenishment rates (u_0) and exponential decay rates (b). Figure 6.13 shows that the magma replenishment parameters (u_0 and b) affects both the lifetime of the magma chamber and steady-state heat output.

For all the different values of u_0 and b, the heat outputs can maintain the steady state for decades. The initial replenishment rate u_0 has a significant control on the decay rate of heat output, and the replenishment decay rate b has a significant control on the convective lifetime. For instance, when b changes from 10^{-9} to 10^{-10}, the life time of convection changes from 60 years to 100 years with the initial replenishment rate of $5x10^{-8}$ m/s.

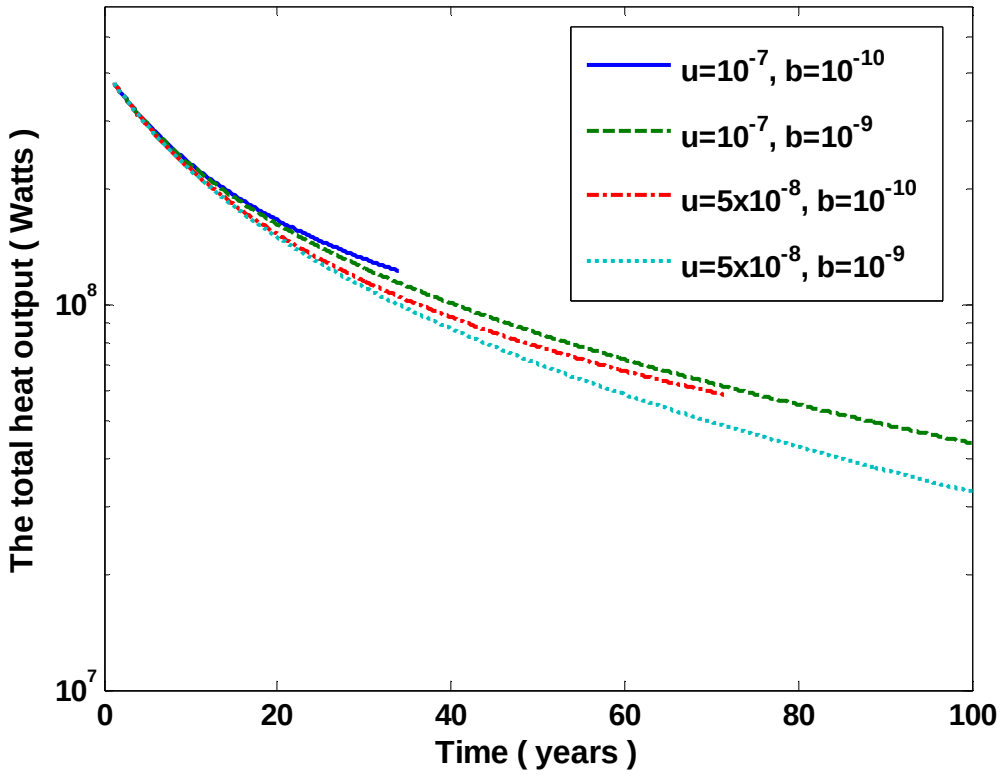

Figure 6.13 Total heat output as a function of time for anhydrous andesites with magma replenishment at various exponential decay rates in crystals settling model.

6.5 Discussion

The mechanism of heat extraction by hydrothermal circulation along mid-ocean ridges is fundamentally the same among fast-, intermediate-, slow, and back-arc basins. Thus, the variations in AMC properties implicate the magmatic processes. In this part, we discuss the effects of liquid magma thickness and replenished magma temperature on the magmatic processes.

6.5.1 Liquid magma thickness in crystals settling model

In this part, we discuss the implication of liquid magma thickness on the total heat flux. For demonstration purpose, we only consider the crystal settling case. Figure 6.14 and Figure 6.15 show the time-varying liquid magma thickness during convection for different magmas with and without magma replenishment, respectively. For the case without replenishment, and an initial magma chamber thickness of 100 m, the thickness of liquid basalt drops to 40 m quickly; indicating rapid decrease in heat output and the end of the convection (see Figure 6.6). In contrast, the thickness of liquid high-silica magma decreases more slowly due to the slow decay of the heat flux (see Figure 6.6), which is induced by the high viscosity. In the magma replenishment case, all the magma chambers grow for 65 years when the initial thickness of magma doubles with the magma replenishment rate of 5×10^{-8} m/s. The liquid magma thickness is greater than 40 m at steady-state for all types of magmas. The thickness of basaltic liquid magma layer decreases rapidly during the first decades of magma chamber cooling and crystallization. A 100 m thick melt lens thins to 45m (55%), because there is more vigorous convection in basaltic magma so that the convective heat loss exceeds the rate of heat input from replenishment. After the heat flux from magma replenishment balances the convective

heat loss, the thickness of liquid magma remains stable over time. Even though the thickness of liquid basaltic magma is less than that of liquid high-silica magmas, the total heat output of basalt system is higher than that of high-silica magma systems (see Figure 6.10).

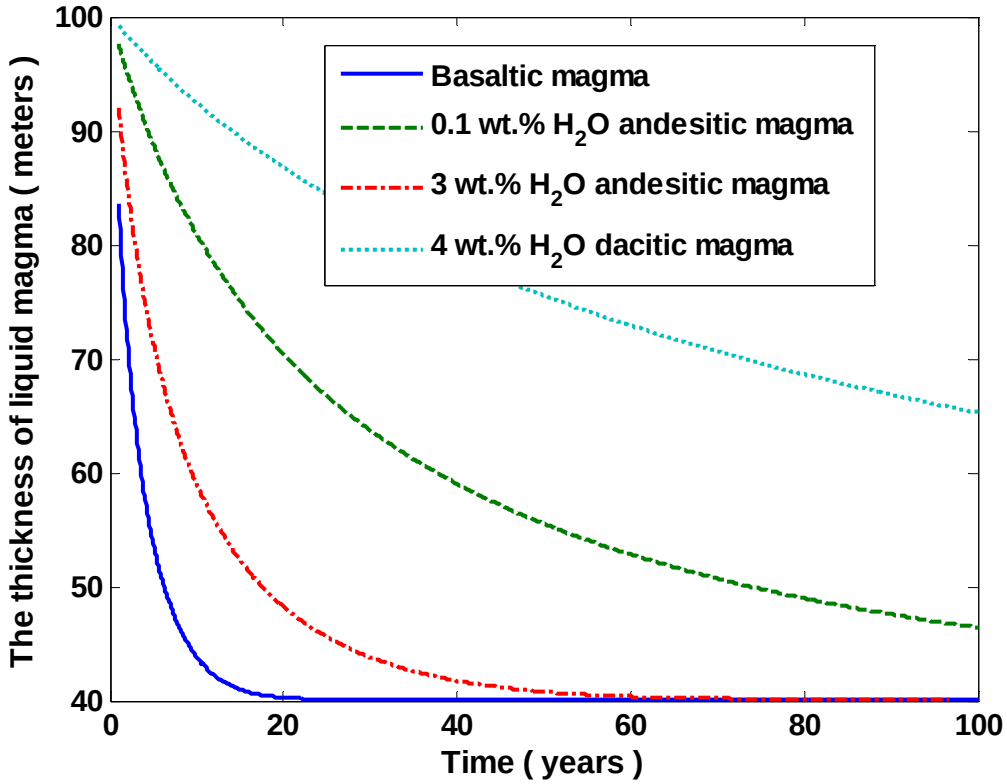

Figure 6.14 The thickness of liquid magma as a function of time for different magmas initially 100 m thick for crystals settling cases without magma replenishment.

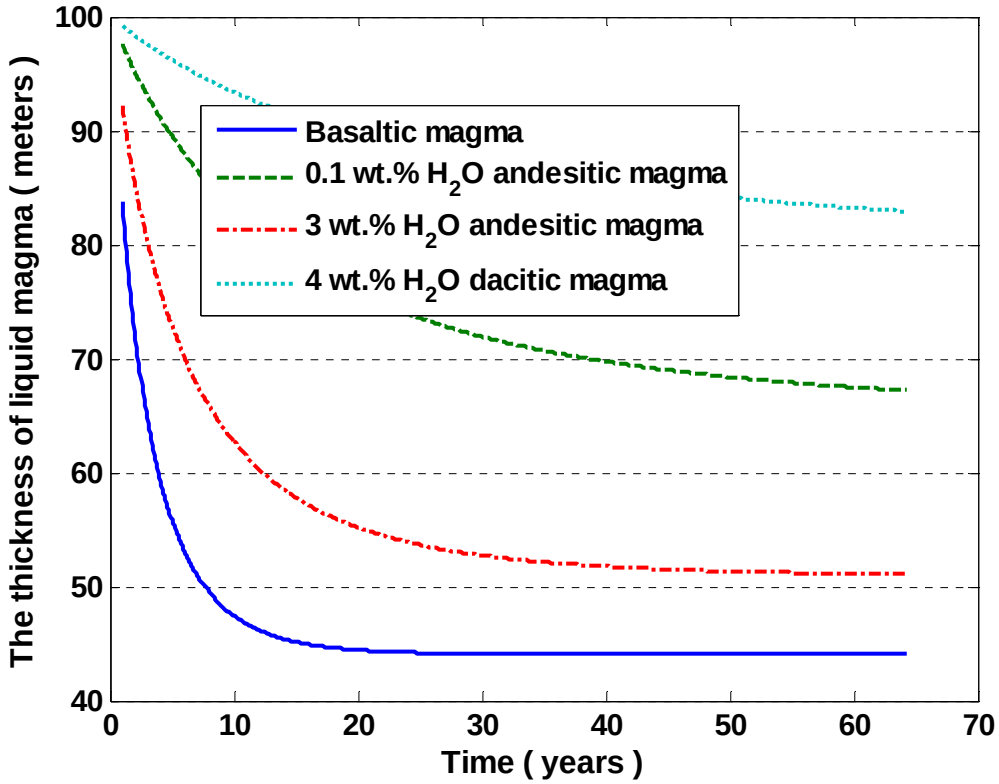

Figure 6.15 The thickness of liquid magma as a function of time for different magmas in crystals settling model with magma replenishment at $5x10^{-8}$ m/s and an initial magma thickness of 100 m.

6.5.2 Evolution of magma and hydrothermal temperature

Based on the magma replenishment equation (16), different magma intrusion temperature may lead to different magma chamber evolution. Assuming that the latent heat is released uniformly between the liquidus and solidus temperatures, magmatic heat is linearly proportional to its temperature, which can be obtained from equation (5) by replacing T_m with T_{in}. In addition, the latent heat is linearly dependent on the liquid fractionation of the added magma, i.e., $L(1-\chi_{in})$. We assumed two scenarios of the replenished magma at temperature of T_{in}. One is that T_{in} is less than liquidus temperature

T_L. In this case, there has already been a certain amount of latent heat loss from the incoming melt. The other is that the original magma has less initial latent heat, i.e., its initial temperature $T_m(0)$ is less than T_L. In this case, we set T_{in} to be T_L, which is larger than $T_m(0)$. Figure 6.16 and Figure 6.17 shows the total heat output of the magma chamber for these two cases, respectively. For both cases, we observe that the lower the intrusion temperature, the faster the decay of the heat flux. However, the effect of the temperature of added magma on the total heat output behavior of the magma chamber is slight.

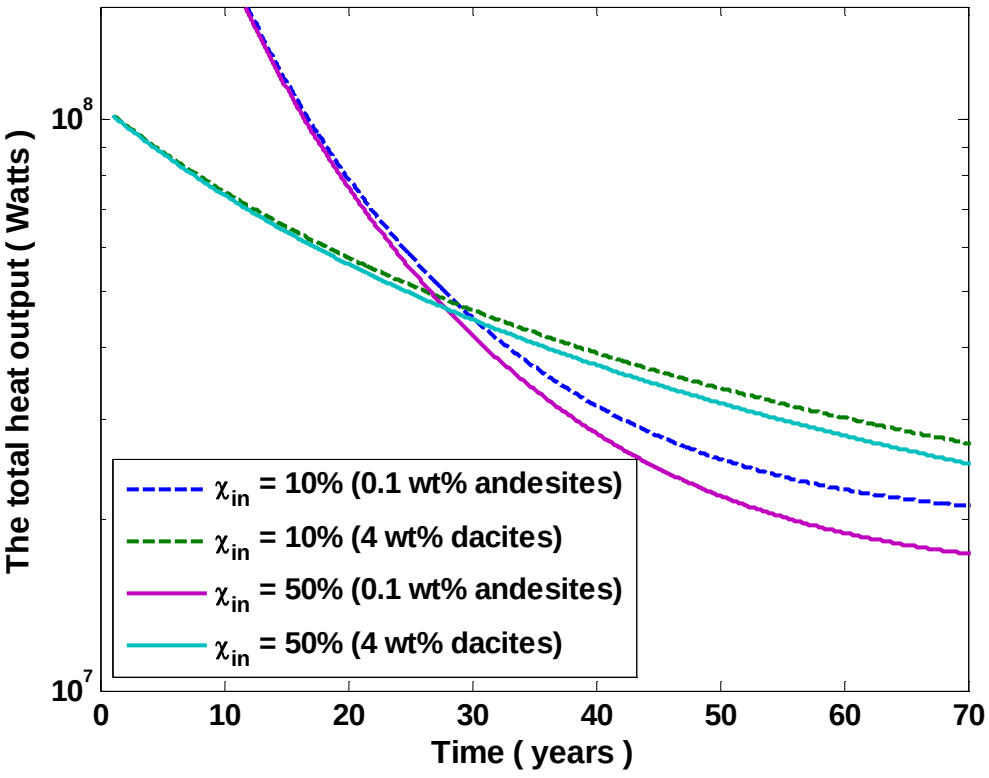

Figure 6.16 Total heat output as a function of time for different magmas in crystals settling case with magma replenishment rate at $5\text{x}10^{-8}$ m/s when T_{in} is less than T_L which means replenished magma with less latent and sensible heat.

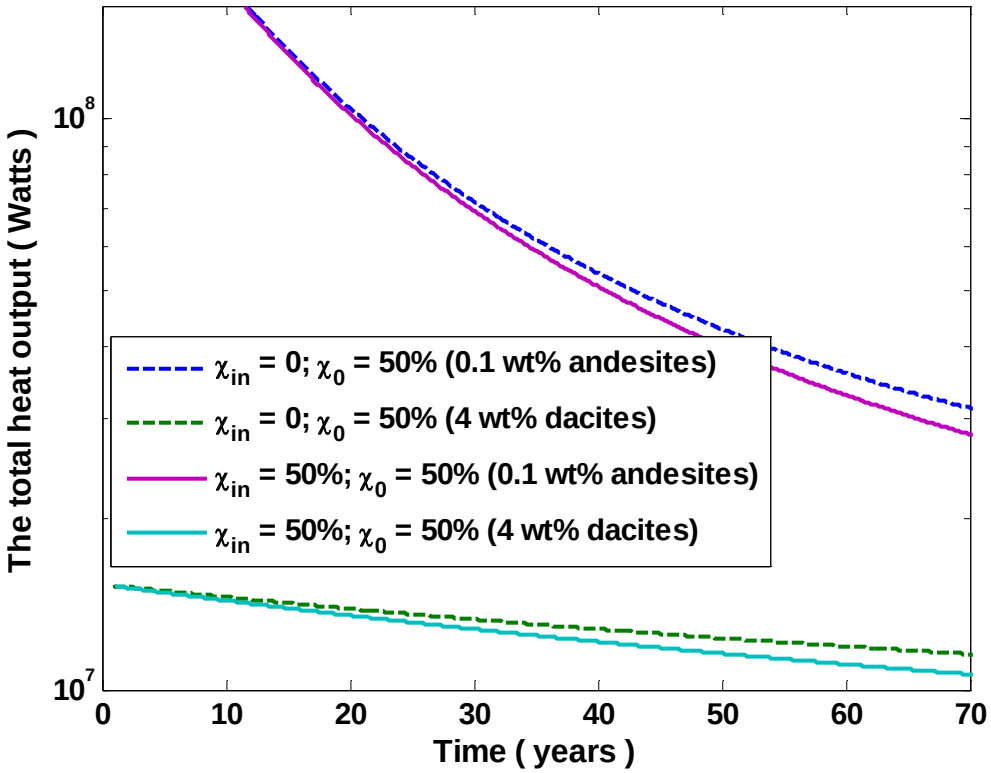

Figure 6.17 Total heat output as a function of time for different magmas in crystals settling case with magma replenishment rate at 5×10^{-8} m/s when we assume replenished magma with liquidus temperature T_L, and original magma in magma chamber with temperature lower than T_L which mean the original magma with a certain amount of crystal content.

[*Liu and Lowell*, 2009] assume that magmatic heat supply is directly coupled to hydrothermal heat flux and vent temperature. Here we employ the same relationships to investigate this link for different host rocks. We assume that no heat loss occurs during the heat transfer between the magma and hydrothermal fluid, and that the variation of hydrothermal temperature T_h and heat flux F_h instantly reflect that in the magma chamber. Thus, we have

$$F_h(t)A_d = F_m(t)A_m(t) \tag{26}$$

where A_d is the area of hydrothermal discharge zone. For a hydrothermal system venting at temperature $T_h(t)$, the heat flux of the hydrothermal venting is

$$F_h(t) = \rho_f c_f u_d(t) T_h(t) \tag{27}$$

where ρ_f is the density of hydrothermal fluid, c_f is the specific heat of the fluid, and $u_d(t)$ is the Darcian upflow velocity. Combining equations (26) and (27), we obtain the temperature of hydrothermal venting as

$$T_h(t) = \left(\frac{F_m(t)A_m v_f}{A_d \rho_f c_f \alpha_f g k} \right)^{1/2} \tag{28}$$

Figure 6.18 shows hydrothermal temperatures resulting from magmatic heat supply for different magma systems with a constant replenishment rate of 10^{-8} m/s. The typical value of permeability k and the area of discharge zone A_d used to calculate the hydrothermal temperature are 10^{-13} m^2 and 10^4 m^2, respectively. Hydrous high-silica magmas have lower initial hydrothermal temperatures because the hydrothermal temperature is proportional to the magmatic heat output as shown in equation (28). In addition, the hydrothermal temperature has a correspondingly slow decay rate, which is consistent with the slow decay rate of magmatic heat output in Figure 6.10. Nevertheless, hydrothermal temperatures of basaltic and anhydrous andesitic magma decrease significantly on decadal timescales during the initial cooling phase of magmatic heat transport but stabilize as the heat input from magma replenishment balances the convective heat loss. Hydrothermal temperatures resulting from convection in the more viscous dacitic and wet andesitic magmas are relatively more stable.

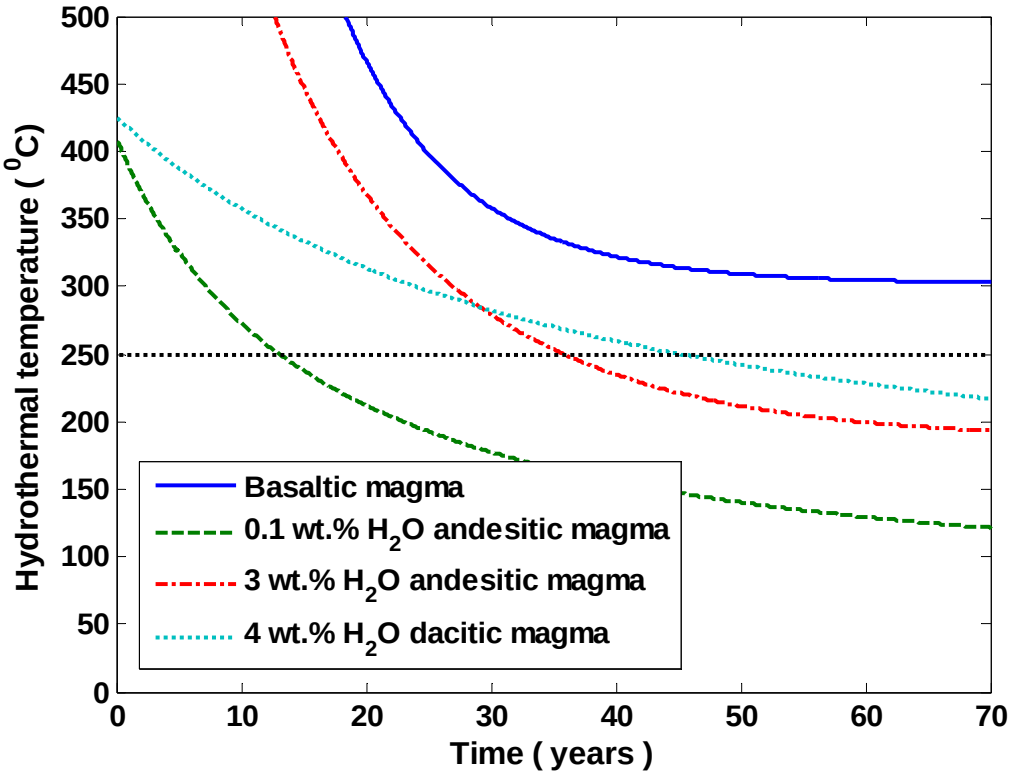

Figure 6.18 The evolution of hydrothermal temperatures for different magma system in the crystals settling case with magma replenishment at 10^{-8} m/s. The typical value of permeability k and the area of discharge zone A_d used to calculate the hydrothermal temperature are 10^{-13} m^2 and 10^4 m^2, respectively. The horizontal line of temperature of 250 °C denotes the lower limit for observed black smoker vent temperatures. The result is for illustration purposes and the basalt hydrothermal T is too high,but it can lowered by using a higher k

6.5.3 Physics of magma replenishment.

In the paper, we have shown that a convecting AMC requires magma replenishment for the stable heat flux. Based on our analysis, the replenishment rate between 10^{-7} and 10^{-8} m/s tends to stabilize the heat output on the decadal timescale for high silica magma chambers. Also, in our comparison of different magma systems, the replenishment rates are assumed to be the same in different magma systems. In reality,

however, magma replenishment rates may depend on the physical processes in the lower crust and upper mantle that depend upon the properties of magma. Several different mechanisms may be involved in magma transport in the lower crust.

As magma initially at its liquidus beneath a colder upper boundary represented by the hydrothermal system begins to crystallize, its volume shrinks. As the internal pressure in magma chamber declines new magma may be driven upward from the reservoir of relatively crystal-rich partial melt that occupies the lower crust [e.g., *Mainprice*, 1997; *Dunn et al*., 2000]. Magmas from the mushy zone may also ascend because of the buoyancy force resulting from the density difference between the melt and crystals in the mush zone as a combination of buoyant porous flow through the mush zone and compaction [*Turcotte and Ahern*, 1978; *McKenzie*, 1984; *McKenzie*, 1985b], or as buoyant crack propagation [*Shaw*, 1980; *Lister*, 1990; *Lister and Kerr*, 1991]. Melt may also be transported by dike propagation from a deeper lying magma body [*Sim*, 2004; *Kelemen et al.*, 1997].

Porous flow models of upward magma migration assume that after pressure release melting in the mantle, interconnected melt along solid grain boundaries generates permeability such that the melt rises at a constant velocity J through the residual solid [*Turcotte and Ahern*, 1978]. The differential buoyancy of the liquid and solid is responsible for the pressure drop with drives the liquid flow out of the solid [*Frank*, 1968]. The velocity of melt in the permeable-porous matrix is given by [*Turcotte and Ahern*, 1978]

$$u = J\theta = \frac{k_\phi}{v_m \rho_m}(\rho_s - \rho_m)g \tag{29}$$

where $k_{\varnothing}$ is the permeability, θ is porosity, ρ_s is the density of solid, respectively. There are many ways to relate the matrix permeability to the porosity, but most formulations suggest that $k_{\varnothing} \propto \theta^3 b^2$, where b is related to an effective grain size. For example, for a set of planar thin vertical cracks of width d and spacing b, $\theta = d/(b+d)$ and

$$k_{\phi} = \frac{\theta^3 b^2}{12} \tag{30}$$

The permeability is proportional to the cube of the volume fraction of liquid magma. For simplicity, we neglect compaction [*McKenzie*, 1984] and apply this model to the lower partially molten zone of the oceanic crust. Figure 6.19 shows the relationship between magma viscosity and magma replenishment rate for porosity θ = 1% or 10% and grain size b = 1 or 10 mm. Porosity has more effect on magma replenishment rate than grain size, since it enters the permeability equation (30) as a cubic rather than a square. The vertical lines in Figure 6.19 show the initial values of viscosity for different crystal free magmas at their liquidus. The figure shows that the higher the viscosity, the lower the velocity of melt through the interconnected porosity. In addition, the magma replenishment rate in almost all cases is much less than the replenishment rate of $\sim 10^{-8}$ m/s needed to stabilize convective heat output between $\sim 10^7$ -10^9 Watts. For the highest porosity and grain size, the velocity is within the needed range only for basaltic magma. These results are generally consistent with the conclusions of *Korenaga and Kelemen* [1998], and suggest that some other mechanism is needed to replenish the AMC on decadal time scales.

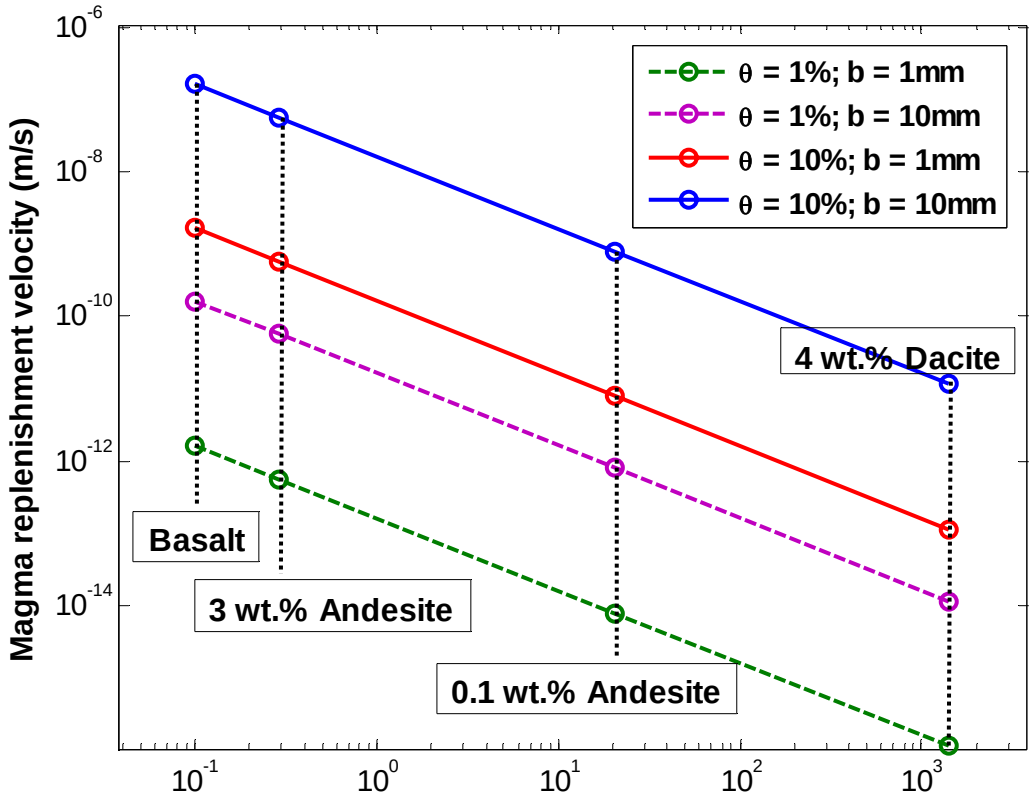

Figure 6.19 The relationship between magma viscosity and magma replenishment rate for basaltic, andesitic and dacitic magma with different values of porosity. θ and b denote the porosity and an effective grain size, respectively .

6.6 Conclusions

Heat transfer from a vigorously convecting crystallizing and replenished magma chamber overlain by a hydrothermal circulation system depends upon magma viscosity, which is a strong function of temperature, chemical composition and water content. In un-replenished magma chambers in which crystals are assumed to settle quickly to the floor, numerical simulations of convection and crystallization in a ~ 100 m thick sill, corresponding to an AMC beneath an oceanic spreading center suggest that the maximum rate of heat transfer and its rate of decay both decrease significantly as the magma

viscosity increases. Assuming a heat output cut-off of 10^7 Watts for the hydrothermal system, the results suggest that higher viscosity magmas such as andesite or dacite may drive longer-lived but lower heat output hydrothermal systems than their basaltic counterparts. Heat output and vent temperature would still decay on decadal time scales, suggesting the need for magma replenishment on these time scales.

Simulations with magma replenishment at a velocity of ~ 5 x 10^{-8} m/s, stabilize heat output and corresponding hydrothermal vent temperatures independent of magma viscosity, though as in the case without replenishment, the resulting heat outputs and hydrothermal temperatures tend to decrease as the viscosity increases. Idealized models of magma flux as buoyancy driven porous flow in the lower crust show that the rate of replenishment depends inversely on magma viscosity. In this model, the magma flux is not sufficient to maintain stable hydrothermal heat output of ~ 10^7-10^9 Watt except possibly for basaltic magmas. Then the porosity (i.e., melt fraction) must be ~ 10% and the grain size (or crack spacing) must be ~ 10 mm.

Table 6.1 Values of the physical parameters for high-silica magma system

Physical meaning	Parameter	Value	Units
Thermal diffusivity of magma	a_m	8×10^{-7}	m^2/s
Vent field discharge area	A_d	10^4	m^2
Horizontal magma area in chamber	A_m	10^6	m^2
Grain size	b	1/10	Mm
Andesitic magma specific heat	c_m	1000	J/kg ºC
Basaltic magma specific heat		1400	J /kg ºC
The total thickness of magma chamber	D		M
The initial thickness of magma chamber	D_0	100	M
The thickness of liquid magma	D_m		M
Magmatic heat flux	F_m		W/m^2
Magma replenishment heat flux	F_r		W/m^2
Acceleration due to gravity	g	9.81	m/s^2
The velocity of melt migration	J		m/s
Permeability of matrix	$k_Ø$		m^2
Latent heat of crystallization of andesite	L	3×10^5	J/kg
Latent heat of crystallization of basalt		4.2×10^5	J/kg
Rayleigh number	Ra		-
Basalt liquidus temperature	T_{bL}	1200	ºC
Basalt solidus temperature	T_{bS}	1030	ºC
Dry Andesite liquidus temperature	T_{aL}	1100	ºC
3 wt.% Andesite liquidus temperature	T_{awL}	1010	ºC
Dry Andesite solidus temperature	T_{aS}	970	ºC
3 wt.% Andesite solidus temperature	T_{awS}	900	ºC
4% dacite liquidus temperature	T_{dwL}	950	ºC
4% dacite solidus temperature	T_{dwS}	800	ºC
Replenishment rate	u		m/s
Initial replenishment rate	u_0		m/s
Thermal expansion coefficient of basalt	α_m	5×10^{-5}	$ºC^{-1}$
Thermal diffusivity	κ	8×10^{-7}	m^2/s
Thermal conductivity	λ_m	2	Wm/ ºC
Density of dry andesite	ρ_a	2.5×10^3	kg/m^3
Density of 3wt.% andesite	ρ_{aw}	2.4×10^3	kg/m^3
Density of basalt	ρ_b	2.7×10^3	kg/m^3
Density of dacite	ρ_d	2.2×10^3	kg/m^3
Density of solid	ρ_s	2.9×10^3	kg/m^3
Porosity	θ	1% /10%	-
Magma kinematic viscosity	v_m	variable	m^2/s
Volume fraction of crystals	χ		-
Critical crystal fraction	χ_c	60%	-
The crystal content of input magma	χ_{in}		-

6.7 References

Allen, D.E. and W.E. Seyfried (2003). Compositional controls on vent fluids from ultramafic hosted hydrothermal systems at mid-ocean ridges: An experimental study at 400°C, 500 bars. *Geochim. Cosmochim. Acta 67*, 1531-1542.

Anderson A.T.Jr., S. Newman, S.N. Williams, T.H. Druitt, C. Skirius, and E. Stolper (1989). H_2O, CO_2, Ci, and gas in Plinian and ash-flow Bishop rhyolite. *Geology 17*:221-25.

Baker, E.T. and G.J. Massoth, (1987). Characteristics of hydrothermal plumes from two vent fields on the Juan de Fuca Ridge, northeast Pacific Ocean. *Earth Planet. Sci. Lett. 85*: 59-73.

Bemis, K.G., R.P. von Herzen, and M.J. Mottl (1993). Geothermal heat flux from hydrothermal plumes on the Juan de Fuca Ridge. *J. Geophys. Res. 98*: 6351-6369.

Binns, R.A. and S.D. Scott (1993). Actively forming polymetallic sulfide deposits associated with felsic volcanic rocks in the eastern Manus back-arc basin, Papua New Guinea. *Econ. Geol*., *88*:2226–2236.

Binns, R.A. (2003). Drilling at Pacmanus; anatomy of a dacite-hosted, active hydrothermal system in a rifted back-arc basin, Abstracts with Programs - *Geological Society of America*, *35*, no.6, pp.13

Blundy, J. and K. Cashman (2001). Ascent-driven crystallisation of dacite magmas at Mount St. Helens, 1980-1986, *Contributions to Mineralogy and Petrology*, *140*, no.6, pp.631-650

Bowen, N.L. (1922). The reaction principle in petrogenesis, *J. Geology*, *30*, 177-198.

Bottinga, Y. and D.F. Weill (1972). Viscosity of magmatic silicate liquids — model for calculation. *Am. J. Sci. 272*, 438–475.

Canales, J.P., S.C. Singh, R.S. Detrick, S.M. Carbotte, A. Harding, G.M. Kent, J.B. Diebold, J. Babcock, and M.R. Nedimovic (2006). Seismic evidence for variations in axial magma chamber properties along the southern Juan de Fuca Ridge, *Earth. Planet. Sci. Lett.*, *246*, 353-366.

Collier, J.S. and M.C. Sinha (1990). Seismic images of a magma chamber beneath the Lau Basin back-arc spreading centre, *Nature*, *346*, 646-648.

Collier, J.S. and M.C. Sinha (1992). Seismic mapping of a magma chamber beneath the Valu Fa Ridge, Lau Basin, *J. Geophys. Res.*, *97*, no. B10, pp.14,031-14,053

Detrick, R.S., P. Buhl, E. Vera, J. Mutter, J. Orcutt, J. Madsen, and T. Brocher (1987). Multi-channel seismic imaging of a crustal magma chamber along the East Pacific Rise, *Nature*, *326*, 35-41.

Detrick, R.S., A.J. Harding, G.M. Kent, J.A. Orcutt, J.C. Mutter, P. Buhl (1993). Seismic structure of the southern East Pacific Rise, *Science*, *259*, no.5094, pp.499-503.

Dingwell, D.B. (1986), Viscosity–temperature relationships in the system $Na_2Si_2O_5$–$Na_4Al_2O_5$. *Geochim. Cosmochim. Acta 50*, 1261–1265.

Dingwell, D.B. (1996). Volcanic dilemma: Flow or blow? *Science 273*, 1054–1055.

Dunn, R.A, D.R. Toomey, and S.C. Solomon (2000). Three-dimensional seismic structure and physical properties of the crust and shallow mantle beneath the East Pacific Rise. *J. Geophys. Res*. *105*. 23537-23556.

Eggler, D.H. (1972). Amphibole stability in H_2O-undersaturated calc-alkaline melts, *Earth. Planet. Sci. Lett.*, *15*, no.1, pp.28-34

Eichelberger, J.C., C.R. Carrigan, H.R. Westrich, and R.H. Price (1986). Non-explosive silica volcanism, *Nature* (London), *323*, no.6089, pp.598-602

Embley, R.W., S. Hammond, K.M. Murphy, C.G. Fox, B. Appelgate, G.J. Massoth, R.A. Feely, E.T. Baker, J. Gendron, G. Lebon, D.A. Butterfield, B. Coughlin, J.E. Lupton, I. Jonnason, M.R. Perfit, J.P. Cowen, V. Tunnicliffe, and D.A. Trivett (1988), Submersible observation of the "megaplume" areas; southern Juan de Fuca Ridge, *Eos, Transactions*, AGU, *69*, no.44, pp.1497

Fouquet, Y., U. Von Stackelberg, J.L. Charlou, J.P. Donval, J. Erzinger, J.P. Foucher, P. Herzig, R.K. Muehe, S. Soakai, M. Wiedicke, and H. Whitechurch (1991). Hydrothermal activity and metallogenesis in the Lau back-arc basin, *Nature*, *349*, 778-781.

Fouquet, Y., U. Von Stackelberg, J.L. Charlou, J. Erzinger, P.M. Herzig, R. Muehe, and M. Wiedicke (1993). Mettallogenesis in back-arc environments: The Lau Basin example, *Econ. Geol.*, *88*, 2154-2181.

Fornari, D.J. and M.R. Perfit, (1982): Sulfide fractionation: its role in the evolution of massive sulfide deposits along the mid-ocean ridge crest. *Eos, Trans.* AGU *63*, 1135.

Francis, P., L. Horrocks, and C. Oppenheimer (2000). Monitoring gases from andesite volcanoes, Philosophical Transactions - Royal Society. *Mathematical, Physical and Engineering Sciences*, *358*, no. 1770, pp.1567-1584

Frank, F.C. (1968). Two-component flow model for convection in the earth's upper mantle, *Nature*, *220*, 350-352.

Fulcher, G.S. (1925). Analysis of recent measurements of the viscosity of glasses. *J. Am. Ceram Soc. 8*(6) 339.

Gamo, T., K. Okamura, J.L. Charlou, T. Urabe, J.M. Auzende, Shipboard Scientific Party of the ManusFlux Cruise, J. Ishibashi, K. Shitashima, and Y. Kodama (1997b). Acidic and sulfate-rich hydrothermal fluid from the Manus basin, Papua New Guinea. *Geology 25*, 139–142.

Ginster, U., M.J. Mottl, and R.P. Von Herzen (1994) Heat flux from black smokers on the Endeavor and Cleft segments, Juan de Fuca Ridge. *J. G.eophys. Res. 99*: 4937-4950.

Giordano, D., C. Romano, B. Poe, D.B. Dingwell, H. Behrens, (2004b). The combined effects of water and fluorine on the viscosity of silicic magmas. *Geochim. Cosmochim. Acta 68*, 5159–5168.

Giordano, D., J.K. Russell, and D.B. Dingwell (2008). Viscosity of magmatic liquids; a model, *Earth. Planet. Sci. Lett.*, *271*, no. 1-4, pp.123-134

Hajash, A., and G.W. Chandler (1981). An experimental investigation of high-temperature interactions between seawater and rhyolite, andesite, basalt, and peridotite. *Contributions to Mineralogy and Petrology 78*:240–254.

Heiken, G., K. Wohletz, and J. Eichelberger (1988). Fracture fillings and intrusive pyroclasts, Inyo Domes, California, *J. Geophys. Res. 93*, no. B5, pp.4335-4350

Hort, M. (1997). Cooling and crystallization in sheet-like magma bodies revisited, *J. Volcanol. Geotherm. Res.*, *76*, 297-317.

Huppert, H.E., and R.S.J. Sparks (1988). The generation of granitic magmas by intrusion of basalt into continental crust, *J. Petrol.*, *29*, 599-624.

Hummel W. and J. Arndt (1985). Variation of viscosity with temperature and composition in the plagioclase system. *Contrib. Mineral. Petrol. 90*, 83–92.

Jacobs, A.M, A.J. Harding, and G.M. Kent (2007). Axial crustal structure of the Lau back-arc basin from velocity modeling of multichannel seismic data, *Earth. Planet. Sci. Lett.*, *259*, no. 3-4, pp.239-255

Johnson, M.C., A.T. Anderson, and M.J. Rutherford (1994). Pre-eruptive volatile contents of magmas: Mineralogical Society of America, *Reviews in Mineralogy*, *30*. P. 281-330.

Jokat, W., O. Ritzmann, M.C. Schmidt-Aursch, S. Drachev, S. Gauger, and J. Snow (2003). Geophysical evidence for reduced melt production on the Arctic ultraslow Gakkel mid-ocean ridge, *Nature*, *423*, no.6943, pp.962-965

Juniper, S.K. and V. Tunnicliffe (1997). Crustal accretion and the hot vent ecosystem, *Phil. Trans. R. Soc. London*, *355*: 459-474.

Kawaguchi, M., T. Yamamoto, and T. Kato (1996). Rheological Studies of Hydrophilic and Hydrophobic Silica Suspensions in the Presence of Adsorbed Poly(N-isopropylacrylamide), *Langmuir*, *12* (26), pp 6184–6187. DOI: 10.1021/la960147x

Kelemen, P.B., K. Koga, and N. Shimizu (1997). Geochemistry of gabbro sills in the crust-mantle transition zone of the Oman Ophiolite: implications for the origin of the oceanic lower crust, *Earth and Planetary Science Letters 146*, pp. 475–488.

Kelley, D.S., J.A. Baross, and J.R. Delaney (2002). Volcanoes, fluids, and life at mid-ocean ridge spreading centers, *Annual Review of Earth and Planetary Sciences*, *30*, pp.385-491

Kelley, D.S., J.A. Karson, D.K. Blackman, G.L. Frueh-Green, D.A. Butterfield, M.D. Lilley, E.J. Olson, M.O. Schrenk, K.K. Roe, G.T. Lebon, and P. Rivizzigno (2001). An off-axis hydrothermal vent field near the Mid-Atlantic Ridge at 30 degrees N, *Nature* (London), *412*, no. 6843, pp.145-149.

Kent, G.M., A.J. Harding, and J.A. Orcutt (1990). Evidence for a smaller magma chamber beneath the East Pacific Rise at 9º30´N, *Nature*, *344*, 650-652.

Korenaga, J. and P.B. Kelemen (1998), Melt migration though the oceanic lower crust: a constraint from melt percolation modeling with finite solid diffusion, *Earth Planet. Sci. Lett*. *156*. pp. 1-11.

Kushiro, I., H.S. Yoder, and B.O. Mysen (1976). Viscosities of basalt and andesite melts at high pressures. *J. Geophys. Res. 81*, 6351–6356.

Lejeune, A.M. and P. Richet (1995). Rheology of crystal-bearing silicate melts - an experimental study at high viscosities. *J. Geophys. Res. 100*, 4215–4229.

Lejeune, A.M., F. Holtz, J. Roux, and P. Richet (1994). Rheology of an hydrous andesite; an experimental study at high viscosities, Eos, *Transactions*, AGU, *75*, no.44, Suppl., pp.724

Liebske, C., H. Behrens, F. Holtz, and R. Lange (2003). The influence of pressure and composition on the viscosity of andesitic melts, *Geochim. Cosmochim. Acta***.** *67* pp. 473–485.

Lister, J.R. (1990). Buoyancy-driven fluid fracture: the effects of material toughness and of low-viscosity precursors, *J. Fluid Mech.*, *210*, 263–280.

Lister, J.R. and R.C. Kerr (1991). Fluid-mechanical models of crack propagation and their application to magma transport in dikes, *J. Geophys. Res.*, *96*, 10,049–10,077.

Liu, L. and R.P. Lowell (2009). Models of hydrothermal heat output from a convecting, crystallizing, replenished magma chamber beneath an oceanic spreading center. *J. Geophys. Res.*, *114*, no. B02102

Lowell, R.P., B.W. Crowell, K.C. Lewis, and L. Liu (2008). Modeling multiphase, multicomponent processes at oceanic spreading centers, *Geophys. Monogr. Ser., 178*, pp.15-44 AGU, Washington, DC.

Mainprice, D. (1997). Modeling the anisotropic seismic properties of partially molten rocks found at mid-ocean ridges, *Tectonophysics 2791*, pp. 161–179.

McKenzie, D.P. (1984). The generation and compation of partially molten rock. *J. Petrol.*, 25: 713-765.

McKenzie, D.P. (1985b). The extraction of magma from the crust and mantle. *Earth Planet. Sci. Lett.*, 74:81-91.

Marsh, B.D. (1981). On the crystallinity, probability of occurrence, and rheology of lava and magma, *Contrib. Mineral. Petrol.*, *78*, 85-98.

Martin, D. (1990). Crystal settling and in situ crystallization in aqueous solutions and magma chambers, *Earth Planet. Sci. Lett.*, *96*, 336-348.

Martin, D. and R. Nokes (1988). Crystal settling in a vigorously convecting magma chamber. *Nature 332*, 534-536.

Martinez, F. and B. Taylor (2002), Mantle wedge control on back-arc crustal accretion, *Nature*, *416*, no. 6879, pp.417-420

McGee, K. A. and A.J. Sutton (1994). Eruptive activity at Mount St Helens, Washington, USA
1984-1988: a gas geochemistry perspective. *Bull. Volcanol*. *56*, 435-446.

Patrick, M., D. Wilson, D. Fee, T. Orr, D. Swanson, A. Sutton, and T. Elias (2008). Gas-pistoning associated with the 2008 summit eruption of Kilauea Volcano, Hawaii, *Eos, Transactions*, AGU, *89*, no. 53, Suppl., Abstract V51E-2082

Pinkerton, H., L. Wilson, and R. MacDonald (2002). The transport and eruption of magma from volcanoes: a review, *Contemporary Physics*, *43*, Issue 3, p.197-210

Ramondenc, P., L.N. Germanovich, K.L. Von Damm, and R.P. Lowell (2006). The first measurements of hydrothermal heat out at 9°50´N, East Pacific Rise, *Earth Planet. Sci. Lett.*, *245*, 487-497.

Resing, J.A., E. Baker, F. Martinez, N. Buck, S. Walker, J. Seewald, G. Proskurowski, J. Lupton, G. Wheat (2008). Hydrothermal Plume Geochemistry along the East Lau Spreading Center. *Eos Trans.* AGU, abstractV53D-07

Richet, P., A.M. Lejeune, F. Holtz, and J. Roux (1996). Water and the viscosity of andesite melts, *Chem. Geol.* 128 pp. 185–197.

Rona, P.A. and S.D. Scott (1993). A special issue on sea-floor hydrothermal mineralization: new perspectives, *Econ. Geol., 88*, 8, 1935-1975.

Rosenberg, N.D., J.E. Lupton, D. Kadko, R. Collier, M.D. Lilley, and H. Pak (1988). Estimation of heat and chemical fluxes from a seafoor hydrothermal vent field using Radon measurements. *Nature*. *334*: 604-607.

Roscoe, R. (1952). The viscosity of suspensions of rigid spheres. *British Journal of Applied Phys.*, *3*, 267-269.

Rudnicki, M.D. and C.R. German (2002). Temporal variability of the hydrothermal plume above the Kairei vent field, 25°S, Central Indian Ridge, *Geochem. Geophys. Geosyst.*, 3(2), 1010, doi:10.1029/2001GC000240.

Rutherford, M.J., H. Sigurdsson, S. Carey, and A. Davis. (1985). The May 18, 1980, eruption of Mount St. Helens; 1, Melt composition and experimental phase equilibria, *J. Geophys. Res.*, *90*, no. B4, pp.2929-2947

Rutherford, M.J. and J.D. Devine (1988). The May 18, 1980, eruption of Mount St. Helens, 3: Stability and chemistry of amphibole in the magma chamber, *J. Geophys. Res., 93*, no. B10, pp.11, 949-11,959

Sauter, D., V. Mendel, C. Rommevaux-Jestin, L.M. Parson, H. Fujimoto, C. Mevel, M. Cannat, and K. Tamaki (2004). Focused magmatism versus amagmatic spreading along the ultra-slow spreading Southwest Indian Ridge; evidence from TOBI side scan sonar imagery, *Geochemistry, Geophysics, Geosystem*s, *5*, no.10, 20 pp.

Scarfe, C.M., B.O. Mysen, and D. Virgo (1987). Pressure dependence of the viscosity of silicate melts. In: Mysen, B.O. (Ed.), Magmatic processes: physicochemical principles. *Spec. Publ. Geochem. Soc., 1*, pp. 504–511.

Schultz, A., J.R. Delaney, and R.E. McDuff (1992). On the partitioning of heat flux between diffuse and point source seafloor venting. *J. Geophys. Res. 97*: 12299-12314.

Shaw, H.R. (1963). Obsidian-H_2O viscosities at 1000 and 2000 bars in the temperature range 700° to 900°C. *J. Geophys. Res*. *68*: 6337-6343.

Shaw H.R. (1972). Viscosities of magmatic silicate liquids: an empirical method of prediction. *Am. J. Sci. 272*, 870–893.

Shaw, H.R. (1980). The fracture mechanisms of magma transport from the mantle to the surface. In: *Physics of Magmatic Processes*, ed. by Hargraves, R. B., Princeton University Press, 201-264.

Silantyev, S.A., M.V. Mironenko, and A.A. Novoselov (2009). Hydrothermal systems hosted in peridotites at slow-spreading ridges. Modeling phase transformations and material balance: Upwelling limb of the hydrothermal cell, *Petrology*. *17*, no. 6, pp. 523-536.

Singh, S.C., G. Kent, M. Sinha, A. Harding, C.H. Tong, P. Barton, R. Hobbs, J. Orcutt, B. White, S. Bazin (1998). 3D nature of the axial magma chamber beneath 9 degrees 03' N overlapping spreading center, East Pacific Rise, *Eos, Transactions*, AGU, *79*, no.45, Suppl., pp.798

Singh, S.C., W.C. Crawford, H. Carton, T. Seher, V. Combier, M. Cannat, J.P. Canales, D. Dusunur, J. Escartin, and J.M. Miranda (2006). Discovery of a magma chamber and faults beneath a Mid-Atlantic Ridge hydrothermal field, *Nature*, *442*, 1029-1032.

Sinton, J.M., L.L. Ford, B. Chappell, M.T. McCulloch (2003). Magma genesis and mantle heterogeneity in the Manus back-arc basin, Papua New Guinea, *Journal of Petrology*, *44*, no.1, pp.159-195.

Sim, Y. (2004). Mechanics of complex hydraulic fractures in the Earth's crust, *Ph. D. Thesis*, 324 p. Georgia Institute of Technology, Atlanta.

Solomatov, V.S. and D.J. Stevenson (1993). Suspension in convective layers and style of differentiation of a terrestrial magma ocean *Journal of Geophysical Research*, *98*, no. E3, pp.5375-5390

Sparks, R.S.J., H.E. Huppert, and J.S. Turner (1984). The fluid dynamics of evolving magma chambers, Philosophical Transactions of the Royal Society of London, Series A: *Mathematical and Physical Sciences*, *310*, no.1514, pp.511-534

Sparks, R.S.J. (2003). Dynamics of magma degassing, *Geological Society Special Publications*, *213*, pp.5-22.

Speer, K.G. and P.A. Rona (1989). A Model of an Atlantic and Pacific hydrothermal plume. *J. Geophys. Res. 94*: 6213-6220.

Spera, F.J. (2000). Physical properties of magma, in *Encyclopedia of Volcanoes*, Academic Press, 171-190.

Thomson, R.E., J.R. Delaney, R.E. McDuff, D.R. Janecky, and J.S. McClain (1992). Physical characteristics of the Endeavour Ridge hydrothermal plume during July 1988. *Earth Planet. Sci. Lett. 111*: 141-154.

Tivey, M.K., P. Craddock, J. Seewald, V. Ferrini, S. Kim, M. Mottl, A. Sterling, A-L. Reysenbach, C. G. Wheat, and the Scientific Party of TUIM05MV (2005). Characterization of six vent fields within the Lau Basin, *Eos Trans.* AGU, *86*, Abstract T31A-0477.

Tunnicliffe, V. and C.M.R. Fowler (1996). Influence of sea-floor spreading on the global hydrothermal vent fauna, *Nature*, *379*, no.6565, pp.531-533

Turcotte, D.L. and J.L. Ahern (1978). A porous flow model for magma migration in the asthenosphere. J. Geophys. Res., 83: 767-772.

Turner, J.S. (1973). *Buoyancy effects in fluids*, Cambridge University Press, London.

Van Ark, E.M., R.S. Detrick, J.P. Canales, S.M. Carbotte, A.J. Harding, G.M. Kent, M.R. Nedimovic, W.S.D. Wilcock, J.B. Diebold, J.M. Babcock (2007). Seismic structure of the Endeavour Segment, Juan de Fuca Ridge; correlations with seismicity and hydrothermal activity, *J. Geophys. Res.*, *112*, B02401, doi: 10.1029/2005JB004210.

Vetere, F., H. Behrens, F. Holtz, D. Neuville, (2006). Viscosity of andesitic melts — new experimental data and a revised calculation model. *Chem. Geol. 228*, 233–245.

Vogel, H. (1921). The temperature dependence law of the viscosity of fluids, *Physikalische Zeitschrift, 22*: 645 (1921).

Von Damm K.L., J.M. Edmond, B. Grant, C.I. Measures, B. Walden, and R.F. Weiss (1985). Chemistry of submarine hydrothermal solutions at 21°N, East Pacific Rise. *Geochimica et Cosmochimica, Acta 49*:2,197–2,220.

Von Damm, K.L. (1995). Controls on the chemistry and temporal variability of seafloor hydrothermal fluids. In : Humphris, S.E., Zierenberg, R.A., Mullineaux, L.S., Thomson, R.E. (Eds.), *Seafloor Hydrothermal Systems: Physical, Chemical, Biological, and Geological Interactions*. *Monograph Series*, *91*, AGU, Washington, D.C.

Wanless, D., M. Perfit, W. Ridley, and E. Klein (2010). Dacite petrogenesis on mid-ocean ridges: Evidence for oceanic crustal melting and assimilation, *J. Petrology* (submitted)

Wetzel, L.R. and E.L. Shock (2000). Distinguishing ultra-mafic from basalt-hosted submarine hydrothermal systems by comparing calculated vent fluid compositions. *J. Geophys. Res 105*:8,319–8,340.

Westrich, H.R., H.W. Stockman, and J.C. Eichelberger (1988). Degassing of rhyolitic magma during ascent and emplacement, *J. Geophys. Res. 93*, no. B6, pp.6503-6511

Whittington, A., P. Richet, F. Holtz (2000). Water and the viscosity of depolymerized aluminosilicate melts. *Geochim. Cosmochim. Acta 64*, 3725–3736.

Whittington, A.G., B.M. Hellwig, H. Behrens, B. Joachim, A. Stechern, and F. Vetere (2009). The viscosity of hydrous dacitic liquids: implications for the rheology of evolving silicic magmas, *Bulletin of Volcanology*. *71*, no. 2, pp. 185-199.

Wiens, D., D. Blackman, C. Fisher (2006). Lau ISS Workshop Report, www.ridge2000.org/science/meetings.

Worster, M.G., H.E. Huppert, and R.S.J. Sparks (1990). Convection and crystallization in magma cooled from above, *Earth Planet. Sci. Lett.*, *101*, 78-89.

CHAPTER 7. CONCLUSIONS AND RECOMMENDATIONS FOR FUTURE WORK

This dissertation developed a mathematical framework and corresponding numerical simulations using MATLAB to characterize the coupling between the hydrothermal systems and magma chamber. Based on this framework, I investigated convective heat transfer to an overlying hydrothermal system from three different types of crystallizing, cooling, replenished magma chambers: basalts, high-silica melts, and Di-An systems. For each scenario, I considered two scenarios of magma convection and crystallization models. One assumes the convective motions in the magma chamber are sufficiently vigorous to keep crystals in suspension and well mixed within the interior of the magma. The other assumed that as crystallization occurs, crystals rapidly settle and accumulate on the floor. In addition, I discussed magma replenishment as a mechanism to maintain the steady state heat output and hydrothermal vent temperatures on time scales of decades.

7.1 Contributions

I summarize below primary contributions of this dissertation:

- Developed general framework to perform numerical analysis of magmatic-hydrothermal systems
- Developed dynamic heat flux and temperature model for both the magma chamber and overlying hydrothermal systems

- Performed parametric analysis of heat output from a convecting, crystallizing, replenished basalt magma chamber beneath an oceanic spreading center, investigating the effects of initial sill size and periodic replenishment
- Proposed a numerical model of viscosity for high-silica magmas capturing its dependence on different physical properties
- Developed dynamic model of the Di concentration in a Di-An systems
- Investigated the effects of convection of a Di-An system on the hydrothermal circulation system through the dynamic modeling of both temperature and heat output

The most important results of this research are:

- Magma replenishment between ~10^{-8}-10^{-7} m/s (i.e., ~ $5x10^5$ and $5x10^6 m^3$/yr) is required to maintain stable heat output of 10^7-10^9 Watts and hydrothermal temperature for decadal time scales.
- The initial heat flux from magma chamber is independent of the thickness of magma chamber, but the decay rate of heat flux is inversely proportional to the initial thickness of magma chamber.
- With episodic magma replenishment rates, magma temperature remains relatively unchanged except for oscillations related to the frequency of replenishment. Hydrothermal responses resulting from periodic changes in magmatic supply might not be observed in the seafloor vents because of two factors related to time delay: the time for heat to be conducted through the thin boundary layers at the top of the magma chamber and at the base of the hydrothermal system

- For two-component Di-An magma chambers, higher initial Di concentration gives rise to more vigorous magma convection, which results in faster heat transfer, more rapid removal of Di from the melt and growth of crystals on the floor. Increasing Di contents of the added magma results in greater stabilized heat flux and hydrothermal temperatures.
- High-viscosity, high silica magmas such as andesite and dacite convect less vigorously basalts, which results not only in lower heat transport and hydrothermal vent temperatures, but also a lower decay rate of the vent temperature.
- Porous flow models of magma replenishment are not likely to provide the necessary replenishment rates, particularly in the case of high viscosity magmas.

7.2 Suggestions for Future Work

The following is a list of interesting research topics that can be pursued as extensions of this dissertation:

- *Magma dynamics and transport.* The current work assumes parametric model of magma replenishment rate. The modeling of magma transport can be improved upon by linking magma replenishment with physical models describing (1) internal pressure in magma chamber together with the stress field and elastic response of the surrounding rocks, (2) deformation and eruption processes, (3) seismicity, etc. Combined with my current heat transfer model, the new magma dynamic model should simulate the migration of magma, dike propagation, magma eruption along fractures, ground deformation, and seismic distribution associated with magma intrusion.

- *Numerical modeling of two-phase flow***.** FISHES can be employed to examine two-phase flow magma-hydrothermal systems. Both time-invariant and time-varying heat flux boundary conditions can be implemented using FISHES in combination with my heat flux model. However, there are many challenging problems about the temporal evolution of seafloor hydrothermal systems in the presence of phase separation. My current dynamic models of hydrothermal flow can be generalized to describe fluid flow in transient porous media and fluid phase separation within hydrothermal systems. In addition, more work can be done with FISHES by itself, for instance, the role of heterogeneous permeability, effect of high-porosity extrusive, circulation near dikes, etc.
- *Complex magma systems***.** The current work assumed a chemically and thermally homogeneous magma chamber. To model the magma system in a more realistic way, chemistry-real magma fractionation, magma density evolution and effects of replenishment on melt composition can be taken into account. Investigating a two component magma chamber using a Di-An model is a good starting point. A better petrological model of magma fractionation and replenishment using a program like MELTS and linking this to the current convection model can be further developed. The new complex magma models should quantitatively model the dynamic processes of magma mixing process and be consistent with the petrology of lavas erupting on the seafloor.
- *Temporal variability of melt injection***.** A related temporal variability in the seafloor hydrothermal systems can be investigated by extending the existing time-dependent periodic melt injection models.

- *Melts transport through the mantle*: To better understand the variable mid-ocean ridge melts that extract from each specific depth of mantle, the linking model between melt transport in the crustal regime and melt generation and transport in the mantle could be investigated.

APPENDIX A: MATLAB CODE

```
%% Basltic magma with magma replenishment in crystal settling case

%PARAMETERS DECLEARATION:
lamd = 5E-5 ;            % coefficient of thermal expansion of the Andesite
K = 8E-7;                % Thermal diffusivity of Andesite
depth = 100;             % Initial thickness of magma
g = 9.81;                % Acceleration due to gravity
Ad = 1E4;                % Discharge zone
Am = 1E6;                % Horizontal basalt area of magma chamber
rhof = 1E6;              % Fluid density
Cf = 6;                  % specific heat of fluid
lamdf = 1E-3;            % Thermal expansion coefficient of fluid
Permf = 1E-12;           % Permeability of fluid
Vf = 1E-7;               % Kinematic viscosity of fluid

param.deltat = 30*24*3600;    % delta time/internal time---one month
param.year = 70;              % simulation time in year
param.u = 0 ;                 % u = 0 is without replenishment

rho = 2.7E6;
C = 0.33;                % specific heat of basalt
L = 100;                 % Latent heat
Tl = 1200;
Ts = 1030;


% initialization
T(1)=Tl;                 % Basalt magma Temperature
Xin = (Tl-Tin)/(Tl-Ts);  % Crystal content of added magma

% Main code
for n = 1:1:year*12;

   %%%%%%%The crystal content and derivative
   X(n)=7200/T(n)-6;
   X_deriv(n)=(-7200)/T(n)^2;

   %%%%%%%The heat flux
   V(n)=1E-1*(Tl/T(n))^(8.5);
   J(n)=0.1*(lamd*g*K^2/V(n))^(1/3);
   tem(n)=rho*C*J(n);
   F(n)=tem(n)*(T(n)-Ts)^(4/3);

   %%%%%%%% The thickness of crystals in mamga chamber
   Ds(n) = depth*X(n);
```

```
   Dm(n) = depth*(1-X(n));
   Fc = lamd*(Tl-T(n))/(Ds(n)+eps);

   %%%%%%% The heat of magma replenishment
   Fr = - X(n)*rho*L*u-rho*C*(Tl-T(n))*u;

   %%%%%%% The depth of mamga chamber
   D(n) = u * (n)*deltat + depth;

   %%%%%%% Rayleigh Number
   Ra(n) = lamd*g*depth^3*(T(n)-Ts)/(K*V(n));

   %%%%%%% Magma temperature
   temp1(n) = rho*u*((1-X(n))*(C*T(n)+(1-X(n))*L)-(C*Tin+L*(1-Xin)));
   temp2(n) = rho*D(n)*X_deriv(n)*(C*T(n)+L*(1-X(n)))+D(n)*rho*(1-
   X(n))*(X_deriv(n)*L-C);
   T(n+1)=T(n)+(F(n)-Fc+temp1(n))/temp2(n)*deltat;
    if D(n) > 2 *depth
      break;
  end
end
   T = T(1:end-1);

%%%%%%%%%%%%%%% total heat output %%%%%%%%%%%%
% change unit from 1cal/s = 4.184watts
% Multiply the results of Fb for 4.184 times;
F=4.184*F;
F=F.*Am;

% Hydrothermal Temperature Coefficient
a = rhof*Cf*lamdf*g*Permf*Ad/Vf;

% hydrothermal temperature
Th = sqrt(F./a);
```